ANALYSIS OF VIROPORINS AND MEMBRANE SYSTEMS WITH NATIVE MASS SPECTROMETRY

by

Julia Townsend

A Dissertation Submitted to the Faculty of the

DEPARTMENT OF CHEMISTRY AND BIOCHEMISTRY

In Partial Fulfillment of the Requirements

For the Degree of

DOCTOR OF PHILOSOPHY

In the Graduate College

THE UNIVERSITY OF ARIZONA

2023

THE UNIVERSITY OF ARIZONA
GRADUATE COLLEGE

As members of the Dissertation Committee, we certify that we have read the dissertation prepared by: Julia Townsend
titled: ANALYSIS OF VIROPORINS AND MEMBRANE SYSTEMS WITH NATIVE MASS SPECTROMETRY

and recommend that it be accepted as fulfilling the dissertation requirement for the Degree of Doctor of Philosophy.

Michael Marty — Date: Jul 13, 2023

Craig Aspinwall — Date: Jul 13, 2023

John Jewett — Date: Jul 13, 2023

Thomas M. Tomasiak — Date: Jul 13, 2023

Final approval and acceptance of this dissertation is contingent upon the candidate's submission of the final copies of the dissertation to the Graduate College.

I hereby certify that I have read this dissertation prepared under my direction and recommend that it be accepted as fulfilling the dissertation requirement.

Michael Marty — Date: Jul 13, 2023
Department of Chemistry and Biochemistry

ACKNOWLEDGEMENTS

I would first like to thank my advisor Dr. Michael Marty. I deeply appreciated his support, patience, and enthusiasm for scientific research. The scientific creativity he has allowed me to explore in his laboratory has allowed me to grow into an independent researcher. Michael believed in my abilities as a researcher long before I believed in them myself. Thanks to the opportunities he has presented me over the last five years, I have grown tremendously.

I would also like to thank my committee members, Dr. Thomas Tomasiak, Dr. John Jewett, and Dr. Craig Aspinwall. I have appreciated the valuable insight each committee member has provided throughout the years. I would also like to thank my instructors and classmates from both the University of Arizona and Binghamton University for helping to shape me as a scientist.

I also greatly appreciate all laboratory members, current and former, of the Marty Lab. You have all been so supportive and have made my time in graduate school far more enjoyable.

Finally, I would like to thank my parents and brother. They have continually supported me and answered my many phone calls when I did not think I would be able to do this. My success in this program would not have been possible without their love and support throughout my life.

CONTENTS

LIST OF ABBREVIATIONS

AMP	Antimicrobial peptide
AmtB	Ammonium transporter B
AqpZ	Aquaporin Z
AUC	Analytical Ultracentrifugation
C8E4	Tetraethylene glycol monooctyl ether
CID	Collision-induced dissociation
CMC	Critical micelle concentration
DDM	*n*-Dodecyl-β-D-maltopyranoside
DMPC	1,2-Dimyristoyl-*sn*-glycero-3-phosphocholine
DMPG	1,2-Dimyristoyl-*sn*-glycero-3- phosphatidylglycerol
DPC	Dodecylphosphocholine
DPPC	1,2-Dipalmitoyl-*sn*-glycero-3-phosphatidylcholine
DSF	Differential scanning fluorimetry
E. coli	*Escherichia coli*
E protein	Envelope Protein
ESI	Electrospray ionization

FPOP	Fast photochemical oxidation of proteins
GC	Glycerol carbonate
HIS	Histidine
IM	Imidazole
IMAC	Immobilized metal affinity chromatography
LC	Liquid chromatography
LDAO	Lauryldimethylamine-N-oxide
LMNG	Laurylmaltose neopentylglycol
M2	Matrix Protein 2
MP	Membrane protein
MS	Mass spectrometry
MSP	Membrane scaffold protein
ND	Nanodisc
OG	*n*-Octyl-β-D-glucopyranoside
PC	Propylene carbonate
PDB	Protein data bank
POPC	1-Palmitoyl-2-oleoyl-*sn*-glycero-3-phosphocholine
POPG	1- Palmitoyl-2- oleoyl-*sn*-glycero-3- phosphatidylglycerol

PC	Phosphatidylcholine
PG	Phosphatidylglycerol
SEC	Size exclusion chromatography
TEV	Tobacco etch virus
Vpu	Viral Protein U

ABSTRACT

Viroporins are a class of viral membrane proteins that play diverse roles in the viral infection cycle. Viroporins are known to play roles in ion transport, inducing membrane curvature, as well as participating in a variety of protein-protein interactions. However, there is little known about the oligomeric state of viroporins. The lack of quantitative data on the oligomeric state of viroporins is due to key analytical challenges associated viroporins, including that they are 1) hydrophobic, and require a membrane mimetic for analysis, 2) small, making viroporins unamenable to some structural biology techniques such as cryo-EM, and 3) contain intrinsically disordered regions, which also poses challenges for structural characterization. To overcome these analytical challenges, this dissertation outlines the application of the unique combination of native mass spectrometry (MS) and nanodiscs for the oligomeric state determination of viroporins.

The unique combination of native MS and nanodiscs can be used to determine the oligomeric state and lipid specificities of membrane proteins (such as viroporins) while embedded within a lipid bilayer using mass defect analysis. This dissertation reviews how to perform mass defect analysis, provides examples of how mass defect analysis has been applied in the past, as well as providing tips for overcoming some of the technical limitations associated with mass defect analysis.

This dissertation also outlines a structure-activity relationship study performed to identify novel charge reducing agents for native MS. Charge reducing agents can be useful for the preservation of fragile complexes, such as viroporins, during native MS. Here, we found improved charge reducing agents that were effective on a wide range of analytes. We also uncovered the

chemical principles governing charge reduction, which may provide a basis for the development of even better novel charge reagents in the future.

The first viroporin characterized with native MS was M2 from influenza A. Here, native MS revealed that M2 assembled into a range of previously undetected oligomers, ranging from monomer through hexamer. Native MS also revealed that M2 oligomerization is highly sensitive to the local environment, being influenced by a range of factors including detergent type, solution pH, and the surrounding lipids. These results suggest that the behavior of M2 may be far more dynamic than initially thought.

The methods developed to characterize M2 were then extended to characterize a broader range of viroporins from other clinically relevant viroporins, including viroporins from HIV, SARS-CoV-2, and polio. Native MS revealed that this broader range of viroporins also had complex patterns of oligomerization and could be highly influenced by the local environment.

Overall, the methods outlined in this thesis detail the methods for determining the oligomeric state of viroporins in a wide range of chemical environments. Native MS revealed that the behavior of viroporins is more dynamic and complex than initially thought. The mass spectrometry approaches outlined in this dissertation provide directions for determining the oligomeric state of membrane proteins while embedded in a lipid bilayer, as well as may enable the development of novel therapeutics targeting viroporin complexes.

CHAPTER 1 INTRODUCTION

1.1 VIRUSES

Viruses pose major public health issues globally each year. One of the major challenges surrounding viral infection is the lack of effective treatments. A better understanding of virus biochemistry is key for the development of improved therapeutics.

Viral genomes are remarkably versatile and can be encoded with either double stranded DNA or RNA. Additionally, the genomes of viruses can be packaged as one long strand or in pieces, as well as being present in both linear and circular forms.[11, 12] Unlike the genetic information of non-viruses, the genomes of viruses are highly diverse and have little very little sequence homology.[13]

Viruses typically have small genomes. Although there are some exceptions, such as the mimivirus which contains about 1,000 genes, a genome that is bigger than many bacteria.[14] However, instances such as this are outliers. Generally speaking, viruses tend to have small genomes.[15] Small genome sizes are advantageous to viral replication, where copies of the viruses genes are exponentially replicated within the infected host cell. The smaller the genome of the virus, the faster the virus can replicate.[16]

Many viruses have evolved a variety of strategies for minimizing the size of their genome. Viruses lack the long stretches of non-coding DNA that are found in non-viruses. Many viruses, such as polio and hepatitis C, do not have individual start and stop codons for each gene, and instead express one long polypeptide chain that is then post-translationally cleaved by viral proteases into its individual protein constituents.[17, 18]

Another strategy used by viruses for minimizing genome size is to encode smaller proteins that function at multiple stages of the viral replication cycle.[19] These proteins can function as small building blocks and generate larger protein assemblies with themselves, other viral proteins, and proteins of the host.[20] The flexible disordered regions of many viral proteins allow for them to easily adopt their fold and conformation as needed under different selective pressures.[21] High conformational flexibility enables viral proteins to interact with many protein partners and still retain specificity, which can allow for the protein to be involved in a wide range of biochemical functions. The diversity in viral protein complexes that can be assembled from a single protein sequence allows for diverse functions from distinct oligomers.[20]

1.2 VIROPORINS

Viroporins are understudied viral proteins that are known to oligomerize and contain large, disordered regions. Viroporins are a class of small membrane proteins found in many viruses.[22] Viroporins are known to play a wide range of roles in the viral life cycle.[23] One of the most widely

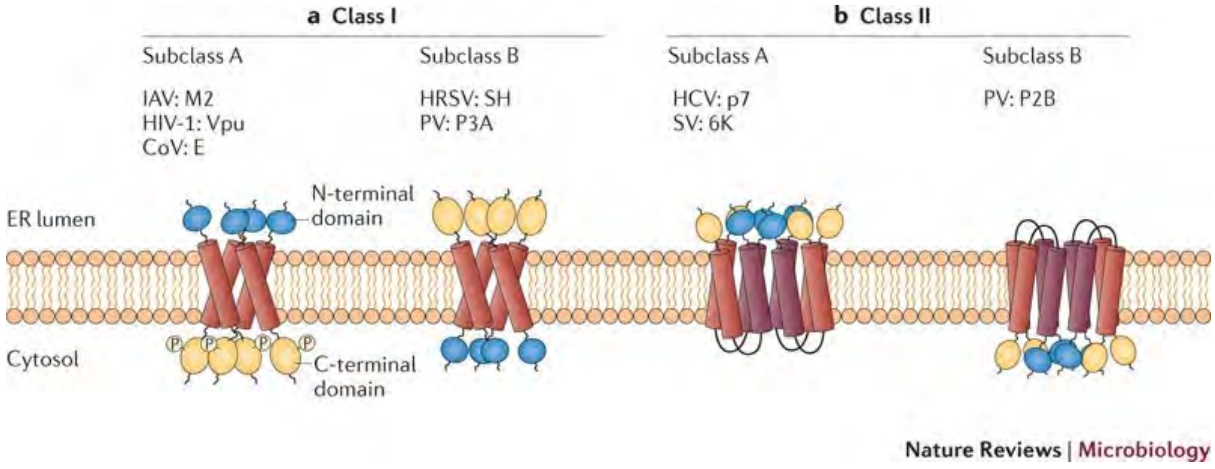

Figure 1-1: Illustration showing the different major classes of viroporins. Class I viroporins are characterized by having one membrane spanning alpha helix. Class I viroporins are also sometimes phosphorylated at their C-terminus. Class II viroporins have multiple helix-turn-helix motifs. Adapted from Nieva, J., et al, *Nat Rev Microbiol.,* **2012**, (10) 563-574.

reported functions of viroporins is their ion channel activity, but they also have a variety of other roles, including inducing membrane curvature and fluidity and aiding in viral budding and fission.[24] Additionally, viroporins are involved in downstream protein-protein interactions that affect viral infection.[24] Due to their critical role in a wide range of viral functions, viroporins can be targeted for the development of therapeutics, including antiviral compounds and vaccines.[22, 25, 26] However, drug development regarding viroporins has yet to be fully explored. Improving the characterization of the dynamics of viroporins can lead to the development of therapeutics targeting this protein class. [27]

Viroporins are typically grouped into two major classes, as illustrated in Figure 1-1. Class one viroporins are characterized by a single transmembrane domain on the monomeric unit, whereas class two viroporins often include helix-turn-helix hairpin motifs embedded within the lipid bilayer.[28] The current paradigm is that viroporins will insert into host membranes and self-oligomerize. It is believed that these fixed oligomers are the functional unit of the protein.[28]

1.2.1 M2 FROM INFLUENZA A

The best characterized viroporin to date is the ion channel M2 from the influenza A virus. One of the best characterized functions of M2 is its role as a selective proton channel. M2 will equilibrate the pH both across the viral lipid membrane during viral entry and across the trans-Golgi membrane of host cells during infection.[29] The transport of protons across the trans-Golgi membrane is essential for viral maturation because it protects nascent hemagglutinin, another influenza A membrane protein, from undergoing premature conformational changes due to low pH.[30-33]

Due to M2's critical role in the life cycle of the influenza virus, it has been an attractive target for potential therapeutic compounds. Currently, M2 is the only viroporin that is a clinically approved drug target.[22] Amantadine was approved for the treatment of Asian influenza in 1966 and for influenza A in 1976.[34] This compound is believed to block the channel formed through M2 oligomerization in the bilayer and prevent the transport of ions across the bilayer, ultimately inhibiting viral replication.[30, 35] However, amantadine resistant strains of influenza A quickly emerged after the drug became widely used. Interestingly, all of the mutations that have led to amantadine resistance in influenza A are located in the transmembrane (TM) domain of M2, such as the S31N mutation.[36]

M2 is made up of 97 amino acid residues including a large C-terminal cytoplasmic tail that is believed to be largely disordered.[37] There are currently over 30 different structures of M2 in the protein data bank (PDB), and nearly all these structures were solved using solution NMR. All the structures in the PDB suggest that M2 assembles into a tetrameric complex. However, none of the

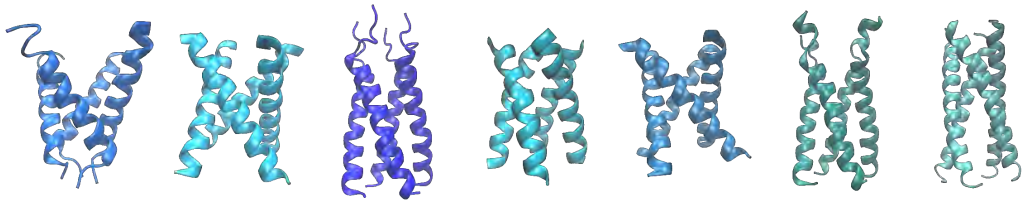

PDB	3C9J	1NYJ	2MUV	3LBW	2KAD	2MUW	6OUG
Membrane Mimetic	OG	DMPC	OG	OG	DLPC	DPC	LCP
Residue #'s	22-46	22-46	22-46	25-46	22-46	19-49	21-61
Drug Added?	✓	X	✓	X	✓	✓	✓

Figure 1-2: Selected experimental determined 3D structures of viroporin M2 embedded in a variety of membrane mimetics. Below each structure shows the length of the construct used, as well as whether amantadine was added to the sample prior to determining the structure. Structure are from PDB files 3C9J[3], 1NYJ[6], 2MUV[7], 3LBW[8], 2KAD[9], 2MUW[7], 6OUG[10].

structures of M2 in the PDB are of the full-length protein, likely because the intracellular and extracellular regions of M2 are expected to be intrinsically disordered.[3]

The majority of the existing structures of M2 consist of the transmembrane domain of the protein (residues 22-46) (shown in Figure 1-2). However, this is a relatively small portion of the entire protein, as highlighted in Figure 1-3, which raises questions of whether the structures or oligomeric states of M2 could be significantly different when examining the full length M2. There have been challenges determining the structure of the full-length M2, thought to be largely due to its intrinsically disordered C-terminal cytoplasmic tail.

Although all existing structures of M2 suggest that it is a tetramer, it appears that the structure of this protein can be highly influenced by its surrounding membrane mimetic. The

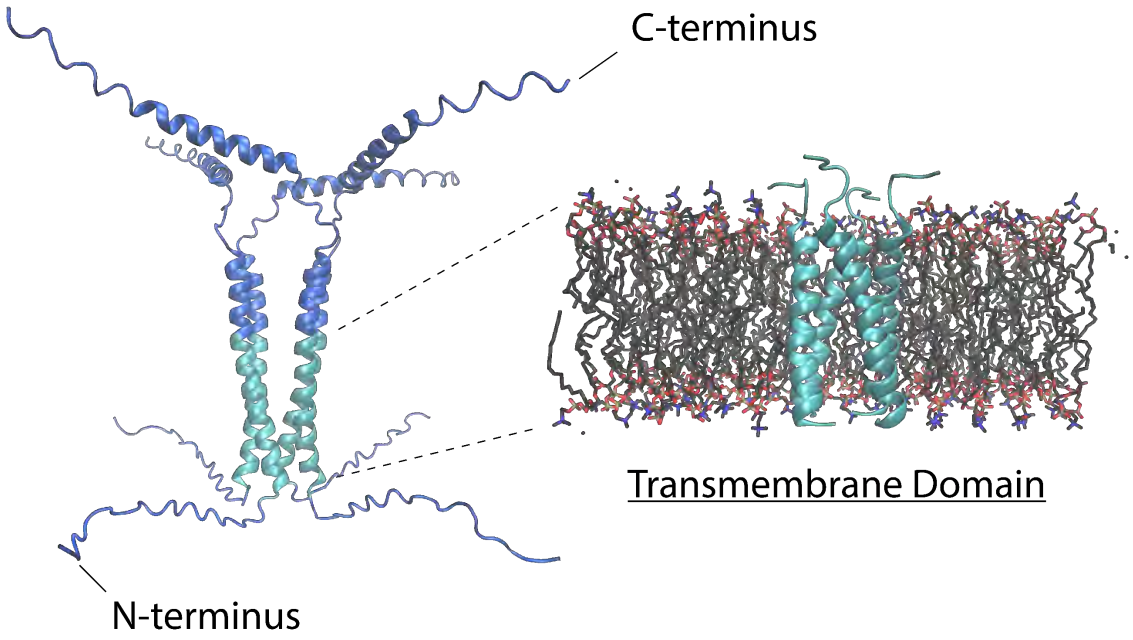

Figure 1-3: An AlphaFold[1] generated structure of full-length M2 shown on the left and an experimentally determined (PDB: 2MUV) structure of the transmembrane domain (residues 22-46) of M2 embedded within a POPC bilayer (bilayer generated in CHARMM-GUI[4]). The N- and C-termini are labeled on the full-length protein.

structure of M2 has been solved in a wide range of membrane mimetics, including both different types of detergents and lipid bilayers. There can be large differences among structures of M2 when the protein is embedded in different membrane mimetics, as highlighted in Figure 1.2.[8, 38] In some instances, even when embedded in the same type of membrane mimetic, there are large differences among structures of the same protein.

Interestingly, it is also reported with many of the different M2 structures that high (millimolar) concentrations of amantadine were added to the sample to help resolve the spectra.[3, 7, 9, 10] The addition of these high concentrations of the drug may also have an unappreciated influence on the structure of M2. In chapter four of this dissertation, we investigate some key questions surrounding M2, including 1) what is the oligomeric state of the full length M2, 2) how does the local environment, including the solution pH and surrounding lipids influence this oligomeric state, and 3) what are the major differences in oligomerization between the full-length M2 and its TM domain?

1.2.2 Viral Protein U (Vpu) from HIV

Viral protein U (Vpu) is a viroporin found in the human immunodeficiency virus (HIV). During virus entry, the glycoprotein on the surface of HIV binds to the CD4 receptor. After initial virus infectivity, Vpu will bind to CD4 to aid in downstream degradation. Degradation of CD4 is critical for the HIV infectivity cycle because it prevents the retention of nascent viruses to the surface of the cell, as well as preventing superinfection of the cell.[39, 40]

It was initially proposed that Vpu may oligomerize to form selective channels due to its similarities in structural features with the M2 protein of influenza.[40, 41] Additionally, early studies of Vpu in frog oocytes suggested that this protein may form cation selective channels.[42] Later

investigations of synthetic Vpu in bilayers supported that Vpu forms cation specific channels.[43, 44] It has been suggested that this cation transport leads to membrane depolarization, which could influence the rate of HIV virus release.[45]

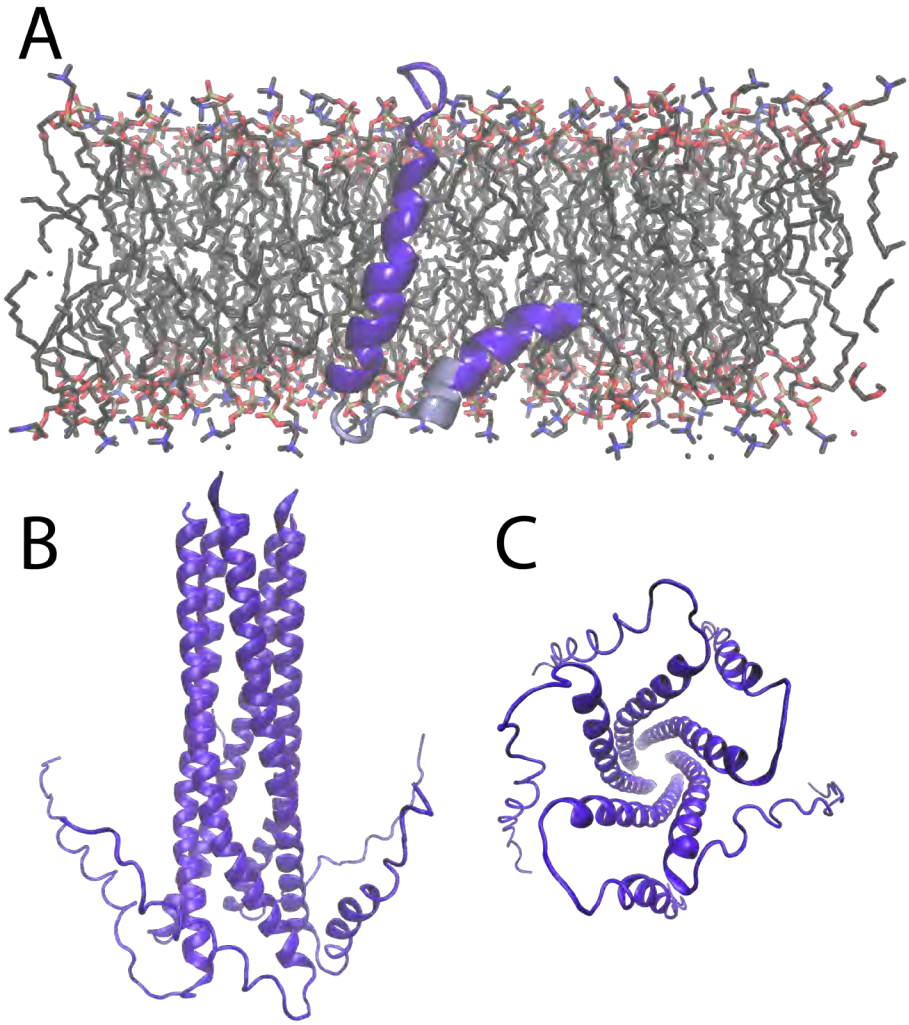

Figure 1-4: A) An experimentally determined structure of the TM domain of Vpu (PDB: 2N29[2]) with the highly conserved "hinge" region of the protein highlighted in light purple in a POPC bilayer (bilayer generated in CHARMM-GUI[4]). B) and C) show an AlphaFold [1]generated model of the full-length Vpu modeled as a pentamer. B) shows this pentamer from the side and C) shows the structure from the bottom, which is the cytoplasmic side of the channel.

Although it is widely agreed that Vpu forms channels in the bilayer, the oligomeric state of Vpu when it self-assembles into these channels is still debated. Some computation studies have suggested that the most energetically favorable structure of the TMD of Vpu would be of a pentamer.[46] Like M2, most of the structural data for Vpu is not of the full-length protein but instead of the shorter transmembrane domain of the protein, as shown in Figure 1-4. Although there are a small handful of structures of full-length Vpu in the PDB, there are no experimentally determined structures indicating the quaternary structure of Vpu; there are only structures of Vpu in its monomeric form.[2, 47, 48]

Vpu has 81 amino acids and is made up of two distinct alpha-helical regions. The most highly conserved region of Vpu is the "hinge" region, which connects these two alpha-helical regions. One region is the N-terminal hydrophobic TM domain, which is believed to form a channel selective for monovalent cations.[39] It has been found that this channel activity can be blocked by the amiloride derivative hexamethylene amiloride.[49] The other major region of Vpu is a cytoplasmic C-terminal domain that is made up of several serines that are known to be phosphorylated within host cells.[44] Despite its high clinical relevancy, there is significantly less known about the structure and function of Vpu than M2. In chapter five of this dissertation, we will cover some of the only reported experimental work of the full length Vpu.

Figure 1-5: A sequence comparison of the envelope (E) protein amino acid sequences from coronavirus. The transmembrane domain is shown in brown, the conserved cysteines in blue, the conserved proline in red, and the PDZ-binding motif in orange. Adapted from Schoeman et al., Front Microbiol. 2020, 11: 2026.

1.2.3 Envelope Protein from SARS-CoV-2

The envelope (or "E") protein is a viroporin found in SARS-CoV-2. Interestingly, the E protein from SARS-CoV-2 shares sequence similarity with the E protein from SARS-CoV-1 and MERS, particularly in the highly conserved N-terminus region,[50] as shown in Figure 1-5. Based on knowledge from earlier coronaviruses, this high degree of conservation provided a basis of what the potential functions of the E protein could be at the start of the pandemic in 2020.[51]

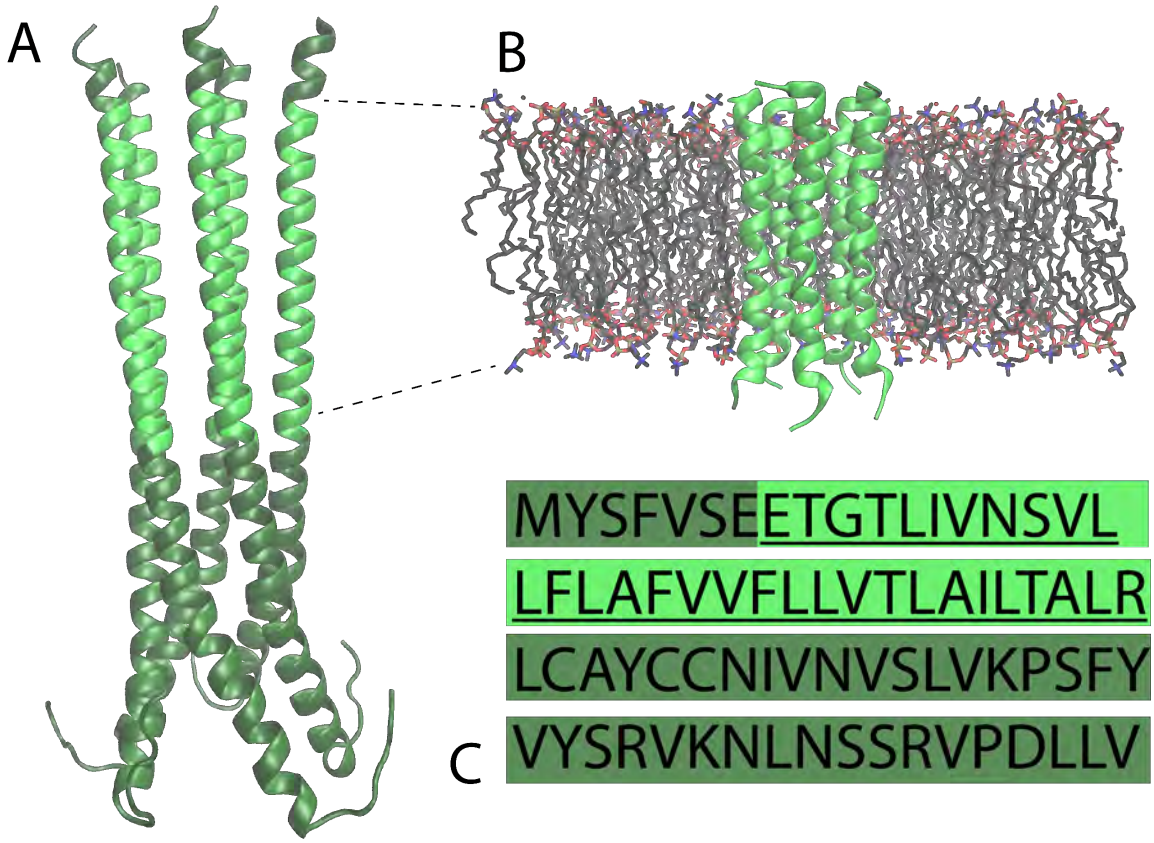

Figure 1-6: An image highlighting the differences between the full-length E protein (A) that was generated in AlphaFold2[1] and the TMD of the E protein (B) that was experimentally determined (PDB: 7K3G[5]). For the full-length protein (A) the TMD is highlighted in light green and the rest in dark green. The amino acid sequence is also shown (C) with the TMD underlined and shown in light green with the rest of the protein sequence shown in dark green.

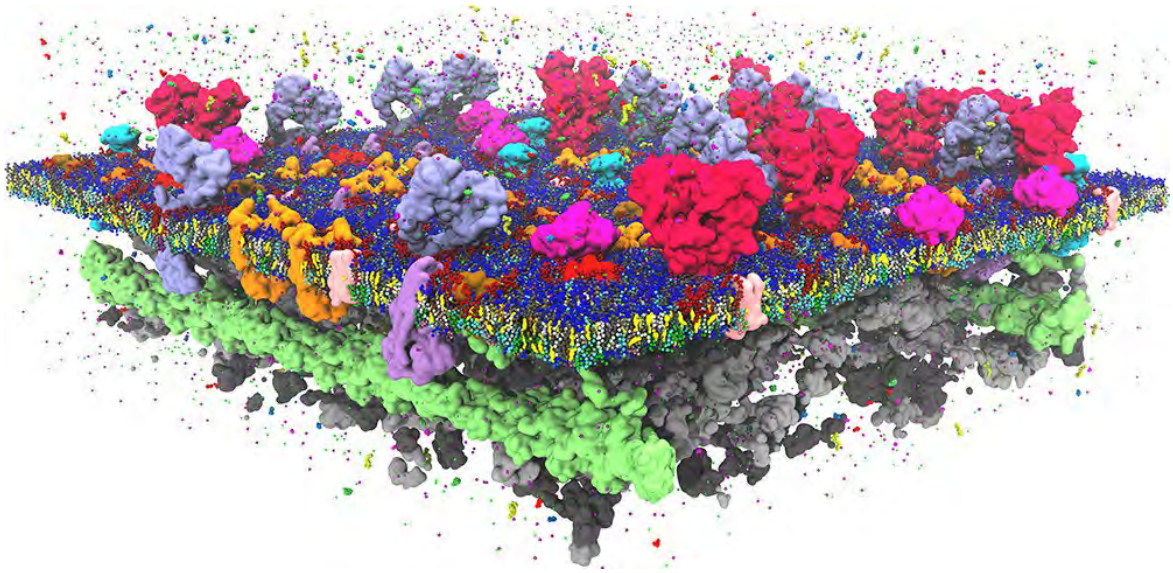

Figure 1-7: Schematic illustrating the complexity and polydispersity of a lipid bilayer. Adapted from Marrink, SJ et al., *Chem. Rev.* **2019**, 119 (9), 6184-6226.

The E protein is known to self-assemble into pores and is thought to potentially form cation-selective channels. Only a small percentage of expressed E proteins will be incorporated into the viral envelope, the majority of E protein is localized in the ER-Golgi intermediate compartment (ERGIC) of cells, where coronaviruses are known to bud and assemble.[52, 53] It has been found that SARS-CoV-2 viruses lacking the E protein gene have a disfigured shape, suggesting that the E protein induces some of membrane curvature that allows the virus to take on its characteristic shape.[54, 55]

It has been found that the E protein channel can be blocked by hexamethylene amiloride (HMA) and amantadine (AMT). Interestingly, it had been previously found that HMA blocks the activity of Vpu and AMT blocks the activity of M2.[35, 56]

Although the E protein plays a critical role in the virus, there have been challenges gaining structural information on the E protein. There is a structure of the E protein solved with solid-state NMR that suggests that the E protein may form pentameric complexes,[57] but this structure is of the isolated transmembrane domain, not the full-length protein. Given that the transmembrane domain is less than half of the full-length protein (as shown in Figure 1-6), it can be challenging to draw conclusions on the structure of the full protein. Additionally, there is still some ongoing debate within the field on whether this pentameric structure is the only functional form of the E protein or if other oligomeric states may exist.[58, 59] Chapter 5 of this dissertation will investigate the patterns of oligomerization of the full length E protein, how this oligomerization is influenced by its local chemical environment, as well as investigating the ion channel activity of the E protein.

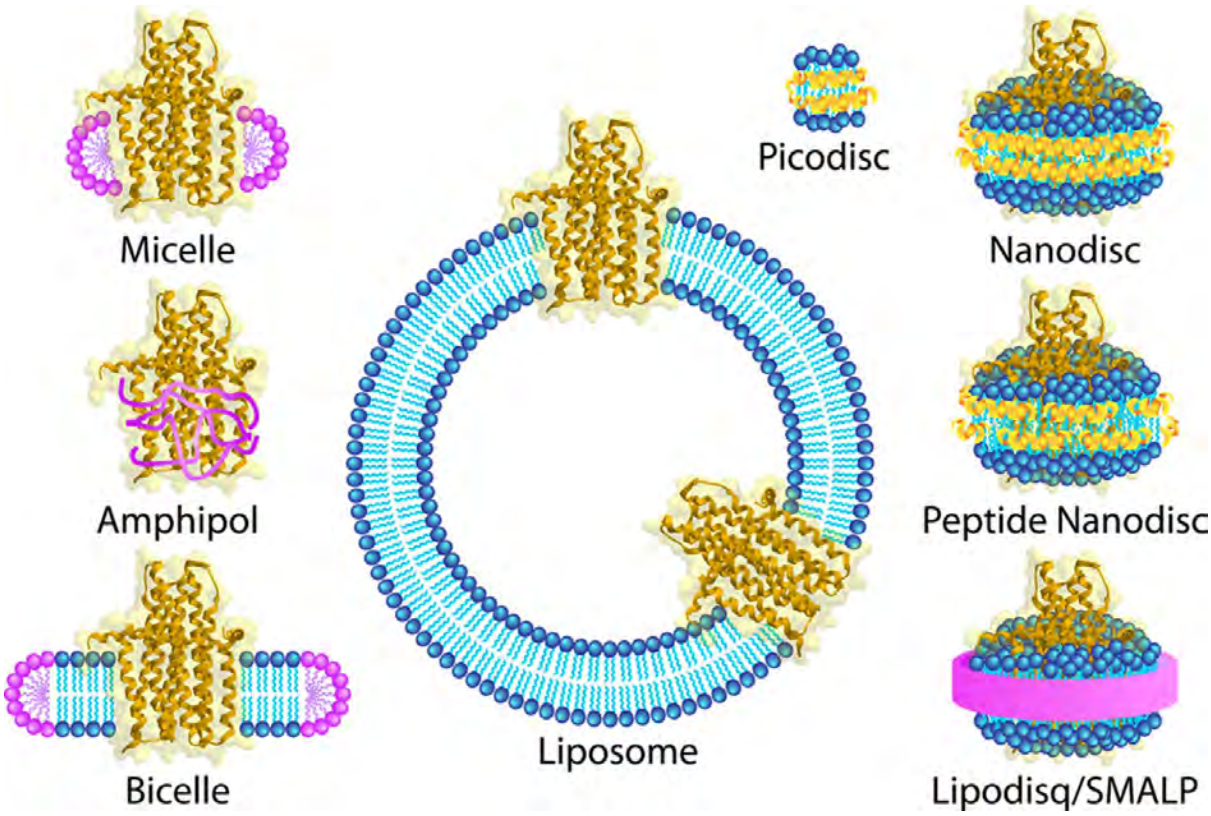

Figure 1-8: Schematic illustrating a membrane protein embedded in the most implemented membrane mimetics applied. Adapted with permission from Marty; et al., *Acc. Chem. Res.* **2016**, 49 (11), 2459-2467.

1.3 ANALYTICAL CHALLENGES WITH MEMBRANE PROTEINS

Cells are surrounded by an amphipathic lipid envelope called the lipid bilayer. This lipid bilayer is what separates the interior of the cell from the outside world. The cell membrane is tremendously complex, being made up of hundreds of different types of lipids, as shown in Figure 1-7.[60] Slight changes in the composition of cell membranes can have a huge influence on the biophysical properties of the bilayer, altering the charge, fluidity, and curvature of the bilayer.[61] All of these properties of the bilayer can directly influence the structures and functions of the membrane proteins embedded within the bilayer.[62]

Membrane proteins constitute about 30% of the total proteome.[63, 64] However, membrane proteins make up only 2-3% of high-resolution structures in the protein data bank (PDB).[65] This is partially due to the analytical challenges associated with studying membrane proteins.

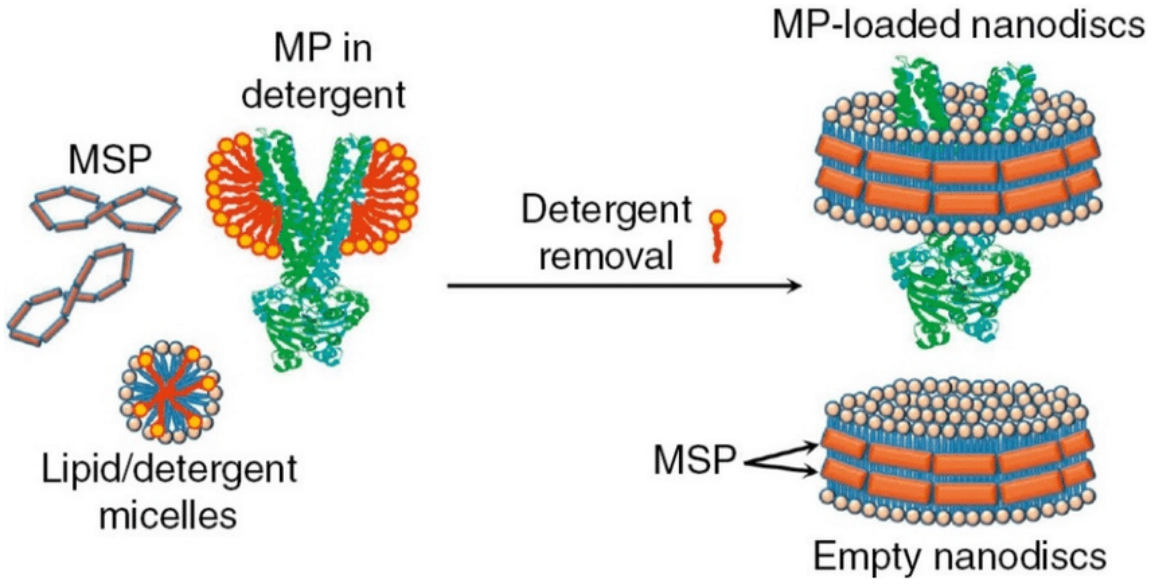

Figure 1-9: Schematic showing the process of the formation of nanodiscs, both with and without membrane proteins (MP). Adapted from Conrard et al. *Biomolecules* **2019**, *9*(10), 513.

1.3.1 Detergent Micelles

One of the major challenges associated with characterizing membrane proteins is their hydrophobic exterior. This requires some form of a membrane mimetic for the analysis of membrane proteins, shown in Figure 1-8. By far, the most common membrane mimetic used for the analysis of membrane proteins is the detergent micelle.[66] Detergents are typically used in the extraction of membrane proteins from the native lipid bilayer, as well as throughout the purification and analysis of the membrane protein.[67] Screening for a suitable detergent is an important part of membrane protein analysis, as not all membrane proteins are stable in all detergent environments. Additionally, some detergents may be more suitable for the extraction of the membrane protein from the native lipid bilayers, whereas other detergents may be more appropriate for different analytical techniques.[68]

Detergents are typically amphipathic molecules that are made up of a polar head group and a nonpolar tail. [67] There a variety of different types of commercially available detergents, including ionic detergents, nonionic detergents, zwitterionic detergents, and bile acid salts.[69] Each detergent molecule has its own critical micelle concentration (CMC), which describes the concentration of detergent molecules in a solution necessary for micelles to spontaneously assemble in solution. The concentration of detergent molecules necessary to self-assemble into micelles generally ranges from as low as 0.025% for DDM detergent to as high as 1.5% for OG detergent.

1.3.2 Nanodiscs

An emerging technology for the analysis of membrane proteins is the nanodisc. Nanodiscs are nanoscale lipid bilayers that are surrounded by two amphipathic helical protein scaffold belts.[70] Nanodiscs are useful because they solubilize the membrane protein in a lipid bilayer, which is a

more native like environment than many other membrane mimetics, such as detergent micelles. The size of nanodiscs can be tuned by switching the length of the protein scaffold belt. The composition of the nanodisc can also be altered by changing the types of lipids incorporated. These factors make nanodiscs a versatile tool for studying membrane proteins. Ultimately, nanodiscs provide significant advantages of other more commonly used membrane mimetics.

Nanodiscs are assembled by mixing lipids that have been solubilized in detergent with this amphipathic membrane scaffold protein (MSP) belt, as shown in Figure 1-9. These MSP belts were derived from the apolipoprotein-A1 (ApoA1) that are often found in high density lipoprotein protein particles.[71] This mixture is then combined with polystyrene Biobeads, which remove the detergent molecules from the solution and promote the spontaneous formation of these nanoscale lipid bilayers.[72, 73] Nanodiscs can then be purified and buffer exchanged using size exclusion chromatography. In Chapter 2, we will discuss more on the earlier work with native MS of nanodiscs.

1.3.3 Techniques for Determining Oligomeric State of Membrane Proteins

There are a variety of analytical tools that can be used for determining the oligomeric states of membrane proteins and peptides. Here, we will describe some of the most common techniques and discuss their strengths and limitations. As we examine these methods, there are three key points to consider.

First, what types of lipid environments can the technique probe? Membrane proteins can be influenced by the lipid bilayer,[74, 75] including properties like fluidity, curvature, and charge.[76, 77] Several techniques, including hydrodynamic methods, mass photometry, nuclear magnetic resonance (NMR), and native mass spectrometry (MS), generally require membrane proteins to be

extracted from their native lipid environment and solubilized in a membrane mimetic, such as detergent micelles.[78, 79] Different membrane mimetics can cause varying types of interference, depending on the technique. Other techniques, including crosslinking and fluorescence methods, can be performed on proteins in diverse environments, including embedded in natural membranes.

Second, how does each technique handle polydispersity? Some techniques, like native MS, mass photometry, and hydrodynamic methods are capable of characterizing polydisperse oligomeric state distributions. Other techniques, including NMR, crosslinking, and some fluorescence methods, generally give average oligomeric state values that will be less useful for polydisperse ensembles.

Third, what is the size range for each technique? Some techniques, like native MS and fluorescence methods generally tolerate a wide range of analyte sizes, ranging from small peptides to large membrane protein complexes. Others, like mass photometry, hydrodynamic methods, and crosslinking, work better for larger proteins. Finally, NMR works best for smaller proteins and peptides and does not scale as well to larger complexes. Overall, no method is perfect, and each has tradeoffs between information content and sample tolerance.

1.3.4 Hydrodynamic Methods

Hydrodynamic methods like analytical ultracentrifugation (AUC) are well-established for determining the oligomeric state of soluble proteins.[80] AUC can be a powerful technique because it can effectively characterize sample polydispersity and quantify the abundance of different oligomers. However, membrane mimetics like detergent micelles are required to solubilize membrane proteins, and they can influence the size and buoyancy of membrane proteins, making

interpretation of AUC data more challenging.[81] AUC can be especially challenging when the sample is polydisperse or the protein interactions are more dynamic.[82]

With size exclusion chromatography coupled with multiangle light scattering (SEC-MALS), the masses of proteins in solution can be measured through the intensity of the scattered light of a sample as it elutes from a SEC column, which also provides a retention time related to mass.[83] Like AUC, the addition of the detergent micelle can significantly interfere with both retention time of a protein from the SEC column and the way that light will scatter around the sample in solution.[84] Thus, the need for membrane mimetics can limit SEC-MALS for determining the oligomeric states of membrane proteins. Other hydrodynamic methods will face similar limitations as AUC and SEC-MALS, where the membrane mimetic can affect the signal. In these cases, it is challenging to study smaller analytes because they contribute less to the overall size of the complex relative to the mimetic.

1.3.5 Mass Photometry

Mass photometry (MP) is a relatively new technique to measure the masses of biomolecules in solution. MP uses light scattering to measure the masses and relative abundances of unlabeled proteins in solution.[85] The major strength of MP is its ability to characterize polydisperse and heterogeneous samples with minimal sample consumption, broad tolerances for buffer conditions, and quick analysis.[86] However, like AUC and SEC-MALS, membrane mimetics are required and can interfere with MP analysis and interpretation.

For detergents, the strong background signal from empty micelles can overwhelm the signal from micelles with protein. To address this problem, researchers have diluted samples to below the detergent critical micelle concentration, which removes the interference. However, even

with these creative approaches and use of non-interfering membrane mimetics like SMALPs and nanodiscs, interpretation still remains challenging due to the mass of the membrane mimetic.[87] Also, although oligomeric changes that cause large changes in the mass of the complex can be easily measured, MP is limited for characterizing smaller proteins and peptides due to limits in resolution and interferences from the membrane mimetic.

1.3.6 NMR

Nuclear magnetic resonance (NMR) spectroscopy is a powerful technique for studying the structure and dynamics of small proteins in solution as well as membrane environments. The most widely used approaches rely on many short range inter-nuclear distance measurements supplemented with angular restraints to constrain the protein to its three-dimensional fold, in part by using restraints on the distances between pairs of nuclei in the protein. However, the lack of long range restraints means that NMR is generally less useful for describing protein-protein interactions, particularly in the cases of small proteins forming homo-oligomers.[88] Relying on distance measurements alone is not straightforward in large part because it is challenging to assign restraint pairs of nuclei in the same or different polypeptide chains.[89, 90]

This limitation of distance restraints can be largely overcome in solid-state NMR studies of proteins in lipid bilayers by employing Centerband-Only Detection Of Exchange (CODEX), which is based upon anisotropic diffusion and using a label such as ^{13}C or ^{19}F.[5, 91] However, CODEX is limited for polydisperse samples and larger protein complexes.[92] Like other NMR techniques, it also needs high sample concentrations, which could drive proteins into non-physiological complexes.[93] The use of angular restraints of aligned bilayer samples[94] can also provide complementary structural information.

1.3.7 Chemical Crosslinking

Chemical crosslinking followed by gel electrophoresis and/or mass spectrometry is another common technique for determining the oligomeric state of proteins.[95] A major strength of crosslinking is that it can be applied while the protein is still embedded in a natural lipid bilayer by using membrane permeable crosslinkers.[96] A challenge of cross-linking experiments is that it relies on have reactive amino acid residues in the correct locations for the cross linking reaction to occur. Smaller complexes might suffer from false negatives if the right residues are not available in the right places. Also, the addition of a crosslinker can also lead to structural distortion and oligomeric artifacts, especially if too much crosslinker is added or the reaction is allowed to proceed for too long.[97, 98] Overall, the potentials for false positives and false negatives make it challenging to confidently determine oligomeric state distributions for polydisperse ensembles from crosslinking data alone.

1.3.8 Fluorescence Methods

Finally, fluorescence methods can inform on the oligomeric state of a membrane protein while in the lipid bilayer.[99] FRET can be used to study dimerization by looking at distance between two labels, and fluorescence recovery after photobleaching (FRAP) provides an average diffusion constant of the protein in the lipid bilayer, which can inform on complex size. An advantage to FRAP is that it can be performed on proteins in living cells.[100] Performing the experiment in living cells adds a dimension of real-time information that none of the other techniques can provide. However, there can be major challenges with FRAP in trying to determine the diffusion coefficient of particles in the membrane, which can lead to artifacts. FRAP is also limited in its ability to resolve polydisperse samples.[101]

1.4 NATIVE MASS SPECTROMETRY OF MEMBRANE PROTEINS

Native, or nondenaturing mass spectrometry (MS) has emerged as a powerful technique for determining the oligomeric state of proteins.[66, 102, 103] Native MS uses non-denaturing sample preparation and gentle ionization to preserve the native fold of proteins in the gas phase and retain protein-protein interactions. Native MS can enable the measurement of protein-protein, protein-lipid, and protein-ligand interactions. Directly measuring the mass of the oligomeric complex usually provides a clear picture of the oligomeric states present and relative changes in the distribution.[103, 104] However, precise quantitation of the oligomeric state distribution can be challenging due to differences in ionization, transmission, and detection efficiency between ions of very different *m/z* ratios.[105, 106]

Native mass spectrometry has the ability to characterize low-abundance and polydisperse samples in ways that other more traditional structural biology techniques, such as X-ray crystallography and cryo-EM are limited.[107] For example, native MS can identify a ligand bound that is only present on a small percentage of the proteins in a sample. Many other techniques would not be able to capture this small portion of the sample population. Beyond just identifying the presence of this ligand, if the protein is made up of multiple subunits, using an activation technique, such as collision induced dissociation (CID) or surface induced dissociation (SID), native MS can be used to identify which subunit this ligand specifically binds to.[108] Additionally, the use of gas-phase activation techniques can be an essential tool for determining protein stoichiometry and oligomerization.[109] Thus, native MS is an invaluable technique in the toolbox of structural biology.

Beyond just information on the *m/z* of biomolecules, recent advancements in ion mobility (IM) when used in combination with native MS can provide details on the collision cross-section (CCS) of the analyte as well.[110] This complementary technique adds an entirely new dimension to the types of structural information that can be gained with native MS, by providing insights on the conformation and folding of the analyte as well. For example, native MS can inform whether the addition of a drug or ligand influences the conformation of a protein. Understanding the dynamics of ligand binding can provide insights on the mechanisms of action of the protein.

1.4.1 Native Mass Spectrometry of Membrane Proteins

Native MS also enables the analysis of membrane proteins in a variety of membrane mimetic environments. The original and most commonly used membrane mimetic for native MS

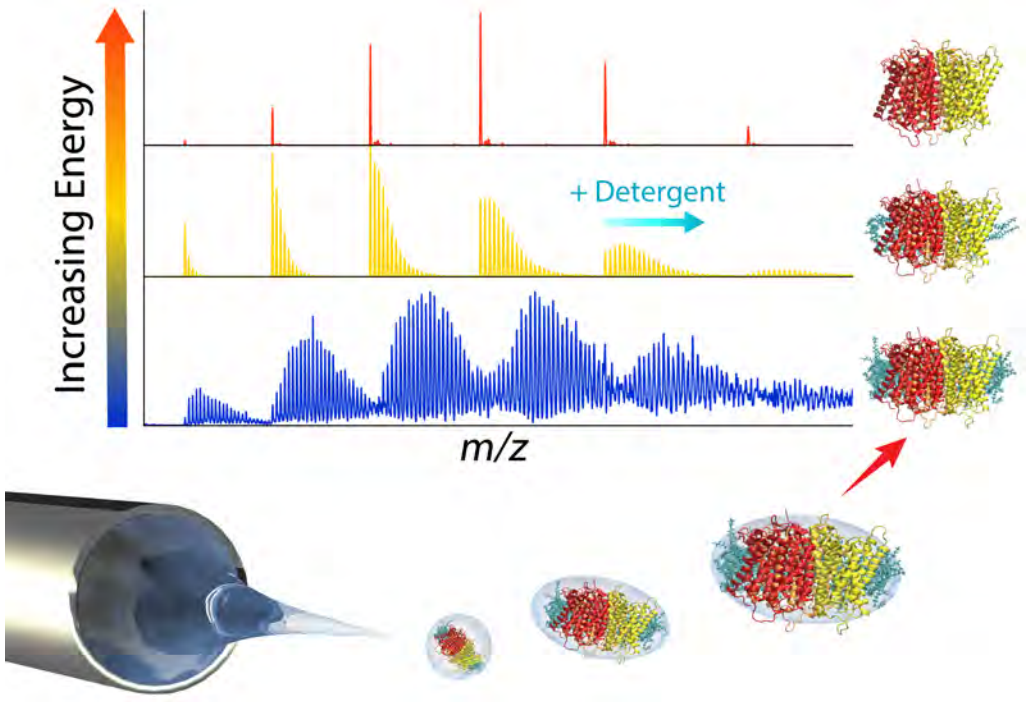

Figure 1-10: Schematic illustrating native mass spectrometry of a membrane protein embedded in a detergent micelle. The schematic shows the removal of detergent molecules from the surface of the analyte as the activation energy is increased inside the mass spectrometer. Adapted from Keener, et al. Anal Chem. **2021**, 93 (*10*), 583-597.

is detergent micelles.[111] When performing native MS of proteins solubilized in detergent, the entire protein-micelle complex is ionized and enters the mass spectrometer. Energy is then applied inside the mass spectrometer and labile detergent molecules are removed from the surface of the protein, as shown in Figure 1-10.[66] The removal of these detergent molecules presents the bare protein complex for mass analysis, which can then be easily interpreted like soluble proteins.

The detergent conditions selected must be carefully considered for native MS of membrane proteins. For example, one common mistake when doing native MS of membrane proteins is that too high of a detergent concentration is used. High detergent concentrations can be problematic for several reasons. First is that too high of a detergent concentration can be destabilizing, even for membrane proteins. Another reason is that if the concentration of detergent micelles is too high, it can make it challenging to resolve the signal for the membrane protein above the signal for the ionized micelle.[112] Conversely, problems can also arise when too low of a detergent concentration is used, leading to non-specific association and aggregation. Typically, a detergent concentration of double the critical micelle concentration (CMC) is appropriate for native MS.[112]

Another important consideration for native MS of membrane proteins is the detergent type selected for analysis. Not all detergents are amenable for native MS, primarily because they create too strong of a micelle around the protein. This makes it challenging to use gas-phase activation techniques to remove the detergent molecules from the surface of the protein for analysis. The first experiments of native MS of membrane proteins typically used saccharide-based detergents, such as *n*-dodecyl-β-D-maltopyranoside (DDM) and *n*-octyl-β-D-glucopyranoside (OG). These were a logical first choice in detergent as this class of detergent is commonly employed in protein purification strategies and in structural biology studies of membrane proteins.[113] However, these

saccharide detergents are prone to excessive adduction to the surface of the analyte in the gas phase.

Later studies of membrane proteins with native MS employed more charge reducing detergent molecules, such as tetraethylene glycol monooctyl ether (C8E4), lauryldimethylamine-N-oxide (LDAO), and Triton X-100.[113-115] These newer detergents were typically more easily removed from the surface of the protein in the gas phase and allowed for better preservation of intact membrane protein complexes.[113] However, the type of detergent selected can have a significant effect on the structure and behavior of a membrane protein. I will discuss more on the influence of detergents on protein oligomerization in Chapters 4 and 5.

Native MS requires less sample than many traditional structural biology techniques, helping to overcome some of the challenges associated with the low yields of membrane proteins.[116] Native mass spectrometry can also provide rich information on ligand and lipid binding interactions to membrane proteins.[117] Better understanding lipid binding is significant because it is known that lipids play a fundamental role in the structure and function of membrane proteins, but it can be challenging to characterize these polydisperse and dynamic interactions.[67] Additionally, native MS allows for membrane proteins to embedded in a wide range of membrane mimetics, ranging from detergent micelles to lipoprotein nanodiscs, allowing the protein to be analyzed in a variety of local environments.

Unlike methods above, native MS uniquely allows detergents to be removed from the membrane protein complex while still preserving the oligomeric assembly for analysis. This technique is broadly applicable to complexes ranging from small membrane proteins/peptides[118] to large membrane protein assemblies.[119] However, detergent are not ideal for membrane sensitive

or highly fragile complexes.[120] As reviewed by Keener *et al.*,[66] there have been a number of other membrane mimetics that have been employed for native MS, including SMALPs,[121] liposomes,[122] and nanodiscs.[123] I will discuss in detail the application of nanodiscs for determining the oligomeric state of membrane proteins with native MS in Chapter 2.

1.4.2 Charge Manipulation

Charge reducing agents can be a valuable tool for native MS because they reduce charge from the surface of the analyte, which reduces electrostatic repulsions and allows for the retention of labile interactions.[124] The reduction of electrostatic forces allows for the analysis of fragile complexes with native MS that otherwise could not be captured. Native MS ionizes samples for analysis by typically using nano-electrospray ionization (nano-ESI). During ESI, a potential difference is applied between the ESI needle and the entrance of the mass spectrometer, leading to the formation of charged droplets at the tip of the needle. These charged droplets then fission off from the tip of the needle and further break down into smaller droplets, until the buffer has evaporated off the of the analyte, leaving just the charge on the surface of the analyte.[125] The charge left on the surface of the analyte can be manipulated using either charge reducing or supercharging reagents.[126]

Conversely, super charge reagent impart additional charge to the surface of the analyte.[127] Increasing the charge of the analyte can be valuable because it can reduce the *m/z* requirements of the mass analyzer. These supercharging reagents can also promote additional dissociation pathways of analytes inside the mass spectrometer.[128] Charge manipulation during ESI can provide rich information about the analyte that could not be obtained through ESI alone. I will discuss more on charge manipulation during native MS in Chapter 3.

1.5 DISSERTATION OVERVIEW

Viroporins are an attractive target for the development of potential therapeutic compounds. However, they are an underexplored area of research, primarily due to the analytical challenges associated with studying viroporins. Some of the biggest analytical challenges associated with studying viroporins is that they are very polydisperse and highly influenced by their local chemical environment. Two of the key unanswered questions related to viroporins currently are:

- What oligomers do viroporins form?
- How is oligomerization influenced by the local chemical environment?

Knowing the oligomeric state of viroporins is important because it is key to have a sense of the architecture of these channels in the development of potential therapeutic compounds.

To answer these questions, this dissertation details the development of methods for better understanding the oligomerization of viroporins in a range of chemical environments. In chapter 2, we will outline protocols for mass defect analysis applied to nanodiscs with native MS. I will describe the wide range of behaviors that we have observed of biomolecules (including membrane proteins, peptides, and amyloid proteins) oligomerizing in different lipid nanodiscs. I will also provide details on what we have learned from mass defect analysis, how to perform mass defect analysis, and how to troubleshoot some of the most seen issues and ambiguities with mass defect analysis.

Then, in chapter 3, we will explore different charge reducing agents for native MS. Charge reducing agents are valuable for native MS because of their ability to preserve fragile complexes in the gas phase, such as some viroporin oligomers. In this chapter, I performed a systematic study of imidazole derivatives that we found to not only be more charge reducing and stabilizing than

many of the existing charge reducing agents, but that these charge reducing agents were also amenable for a wide range of analytes, including soluble proteins, membrane proteins, and nanodiscs containing peptides. Additionally, in this chapter I also explored some of the chemical principles governing charge reduction during electrospray ionization, providing a basis for the development of even more effective charge reducing agents in the future.

In chapter 4, I describe performing native MS on viroporin M2 to study how changes in the local chemical environment affect its oligomerization. There are currently dozens of experimentally solved structures of M2 in the PDB, and M2 is the best characterized viroporin to date. All these structures suggest that M2 forms a tetrameric complex. However, we performed native MS on M2 in a wide range of chemical environments, including varied detergents, solution pH, and lipids, and did not find the M2 forms exclusively a tetrameric complex. Instead, we found the M2 forms a variety of oligomers that seem to be highly dependent on its local environment, which raised the question for us of whether viroporins as an entire protein class may potentially be more polydisperse than previously thought.

Building upon this initial viroporin work, in chapter 5, we went on to characterize less studied viroporins with native MS. We first investigated Vpu (from HIV). Vpu assembled into a range of oligomers and was dependent on its local environment, similar to what we saw with M2. Next, we characterized the E protein (from SARS-CoV-2) and found that it assembled into dimeric complexes and did not appear to be greatly influenced on the local environment. Finally, we explored the oligomerization of VP4, a potential viroporin from Polio. VP4, unlike any of the other viroporins previously explored, appeared to be monomeric. This suggested that the behavior of VP4 may be more complex than previously thought and may need a posttranslational modification or another protein to facilitate its channel formation.

Overall, this thesis contains the optimized methods of creating viroporins and characterizing their polydispersity in a range of chemical environments with native MS. These methods will provide an understanding of how viroporins self-assemble and are affected by different environments. Characterizing the oligomeric state and how this oligomerization is influenced by the local chemical environment will hopefully enable the development of improved therapeutics for viruses in the future.

CHAPTER 2 USING MASS DEFECTS TO STUDY OLIGOMERIZATION OF MEMBRANE PROTEINS AND PEPTIDES IN NANODISCS WITH NATIVE MASS SPECTROMETRY

2.1 INTRODUCTION: OLIGOMERIZATION OF MEMBRANE PROTEINS AND PEPTIDES

Between 30–50% of proteins are thought to form oligomers.[129] Some membrane proteins, such as the ATP-binding cassette transporter, TmrAB, form monodisperse and static complexes.[130, 131] Other proteins, such as the receptor tyrosine kinase family, have more dynamic interactions.[132-135] In a number of cases, their oligomerization is not well understood, such as with GPCRs.[136-138] Understanding this fundamental aspect of protein quaternary structure is important because the oligomeric state can have a significant effect on the activity of the protein.[139] For example, oligomerization of membrane proteins can affect crucial cellular functions, such as apoptosis, tumor formation, and signal transduction.[140] Similarly, membrane active peptides can oligomerize in bilayers, and complex formation can be critical to their antimicrobial properties.[141] However, direct measuring the oligomeric state of membrane proteins poses a variety of analytical challenges.[142]

Here, we will review our recent work studying the oligomerization of membrane proteins and peptides in lipid nanodiscs using native mass spectrometry (MS). We detail the data analysis methods, limitations of the technique, and strategies used to overcome these limitations. Finally, we will review the unique biophysical insights gained by applying these techniques to study viroporins, antimicrobial peptides, and amyloid proteins.

2.1.1 NANODISC NATIVE MS

Nanodiscs are a promising platform for the analysis of membrane proteins.[70] Nanodiscs are typically 10–13 nm bilayers, however they can be as small as 6 nm[143] and as large and 90 nm.[144] These bilayers are surrounded by a membrane scaffold protein (MSP) belt (Figure 2-1A). The lipid composition and size of nanodiscs can both be tuned to suit the needs of the analyte.[70, 71] Nanodiscs enable membrane proteins to be embedded in a soluble lipid bilayer.[145] Prior studies have suggested that embedding membrane proteins in nanodiscs can be more effective at preserving membrane protein activity than detergent micelles, likely because the nanodisc bilayer more closely mimics the natural lipid bilayer.[71, 146, 147]

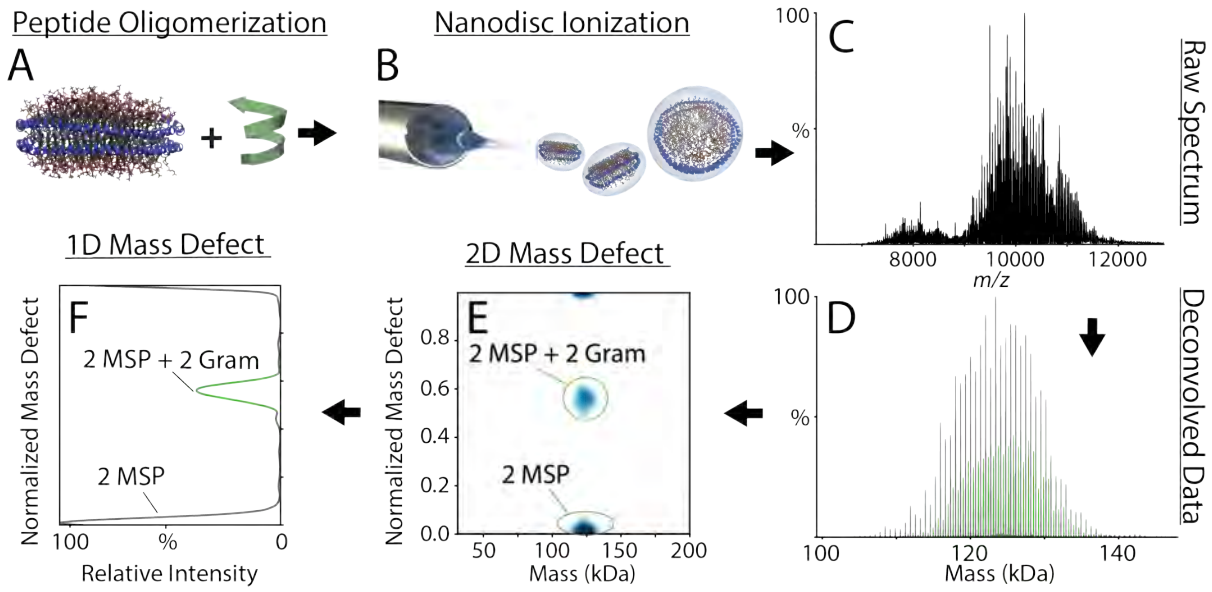

Figure 2-2: Schematic illustrating the experimental workflow for determining the number of peptides associated with a DMPC nanodisc. Gramicidin A (illustrated as green alpha helix) was directly added to nanodiscs (A) prior to electrospray ionization (B) for native mass spectrometry (C). The data was then deconvolved (D), and nanodiscs that contain only DMPC and MSPs are shown in grey. Nanodiscs that have two gramicidin peptides added are in green. Mass defects were calculated and are shown as a function of the overall mass of the nanodisc with specific signals labelled (E). The relative intensities of each species can be determined by summing the intensities of mass defects across all mass values (F).

Over the last decade, we have worked to combine the emerging technologies of native MS and nanodiscs to enable the direct, label free measurement of the stoichiometry of membrane proteins in an intact lipid bilayer. The earliest reports of coupling native MS and nanodiscs was in 2014 by Marty et al.[148] These experiments included characterizing DMPC nanodiscs with native MS and describing how to analyze the data and quantify the loss of lipids from the nanodisc in the gas-phase. Since then, this work has been built upon to use native MS to characterize much more complex lipid mixtures in nanodiscs,[149, 150] intact membrane protein-nanodisc complexes,[151] to determine the stoichiometries and lipid specificities of antimicrobial peptides,[152-154] and to elucidate the oligomerization patterns of viroporins.[155] The unique combination of native MS and nanodiscs has emerged as a valuable blend of tools for better understanding the biochemistry of membrane systems.

Native MS is gentle enough to preserve the noncovalent interactions of the entire membrane protein-nanodisc complex for mass analysis (Figure 2-1B),[123, 156, 157] which yields complex mass spectra of the intact nanodisc (Figure 2-1C). This raw data can then be deconvolved[158] to combine the multiple charge states in the *m/z* spectrum into a summed mass distribution (Figure 1D).

Nanodiscs have a series of masses due to the intrinsic heterogeneity in number of lipids per particle. For example, MSP1D1(-) nanodiscs typically contain between 140–160 1,2-dimyristoyl-*sn*-glycero-3-phosphotidylcholine (DMPC) lipids, as shown in Figure 1D.[145, 159] Because there is a polydisperse and variable number of lipids per nanodisc, it can be challenging to determine the stoichiometry of complexes embedded within the nanodisc, especially for small proteins or

peptides. If we assume that the number of lipids remains constant, it is sometimes possible to infer binding stoichiometry from global shifts in the mass, such as seeing a 12 kDa shift in mass caused by binding of three 4 kDa peptides.[160] However, membrane proteins/peptides often displace lipids upon incorporation in the nanodiscs, leading to either no global shift in mass or an uncertain number of lipids in the nanodisc.

To overcome this challenge, we developed the use macromolecular mass defect analysis to measure small shifts in mass caused by addition of proteins or peptides to the complex.[161, 162] These small shifts are independent of the total number of lipids and thus are more informative than the global mass. Here, we will present a detailed walkthrough to cover what mass defect analysis is, how mass defect analysis is performed, what it can teach us, and what we have learned from it.

2.2 MACROMOLECULAR MASS DEFECT ANALYSIS

2.2.1 WHAT IS MASS DEFECT ANALYSIS?

Mass defect analysis aids in the visualization of complex mass spectra, especially when there are regular patterns of mass differences separating the peaks.[163] Our implementation of macromolecular mass defect analysis is analogous to Kendrick mass defect analysis, which is typically used in hydrocarbon analysis.[164] Mixtures of hydrocarbons often have species within the same class of molecules (such as fatty acids) that differ only in length of the chain. To help cluster classes, classic Kendrick analysis plots the mass of each hydrocarbon species relative to a repeating methylene (CH_2) unit.[165, 166] Thus, compounds that differ by any number of additional CH_2 units but are otherwise identical, cluster together.

The Kendrick mass defect is calculated by dividing the measured mass by the reference mass, classically the mass of methylene, and taking only the remainder. This remainder is the mass

defect value, and it can be normalized between 0 and 1 or converted back into absolute mass by multiplying by the reference mass.[153, 157, 162, 164] Species that have exactly one additional methylene will have different integer quotients but the same remainder (mass defect). Kendrick analysis is usually visualized in two dimensions, and plots typically show the mass defect as the y-axis and the x-axis as either the integer quotient (the Kendrick mass number), the exact measured mass, or the Kendrick mass, which is a slightly corrected mass value. Although originally used in hydrocarbon analysis, Kendrick mass defect plots are also useful in clustering lipid species, and mass defect analysis in general has diverse applications in data interpretation.[167-169] Macromolecular mass defect is analogous to Kendrick mass defect, but it uses a molecule rather than methylene as the reference mass.

2.2.2 Mass Defect Analysis with Nanodiscs

To illustrate how macromolecular mass defect is performed and interpreted for nanodiscs, we will walk thorough an example of applying macromolecular mass defect analysis to determine the number of gramicidin A peptides embedded within an intact nanodisc (Figure 2-1).[162, 170] We use the mass of the lipid in the nanodisc as the repeating unit reference mass.

When examining an intact nanodisc by native MS, we can generally assume that all nanodiscs contain two MSP belts, except in strange and undesirable cases.[149] For example, consider nanodiscs made up of DMPC lipids and two MSP1D1(-) belts. The mass defect value of the two MSP is determined by adding the mass of the two belts together (2 × 22,044 = 44,088 Da) and dividing it by the reference mass of DMPC (678 Da). This division yields: 44,088 Da /678 Da = 65.03. Removing the integer component of 65 gives us the normalized mass defect value of 0.03.

Comparing this predicted mass defect value with the measured mass defect value (Figure 2-1E) confirms the number of MSP belts on the nanodisc.[161]

The mass defect can be expressed as unitless parameter (normalized to between 0 and 1), or it can be converted back into Da by multiplying by the reference mass (0.03 * 678 Da = 20 Da).[162] This conversion tells us that nanodiscs with 2 MSP1D1(-) belts are 20 Da heavier than the nearest multiple of the DMPC lipid mass, which would be 65 * 678 Da = 44070 Da, with slight errors from rounding. Here, we will primarily discuss normalized mass defects for simplicity.

Importantly, each additional lipid changes only the integer and not the remainder of the division, so the mass defect is independent of the number of lipids in the nanodisc and informs exclusively on the number of proteins/peptides incorporated into the nanodisc.[123] Any lipids added to the 2 MSP belts to form a nanodisc will not shift the mass defect. For example, if one lipid is added, the mass will be 44,088 + 678 = 44,766 Da. Dividing by the reference mass yields: 44,766 / 678 = 66.03. Adding a lipid increases the integer component of the division (from 65 to 66), but the mass defect (0.03) remains unchanged. This principle holds for 10, 100, or 1000 bound lipids, which would change the integer to 75, 165, and 1065, respectively, but would not change the mass defect, 0.03.

2.2.3 Calculating Mass Defects from Native Mass Spectra

The discussion above has focused on predicting mass defect values from known masses. When applied to measured data, the same process for calculating mass defect is repeated for each deconvolved mass data point. Thus, we supplement our data of mass and intensity with a third column of mass defect. There are two typical ways that the data for macromolecular mass defect analysis can be presented, as 1D and 2D plots. With the 2D plots (Figure 2-1E), the data is plotted

as the mass defect value (y-axis) versus the overall mass of the entire complex (x-axis). The 2D plots have the relative intensity of each species displayed in color as a heat map (z-axis).

With the 1D plots (Figure 2-1F), the mass defect value is plotted against the relative summed intensity from all mass data points, summing across the x-axis of the 2D plots. Ideally, each peak in the plots corresponds to a different number of oligomers associated with the nanodisc. The 1D plots more clearly reveal the global distributions of different oligomeric states, but the 2D plots preserve useful information on absolute mass that can be useful for assignments and observing shifts in the mass (discussed below). The intensities of the peaks can be extracted from the 1D and 2D plots and averaged over replicates. These average intensities can then be plotted in a grid or bar chart for different oligomeric states and under different conditions to gain insight on trends and specificities across species and lipid types (see below).

The approach described above relies on first deconvolving the data from *m/z* into mass. However, it is possible to use the phase information in a Fourier transformed *m/z* spectrum to reconstruct a macromolecular mass defect trace.[164] Although it is only currently possible to get phase information from the entire spectrum to assemble a 1D plot, it may be possible to create similar 2D plots with a Gabor transform.[171] Excitingly, there is excellent agreement between mass defect profiles measured with direct Fourier methods and with deconvolved data.[164]

2.2.4 Measuring Association of Biomolecules to Nanodiscs

Because the lipids do not affect the mass defect, the mass defect value reflects the mass of the non-lipid species incorporated into the nanodisc. Thus, after we know the mass defect shift caused by the MSP belts, we can examine additional shifts to measure association of other biomolecules. For example, by adding antimicrobial peptides (AMPs) to nanodiscs, we can

measure the stoichiometries of peptides associating with nanodiscs using mass defect analysis (Figure 2-1).[152-154] After the raw mass spectra are deconvolved, the normalized mass defect values are compared to predicted values to reveal the different stoichiometries associated with the nanodisc (Figure 2-1E and F).

For example, based on the mass of gramicidin A (GA, 1882.3 Da), we can calculate the mass defect value for each possible stoichiometry in the nanodisc (shown in Table 1). Because all nanodiscs have two MSP belts, we calculate the predicted mass defect by adding the mass of GA to the mass of the two MSP belts and dividing it by the lipid mass. For example, a DMPC nanodisc containing 4 GA peptides would be determined by: (44,088 + (1882.3 × 4)) / 678 = 76.13. The mass defect value is the remainder value of this division, so the mass defect value for 4 GA peptides in a DMPC nanodisc would be 0.13, as shown in Table 2-1.

Mass defects for oligomeric complexes can also be calculated by combing individual mass defects with a form of modular arithmetic. Addition and multiplication of mass defects follow standard arithmetic except that

Table 2-1: The expected mass defect values for gramicidin A in nanodiscs with MSP1D1(-) belts comprised of DMPG and DMPC lipids.

Stoichiometry	DMPG (667 Da)	DMPC (678 Da)
0	0.09	0.03
1	0.92	0.80
2	0.74	0.58
3	0.57	0.36
4	0.39	0.13
5	0.21	0.91
6	0.03	0.68
7	0.85	0.46
8	0.68	0.24
9	0.50	0.01
10	0.32	0.79

the integer part is subtracted (or added, as shown in the next paragraph) to normalize the mass defect between 0 and 1. Thus, mass defect arithmetic will "wrap around" to stay within the 0 to 1 window. For example, gramicidin A has a mass defect of 0.78 (1882.3 / 678 = 2.78 = 0.78) in DMPC. As shown above, 2×MSP1D1(-) has a mass defect of 0.03. Thus, a GA monomer in nanodiscs will be 0.03 + 0.78 = 0.81. Two GA in nanodiscs will be 0.03 + 2 × 0.78 = 1.59, but the integer is dropped to yield simply 0.59. Adding another GA monomer to calculate three GA in nanodiscs will yield 0.59 + 0.78 = 1.37, which wraps around again to yield 0.37. Numbers are only slightly different from Table 2-1 due to rounding.

We can use this modular wrapping for convenience in calculations. For example, we could view a mass defect of 0.78 as equivalent to –1 + 0.78 = –0.22, wrapping it down to a window of –1 to 0. Here, two GA in nanodiscs would be calculated by taking the mass defect of the monomer and subtracting 0.22: 0.81 – 0.22 = 0.59. For any negative values calculated this way, we simply need to add enough integers to get the value within 0 to 1. For example, monomeric GA in nanodiscs could be calculated by 0.03 – 0.22 = –0.19 + 1 = 0.81. In fact, we can choose any convenient window for normalized mass defects, provided it has a width of 1. It is sometimes useful to wrap to a window of –0.5 to 0.5. Thus, mass defects can be combined in useful and predictable ways.

We can compare these predicted mass defect values of each stoichiometry to measured shifts in the mass defect plots to determine the number of proteins or peptides associated with the nanodisc. In Figure 1, clear signals are observed for 0 GA (mass defect of 0.03) and 2 GA (mass defect of 0.58) per nanodisc. It is not uncommon that measured mass defect values will be slightly higher than predicted due to adduction or incomplete desolvation.

The distributions of stoichiometries provide important information on the oligomeric specificities of membrane proteins/peptides. As shown in Figure 1, there is a clear signal for 0 and 2 GA per nanodisc, but not for 1 and 3. If GA incorporated as only monomers or nonspecific complexes, it should show a roughly Poisson distribution of stoichiometries. Because only even stoichiometries are observed, this peptide incorporates preferentially in units of 2. However, the distribution of dimers is roughly Poisson, which indicates that specific higher order tetramer or hexamer complexes are not preferred under these conditions.[153] Instead, these nanodiscs likely accommodate multiple dimers that lack specific inter-dimer interactions. Examining the distributions of different species present with mass defect analysis can thus reveal specific complex formation, as described with examples below.

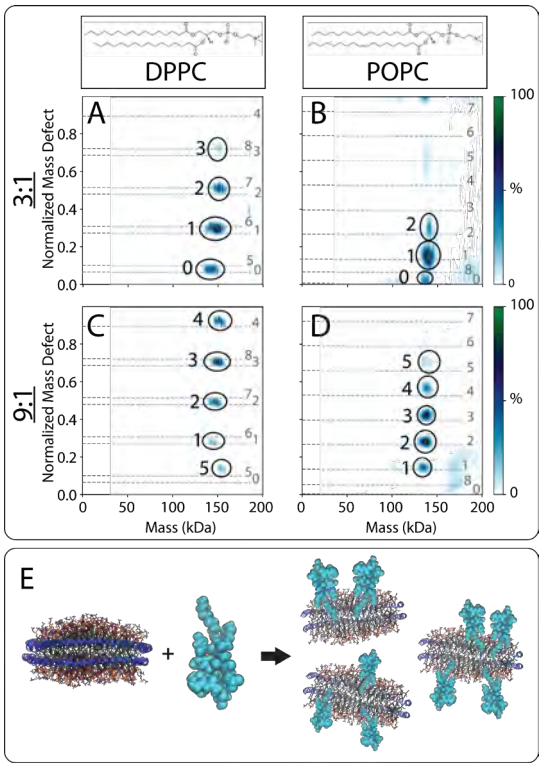

Figure 2-2: Mass defect heatmaps of daptomycin incorporated into DPPC nanodiscs (A, C) and POPC nanodiscs (B, D) at ratios of 3 daptomycin per nanodisc (A, B) and 9 daptomycin per nanodisc (C, D). The possible stoichiometries based on the mass defect values are annotated in dashed gray lines, and the assigned stoichiometries are circled in black on each heatmap (A-D). Panel E illustrates the possible incorporation of daptomycin into nanodiscs.

2.3 AMBIGUITIES AND WORK AROUNDS

Although macromolecular mass defect analysis can be a powerful technique for determining the oligomeric states of membrane proteins and peptides in nanodiscs, it also has limitations. The primary limitation is that some combinations of protein/peptide mass and lipid reference mass yield mass defect values of

different oligomers that are very similar, making it challenging to assign the stoichiometry. In the most extreme case, where the mass defect of the monomer is exactly 0, the protein/peptide mass is equal to an integer number of lipids. Thus, each oligomer would be indistinguishable from lipids or from one another, making it impossible to assign a given peak to stoichiometries from mass defect alone. Anytime when mass defects are close to 0, ambiguous overlaps will occur.

In a less extreme case, when daptomycin, a cyclic lipopeptide antibiotic,[172, 173] is added to nanodiscs made up of 1,2-dipalmitoyl-*sn*-glycero-3-phosphocholine (DPPC) lipids, there is near overlap of several stoichiometries, including the mass defects for 0 and 5, 1 and 6, 2 and 7, and 3 and 8 (shown in gray dashed lines in Figure 2-2A and 2-2C). This near overlap makes it challenging to confidently assign the stoichiometry of the peptide inside the nanodisc from a single spectrum.

For example, the mass defect for a DPPC nanodisc with one daptomycin incorporated is determined by the remainder after dividing the mass of the two MSP belts plus the one daptomycin (1,619.7 Da) by the reference mass, or (44,088 Da + 1,619.7 Da)/734 Da = 62.27. The mass defect value of 0.27 is similar to the mass defect value for six daptomycin incorporated into the same nanodisc, which is (44,088 + 1619.7*6)/734 = 73.30 or 0.30. This difference in mass defect of 0.03 corresponds to an absolute mass difference of 22 Da, which is not possible to resolve with assemblies this large and complex.

To reframe these calculations, the mass defect daptomycin alone (no MSP belts) is 1,619.7/734 = 0.207. A stoichiometry of 5 daptomycin molecules will have a mass defect of 5 × 0.207 = 0.03. Thus, any stoichiometries that differ by 5 are only 0.03 apart in mass defect, which

is impossible to distinguish in practice. In general, combinations of protein/peptide and reference masses that yield mass defects close to simple fractions (1/2, 2/3, 1/4, etc.) will be prone to overlap.

Due to these ambiguities in assignment, we cannot tell from this spectrum alone whether the distribution in Figure 2C should be assigned as sets of [0, 1, 2, 3], [5, 6, 7, 8], or some mixture of these assignment sets. However, several strategies can be used to help disambiguate these assignments.

2.3.1 Strategies for Disambiguating Mass Defect Assignments

Strategy 1: Leverage Statistics. The first strategy for disambiguation is to carefully examine the statistical distribution. If we can make assumptions about the distribution, like assuming a Poisson distribution, we can exclude assignments that do not fit the distribution. For example, in Figure 2-2A, the distribution fits a roughly Poisson distribution for [0, 1, 2, 3]. However, a distribution of [5, 6, 7, 8] is lacking key intensity for 4 that would be expected. Thus, we can infer that [0, 1, 2, 3] is the more likely assignment set. However, not all systems show obvious statistical distributions, as described below. Thus, this strategy relies on our ability to make assumptions about the statistical distribution, which often requires comparison of multiple spectra.

Strategy 2: Compare Spectra Across Different Conditions. Another useful strategy for disambiguation is to look at sets of spectra rather than an individual spectrum. For example, we can assume that distributions will shift to higher stoichiometries at higher concentrations of added peptide/protein. We can thus rule out any distributions that do not fit logically. For example, if we assign the 9:1 ratio of peptide:nanodisc in Figure 2C as [1, 2, 3, 4, 5], the more dilute peptides in Figure 2-2A at the 3:1 ratio are more likely to be [0, 1, 2, 3] than [5, 6, 7, 8]. We can also rule out stoichiometries that do not make sense considering the global ratios. For example, a larger set of

[10, 11, 12, 13] would have similar mass defect values to [0, 1, 2, 3], but it is impossible to have this larger set of stoichiometries if the global ratio is only 3:1 peptide:nanodisc.

Similarly, we have previously used collisional activation inside the mass spectrometer as a way to help disambiguate spectra.[153, 174] Collisional activation is a technique where voltages are increased inside the mass spectrometer to increase the speed that the analyte collides with inert gas molecules inside the instrument. Collisional activation can eject molecules from the nanodiscs.[157, 175] With peptide nanodiscs, we can perform collisional activation to eject some of the peptides from the nanodisc. Shifting the distribution down to lower stoichiometries with ejection has similar value as shifting the distribution up by adding more peptide. Because Poisson distributions will distort as they approach zero (described in Strategy 1), activation can help determine the stoichiometry of peptides in the nanodisc by breaking the symmetry of the distribution. However, not all systems eject efficiently and predictably with collisional activation. For example, many membrane proteins break off the MSP belt rather than eject protein subunits.[161]

Strategy 3: Look for Spectral Shifts. If we see clear shifts in the absolute mass of the nanodisc, we can use these to aid in disambiguation. For example, in Figure 2-2A and 2-2C, we can see that each additional daptomycin molecule shifts the mass slightly higher. Thus, in Figure 2-2C, the 0 and 5 state could each be populated based on the distribution (Strategy 1) and on comparisons with a broader data set (Strategy 2), but the slight increase in mass over the neighboring state with 1 incorporated suggest that 5 is more likely.

However, not all peptides show a clear mass shift upon incorporation. Many, like α-syn shown below in Figure 2-5C, do not shift the overall mass of the nanodisc upon incorporation,

likely because the same mass of lipids is displaced upon addition of the protein/peptide mass to the bilayer.[176]

Strategy 4: Change the Reference Mass. Similar to Strategy 2, a different lipid with a different reference mass can be used to disambiguate assignments.[153, 162] As shown in Figure 2-2B and 2-2D, using 1-palmitoyl-2-oleoyl-*sn*-glycero-3-phosphocholine (POPC) lipids in the nanodisc shifts the possible mass defect values so that they are no longer ambiguous. For example, with one daptomycin incorporated into a POPC nanodisc, the mass defect value is 0.41, which is determined by (44,088 Da+1619.7 Da)/760.1 Da = 60.13 for a mass defect of 0.13. This value is now considerably different from the mass defect value for six daptomycin incorporated into a DMPC nanodisc, which is 0.78. The use of different lipids can be a powerful tool for disambiguating the assignments for mass defect analysis.

One major challenge associated with using different lipids to aid in the assignment of mass defect values is that this strategy relies on the protein behaving identically in both lipid conditions. This assumption can pose issues as some proteins will take on markedly different oligomeric states in different lipid environments, as shown in Figure 2-3 and Figure 2-4.[152-155]

Strategy 5: Change the Protein/Peptide. If changing the lipid reference changes the oligomeric state distribution, the mass of the protein or peptide be changed instead. It is important that these changes result in mass shifts great enough to alter the mass defect values without perturbing the natural oligomeric state of the protein. This could be done by creating proteins that are labeled with stable isotopes, such as ^{15}N.[177] Another way that the mass of the protein could be slightly shifted is through the addition of one or two amino acids to the protein through genetic

engineering in sites that do not affect the structure or function.[161] Both methods are useful for disambiguating the oligomeric states of proteins with mass defect analysis.

2.3.2 Additional Challenges and Considerations

Another limitation of mass defect analysis is that it provides little structural information on the proteins inside of the nanodisc. Mass defect analysis can only inform on the number of proteins or peptide incorporated into the bilayer, not the orientation of these molecules (Figure 2-2E). However, mass defect analysis can be done alongside other experiments that can provide structural information on the oligomeric state and the solvent exposed regions of the protein, such as hydrogen-deuterium exchange MS or fast photochemical oxidation of protein (FPOP).[178, 179] The combination of mass defect analysis with footprinting can provide a depth of information on the structure, lipid specificities, and protein-protein interactions of membrane proteins.[180]

Another challenge in macromolecular mass defect analysis is that the mass spectra for this data can sometimes be noisy and challenging to resolve. It is important with mass defect analysis of nanodiscs that all components of the nanodisc are free of impurities and adductions. We have found that common sources of impurities are the lipids used or the membrane protein embedded within the nanodisc. These impurities can be identified more easily if there is upstream characterization of these materials prior to nanodisc assembly. We typically characterize membrane proteins with native MS in detergent prior to nanodisc assembly to confirm the purity and mass. We also create control nanodiscs with no membrane protein embedded to ensure that there are not any contaminants present in the lipids that could interfere with the mass defect analysis. For example, with pIAPP, a low-level contaminant was present in all samples that was disregarded due to its presence in the control.[181]

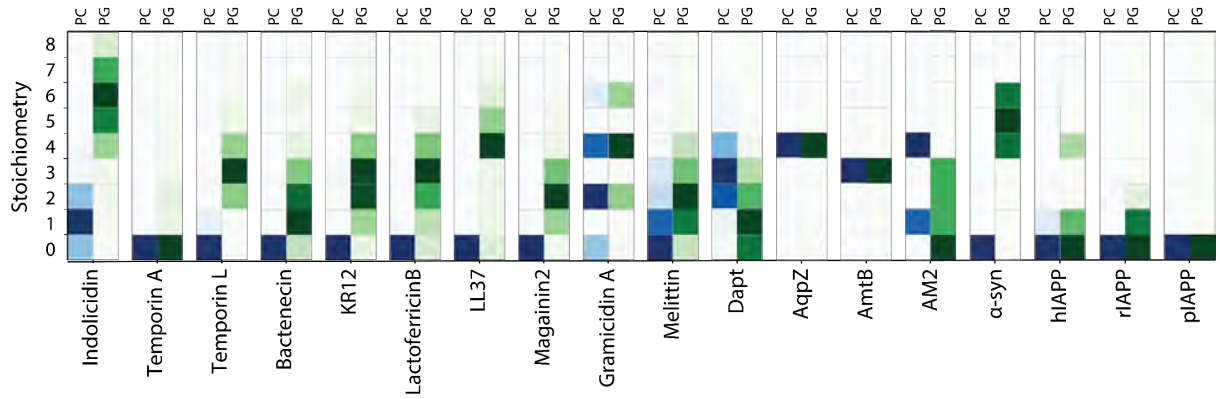

Figure 2-3: The abundances (shown by color density) of different stoichiometries of different peptides and proteins incorporated into nanodiscs made of PC (blue) and PG lipids (green), characterized with native mass spectrometry of peptide or protein-nanodisc complexes. The abundances of the proteins and peptides were obtained by averaging the extracting the normalized mass defect values for each stoichiometry. All molecules (except proteins AqpZ, AmtB, and AM2) were added at a ratio of 9:1 peptide to nanodisc.

Another challenge with mass defect analysis can be the loss of labile interactions. Although native mass spectrometry is gentle enough to preserve noncovalent interactions, fragile interactions are sometimes disrupted inside the instrument. These energy necessary for these disruptions can vary based upon the analyte. These disruptions can also affect mass defect analysis results. For example, daptomycin showed lower incorporation in 1,2-dimyristoyl-*sn*-glycero-3-phosphoglycerol (DMPG) lipid bilayers by native MS and mass defect analysis, but FPOP analysis clearly showed similar membrane association to DMPC. Our interpretation was that the interactions are relatively weak and do not survive native MS analysis.[180] Fragile interactions can be better preserved for native MS by using low concentrations of charge manipulation reagents. Previous work has revealed that charge reducing agents, such as imidazole, triethylammonium acetate, and trimethyl amine oxide, can be useful for preserving noncovalent interactions inside the mass spectrometer.[153, 182-184]

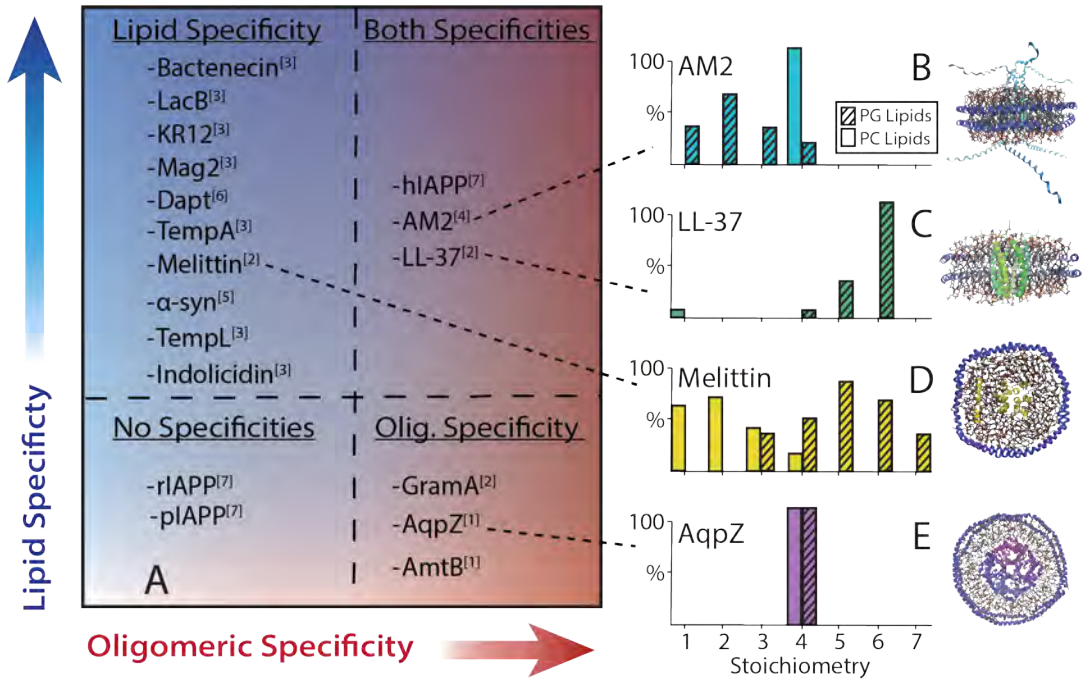

Figure 2-4: Schematic illustrating the variations in stoichiometry and lipid specificities of biomolecules characterized through mass defect analysis (A). Parts B, C, D, and E highlight some examples of different biomolecules shown. (B) AM2, a viroporin, showed high levels of oligomeric specificity in some lipids and little specificity in other lipid conditions. (C) LL-37, an AMP, only incorporated in phosphatidylglycerol (PG) nanodiscs and appeared to have some oligomeric specificity. (D) Melittin, another AMP, had no oligomeric specificity but incorporated into PG lipids at higher levels than phosphatidylcholine (PC) lipids. (E) AqpZ, a tetrameric membrane protein, had high oligomeric specificity but no lipid preferences. Superscripts next to protein/peptide name indicate reference number.

2.4 Applications of Mass Defect Analysis with Nanodiscs

Over the last several years, macromolecular mass defect analysis has been used to characterize both the oligomeric and lipid specificities of a variety of biomolecules, including AMPs, amyloid proteins, viroporins, and larger membrane protein complexes. Lipid specificity can be determined by comparing the association of proteins/peptides into nanodiscs containing different lipids. Either the total levels of association[154, 180] or the specific distributions[152] can be

compared to explore how lipid head groups and tails affect protein/peptide association with the nanodisc bilayer.

Although mass defect analysis only directly measures the stoichiometry of membrane protein/peptides associated with the nanodisc, examining the statistical distribution of stoichiometries can reveal whether the proteins associating with the nanodisc are forming specific oligomeric complexes or are simply randomly associating with the nanodisc. Proteins/peptides that interact nonspecifically with the nanodisc, either by associating as monomers or by forming nonspecific oligomeric complexes, exhibit a roughly Poisson distribution of stoichiometries that increases with higher concentrations. In contrast, proteins/peptides that form specific complexes exhibit a non-Poisson distribution, such as the GA peptide in Figure 2-1.[153] Our experiments have discovered a wide range of behaviors for these complexes, as shown in Figure 2-3 and Figure 2-4. We will begin by discussing examples of highly specific oligomeric complexes before continuing to nonspecific complexes and closing with systems that show partial specificity.

2.4.1 Specific Membrane Protein Complexes

Highly specific oligomeric complexes can show only a single oligomeric state within the nanodiscs, which we observed with several stable membrane protein complexes. These specific oligomers tend to show minimal lipid specificities, forming a single oligomer in different lipid environments. For example, the membrane protein aquaporin Z (AqpZ) had exactly four monomers per nanodisc (Figure 4E), which indicates highly specific tetramers, consistent with known structures.[185, 186] AqpZ incorporated as only tetramers in bilayers of either PC or PG lipids, demonstrating no lipid preferences.[157] Similar results were seen for AmtB, which formed monodisperse trimers in both lipid environments. Gram A, discussed above, was also largely lipid

insensitive, and although multiple dimers could incorporate into a single nanodiscs, we only saw evidence for specific dimer complexes.[153]

2.4.2 Non-specific Peptide Complexes

In contrast with highly specific membrane proteins, many antimicrobial peptides had nearly Poisson distributions that indicated nonspecific association with the nanodiscs. For example, melittin did not assemble specific complexes, as shown in Figure 2-4D.[153] However, melittin incorporated into PG bilayers at higher stoichiometries than PC bilayers, showing clear lipid specificity. The tendency of AMPs to show some preference for more anionic PG lipids over zwitterionic PC lipids but little oligomeric specificity was common across many of the AMPs studied (Figure 2-3 and Figure 2-4).[152-154] This trend may provide insight to the mechanisms of action for AMPs, suggesting that AMPs target the anionic bacterial membranes but generally do not need to form specific oligomers to have antimicrobial effects.[187, 188]

Mass defect analysis was also able to reveal the oligomeric states and lipid specificities of α-synuclein (α-syn), as shown in Figure 2-3 and Figure 2-5. We discovered that α-syn incorporated in stoichiometries up to five α-syn per nanodiscs and preferred PG lipids.[176] However, no specific α-syn oligomers were detected. Similar results were observed for rat islet amyloid polypeptide.[181]

2.4.3 More Complicated Oligomerization

Between the two extremes of highly specific and nonspecific, several systems had more complex oligomeric behaviors. Unlike most other AMPs, LL-37 tended to associate with nanodiscs with a greater degree of oligomeric specificity, associating preferentially in units of six that indicate preference for hexamer. LL-37 had significant lipid specificity and only incorporated in appreciable numbers into PG bilayers (Figure 2-3 and Figure 2-4C). Interestingly, LL-37

showed lipid tail dependence in how it assembled complexes, preferring dimer intermediates in DMPG and trimer intermediates in DPPG. Other mass spectrometry-based techniques also showed tail-dependent oligomerization of LL-37.[160] Overall, the preference of LL-37 for hexamers with dimer or trimer intermediates was unique and complex.

Another unusual example of lipid and oligomeric specificity is the case of viroporin M2 from influenza A (Figure 2-4B). In DMPG lipids, there was a roughly Poisson distribution of stoichiometries measured, ranging from one to four AM2 associated with the nanodisc. This statistical distribution of species suggests that there is likely no specific complex formation for AM2 in PG lipids. Similarly, when added to DMPC lipids, there also appeared to be a Poisson distribution of AM2 incorporation. However, when embedded in DPPC lipids, which form a thicker bilayer, AM2 only incorporated in units of four and one (Figure 2-3, 2-4B, and 2-6A). The specificity for units of four suggests that AM2 may be forming a specific tetramer complex in the DPPC lipids.[155] These differences in incorporation among lipid types suggest that bilayer thickness may affect complex formation.[189] The behavior of M2 is discussed in greater depth, along with experimental details, in Chapter 4.

These applications of mass defect analysis show the variety of behaviors that peptides and proteins exhibit when associated with nanodiscs. This wide range of behavior is illustrated in Figure 2-3 and Figure 2-4, which show most of the proteins and peptides analyzed with nanodisc mass defect analysis to date. Some proteins and peptides appear to self-assemble into highly specific oligomers regardless of the types of lipids they are surrounded with, such as AqpZ, AmtB,

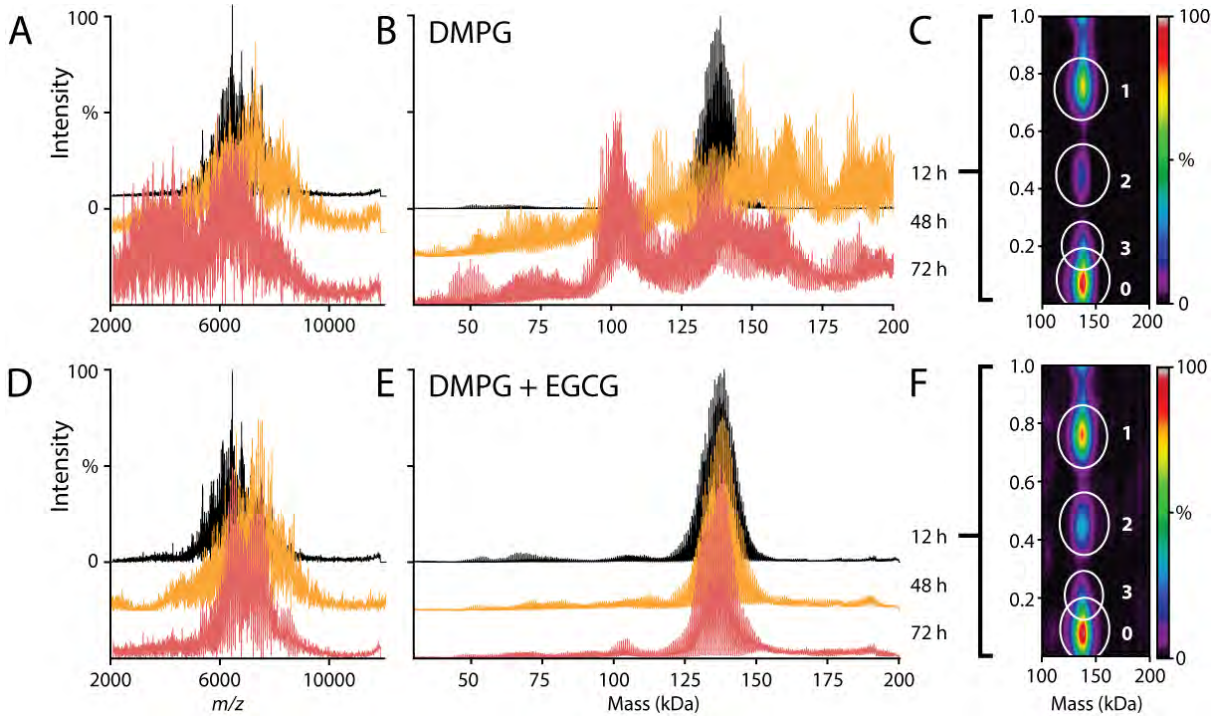

Figure 2-5: Native mass spectra of α-syn:DMPG nanodiscs that have been incubated for 12 h (black) 48 h (orange) and 72 h (red). The raw (A) and deconvolved (B) mass spectra suggest a disruption of the nanodisc by 48 h without the addition of EGCG. The 2D mass defect plot (C) indicates the association of up to 3 α-syn to the nanodisc at 12 h, prior to nanodisc disruption. With the EGCG, the raw (D) and deconvolved (E) mass spectra reveal that the nanodisc has remained intact. The 2D mass defect plot (F) shows the association of up to 3 α-syn into the nanodiscs, nearly identical to (C) without EGCG. Figure reproduced with permission from Sanders, H.M., Kostelic, M.M., Zak, C.K., and Marty, M.T. "Lipids and EGCG Affect α-Synuclein Association and Disruption of Nanodiscs**."** *Biochem*. **2022** *61* (11), 1014-1021. Copyright 2023 American Chemical Society.

and Gramicidin A. Conversely, other biomolecules exhibited little oligomeric specificity but had significant preference for certain lipid environments, such as Bactenecin and LacB. Others, like LL-37 and AM2 had more complex behaviors. Thus, mass defect analysis can be a powerful technique for characterizing the behavior of membrane-bound molecules.

2.4.4 Measuring Drug Binding and Effects

Beyond determining the stoichiometries of proteins in nanodiscs, mass defect analysis can also reveal how small molecules affect membrane interactions. For example, we used mass defect

analysis to study the influence of small molecule (−)-epigallocatechin 3-gallate (EGCG) on α-syn in nanodiscs.[176] EGCG is a flavonoid found in green teas that inhibits the formation of amyloid fibrils.[190, 191] When adding α-syn to a DMPG nanodisc for 48 h or greater, the nanodiscs were significantly disrupted, as indicated by the unresolvable spectra (Figure 2-5A and B). However, when EGCG was added in addition to the α-syn and DMPG nanodiscs, the nanodisc remained intact (Figure 2-5D and E). Interestingly, mass defect analysis revealed that, at 12 h or less, samples with and without EGCG had the same amount of α-syn associated with the nanodisc (Figure 2-5C and F). The striking similarities suggest that the addition of EGCG prevents lipid bilayer disruption in nanodiscs that contain α-syn, but it does not prevent the initial association of α-syn with the nanodisc.

Finally, mass defect can also be used to detect drug binding to membrane protein complexes in intact nanodiscs by detecting small shifts in the mass of the assembly, as discussed in Chapter 4. In DPPC nanodiscs, AM2 assembled into stoichiometries of one and four, as described above and shown in Figure 2-6A. Amantadine (AMT) specifically binds to the AM2 tetramer,[35, 192] but prior research had suggested the possibility of either one or four AMT molecules binding per tetramer complex.[193, 194] After adding 40 μM AMT to AM2 nanodiscs with DPPC lipids, we measured shifts in the mass defect heat map that corresponded to the binding of AMT to the AM2 tetramer but not the monomer (Figure 2-6B). We were also able to resolve the stoichiometry of drug binding, measuring both one and four amantadine bound to the tetrameric M2. Adding higher concentrations of AMT increased in the intensity of the tetramer with four AMT bound (Figure 2-6C). These exciting results show how mass defect analysis can be applied to characterize the relationships between the small molecules that may interact with proteins and lipid bilayers.

2.5 OUTLOOK AND FUTURE DIRECTIONS

The increasing prevalence of high-resolution mass spectrometry has enabled the analysis of increasingly heterogenous assemblies. Macromolecular mass defect analysis aids in the visualization and analysis of these complex mass spectra. There is a wide range of future applications for macromolecular mass defect analysis, including analyzing data of polymer-conjugated proteins[195] and proteins with complex glycosylation patterns.[196, 197] Here, an individual glycan unit such as a mannose can be used as the reference mass. All glycoforms that differ only in mannose units will cluster together. Similarly, the monomer mass could be used as the reference in polymer spectra to explore modifications to the chain.

Macromolecular mass defect analysis is also useful to visualize binding to oligomeric complexes. If the protein monomer mass is used as the reference mass, everything that differs only in the number of protein monomers will cluster together, giving distinct clusters for ligand or adduct binding. This approach may be powerful for characterizing drug binding to proteins and

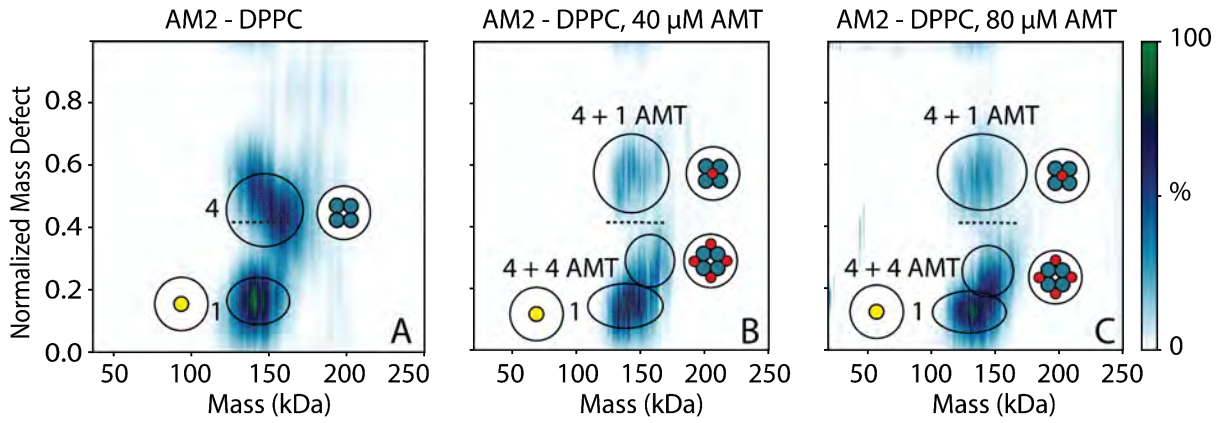

Figure 2.6: Mass defect heat maps of AM2 in DPPC nanodiscs (A) with 40 µM amantadine added (B) and 80 µM amantadine (AMT) added (C). The dashed line indicates the shift in the tetramer upon the binding of AMT. Figure adapted with permission from Townsend et al., Influenza AM2 Channel Oligomerization Is Sensitive to Its Chemical Environment. *Anal Chem.* **2021,** *93* (48): 16273-16281. Copyright 2023 American Chemical Society.

can provide information on which oligomers bind the drug. In general, macromolecular mass defect analysis can be effective for visualizing any complex spectra where it is useful to cluster things that differ by a specific reference mass.

2.6 CONCLUSIONS

Macromolecular mass defect analysis provides an effective bridge to combine the unique technologies of native mass spectrometry and nanodiscs. Mass defect analysis enables direct, label-free measurement of oligomerization of proteins and peptides in lipid nanodiscs. By combining these technologies, we can characterize the patterns of oligomeric and lipid specificities of a wide range of peptides and proteins, as well as characterizing the influence of small molecules on proteins and nanodiscs. Our hope is that this chapter provides a foundation for others to both use and interpret mass defect data, inspiring new applications to understand complex biophysical interactions. The methods reviewed in this chapter are foundational for the experiments outlined in the next three chapters.

The preprint article of this chapter can be found online at
https://chemrxiv.org/engage/chemrxiv/article-details/64406ef67be842788dec9ddf .

CHAPTER 3 IMIDAZOLE DERIVATIVES IMPROVE CHARGE REDUCTION AND STABILIZATION FOR NATIVE MASS SPECTROMETRY

3.1 INTRODUCTION

By preserving noncovalent interactions during electrospray ionization (ESI), native MS enables quantitation of protein complex stoichiometry, ligand binding, and lipid interactions.[198-201] It has been applied to a range of different complexes, including soluble proteins, viroporins, nucleic acids,[202, 203] and lipid nanoparticles.[204, 205] However, even under nondenaturing ESI conditions, labile interactions can be disrupted. Because lowering the charge of ions reduces electrostatic repulsions that drive dissociation in the gas phase, charge reduction is widely used to mitigate gas-phase dissociation and unfolding.[184, 206-211] Charge reducing reagents may also improve stability of complexes by reducing the internal energy of ions through evaporative cooling as weakly-bound adducts are released in the gas phase.[207, 212] This can be useful for preserving fragile complexes, such as viroporin oligomers, inside the mass spectrometer. In addition to improving stability, charge reduction can also aid data analysis by reducing overlap between charge states and narrowing the charge state distribution, which improves the signal-to-noise ratio.

Several approaches to charge reduction have been employed for native MS. The most commonly used method is to add charge reducing reagents to solution prior to ESI. Imidazole[207] and triethylamine (TEA)[211] are commonly used, but recent work has shown that trimethylamine oxide (TMAO) can be a potent charge reducing reagent.[213-215] However, TMAO tends to form adducts with protein complexes, which is an important component of its activity.[215]

Our prior studies have explored the effects of imidazole as a charge reducing reagent on lipoprotein nanodiscs with only lipids, with embedded membrane proteins,[151] and with incorporated transmembrane peptides.[216] TEA is less effective than imidazole for stabilizing nanodiscs, and TMAO forms adducts with nanodiscs that are not easily removed. Empty nanodiscs and nanodiscs with transmembrane peptides are significantly stabilized by imidazole, and charge reduction is essential for retaining labile lipids like cholesterol.[150] However, cholesterol nanodiscs are not fully stabilized by imidazole, indicated by the fact that more cholesterol is retained in negative ionization mode.

To find more effective charge reducing reagents, we hypothesized that a systematic study of imidazole derivatives would provide not only more effective reagents but also inform on the chemical principles governing charge reduction. We discovered that the addition of hydrocarbon substituents to the 2 position on imidazole allowed for greater charge reduction, improved signal-to-noise ratios, and resulted in cleaner spectra across a range of different systems, including a soluble protein complex, a membrane protein complex, and lipoprotein nanodiscs. We also found that these derivatives could better stabilized noncovalent interactions during native MS. To explore the chemical factors contributing to the behavior of these new charge reducing reagents, we tested their influence on solution-phase thermal stability of proteins and calculated their gas-phase basicities, proton affinities, and interaction energies with protein side chain models. Together, these results reveal not only largely explain the efficacy of these new charge reduction reagents but also provide heuristics for development of future reagents.

3.2 METHODS

3.2.1 MATERIALS AND SAMPLE PREPARATION

Imidazole and trimethylamine oxide were purchased from Arcos Organics. Ammonium acetate, Amberlite XAD-2, 4(5)-hydroxymethylimidazole, 4(5)-methylimidazole, 2-methylimidazole, 1-methylimidazole, 2-ethylimidazole, and 5-ethylimidazole were purchased from Sigma Aldrich. 2-isopropylimidazole and 2-propylimdazole were purchased from Tokyo Chemical Industry. 1,2-dimyristoyl-sn-glycero-3-phosphocholine (DMPC), 1,2-dimyristoyl-sn-glycero-3-phosphoglycerol (DMPG), and 1-palmitoyl-2-oleoyl-sn-glycero-3-phosphoethanolamine (POPE) lipids were purchased from Avanti Polar Lipids. Streptavidin was purchased from GBioscience. LL-37 was purchased from Bachem.

Stock solutions of streptavidin were prepared by dissolving it into 0.2 M ammonium acetate at 1 mg/ml. Samples were then buffer exchanged into ammonium acetate using Micro Bio-Spin Columns (Bio-Rad Laboratories Inc) to remove residual salts. From a single stock, replicate streptavidin samples were buffer exchanged and measured in triplicate.

As previously described,[151, 217] AmtB-TEV-MBP-HIS was expressed in *E. coli* and purified by immobilized metal affinity chromatography (IMAC) and size exclusion chromatography (SEC) on a Superdex 200 16/600 (GE Healthcare) with buffers containing 0.025% dodecyl-maltoside (DDM) from Anatrace. AmtB was prepared by incubating with TEV protease overnight to cleave the poly-histidine tags. The cleaved protein was then purified by reverse IMAC and detergent exchanged by SEC into 0.5% C8E4 detergent in 0.2 M ammonium acetate. Membrane protein detergent solutions were detergent exchanged and measured in triplicate. For lipid titration experiments, 2.5 mM POPE lipids were added to a solution of 50 μM AmtB containing 40 mM charge reducing reagent, diluting the charge reducing reagent to 36 mM.

MSP1D1(-) was expressed, purified, and assembled into nanodiscs as previously described.[72, 217, 218] Briefly, nanodiscs were assembled by solubilizing dried DMPC or DMPG in sodium cholate. MSP1D1(-) was added to the lipids and the sodium cholate was removed by addition of Amberlite XAD-2 beads. Nanodiscs were purified by SEC using a Superose 6 Increase 10/300 column (GE Healthcare) in 0.2 M ammonium acetate and diluted to 2.5 μM. LL-37 was dissolved in methanol to a concentration of 0.1 mM. To create peptide-nanodisc complexes, the DMPG nanodiscs were mixed 19:3 v/v with 0.1 mM LL-37 for a final concentration of 0.01 mM. Nanodisc samples were assembled and measured in triplicate.

3.2.2 Charge Reduction

Stock solutions of imidazole, TMAO, and all imidazole derivatives were dissolved in water at a concentration of 400 mM. The pH was lowered to 7 using acetic acid. Preliminary experiments with streptavidin, AmtB in C8E4, and peptide-nanodiscs optimized the concentration of charge reducing agents in each sample. For streptavidin, protein was mixed 9:1 v/v for a final concentration of 40 mM. For charge reduction of AmtB, protein was mixed with charge reducing reagent 9:1 v/v for a final concentration of 40 mM. For AmtB lipid binding experiments, protein and lipid were mixed 10:1 v/v for a final concentration of 36 mM of charge reducing reagent. Empty nanodiscs were mixed 41:1 v/v for a final concentration of 10 mM. Peptide-nanodiscs were mixed 45:1 v/v with 400 mM charge reducing reagent for a final concentration of 9 mM.

3.2.3 Mass Spectrometry

Native MS was performed as previously described.[216, 217, 219] Briefly, electrospray ionization (ESI) was performed with borosilicate needles pulled with a P-1000 micropipette puller (Sutter Instrument, Novato, CA). Mass spectrometry was performed with a Q-Exactive HF

Orbitrap mass spectrometer equipped with the Ultra-High Mass Range (UHMR) research modifications (Thermo Fisher Scientific).[220] Instrumental parameters applied to each of the samples tested included 200 °C capillary temperature, 1.1-1.5 kV capillary voltage, and resolution setting of 15,000 with 10 microscans summed into one scan. For AmtB, empty nanodiscs, and peptide-nanodiscs, an additional 50 V of source fragmentation was applied. Streptavidin scans were collected from 1,000-20,000 m/z with a trapping gas pressure of 3. The applied HCD voltage was increased from 0-200 V in 20 V increments of one minute for each voltage step. AmtB scans were collected from 2,000-30,000 m/z with a trapping gas pressure of 7. HCD voltage was increased from 0-200 V in 50 V increments for 1-minute acquisitions at each step. Peptide-nanodisc and empty nanodisc scans were collected from 2,000-25,000 m/z with a trapping gas pressure of 7. In-source trapping was increased from 0-200 V in 20 V increments of one minute for each step.

3.2.4 Mass Spectrometry Data Analysis

Native mass spectra were deconvolved using UniDec[221] and MetaUniDec.[219] The deconvolution settings for streptavidin included a mass range of 1−60 or 70 kDa, a charge range of 1−50, and a Gaussian peak FWHM of 1 m/z. A charge smooth width and point smooth width of 1.0 were also applied. The deconvolution settings for AmtB included a mass range of 5-500 kDa, a charge range of 1-30, and a Gaussian peak FWHM of 0.85 m/z. A charge smooth width and point smooth width of 1.0 were also applied. The settings for deconvolution of the nanodiscs included a mass range between 20-210 kDa and a charge range of 5-25. A Gaussian peak FWHM of 10.0 was also used. A charge smooth width and mass smooth width of 1.0 were applied with the mass of the lipid set as the mass difference. For the analysis of all spectra, a curved background subtraction of 100 was applied.

To determine the number of peptides incorporated into the nanodiscs, we used mass defect analysis[222] in MetaUniDec. Mass defect analysis involves dividing the measured mass by a reference mass. Here, the reference mass was the mass of DMPG, 667 Da. The total intensities of the mass defects were summed across all masses to determine the number of peptides incorporated into the nanodisc as previously described.[216] Any ambiguities in matching the mass defect peaks with the corresponding number of peptides were resolved using collisional dissociation experiments.

3.2.5 Nano-Differential Scanning Fluorimetry

Nano-differential scanning fluorimetry measurements were made using a NanoTemper Tycho NT.6 NanoDSF instrument as previously described.[151] Streptavidin was mixed 9:1 v/v with 400 mM charge reducing reagent for a final concentration of charge reducing reagent of 40 mM. AmtB solubilized in C8E4 detergent was mixed 9:1 v/v with 400 mM charge reducing reagent for a final concentration of charge reducing reagent of 40 mM. 10 μL of each of the samples were added to Tycho NT.6 Capillaries (Nano Temper Technologies), and the temperature was raised from 35–95 °C while measuring the ratio of fluorescence at 320 and 350 nm. The change in the ratio of fluorescence was plotted against the change in temperature to determine the melting point of each sample. All the samples were tested in triplicate.

3.2.6 Calculations

Computational modelling was performed using the University of Oregon's High-Performance Computing Cluster, Talapas. Initial structures for neutral and protonated conformers of charge stripping reagents were constructed in the molecular modelling program Avogadro v. 1.2.0 to determine the respective molecule's proton affinity and gas basicity. Proton bound dimers

of charge stripping reagents bonded to *n*-butylamine were also constructed to simulate the respective charge stripping reagent bound to a protonated lysine side chain of a protein ion. For each base, low-energy structures identified from a search of 5,000-conformers in Avogadro were optimized using the MMFF94 force field. The resulting structures were geometry optimized in Gaussian 09 (Gaussian, Inc.) first at the B3LYP/6-31G* level of theory. Output structures were then further geometry optimized and harmonic vibrational frequencies were computed using the B3LYP/6-31++G** level of theory. Enthalpies and Gibbs free energies at 298 K were calculated without rescaling of the vibrational frequencies. Proton affinities (PA) and gas-phase basicity (GB) values were computed as previously described.[151] In short, the PA and GB of a given molecule were calculated by subtracting the 298 K enthalpy or Gibbs free energy, respectively, of the protonated structure from that of the neutral structure and then correcting for the standard 298 K enthalpy or Gibbs free energy[223] of formation for a proton gas. When this method is applied to imidazole, the PA and GB are calculated to be 947.7 kJ/mol and 915.5 kJ/mol, respectively, at the B3LYP/6-31++G** level of theory. These computed values agree well with experimentally determined values reported by Hunter and Lias[224] (942.8 and 909.2 kJ/mol, respectively). 298 K enthalpies and Gibbs free energies of binding for proton-bound dimers of charge reducing reagents with *n*-butylamine were computed by adding the 298 K enthalpy or Gibbs free energy, respectively, of the protonated structure of the more basic substituent to that of the neutral structure of the other substituent. The 298 K enthalpy or Gibbs free energy of the proton bound dimer complex was then subtracted from the sum to yield the dimer enthalpy or Gibbs free energy of binding.

3.3 RESULTS AND DISCUSSION

3.3.1 CHARGE REDUCTION AND STABILIZATION OF STREPTAVIDIN

Based on prior results with trialkylamines,[225] we predicted that imidazole derivatives with added nonpolar substituents and higher gas-phase basicities would provide greater charge reduction and enhance the stability of biomolecular complexes during native MS. We first tested our hypothesis with streptavidin, a soluble tetrameric protein. Control spectra were collected for streptavidin with no additive, with imidazole, and with TMAO (Figure 3-1 A-D). Addition of imidazole significantly reduced the charge states of streptavidin compared to spectra without additives. We found that TMAO resulted in an even greater charge reduction, but only when collision voltage was applied (Figure 3-1D). TMAO spectra were poorly resolved without collision

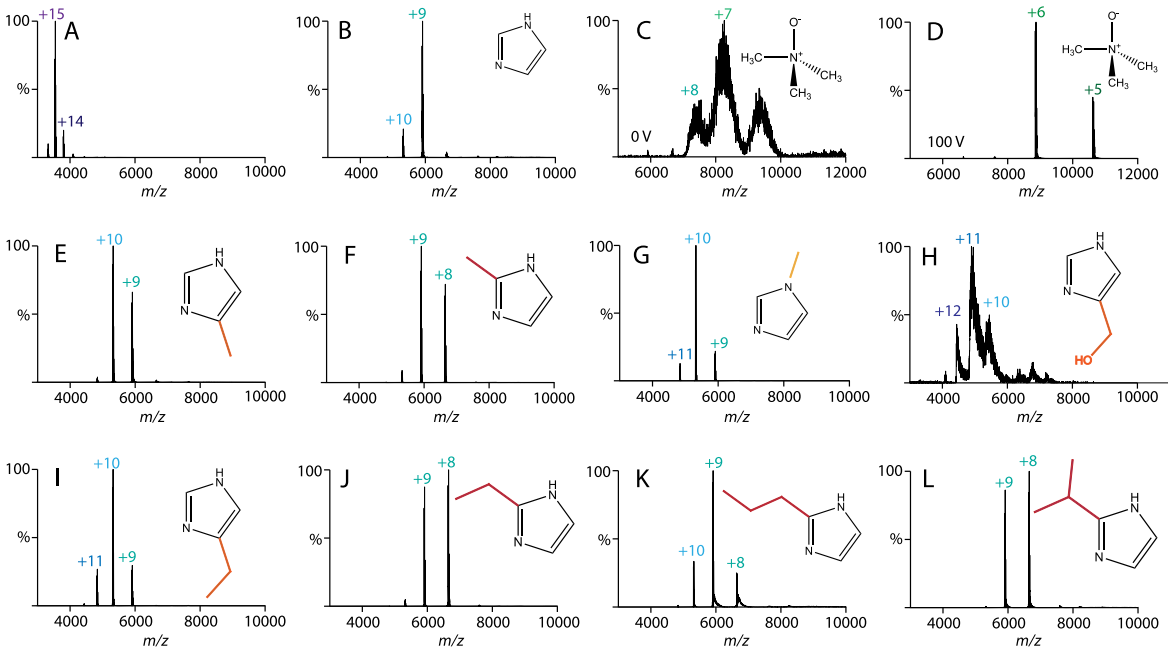

Figure 3-1 Native mass spectra of streptavidin with 40 mM of charge reducing agent added. All spectra were collected at 0 V in-source trapping collision voltage except (D), which was 100 V. Additives were (A) water, (B) imidazole, (C, D) TMAO, (E) 4(5)-methylimidazole, (F) 2-methylimidazole, (G) 1-methylimidazole, (H) 4(5)-hydroxy methylimidazole, (I) 4(5)-ethylimidazole, (J) 2-ethylimidazole, (K) 2-propylimidazole, and (L) 2-isopropylimidazole.

voltage, likely due to formation of TMAO adducts that require collisional activation to remove (Figure 3-1C).

We then monitored the effects of adding a methyl to imidazole at three different locations: 4(5)-methylimidazole, 2-methylimidazole, and 1-methylimdazole (Figure 3-1 E-G). Interestingly, 4(5)-methyl and 1-methyl derivatives were less charge reducing than imidazole, but the 2-methyl derivative was more charge reducing. Switching to a hydrophilic substituent, such as 4(5)-hydroxymethylimidazole, resulted in spectra that were poorly resolved, likely due to adduction to

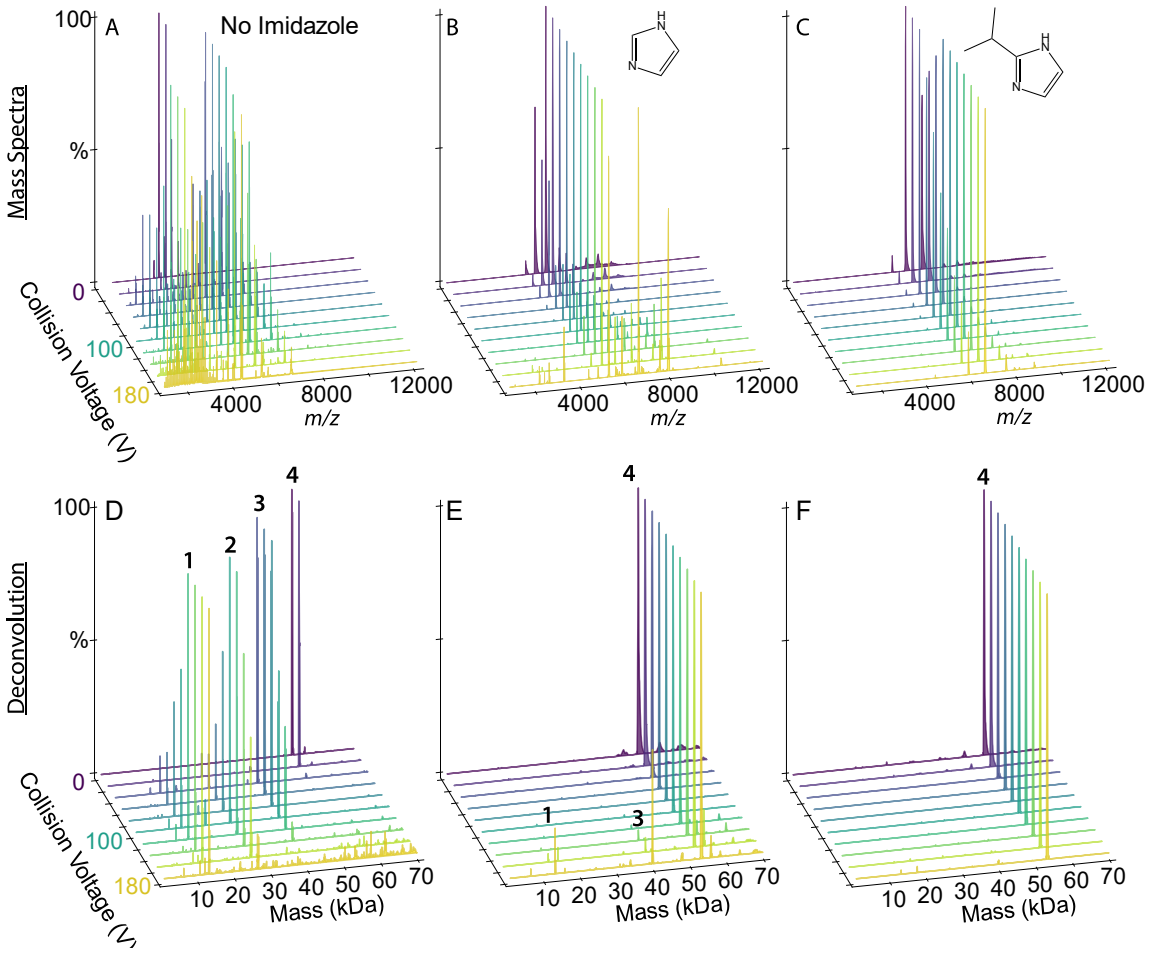

Figure 3-2 The mass spectra (A, B, C) and deconvolved mass distributions (D, E, F) of streptavidin in the presence of no additive (A, D), 40 mM imidazole (B, E), and 40 mM 2-isopropylimidazole (C, F). The in-source trapping collision voltage was increased from 0-180 V in increments of 20 V as shown by various colors.

the protein complex (Figure 2.1H). Thus, we concluded that non-polar derivatives are superior to polar derivatives.

Returning to non-polar derivatives, we next tested 5-ethylimidazole and 2-ethylimidazole (Figure 3-1I and 3-1J). Like the methyl derivatives, ethyl derivatives were more effective at the 2 position. Furthermore, 2-ethylimidazole was slightly more charge reducing than 2-methylimidazole, which suggested that longer carbon chains might be more effective. Thus, we tested 2-propylimidazole and 2-isopropylimidazole (Figure 3-1K and 3-1L). Here, the 2-propyl

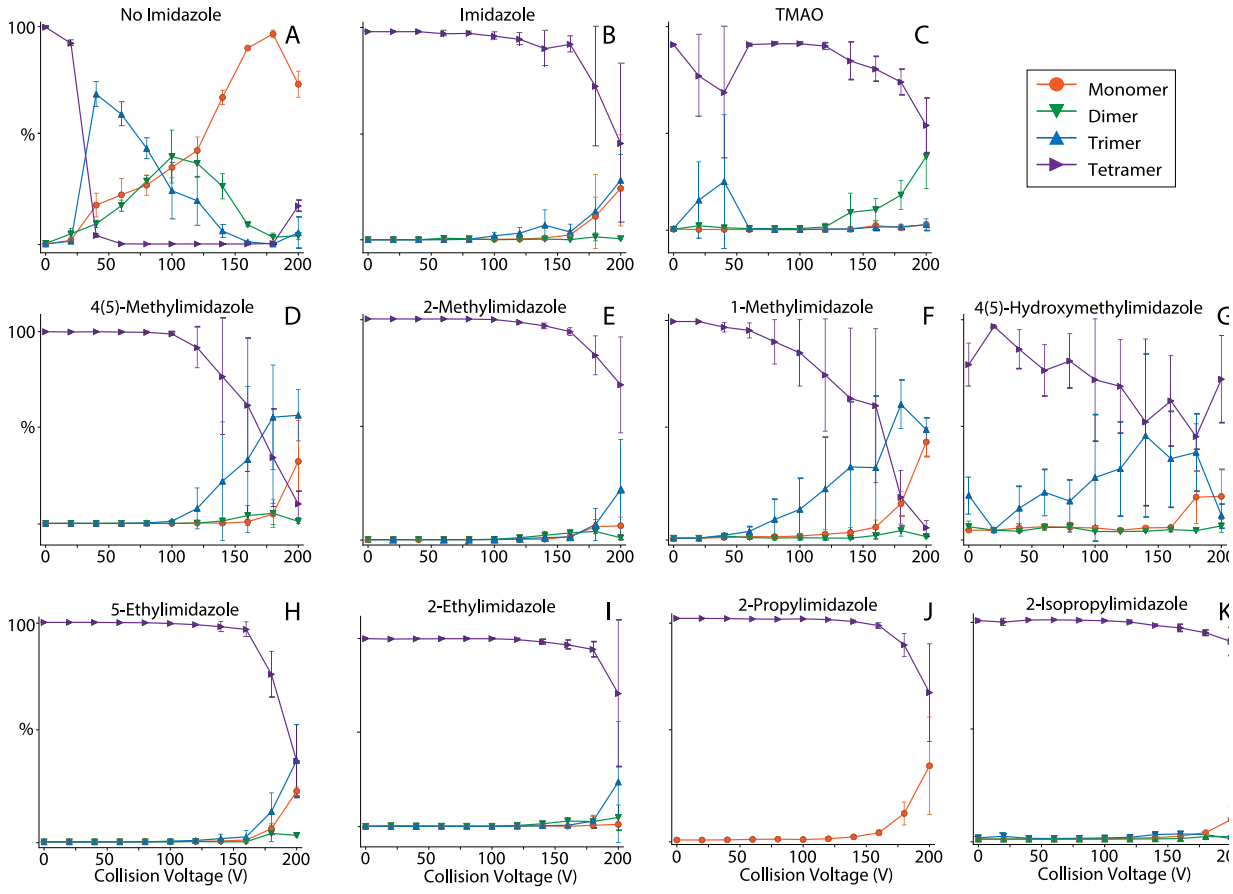

FIGURE 3-3 Streptavidin in the presence of (A) no additive or 40 mM (B) imidazole, (C) TMAO, (D) 4(5)-methylimidazole, (E) 2-methylimidazole, (F) 1-methylimidazole, (G) 4(5)-hydroxy methylimidazole, (H) 5-ethylimidazole, (I) 2-ethylimidazole, (J) 2-propylimidazole, and (K) 2-isopropylimidazole. The collision voltage was increased from 0-200 V in 20 V increments.

derivative was less effective whereas the 2-isopropyl derivative was slightly more charge reducing than the 2-ethyl derivative. Butyl and tert-butyl derivatives were not sufficiently soluble in ammonium acetate solution and were thus not explored further.

To test whether these imidazole derivatives also improved improved the overall stability of streptavidin, we performed collision induced dissociation (CID) experiments by increasing the collision voltage from 0-200 V (Figure 3-2 and 3-3). Without charge reducing reagents, we observed significant dissociation from tetramer to trimer by 40 V and mostly monomer and peptide fragments by 200 V. With added imidazole, streptavidin dissociation did not begin until around 150 V. Across the imidazole derivatives, gas-phase stability correlated with charge reduction. Interestingly, the 2-ethyl, 2-propyl, and 2-isopropyl derivatives were more stabilizing than TMAO despite having overall higher charges. This suggests that additional factors such as evaporative cooling[207, 212] contribute to the improved stability. With all the charge reducing reagents tested, we

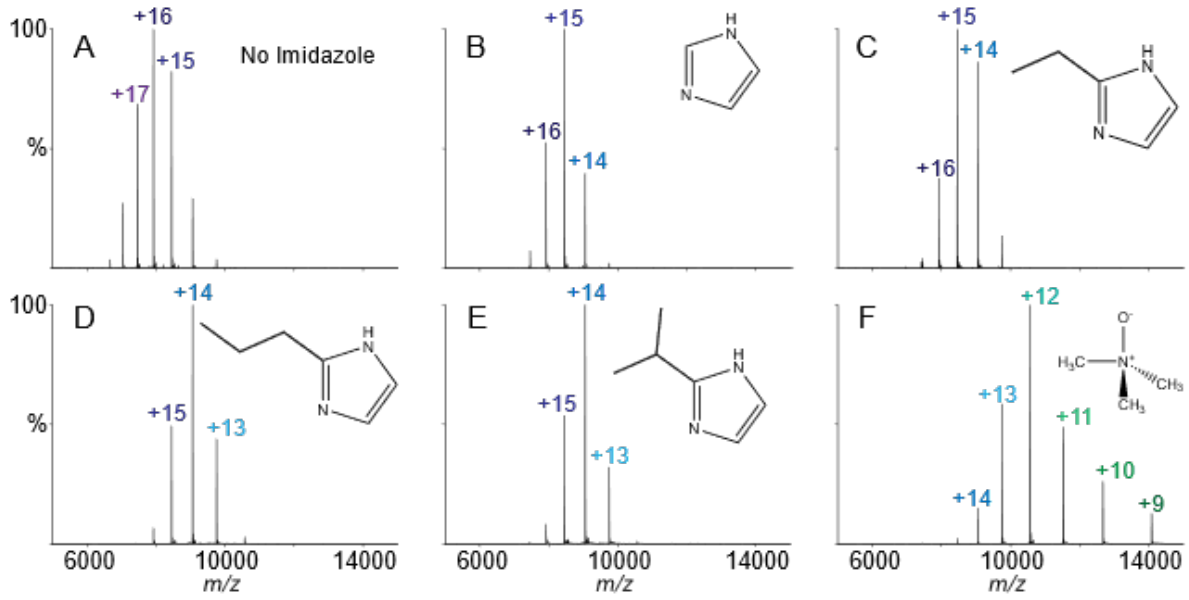

Figure 3-4 Charge states of AmtB with 40 mM charge reducing agent added. The charge reducing agents tested were (A) with water added as a control, (B) imidazole, (C) 2-ethylimidazole, (D) 2-propylimidazole, (E) 2-isopropylimidazole, and (F) TMAO.

observed fragmentation into peptides at 200 V, which is consistent with prior results with low

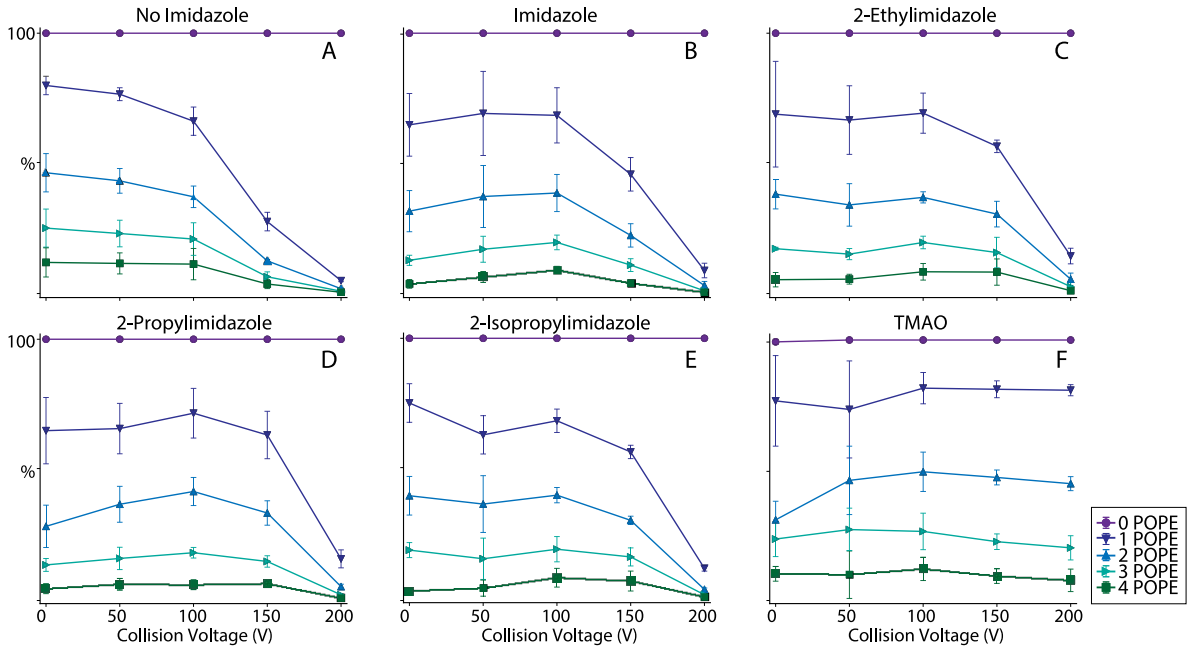

Figure 3-6 The retention of POPE lipids on AmtB in C8E4 as the collision voltage was increased from 0-200 V in 50 V increments with the addition of (A) no additive, or 40 mM of (B) imidazole, (C) 2-ethylimidazole, (D) 2-propylimidazole, (E) 2-isopropylimidazole, and (F) TMAO.

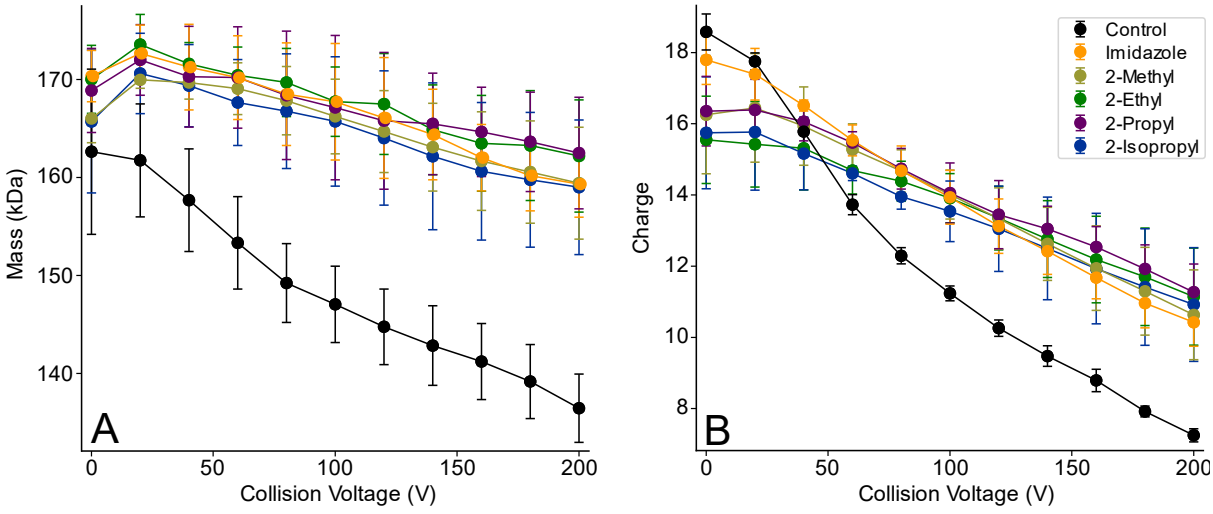

Figure 3-5 The addition of 10 mM imidazole derivatives to empty DMPC nanodiscs (A) stabilizes the average mass towards increasing collision voltage and (B) reduces the initial average charge. Water was added as a control. The collision voltage was increased from 0-200 V in 20 V increments.

charge states of TTR.[226] Comparing the laboratory collision energy[227]—defined as the applied collision voltage times the average charge state—revealed that the stability enhancements were not simply the result of lower effective collision energy. Overall, the addition of 2 or 3 carbon alkyl substituents at the 2 position of imidazole reduced the charge and improved the stability of streptavidin for native MS.

3.3.2 Charge Reduction and Lipid Retention with AmtB

Using the imidazole derivatives that were effective with streptavidin, we next tested their effects on AmtB, a membrane protein trimer, in C8E4 detergent. AmtB with no additive, with imidazole, and with TMAO were compared as controls. Because C8E4 is known to be charge

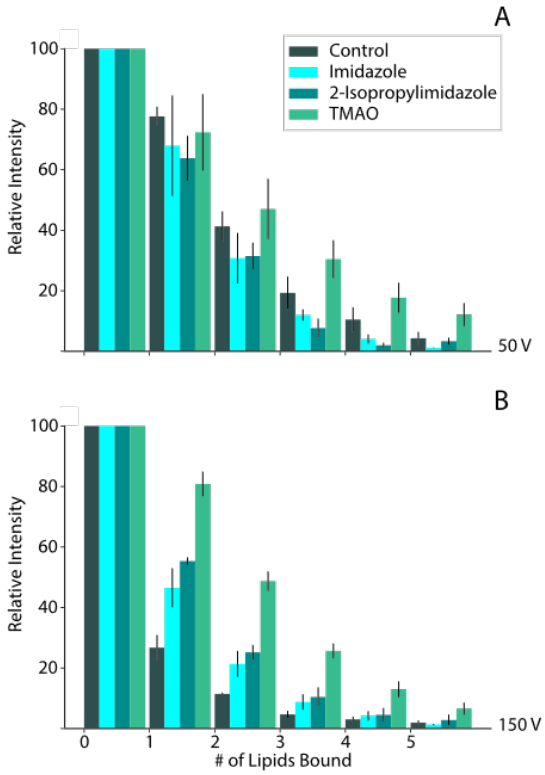

Figure 3-7 The binding of POPE lipids under A) 50 V and B) 150 V collisional activation in the presence of no additive or 40 mM imidazole, 2-isopropylimidazole, and TMAO.

reducing,[114] addition of imidazole had less of a charge reduction effect for AmtB than for streptavidin (Figure 3-4A and 3-4B).

Like streptavidin, we discovered that imidazole derivatives with the longer hydrocarbon substituents were more charge reducing for AmtB (Figure 3-4 C–E). For example, the predominant charge state was +15 with imidazole, but the predominant charge state was +14 for both 2-propylimidazole and 2-isopropylimidazole. Adding TMAO produced the lowest charge state but created a wider charge state distribution (Figure 3.4F), which has the potential to reduce the signal to-noise ratio. Because collisional activation is needed to remove detergents from AmtB, we did not observe any TMAO adducts on AmtB. Overall, the most charge reducing imidazole derivatives for AmtB were 2-propylimidazole and 2-isopropylimidazole.

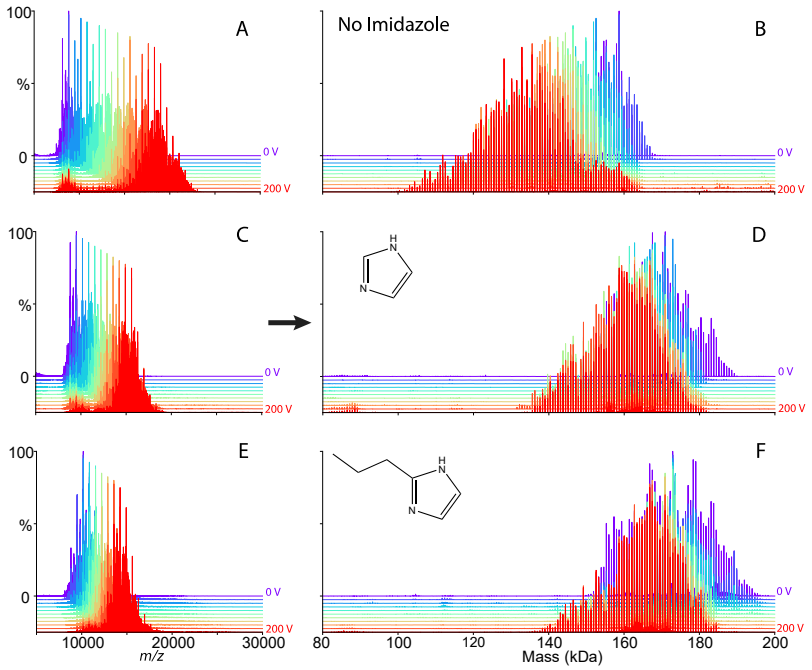

Figure 3-8 The effect of the addition of 10 mM charge reducing agent on the average (A) mass and (B) charge of empty DMPG nanodiscs with increasing collisional voltage. The collision voltage was increased from 0-200 V in 50 V increments.

To evaluate how imidazole derivatives impacted stability of lipid bound AmtB, we added POPE at a final concentration of 0.21 mM. We then performed CID from 0-200 V in 50 V steps. There were only minor differences in initial lipid binding, but we found that the presence of imidazole and imidazole derivatives stabilized bound lipids at higher collision voltages, as shown in Figure 3-5 and 3-6. Although TMAO was more stabilizing in this case, imidazole derivatives were as effective as imidazole at stabilizing membrane protein-lipid complexes.

3.3.3 Charge Reduction on Nanodisc-Peptide Complexes

Finally, we tested the most promising imidazole derivatives on lipoprotein nanodiscs. Prior research has shown that imidazole is charge reducing and stabilizing for "empty" nanodiscs with both zwitterionic and anionic embedded lipids.[151] We first tested DMPC nanodiscs, which eject lipids under increasing collisional activation.[228] Although imidazole has a clear charge reduction and

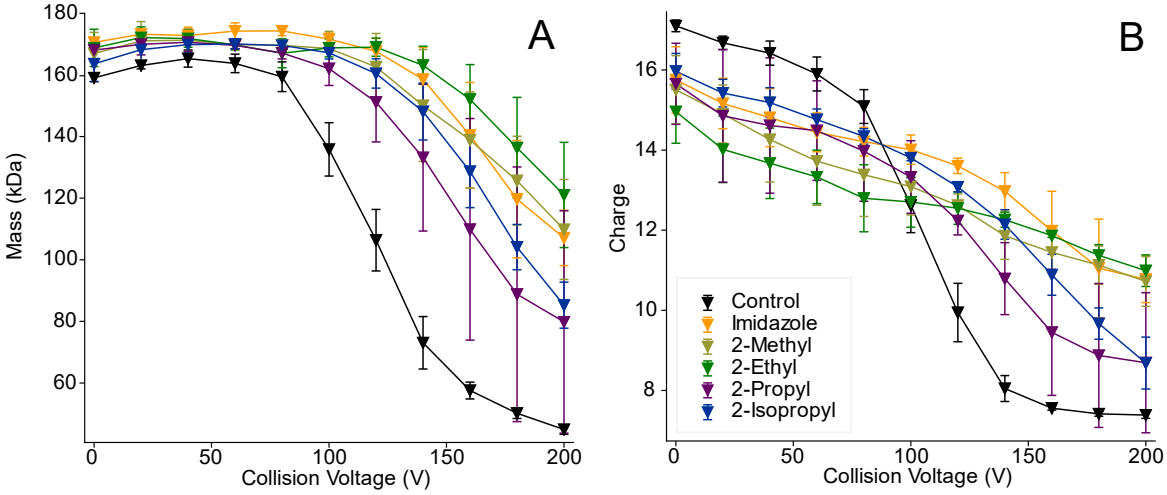

Figure 3-9 The effect of the addition of 10 mM charge reducing agent on the average (A) mass and (B) charge of empty DMPG nanodiscs with increasing collisional voltage. The collision voltage was increased from 0-200 V in 50 V increments.

stabilizing effect on DMPC nanodiscs, 2-methyl, 2-ethyl, 2-propyl, and 2-isopropyl derivatives showed only minor differences from imidazole (Figure 3-7 and 3-8). Similar results were observed for empty DMPG nanodiscs (Figure 3-9 and 3-10). Thus, although these imidazole derivatives are useful for stabilizing empty nanodiscs for ESI, they are not significantly better than conventional imidazole.

However, significant differences were observed upon addition of an antimicrobial peptide to nanodiscs. We previously found that imidazole stabilizes peptide-nanodisc complexes and allows for the detection of higher stoichiometries of peptides in nanodiscs.[216] To test whether imidazole derivatives would further stabilize peptide-nanodisc complexes, we added LL-37, an

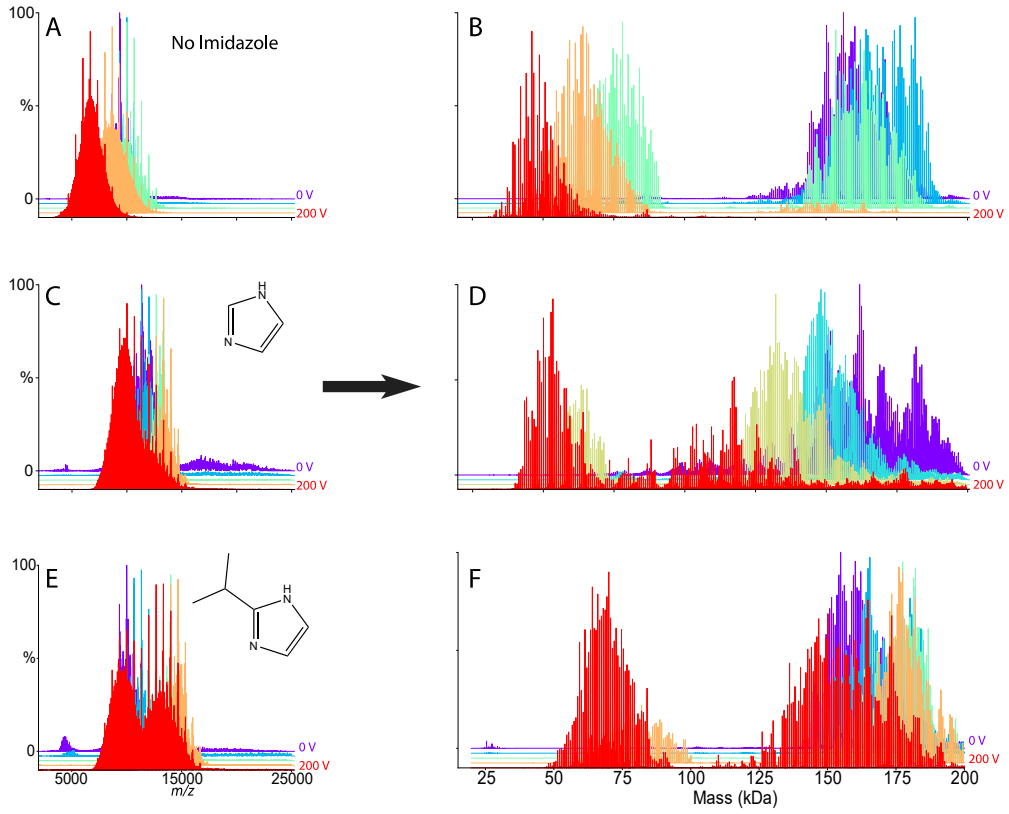

Figure 3-10 The mass spectra (A, C, E) and deconvolved mass distributions (B, D, F) of empty DMPG nanodiscs in the presence of (A, B) no additive, or 10 mM (C, D) imidazole and (E, F) 2-isopropylimidazole. The collision voltage was increased from 0-200 V in increments of 50 V.

antimicrobial peptide, at a 6/1 molar ratio with DMPG nanodiscs. As a control, we collected spectra with no additive, imidazole, and TMAO. There was poor signal intensity and unresolvable spectra when TMAO was added to nanodisc samples.

Adding imidazole increased the average number of incorporated peptides from 2.17±0.07 with controls to 2.80±0.08 (Figure 3-11). 2-methylimidazole did not significantly increase the average number of peptides and caused a wider standard deviation between replicate samples. In contrast, 2-ethyl, 2-propyl, and 2-isopropyl all significantly increased the average number of

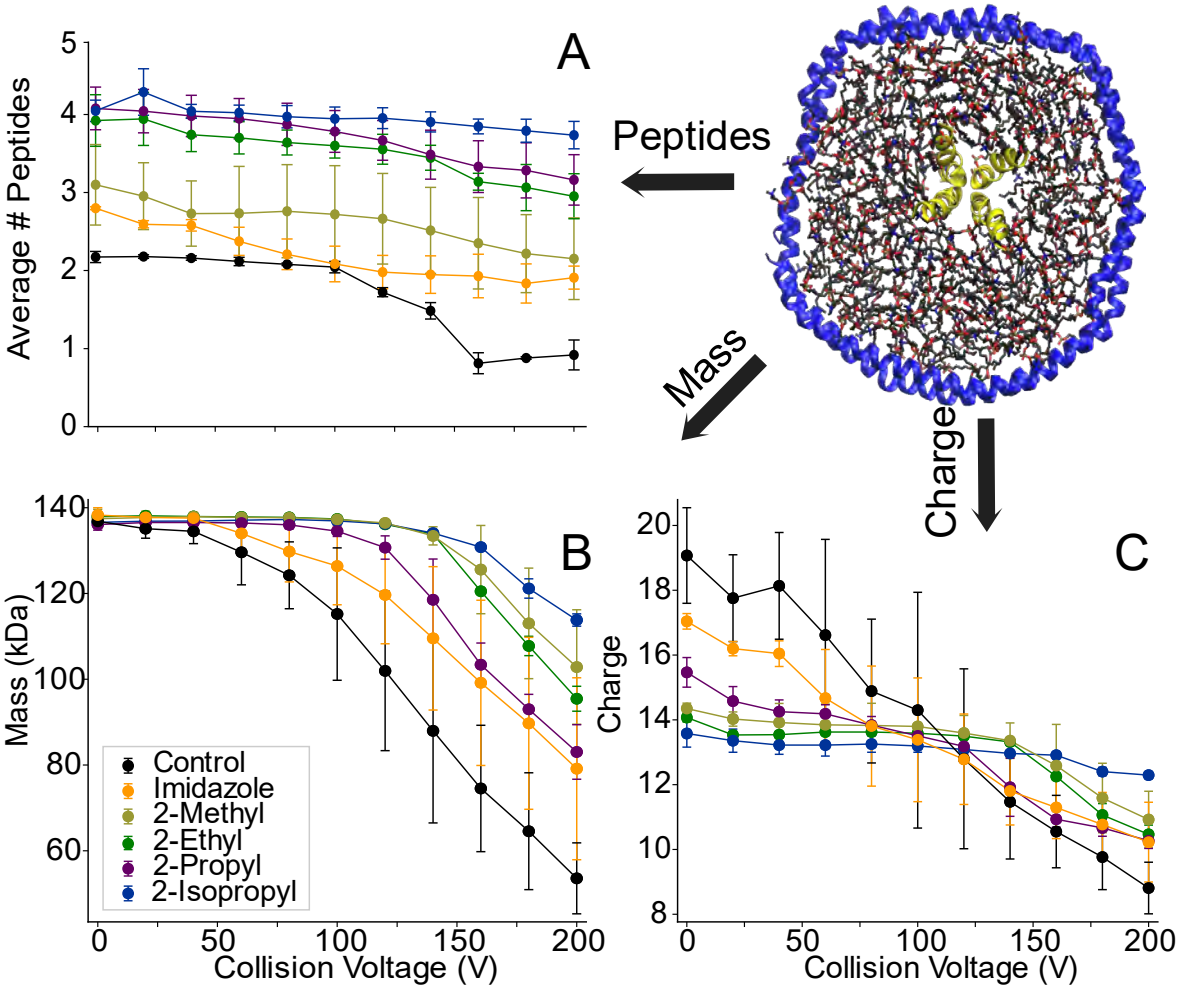

Figure 3-11 (A) The average number of peptides incorporated, (B) average mass, and (C) average charge of DMPG nanodiscs with 6/1 LL-37 and different charge reducing agents added. The collision voltage was increased from 0-200 V in 20 V increments.

peptides incorporated to around 4. Thus, imidazole derivatives improve retention of labile peptides and provide more accurate quantitation of the stoichiometry of peptides associated with nanodiscs.

To investigate the effects of imidazole derivatives on the stability of peptide-nanodisc complexes, we performed CID and monitored the average number of peptides incorporated, the average mass of the entire nanodisc complex, and the average charge (Figure 3-11). Deconvolved mass distributions are also shown in Figure 3-12. Without charge reducing reagents, there was a substantial loss of peptides, mass, and charge at increasing CID. Some degree of stabilization was observed with imidazole, but imidazole derivatives were more stabilizing towards peptide and average mass loss and showed lower charge states. Interestingly, stability of mass is not always correlated with stability of peptide incorporation. For example, the 2-propyl derivative was

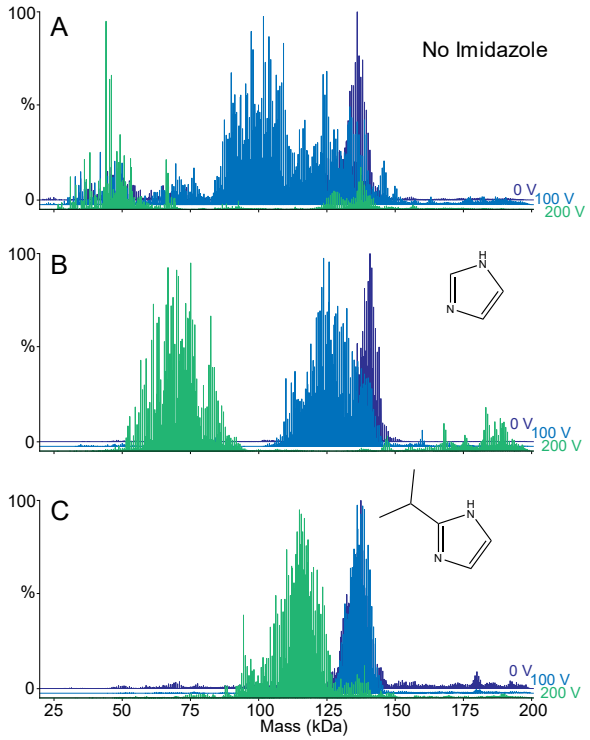

Figure 3-12 Mass spectra of DMPG nanodiscs and 6/1 ratio of LL-37 in the presence of (A) no additive, (B) 9 mM imidazole, and (C) 9 mM 2-isopropylimidazole. The collision voltage was increased from 0-200 V in increments of 100 V.

significantly more stabilizing towards peptide loss than the 2-methyl derivative but less stabilizing towards overall mass loss. This could be due to different reagents shifting the competition between dissociation of lipids and dissociation of peptides. It could also be due to interactions of the more hydrophobic derivatives with the lipid bilayer that alter dissociation pathways. In any case, the 2-isopropyl derivative was the most stabilizing across all three measures of dissociation. Thus, 2-isopropylimidazole provides an improved reagent for native MS of nanodisc complexes with embedded antimicrobial peptides.

3.3.4 Mechanisms of Improved Charge Reduction

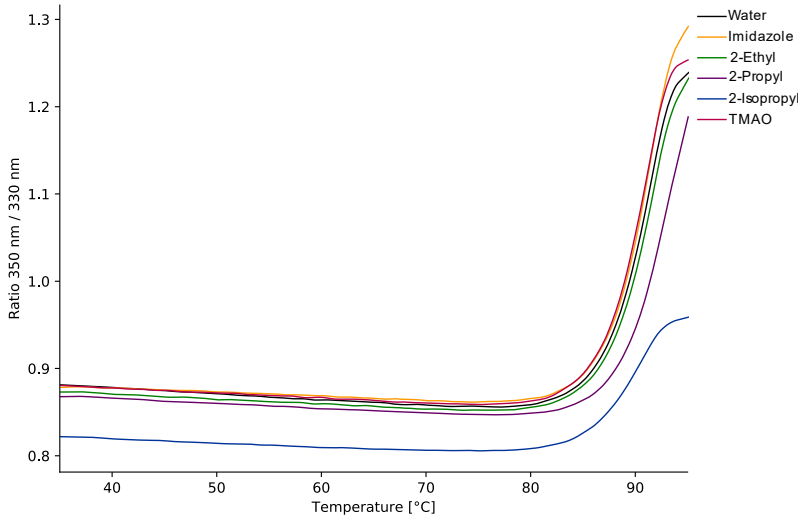

Figure 3-13 A representative nanoDSF data set of the three thermostability experiments for streptavidin. The charge reducing reagents were added at a concentration of 40 mM.

To understand why the imidazole derivatives were superior charge reducing reagents, we first sought to rule out solution-phase effects. Thus, we tested the thermal stability of streptavidin, AmtB, and empty nanodiscs by nano-differential scanning fluorimetry (DSF).[151] Addition of imidazole, TMAO, and imidazole derivatives generally did not significantly influence the melting temperature (Figure 3-13 and Table 3-2). Thus, we do not expect that solution-phase stability is

Table 2.1 The average unfolding temperatures, Tm (°C), for NanoDSF experiments with streptavidin, AmtB, and empty DMPC nanodiscs in the presence of charge reducing reagents. Each sample was measured with each of the charge reducing reagents in triplicate. The unfolding temperature for streptavidin in the presence of 2-propylimidazole was not detected because it was above of the upper limit of detection

Reagent	**Streptavidin**	**AmtB**	**Nanodiscs**
Water	91.05±0.03	76.85±0.15	79.40±1.13
Imidazole	91.15±0.04	76.94±0.01	73.34±0.84
2-Ethylimidazole	91.27±0.04	76.98±0.07	75.17±0.92
2-Propylimidazole	ND	76.53±0.16	74.53±0.78
2-Isopropylimidazole	90.40±0.20	76.34±0.25	77.37±1.37
TMAO	90.64±0.11	76.90±0.05	80.12±3.85

affected by these reagents. Imidazole is often used in protein purification and likely has only minor influences on protein activity and interactions in most cases. However, we cannot rule out that imidazole derivatives might interact with the protein in some cases, particularly with the more hydrophobic reagents.

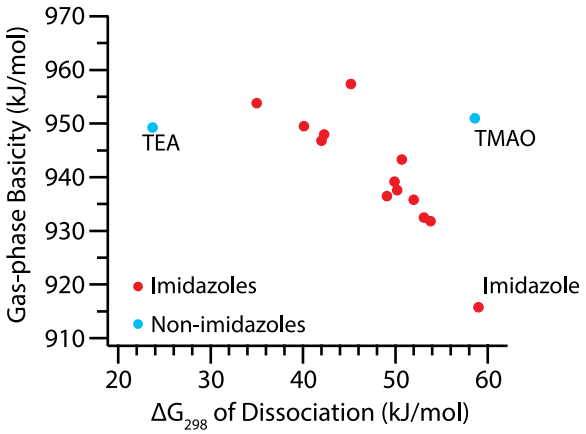

Figure 3-14 A comparison of computed gas-phase basicities against the ΔG_{298} of dissociation for proton-bound dimer with *n*-butylamine. Imidazole and its derivatives are shown in *red*. TMAO and TEA are shown in *blue*.

We next considered the gas-phase interactions of the different derivatives with protons and

Table 2.3 Calculated ΔG_{298} of dissociation for proton-bound dimer with *n*-butylamine, proton affinity (PA), and gas-phase basicity (GB) values for different charge reduction reagents. All values are reported in kJ/mol. PA and GB values reported in parentheses are experimental values from Hunter and Lias, 1998. Our values are systematically higher than those from Hunter and Lias, due to the difficulty of establishing an accurate experimental anchor value for PA/GB measurements as well as computational error, thus we expect the computed differences in PA/GB between different bases are more reliable than their absolute values. Dimer dissociation energies were not computed for *n*-butylamine and methylguanidine.

Reagent	**ΔG_{298} Diss.**	**PA**	**GB**
imidazole	59.0	947.8 (942.8)	915.5 (909.2)
1-methylimidazole	52.0	968.2 (959.6)	935.5 (927.7)
2-methylimidazole	50.2	973.0 (963.4)	937.3 (929.6)
4-methylimidazole	53.1	964.4 (952.8)	932.2 (920.9)
4-hydroxymethylimidazole	53.8	963.8	931.5
1-ethylimidazole	50.7	975.1	943.0
2-ethylimidazole	49.9	978.3	938.9
4-ethylimidazole	49.1	967.8	936.2
2-propylimidazole	42.3	979.6	947.7
1-isopropylimidazole	40.1	981.6	949.2
2-isopropylimidazole	42.0	979.9	946.5
1-*t*-butylimidazole	45.2	989.6	957.1
2-*t*-butylimidazole	35.0	984.5	953.5
TMAO	58.4	980.5	950.7
TEA	22.0	981.5 (981.8)	949.0 (951.)
n-butylamine	--	923.0 (921.5)	891.6 (886.6)
methylguanidine	--	1012.6	982.2

with model side chains. Our hypothesis was that more effective charge reducing reagents would show stronger interactions with protons but weaker interactions with proteins. Gas-phase basicity (as measured by PA, negative ΔH of protonation, or GB, negative ΔG of protonation) has been shown to correlate with the degree of charge reduction for other reagents and to be an important factor in gas-phase ion structure.[209, 211, 225, 229-231]

Experimental GB values are not available for many of the reagents studied here, so we used *ab initio* computations to determine them, as well as the PA and GB of models of lysine and arginine side chains (*n*-butylamine and methylguanidine, respectively). Computational results for PA and GB affinity are summarized in Figure 3-14 and Table 2-3. Because GB showed nearly identical trends to PA, we focus the discussion on PA. All charge reducing reagents were found to be less basic in the gas phase than methylguanidine but more basic than *n*-butylamine, indicating that these reagents likely will not deprotonate arginine side chains upon dissociation but should be able to deprotonate many lysines, histidines, and other less basic groups on the protein, thereby reducing the charge.

Imidazole derivatives showed higher PA values with larger alkyl substituents. Thus, the trend of increased charge reduction with increasing alkyl chain length can be partially explained by increasing PA. Derivatives in the 4 position had lower PA than those in the 1 or 2 position, in line with the observed lower efficacy of 4-subsituted reagents at charge reduction. Derivatives in the 2 position had similar GB values to derivatives in the 1 position, indicating that factors not well-described by these computations, such as sterics, likely play a role in the observed differences between 1- and 2-substituted isomers in the experiments. A notable exception to the strong correlation between PA and ability reduce charge was unsubstituted imidazole, which had a much lower calculated PA than the other imidazole derivatives (though still higher than *n*-butylamine)

despite its excellent charge reduction capabilities. TEA and TMAO have similar PA values to one another and to propyl and isopropyl imidazole derivatives but have very different charge reducing effects, indicating that factors beyond basicity contribute to charge reduction efficacy.

To understand why some charge reducing reagents are more prone to adduction during ESI, we computed dissociation energies of proton-bound heterodimers formed between each charge reducing reagent and *n*-butylamine, a model of the lysine side chain. For imidazole derivatives, heterodimer dissociation energies were generally found to decrease with increasing alkyl chain length due to an increasing difference between the PA of the charge reducing reagent and that of *n*-butylamine. Thus, higher PA values led to derivatives that are easier to dissociate and hence less prone to adduction to lysines and other basic protein side chains. Interestingly, despite having a high PA, TMAO has an especially high dimerization energy with *n*-butylamine. This can be explained by the large charge rearrangement in the polar N-O bond that occurs upon dimerization with lysine and which does not occur for the other bases studied, including TEA. This result is consistent with TMAO's tendency to remain adducted to positively charge biomolecular ions under low-activation conditions (Figure 3-1C).[214, 215] In contrast, TEA has a similar PA to TMAO, but TEA undergoes little change in C-N bond polarity upon dimerization with *n*-butylamine, resulting in a relatively low dimerization energy as compared to TEA or the imidazole derivatives studied. This result is consistent with TEA's low tendency toward adduction. As for the calculated PA/GB results discussed above, unsubstituted imidazole is an exception, with a relatively high computed proton-bound dimerization energy (ΔG of 59 kJ/mol at 298 K), even higher than TMAO (57 kJ/mol), but it does not show adduction like TMAO. 4-hydroxymethylimidazole shows much higher adduction but similar dimerization energies to other

methyl derivatives, likely because our calculations do not fully reflect the contributions of the hydroxyl interacting with other hydrogen-bonding sites on the protein.

Comparing computations with experimental results, imidazole derivatives with higher computed PA/GB values and lower shared-proton dimer binding energies with *n*-butylamine are generally more effective at charge reduction while avoiding adduction. Based on the experimental data presented above and these computational data, we conclude that the following factors are helpful in optimizing ESI charge-reducing reagents for protonated biomolecular ions: 1) the reagent should have a high PA/GB; 2) it should have a low proton-bound dimer dissociation energy with *n*-butylamine; and 3) other chemical properties, such as solubility in the electrospray solvent, volatility, and strength of interactions with the analyte, should be taken into consideration as appropriate.

3.4 CONCLUSIONS

We have shown that the imidazole derivatives with alkyl substituents, particularly isopropyl, in the 2 position can provide superior charge reduction and stability for a range of different biomolecular complexes, including a soluble protein, a membrane protein in detergent, and lipoprotein nanodiscs with embedded transmembrane peptides. Given their superior performance and ease of use, we expect that these reagents will have wide-ranging impacts in native MS analysis. These improvements are largely explained by increases in computed gas-phase basicity/proton affinity and decreases in proton-shared heterodimer energies between imidazole derivatives and lysine side chains, which reveal opportunities for future development of charge reduction reagents with even more potent effects.

CHAPTER 4 INFLUENZA A M2 CHANNEL OLIGOMERIZATION IS SENSITIVE TO ITS CHEMICAL ENVIRONMENT

4.1 INTRODUCTION

As discussed in Section 1.2, viroporins are a class of small transmembrane proteins that oligomerize to form channels in membranes.[22] Found in a range of different viruses, they are involved at multiples stages of infection, including uncoating, replication, assembly, and budding[232, 233] Matrix protein 2 from influenza A (AM2) is a multifunctional viroporin and a clinically approved drug target for amantadine and rimantadine.[233-235] AM2 is made up of three regions, the extracellular domain, the transmembrane (TM) domain, and the cytosolic tail (Figure 4-1A). The 20-residue single-pass TM domain of AM2 is necessary and sufficient for oligomerization and formation of a pH-mediated ion channel.[31, 233, 236] There are several dozen X-ray or NMR structures of the AM2 TM domain in a variety of membrane mimetics, all depicting monodisperse homotetramers.[237-240] Despite the uniform oligomeric state, there are significant differences among many of the AM2 structures, and the membrane mimetic used to solubilize AM2 can have major influences on its structure.[238, 241] However, traditional structural biology techniques are limited in their ability to study oligomeric polydispersity, so these existing structures may not capture the full range of possible states. Indeed, earlier fluorescence resonance energy transfer studies suggested that the dimer might be the minimal proton-conducting unit for the full-length AM2 in cells.[242]

For conventional native MS of membrane proteins, the entire protein-micelle complex is ionized with electrospray ionization (ESI).[66] The detergent adducts are then removed from the protein using collision induced dissociation (CID), and the mass of the bare membrane protein

complex reveals the protein stoichiometry and noncovalent ligands that remain bound (Figure 4.1). Other membrane mimetics, such as nanodiscs, allow membrane proteins to be solubilized in lipid bilayers during native MS.[66, 123, 243] Thus, native MS provides rich information and can capture the polydispersity of membrane proteins in different lipid and detergent environments.

Here, we performed native MS on both the full-length and TM AM2 in detergents and nanodiscs. Based upon the existing structures, we predicted that AM2 would form robust tetramers. However, we discovered that AM2 assembled into a range of oligomeric states from dimer to hexamer. Further investigation showed that the oligomeric state of AM2 was influenced by the membrane environment, solution pH, and drug binding. Together, these results reveal that AM2 could be more polydisperse than previously suggested and more sensitive to its chemical environment.

4.2 MATERIALS AND METHODS

4.2.1 Preparation of AM2 in Different Detergents and pH

Full-length AM2 was expressed and purified as previously described, and details are provided in the Supporting Information. Purity was confirmed by SDS-PAGE and native MS, which both showed no detectable contaminants. Protein activity was confirmed with proton flux assays with POPC liposomes (Figure 4-23). A series of ammonium acetate solutions were first adjusted to pH 4, 5, 6, 7, 8, and 9 with acetic acid or ammonium hydroxide. All detergents were purchased from Anatrace. Each detergent solution was created by adding twice the critical micelle concentration (CMC) of the detergent to the ammonium acetate solution at each pH. AM2 was exchanged into each of these detergent solutions using Bio-Spin 6 columns (Bio-Rad) and diluted to a final concentration of 50 μM (per monomer) prior to analysis in the relevant solution, except

where different concentrations are noted. Samples were allowed to briefly equilibrate at room temperature prior to analysis, but no significant changes were observed in the oligomeric state distributions over time or at colder temperatures. For TM-AM2, the peptide was synthesized as previously described[30] and diluted to 50 μM in each detergent solution. For drug binding experiments, amantadine (Sigma Aldrich) was diluted to 1.5, 0.75, 0.375, and 0.188 mM in water. 0.5 μL of amantadine was added to 4.5 μL of AM2, for a final drug concentration of 150, 75, 37.5, and 18.8 μM. Mixtures were incubated with amantadine for 5−10 minutes prior to analysis.

4.2.2 Nanodisc Assembly and Sample Preparation

AM2 nanodiscs were assembled using a 4:1 AM2 to nanodisc ratio. Lower ratios of incorporation showed less AM2 incorporated and higher ratios showed complex spectra that were difficult to resolve and interpret. For nanodiscs containing DMPC and DMPG lipids, the lipids (Avanti Polar Lipids) solubilized in cholate (Sigma Aldrich) were added at an 80:1 ratio of lipid to membrane scaffold protein (MSP). Details on MSP expression and purification are provided in the Supporting Information. For nanodiscs containing DPPC lipids, the lipids were added at a 90:1 ratio of lipid to MSP. All nanodiscs were assembled overnight by adding Amberlite XAD-2 hydrophobic beads (Sigma Aldrich) at the phase transition temperature of the lipid. To isolate nanodiscs containing AM2 from empty nanodiscs, nanodiscs were purified using a HisTrap HP 1 mL column (GE Healthcare). The column was equilibrated with buffer containing 40 mM Tris, 0.3 M NaCl, and 20 mM imidazole at pH 7.4. AM2 nanodiscs were then eluted from the column with buffer containing 40 mM Tris, 0.3 M NaCl, and 400 mM imidazole at pH 7.4. Nanodiscs were then concentrated and purified on a Superose 6 10/300 GL (GE Healthcare) equilibrated with 0.2 M ammonium acetate. For all nanodisc drug binding experiments, 1 μL of 400 or 800 μM drug

were added to 9 μL of nanodiscs for final drug concentrations of 40 and 80 μM. These samples were allowed to incubate for ten minutes at room temperature prior to analysis.

Nanodiscs for peptide experiments were assembled at a 90:1 and 80:1 ratio of lipid to MSP for DPPC and DMPC nanodiscs respectively. All nanodiscs were assembled overnight by adding Amberlite XAD-2 hydrophobic beads (Sigma Aldrich) at the phase transition temperature of the lipid. Nanodiscs were then purified on a Superose 6 10/300 GL (GE Healthcare) equilibrated with 0.2 M ammonium acetate. After purification, all nanodiscs were diluted to a final concentration of 2.2 μM. Nanodiscs were then mixed with peptide at a 16:1, 8:1, 4:1, 2:1, and 1:1 ratio of peptide to nanodisc and allowed to incubate for 30 minutes at room temperature prior to analysis.

4.2.3 Native Mass Spectrometry

Native MS was performed using a Q-Exactive HF Orbitrap (Thermo Scientific, Bremen) mass spectrometer with ultra-high mass range modifications except where noted as a Synapt XS Q-ToF mass spectrometer (Waters Corporation, Manchester). The native mass spectra were deconvolved and quantified using UniDec, and macromolecular mass defect analysis was used to quantify the stoichiometries of AM2 and amantadine in nanodiscs.[157, 158, 183] Full details are provided in the Supporting Information. Prior published results with streptavidin, a similarly sized tetramer, with similar instrument conditions provided a positive control demonstrating the ability of native MS to preserve and detect specific noncovalent complexes of the same size.[183] Similar experiments on a small transmembrane protein complex, semiSWEET, also demonstrate the ability of native MS to detect specific complexes of small membrane proteins.[118]

4.2.4 Protein Expression and Purification

The full-length AM2 with C-terminal polyhistidine tag and cysteines converted to serines was overexpressed in BL21(DE3) pLysS cells. The sequence is shown in Figure 4-1A without the N-terminal methionine, which is cleaved during expression. Cells were grown at 37 °C in terrific broth media (Thermo Fisher Scientific) to an optical density of 0.8-1.0. Overexpression was induced with isopropyl β-d-1-thiogalactopyranoside at a final concentration of 1 mM for three hours, and cells were then harvested through centrifugation. Cells were resuspended in lysis buffer containing 150 mM NaCl, 50 mM Tris, 40 mM octyl-glucoside (OG), and protease inhibitor. After resuspension, cells were lysed using the LM20 Microfluidizer High Sheer Homogenizer. Lysed cells were then stirred at 4 °C for 1–3 hours to allow for membrane solubilization. The lysate was clarified through centrifugation at 48,380×*g* for 20 minutes. Prior to protein purification, a HisTrap HP 5 mL column (GE Healthcare) was equilibrated with buffer A (150 mM NaCl, 50 mM Tris, 40 mM OG, 20% glycerol, and 20 mM imidazole). The sample was then filtered, loaded to the column, and washed with 10–15 column volumes of buffer A. To remove any nonspecific protein binding, the column was then washed with 5–10 column volumes of 5% buffer B (150 mM NaCl, 50 mM Tris, 4 mM OG, 20% glycerol, and 300 mM imidazole). AM2 was then eluted with 100% buffer B. It was then diluted with buffer A to a final monomer concentration of 580 μM, aliquoted, and flash frozen. The S31N mutant of AM2 was expressed and purified using the same protocol as AM2 wild type.

Membrane scaffold protein, MSP1D1(–) was expressed and purified as previously described.[159, 244] Briefly, MSP1D1 was expressed in *E. coli* and purified using immobilized metal affinity chromatography (IMAC). Following cleavage of the polyhistidine tag, MSP1D1(–) was purified by reverse IMAC.

4.2.5 NATIVE MASS SPECTROMETRY

Native mass spectrometry was performed as previously described[157, 183] using a Q-Exactive HF Orbitrap (Thermo Scientific, Bremen) mass spectrometer with Ultra-High Mass Range Modifications except where stated otherwise. Nano-electrospray ionization in positive ion mode was performed using borosilicate needles pulled using a P-1000 micropipette puller (Sutter Instruments).

Detergent-solubilized AM2 was analyzed with a range of 1,500−15,000 *m/z* at a resolution of 15,000. The trapping gas pressure was set to 5, and the spray voltage ranged from 1.1−1.5 kV. To aid in desolvation and detergent removal, 10−50 V of higher-energy collisional dissociation (HCD) energy and 10–50 V of source fragmentation were applied to each sample, as previously described.[183] The precise collision voltages were adjusted slightly for each sample, and results are shown for the lowest value that gave a well-resolved spectrum. An open vial with 2–5 mL of acetonitrile was placed in the source of the mass spectrometer to allow for vapor charge reduction of all samples, which we found helped stabilize complexes during native MS.[245] Mass spectrometry data was collected as single measurements for three sets of dilutions after the protein was buffer exchanged. Spectra are shown for a single representative replicate, and error bars show the standard deviation of the three replicates.

Nanodiscs were analyzed with a range of 2,000−25,000 *m/z* at a resolution of 15,000. The trapping gas pressure was set to 5 with a spray voltage of 1.1−1.3 kV. For nanodiscs with 1,2-dimyristoyl-*sn*-glycero-3-phosphocholine (DMPC) or 1,2-dimyristoyl-*sn*-glycero-3-phosphorylglycerol (DMPG) lipids, 50−100 V of HCD collisional energy and 10−50 V of source voltage was applied to aid in the desolvation. To aid in the analysis of 1,2-dipalmitoyl-*sn*-glycero-3-phosphocholine (DPPC) nanodiscs, a super charging reagent, propylene carbonate, was added

prior to ionization at 5% propylene carbonate by volume.[157] For DPPC nanodiscs, 100−200 V of HCD collisional activation was added to remove propylene carbonate. Representative spectra are shown from three replicate nanodisc assemblies.

Ion mobility-mass spectrometry (IM-MS) analysis was performed on a Synapt XS HRMS Q-ToF mass spectrometer (Waters Corporation, Manchester) using a nano-electrospray ionization source with borosilicate glass capillaries prepared as described above. MS conditions were applied to remove detergent adducts without disrupting structure prior to detection with instrument parameters as follows: capillary voltage, 1.5–1.8 kV; sampling cone, 150 V; trap collision energy, 100 V; transfer collision energy, 10 V; trap gas, 10 mL/min; helium cell gas, 120 mL/min; backing gas, 2.85 mbar. The parameters for IM were as follows: IM cell wave height, 40 V; IM cell wave velocity, 1000 m/s; transfer wave height, 4 V; transfer wave velocity, 69 m/s. Arrival time distributions (ATDs) were viewed using DriftScope 2.9 (Waters Corporation). CCS values were calculated as previously described using standards with published values.[2] All reported CCS values were the result of triplicate experiments, and error bars are shown as the standard deviation of the CCS for different charge states.

4.2.6 Native MS Data Analysis

The native mass spectra for AM2 solubilized in detergent were deconvolved using UniDec as previously described.[183] The settings for the deconvolution of AM2 in all conditions included a mass range of 1−110 kDa, a charge range of 1−50, and a FWHM of 1 *m/z*. A curved background subtraction of 100, as well as point smooth width of 1 and a beta value of 50 were also applied for all data.[149, 246] The native mass spectra for the AM2 nanodiscs were analyzed using UniDec as

previously described.[153] The mass range was extended to an upper limit of 250 kDa. For nanodiscs made of DMPG and DMPC lipids, the charge range was set 1−25. For nanodiscs made of DPPC lipids, the charge range was set 1−16. The mass of the lipid was used with mass smoothing set to -1.

To determine the stoichiometry of both full-length AM2 and TM-AM2 in nanodisc samples, we used mass defect analysis.[153, 222] Mass defect analysis divides the mass of the sample by a reference mass (the mass of the lipid), and the remainder of the division is then plotted. The plotted remainder is then normalized between 0 and 1.[153] Nanodiscs with the same number of proteins or peptides associated but varying numbers of lipids incorporated will have the same mass defect. This allows for us to sum the mass defect of the protein or peptide across nanodiscs with different numbers of total lipids, yielding the overall mass defect distribution. Mass defect analysis thus reveals the number of AM2 molecules associated with an intact nanodisc inside the mass spectrometer. The addition of each full-length AM2 incorporated into the nanodisc also shifted the overall mass of the complex by about 10 kDa, which further helped in the assignment of the stoichiometry of the protein-nanodisc complexes.

4.2.7 AM2 Model Structures and Predicted Collisional Cross Sections

CCS values expected for native, globular proteins were determined using the empirical relationships between mass and CCS for a variety of proteins.[247, 248] Model structures of AM2 oligomers were generated in PyMol[249] using PDBs 2N70[250] and 4N8C[251] as templates for the transmembrane and intracellular domains. Any discrepancies in sequence were changed, and missing extracellular domain residues were added manually in PyMol to generate a model AM2 monomer. This monomeric structure was then subjected to a brief (1 ns) relaxation in water using

GROMACS, and the resulting simulated structure was used to construct all model oligomeric complexes with PDB 2KIH[38] as a template for subunit arrangement.

In vacuo molecular dynamics simulations of each model AM2 structure were then performed using the GROMOS96 43a2 force field in GROMACS, as previously described.[252] Briefly, the center of the experimental charge state distribution was chosen for each AM2 oligomer, and a low-energy configuration of positive charges was determined using the charge placement algorithm in Collidoscope.[253] This configuration was used to assign charges during topology file generation, and then each model AM2 structure was allowed a brief energy minimization step, followed by a 5 ns *in vacuo* MD production run at 300 K with a modified Berendsen thermostat. CCSs for simulated structures were computed using nitrogen buffer gas and the Trajectory Method in Collidoscope after identifying a low-energy charge configuration for the compacted structures.

4.2.8 Size Exclusion Chromatography

Analytical size exclusion chromatography (SEC) was performed using a Superdex 200 Increase 10/300 (GE Healthcare) equilibrated with 1 column volume of each solution, and 100 μL of concentrated AM2 (580 μM) was injected in duplicate.

4.2.9 Analytical Ultracentrifugation

Samples for analytical ultracentrifugation (AUC) were prepared similarly to native MS samples by buffer exchanging full-length AM2 into 0.2 M ammonium acetate at pH 5 with twice the critical micelle concentration of either C8E4 or LDAO detergent with a final protein concentration of 2 mg/ml. Experiments were performed using a Beckman Optima Analytical Ultra Centrifuge with a 4 cell An-60 Ti rotor. After equilibrating 4 hours at 25 °C, samples were spun at

40,000 rpm for sedimentation velocity experiments. The absorbance data was collected at 280 nm every 2 minutes overnight (>12 hours or until the baseline was well established by protein depletion). All AUC data was collected in triplicate from separate spins. Data from absorbances at 280 nm were fit with direct boundary modeling and analyzed using the c(s) distribution in Sedfit.[254] Buffer density was estimated at 1.00 g/L, and the viscosity was assumed to be 1.00 cP. Partial specific volume for the protein was assumed to be 0.73 mL/g.

4.2.10 Liposome Assays

Proton flux assays were performed on AM2 by assembling AM2 into liposomes made of 1-palmitoyl-2-oleoyl-*sn*-glycero-3-phosphocholine (POPC) lipids. Liposomes were assembled

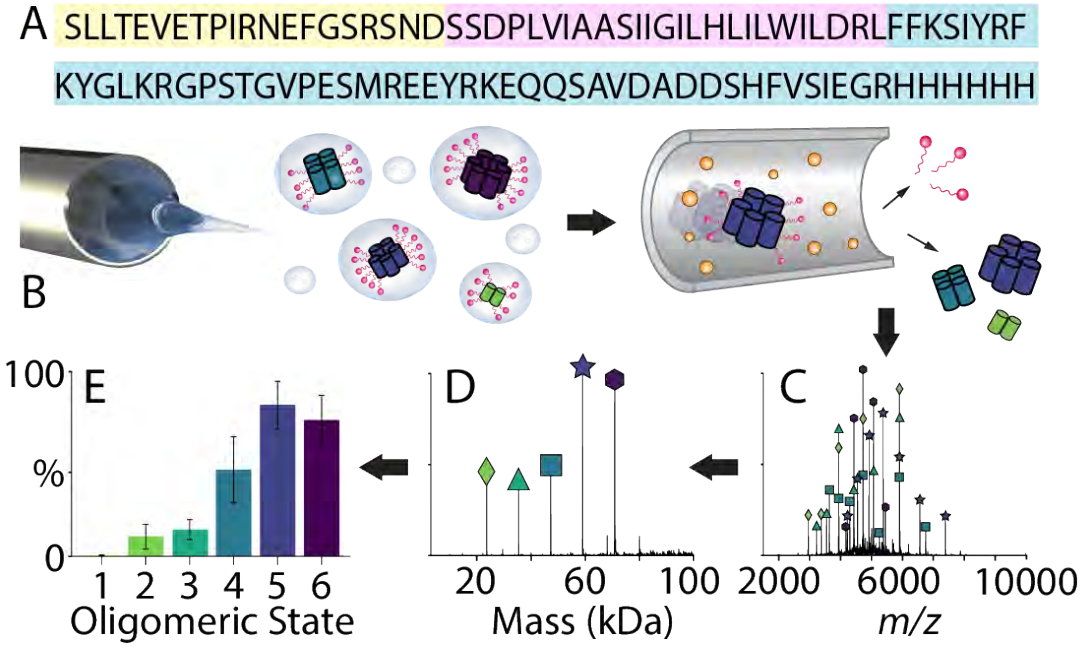

Figure 4-1 Native MS reveals the oligomeric state distribution of AM2. (A) The sequence of AM2 with the short extra-viral domain colored in yellow, the transmembrane domain in pink, and the intra-viral region in blue. (B) A schematic of ESI with CID to remove detergent from AM2, (C) the mass spectrum of AM2 (at 50 μM per monomer) in C8E4 detergent at pH 5, (D) the deconvolved mass spectrum, and (E) the extracted normalized peak areas of each oligomeric state.

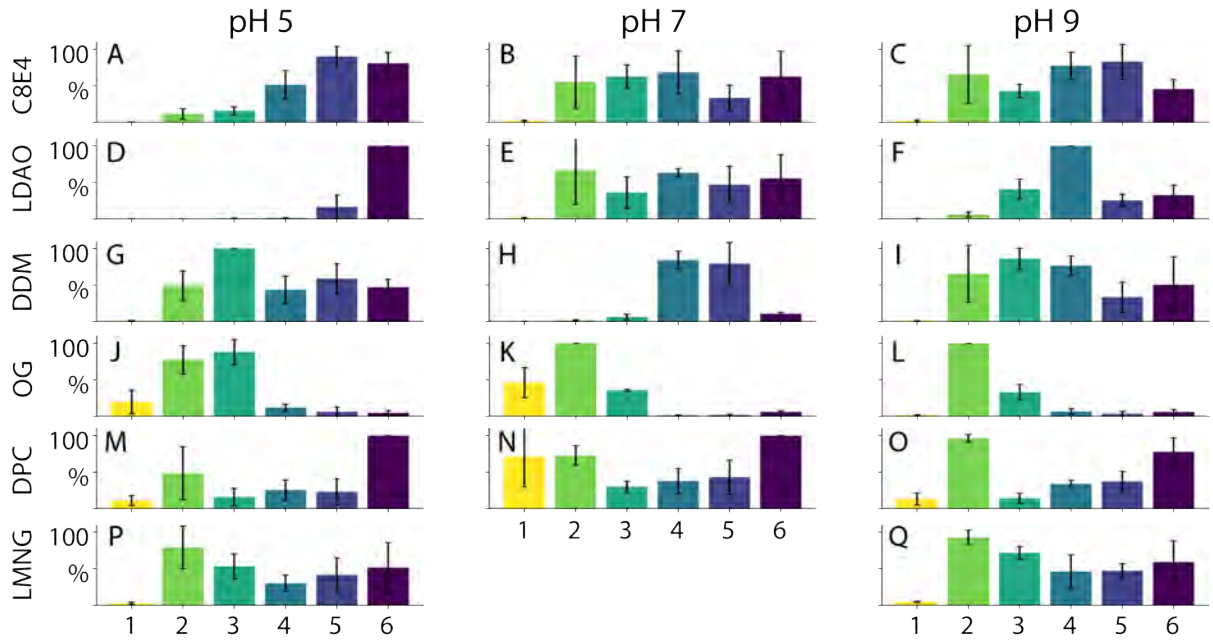

Figure 4-2: The average relative peak areas measured by native MS of different oligomeric states of WT full-length AM2 (at 50 µM monomer) at pH 5 (A, D, G, J, M, P), pH 7 (B, E, H, K, N), and pH 9 (C, F, I, L, O, Q) while solubilized in C8E4 (A–C), LDAO (D–F), DDM (G–I), OG (J–L), DPC (M–O), and LMNG (P, Q). AM2 was not stable in pH 7 with LMNG and no mass was detected under these conditions. Error bars indicate the standard deviation of measurements from triplicate samples. Representative native mass spectra of select conditions are shown in Figure 3.2.

with 10 mg of POPC solubilized in 0.1 M sodium cholate, 20 nmol of full-length AM2 solubilized in OG detergent, and 0.2 nmol of valinomycin. The internal liposome buffer (50 mM phosphate, 50 mM citrate, 122 mM KCl and 122 mM NaCl) was added to a final mixture volume of 500 µL. Amberlite XAD-2 hydrophobic beads (Sigma Aldrich) were added to the mixture, and liposomes were assembled at 4 °C. The liposomes were then extruded, and the assay was performed as previously described.[38] Solution pH measurements were made using a pH microelectrode (InLab) and measurements were made each second. Assays were performed by adding 2 µL of 1 M HCl to the solution being mixed with a stir bar. An increase in the solution pH after acid was added was only observed in liposomes where both AM2 and valinomycin were present. Controls were

performed on liposomes without AM2 and without valinomycin, and there was no proton flux measured in these conditions.

4.3 RESULTS

4.3.1 AM2 Oligomerization is Sensitive to Detergent and pH

Our initial goal was to investigate drug binding to AM2 using native MS. Based on prior studies,[233, 235, 238] we expected to find a monodisperse AM2 tetramer. However, initial results immediately revealed a more complex oligomeric state distribution. To identify conditions that

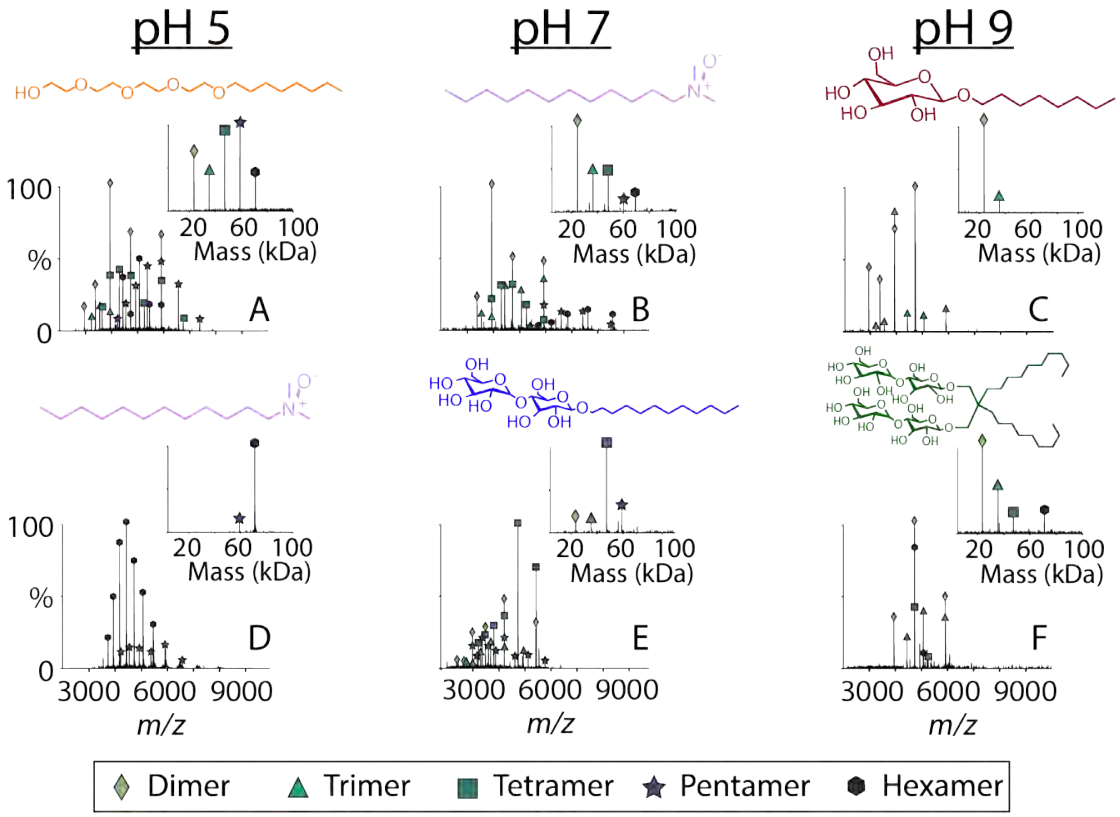

Figure 4-3: Representative native mass spectra with the deconvolved mass spectra in the inset of AM2 (at 50 µM per monomer) solubilized in (A) C8E4 at pH 5, (B) LDAO at pH 7, (C) OG at pH 9, (D) LDAO at pH 5, (E) DDM at pH 7, and (F) LMNG at pH 9. Each detergent is shown above the spectrum. Average oligomeric state distributions collected in triplicate are shown in Figure 4-2.

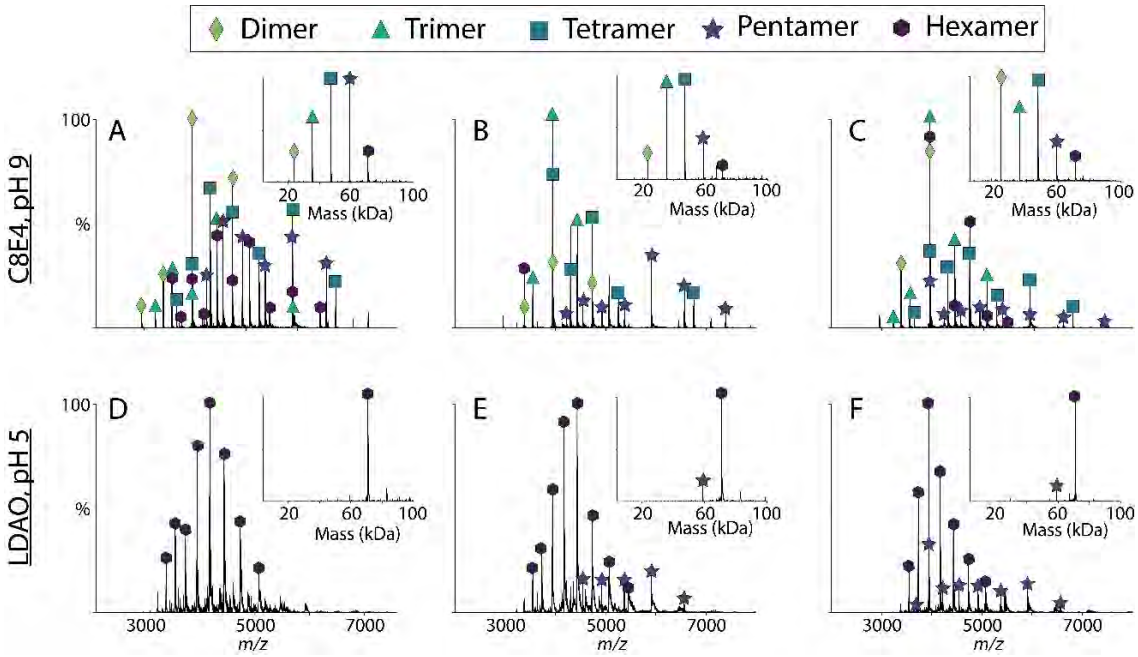

Figure 4-4: Native mass spectra and deconvolved mass spectra (inset) of WT full-length AM2 (at 50 μM monomer) in C8E4 detergent at pH 9 (A–C) and in LDAO at pH 5 (D–F) shown for three separate replicates.

would promote the formation of a monodisperse tetramer, we performed native MS on full-length AM2 to quantify the oligomeric state distribution (Figure 4-1) in a range of different conditions. We screened different detergents by exchanging AM2 into solution containing tetraethylene glycol monooctyl ether (C8E4), lauryldimethylamine oxide (LDAO), *n*-octyl-β-D-glucopyranoside (OG), *n*-dodecyl-phosphocholine (DPC), *n*-dodecyl-β-maltoside (DDM), and lauryl maltose neopentyl glycol (LMNG). We selected detergents that have been previously used for AM2 structural biology studies, including OG and DPC,[3, 7, 255-257] as well as detergents that are commonly-used for native MS, such as C8E4, LDAO, and DDM.[113, 258] LMNG was selected for additional structural diversity. For each detergent, we tested pH 5, 7, and 9, which encompass the

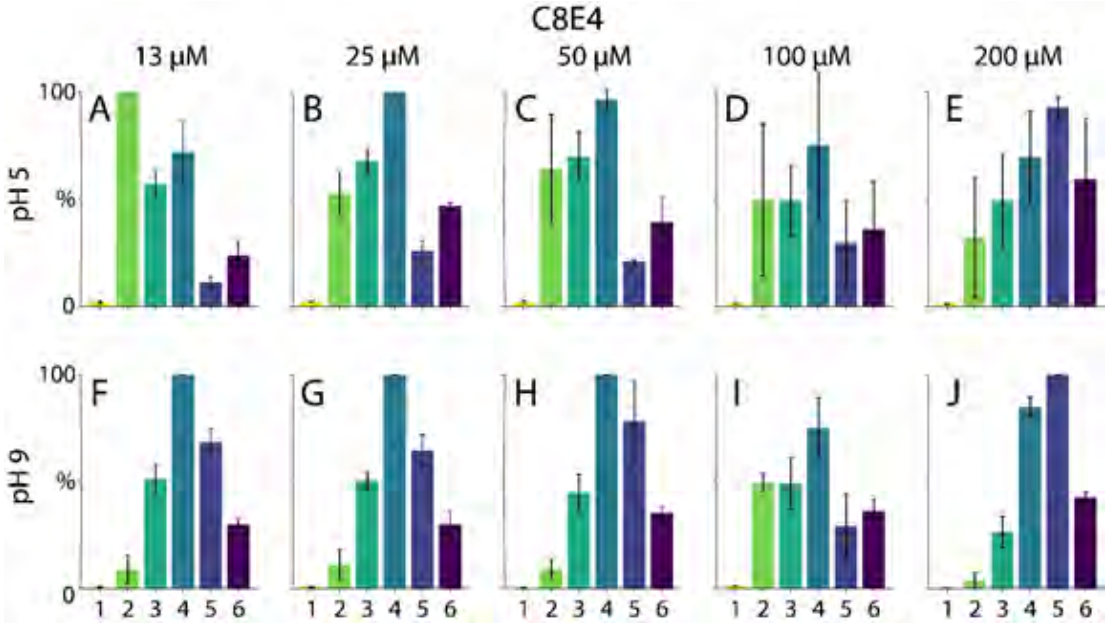

Figure 4-5: The average relative peak areas measured by native MS of different oligomeric states of WT full-length AM2 solubilized in C8E4 at AM2 monomer concentrations of (A, F) 13, (B, G) 25, (C, H) 50, (D, I) 100, and (E, J) 200 µM at pH 5 (A-E) and pH 9 (F-J).

pH conditions that have been previously investigated with AM2.[259, 260] Selected spectra are shown in Figure 4-3 with oligomeric state distributions for all plotted in Figure 4-2.

We began by investigating C8E4, which is commonly used for native MS because it is easy to dissociate from membrane proteins.[261, 262] At all pH conditions tested for C8E4, AM2 showed a

Table 4-1: The theoretical masses, mean measured masses, and standard deviation of the mass measurement of AM2 in C8E4, LDAO, and OG detergents at pH 5 and 9.

Theoretical Mass (Da)	Mean Measured Mass (Da)	Standard Deviation (Da)
11810	11821.0	19.8
23620	23616.7	0.5
35430	35447.9	20.9
47240	47280.8	12.8
59050	59090.6	13.2
70860	70940.2	22.1

polydisperse mixture of oligomers that ranged from dimers to hexamers (Figures 4-2, 4-3A and 4-5, Table 4-1). The precise oligomeric state distribution varied somewhat between replicate measurements, potentially indicating more dynamic oligomers (see Figure 4-4). Our interpretation is that these more variable oligomers are more sensitive to minor fluctuations in the chemical environment between samples, but the overall trend of forming polydisperse oligomers is highly reproducible. When it was diluted at pH 5, AM2 shifted to lower oligomeric states, indicating weaker interactions in this condition, but it retained higher order oligomers upon dilutions at pH 9 (Figure 4-5). Overall, AM2 in C8E4 was relatively polydisperse and not heavily influenced by the pH.

In contrast, the oligomeric state of AM2 was more monodisperse and highly dependent on pH when it was solubilized in LDAO. At pH 6 and below, AM2 in LDAO was almost exclusively

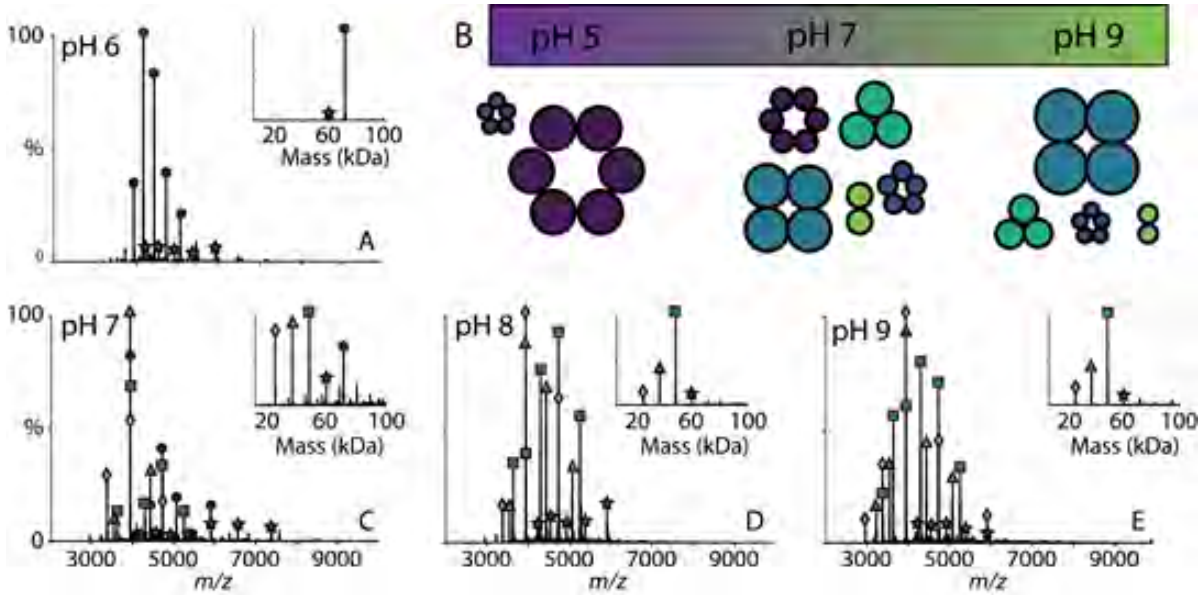

Figure 4-6: Representative native mass spectra with deconvolved mass spectra (inset) of AM2 (at 50 μM per monomer) solubilized in LDAO detergent at pH (A) 6, (C) 7, (D) 8, (E) 9, with (B) a schematic of the different oligomers of AM2 versus pH where the sizes of the oligomers indicate their relative intensities in the spectra. The average oligomeric state distributions collected in triplicate are shown in Figure 4-7.

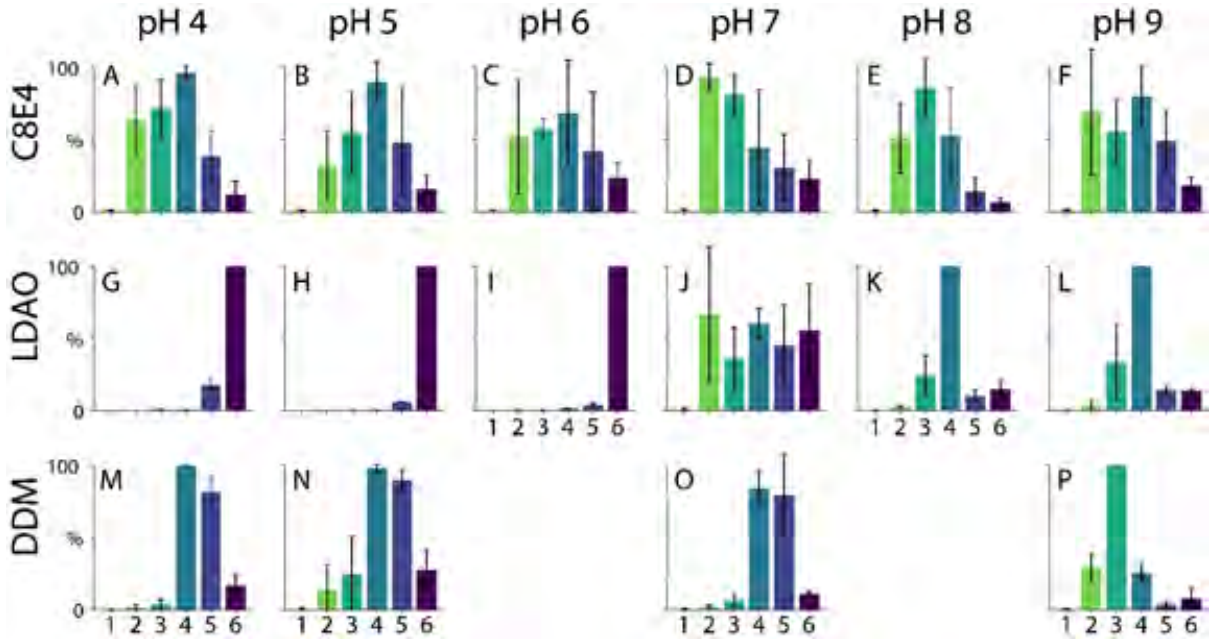

Figure 4-7: The average relative peak areas measured by native MS of different oligomeric states of WT full-length AM2 (at 50 μM monomer) at pH 4 (A, G, M), pH 5 (B, H, N), pH 6 (C, I), pH 7 (D, J, O), pH 8 (E, K), and pH 9 (F, L, P) while solubilized in C8E4 (A–F), LDAO (G–L), and DDM (M-P). AM2 was not stable in DDM at pH 6 and 8, so no data is shown. Representative native mass spectra of AM2 in LDAO are shown in Figure 4-6.

hexameric, with a small amount of pentamer present (Figures 4-4, 4-6, and 4-7). Additionally, there was almost no variation among replicates of AM2 under this condition, indicating the formation of specific hexameric complexes. However, at pH 7, AM2 in LDAO formed a polydisperse mixture from dimers to hexamers (Figures 4-2 and 4-6C). At pH 8 and 9, AM2 was less polydisperse than at neutral pH, forming primarily tetramer with a significant amount of trimer (Figure 4-6D and E). In contrast with C8E4, these more monodisperse oligomers at pH 5 and 9 remained intact upon dilution, further confirming their specificity (Figure 4-8). Overall, AM2 formed more selective complexes in LDAO detergent, and the oligomeric states were strongly influenced by the pH.

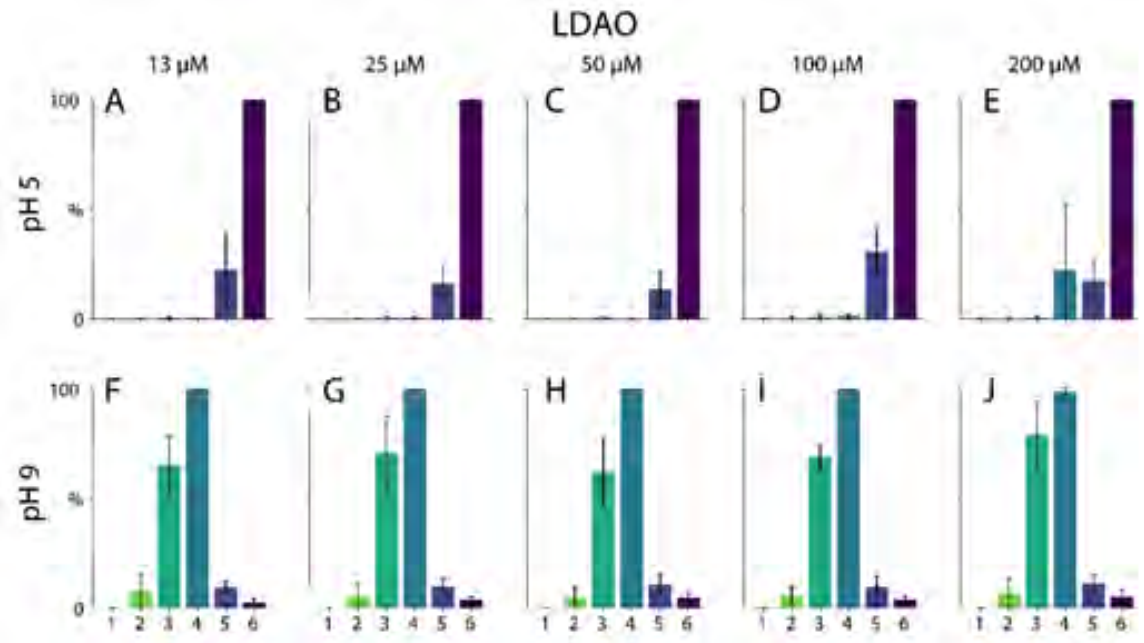

Figure 4-8: The average relative peak areas measured by native MS of different oligomeric states of WT full-length AM2 solubilized in LDAO at an AM2 monomer concentrations of (A, F) 13, (B, G) 25, (C, H) 50, (D, I) 100, and (E, J) 200 μM at pH 5 (A-E) and pH 9 (F-J).

The pH also had strong influences on the oligomerization of AM2 in DDM (Figure 4-2 and 4-7). At pH 7 and below, AM2 was primarily a mixture of tetramers and pentamers. At pH 9, AM2 in DDM was predominantly trimer with significant amounts of dimer and tetramer (Figure 4-7). These oligomers also remained intact upon dilution (Figure 3.8). In contrast, the solution pH did not appear to have a strong influence on the oligomerization of AM2 in OG and DPC detergents (Figure 4-6). Despite the fact that AM2 has previously been studied in OG and DPC detergents,[3, 256, 257, 263] we did not observe monodisperse tetramers, perhaps due to the lower concentrations used here. Instead, there was a general preference for dimer and hexamer. In LMNG, AM2 preferred dimer and trimer at both pH 5 and 9 but was not stable at pH 7 (Figures 4-2 P–Q).

Because oligomerization is driven by the transmembrane domain, we next tested the TM domain peptide oligomeric state in select conditions. Similar to the full-length protein, TM-AM2

was polydisperse in C8E4 and OG (Figure 4-10). In LDAO, TM-AM2 was monodisperse and mostly hexameric at low pH but transitioned to polydisperse above pH 7 (Figure 4-10). Interestingly, TM-AM2 appeared to have slightly higher preferences for tetramer and hexamer than the full-length AM2 in C8E4 and LDAO detergents. However, the TM peptide overall qualitatively agreed with results from the full-length protein.

Overall, although tetramers were preferred in several conditions, there were no conditions where we found exclusively tetramers (Fig 4-2 and 4-10). Instead, we discovered that AM2 oligomerization is influenced by both its detergent environment and solution pH. Depending on the conditions, AM2 can form either highly variable and polydisperse oligomers or relatively selective oligomers of different sizes. Interestingly, the most stable and monodisperse oligomer we found was the hexamer in LDAO under acidic conditions (Figure 4-6A). It is known that AM2

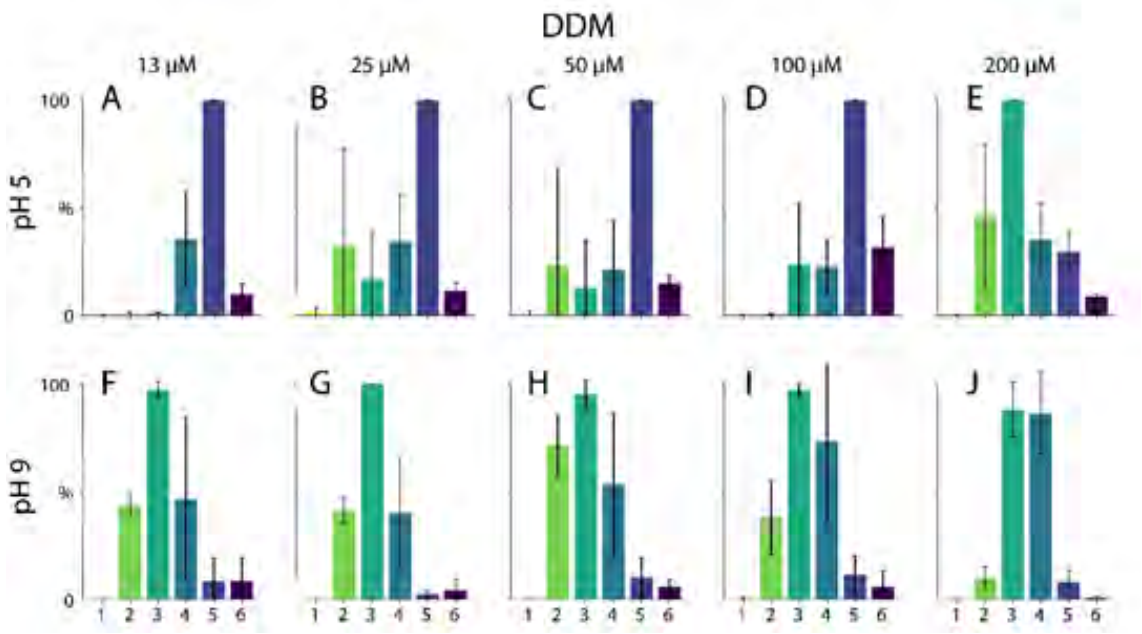

Figure 4-9: The average relative peak areas measured by native MS of different oligomeric states of WT full-length AM2 solubilized in DDM at an AM2 monomer concentrations of (A, F) 13, (B, G) 25, (C, H) 50, (D, I) 100, and (E, J) 200 µM at pH 5 (A-E) and pH 9 (F-J).

is a pH-mediated proton channel, and it is possible that the LDAO detergent is the only conidition tested that allows for the remodeling of the AM2 oligomer into this hexameric form.

4.3.2 Orthogonal Measurements Support Oligomeric Variability

Native MS gives accurate relative quantitation for similar species across narrow *m/z* ranges, but differences in ionization, transmission, and detector efficiency make quantitation across wide *m/z* ranges difficult.[264] To help rule out instrumental biases, we repeated select measurements using a mass spectrometer with a different type of detector. Both the Orbitrap and time-of-flight (ToF) detectors gave similar results (Figures 4-11 and 4-12), which support our qualitative conclusions and demonstrates that the results are consistent on different types of mass spectrometers.

We also used ion mobility-mass spectrometry to measure the collisional cross section (CCS) of some of the complexes (Figure 4-11 and 4-13).[247, 265] We modeled potential structures

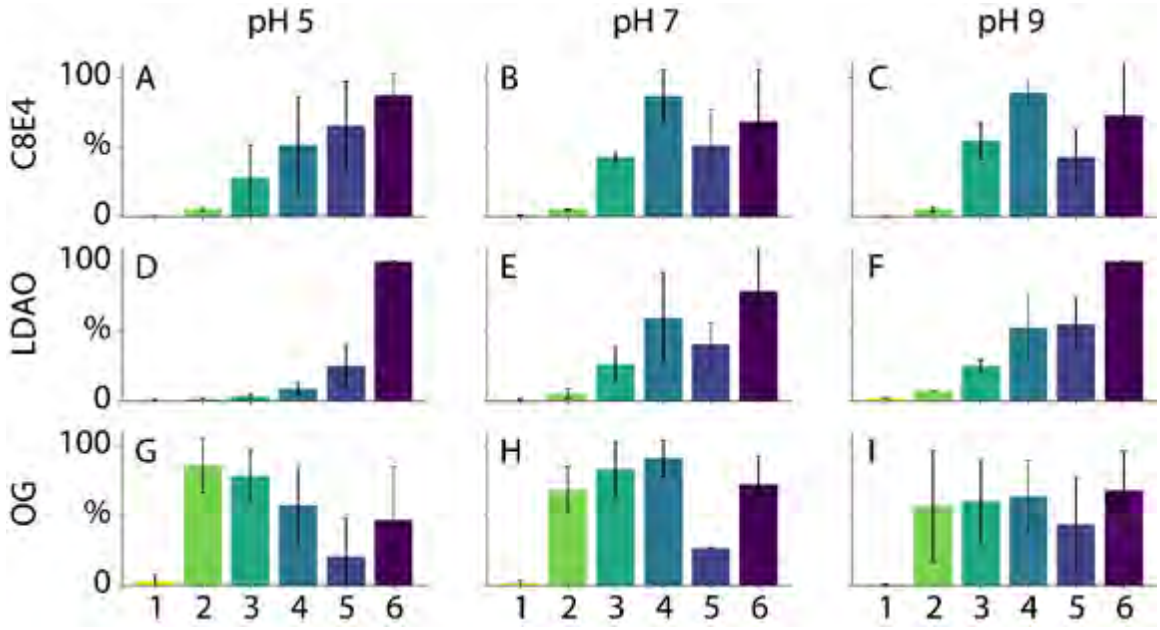

Figure 4-10: The average relative peak areas of the different oligomeric states of the TM domain of WT AM2 (at 50 μM per monomer) at pH 5 (A, D, G), pH 7 (B, E, H), and pH 9 (C, F, I) while in C8E4 (A–C), LDAO (D–F), and OG detergents (G–I). Error bars indicate the standard deviation of measurements from triplicate samples.

assuming oligomerization of the transmembrane domain and disordered soluble domains.[252] Our experimental CCS values agreed with modeled gas-phase structures, where the disordered regions collapse. Our results also matched predicted CCS values for globular proteins of a similar size,[247] and the observed charge states are also consistent with a compact structure. Together, these results point to compact oligomers consistent with oligomerization in the transmembrane domain. Based on the observed charge states and CCS values, we can rule out highly extended oligomeric structures and also rule out gas-phase dissociation, which would cause unfolding of the complex and higher CCS values. Also, we would expect any dissociation or complex disruption during native MS to yield a significant population of monomers, which are generally absent. Thus, there is no evidence for complexes being disrupted during native MS. In our interpretation of the data,

we have been careful to avoid any conclusions that could be distorted by different ionization efficiencies.

Although both instruments showed similar oligomeric state distributions, we cannot rule out differences in ionization efficiency that could skew the distribution measured by native MS. To further confirm our results, we performed size-exclusion chromatography (SEC) with AM2 in select conditions. It is challenging to directly compare the elution times between different detergents because the micelle sizes can vary. However, qualitative comparisons of the chromatograms of AM2 in different conditions supported the native MS results. Conditions with a wide range of oligomers in native MS, such as C8E4 at pH 9, had broader SEC peaks and more

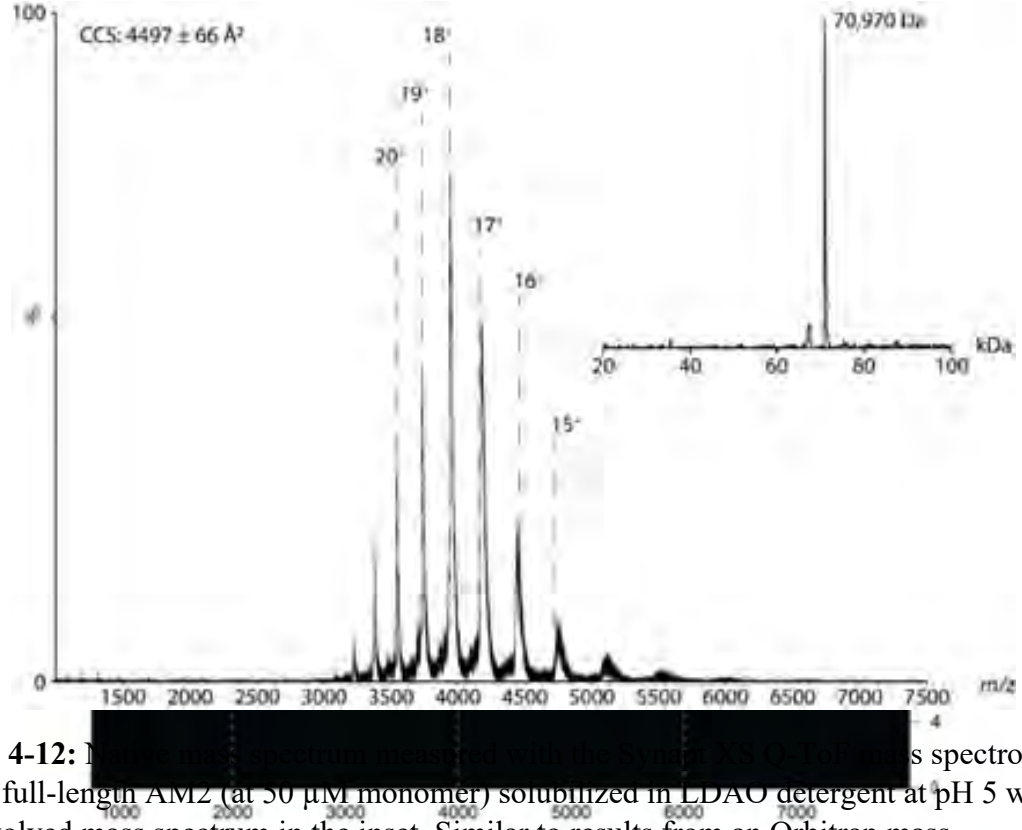

Figure 4-12: Native mass spectrum measured with the Synapt XS Q-ToF mass spectrometer of WT full-length AM2 (at 50 µM monomer) solubilized in LDAO detergent at pH 5 with the deconvolved mass spectrum in the inset. Similar to results from an Orbitrap mass spectrometer (Figure 2D), a mostly monodisperse hexamer of AM2 is observed. The CCS value for the hexamer is 4497 ± 66 Å^2.

variability between replicate injections (Figure 4-14). In conditions where AM2 was more monodisperse, such as LDAO at pH 5, we saw narrower and more reproducible peaks.

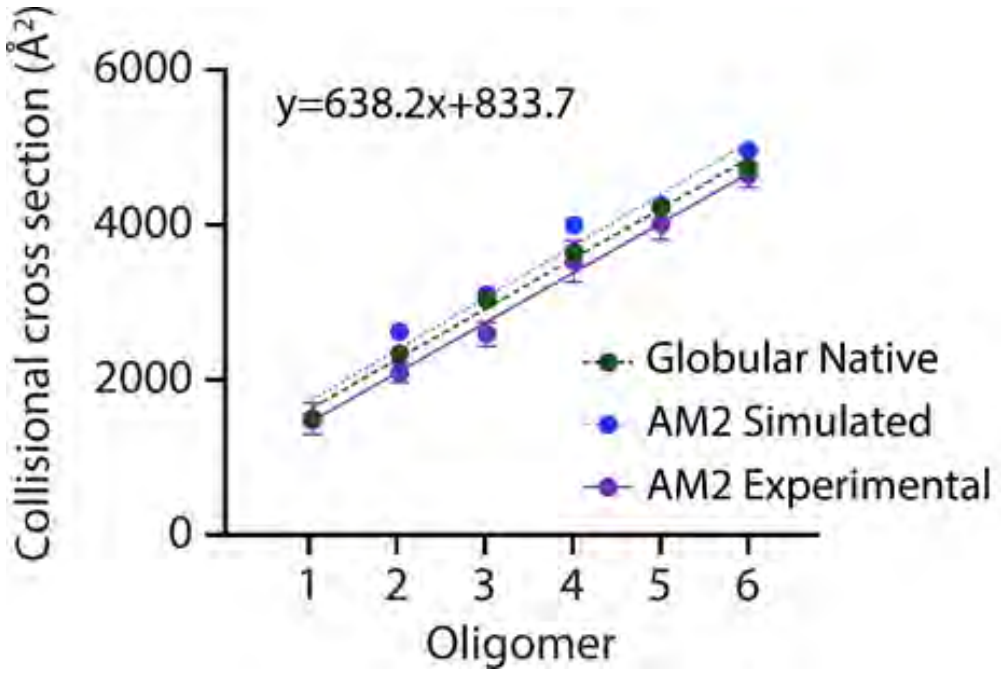

Figure 4-13: Experimental collisional cross sections (CCS) of AM2 oligomers in C8E4 at pH 9 (*purple*) compared to CCSs expected for native globular proteins (*green*) and to CCSs calculated for model structures (*blue*). A linear fit to the experimental data is annotated and shows that each monomer added to the oligomeric complex contributed around 638 Å^2 in CCS.

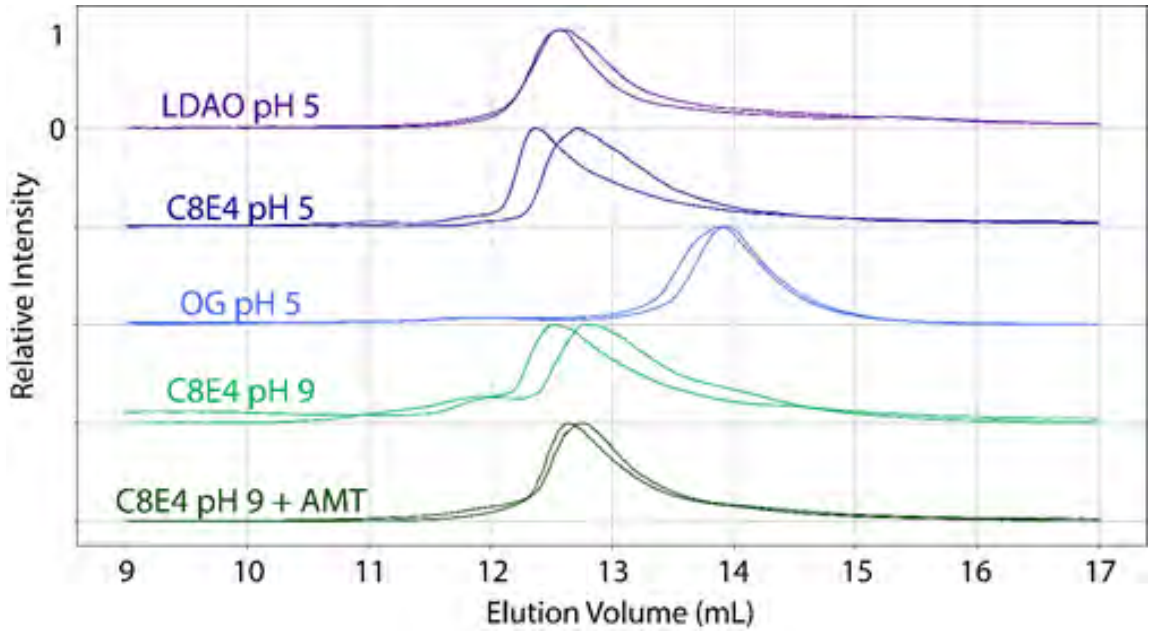

Figure 4-14: The relative absorbances at 280 nm of AM2 in LDAO pH 5, C8E4 pH 5, OG pH 5, C8E4 pH 9, and C8E4 pH 9 with 300 µM amantadine during size exclusion chromatography. For comparison, standards were analyzed on the same column: thyroglobulin (eluted at 9.2 mL), catalase (9.6 mL), alcohol dehydrogenase (12.96 mL). carbonic anhydrase (16.39 mL), and ribonuclease A (17.59 mL). Duplicate injections are shown for each.

LDAO and C8E4 at pH 5. AUC trends were consistent with native MS. The more polydisperse sample (C8E4) showed several species with AUC, while the more monodisperse sample (LDAO) showed one single species (Figure 4-15). Thus, these data help support the qualitative descriptions of the oligomeric state distributions and also show changes in the size and polydispersity of the complex in response to the chemical environment. Together, these orthogonal measurements support the qualitative conclusions from native MS.

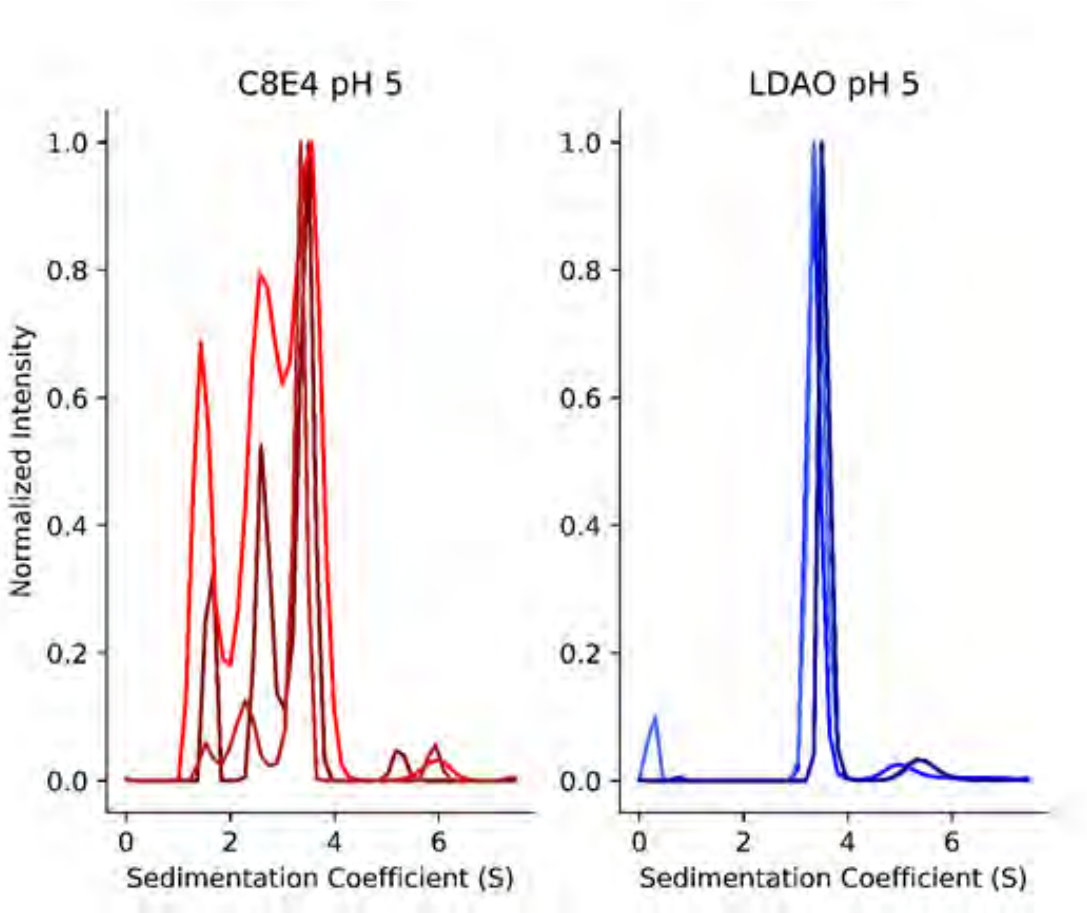

Figure 4-15: The fit sedimentation coefficients (s20,w) from AUC of WT full-length AM2 solubilized in LDAO and C8E4 at pH 5 shown in triplicate.

4.3.3 Drug Binding Can Remodel AM2 Oligomers

We next measured the effects of amantadine, a clinically-approved inhibitor of AM2,[266] by adding the drug at different concentrations in all the detergent and pH conditions. Interestingly, we discovered a shift in the oligomerization when amantadine was added to AM2 in C8E4 at pH 9. At low concentrations of amantadine, AM2 formed a range of variable oligomers. At higher concentrations of amantadine, AM2 shifted towards relatively monodisperse tetramers (Figure 4-16). A similar trend was observed on the ToF platform (Figure 4-17). We also compared the drug-resistant S31N mutant of AM2 under the same conditions.[267] Even at high concentrations of amantadine, there were no major changes in the oligomeric state of AM2 S31N.

The S31N mutant appeared to have a similar oligomeric state distribution without added drug (Figure 4-18). Further experiments in a range of different detergents, pH conditions, and with

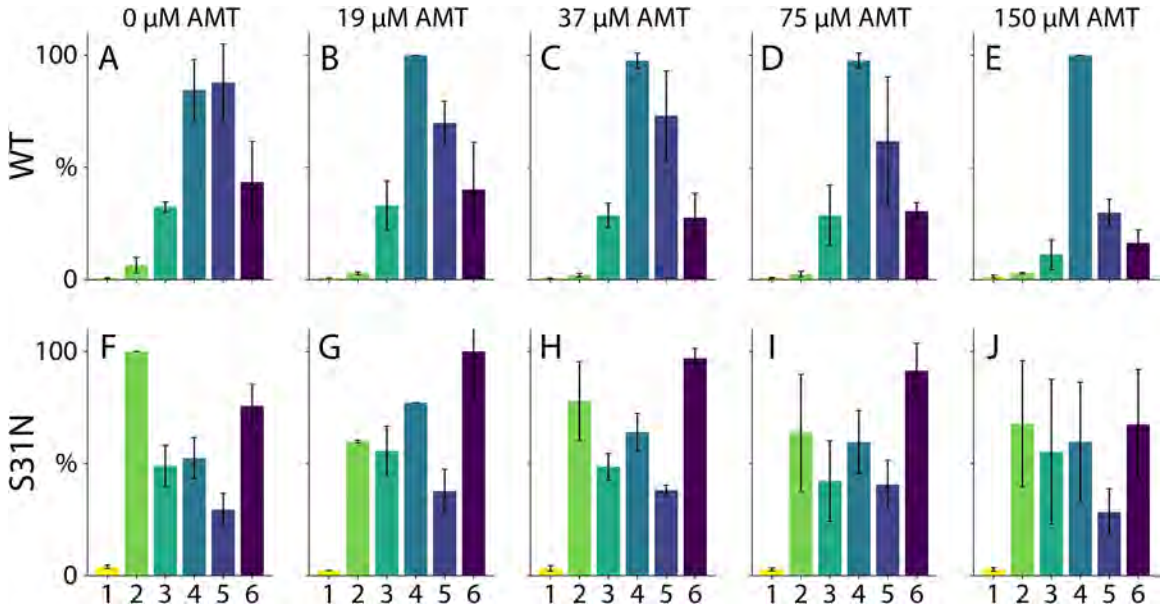

Figure 4-16: The average oligomeric state of AM2 wild type (A-E) and drug-resistant S31N (both at 50 µM per monomer) (F-J) with 0 µM (A, F), 19 µM (B, G), 37 µM (C, H), 75 µM (D, I), and 150 µM (E, J) amantadine added. Both AM2 WT and S31N were solubilized in C8E4 at pH 9.

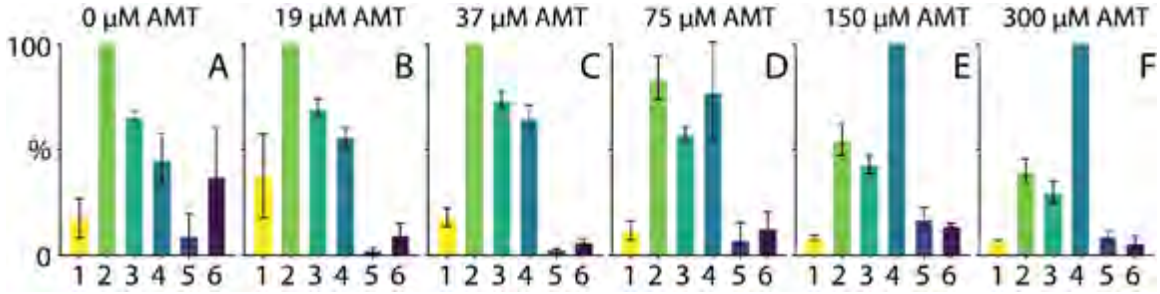

Figure 4-17: The average relative peak areas of different oligomeric states of WT full-length AM2 in C8E4 (at 50 µM monomer) at pH 9 with increasing concentrations of amantadine added measured with the Synapt XS Q-ToF mass spectrometer. Increasing concentrations of drug drive formation of more monodisperse tetramer complexes.

the full-length and TM peptides of the S31N mutant revealed an overall qualitatively similar oligomeric state pattern (Figure 4-19). The S31 mutant was generally polydisperse in most conditions but formed monodisperse hexamers in LDAO at pH 5. However, there was some bias

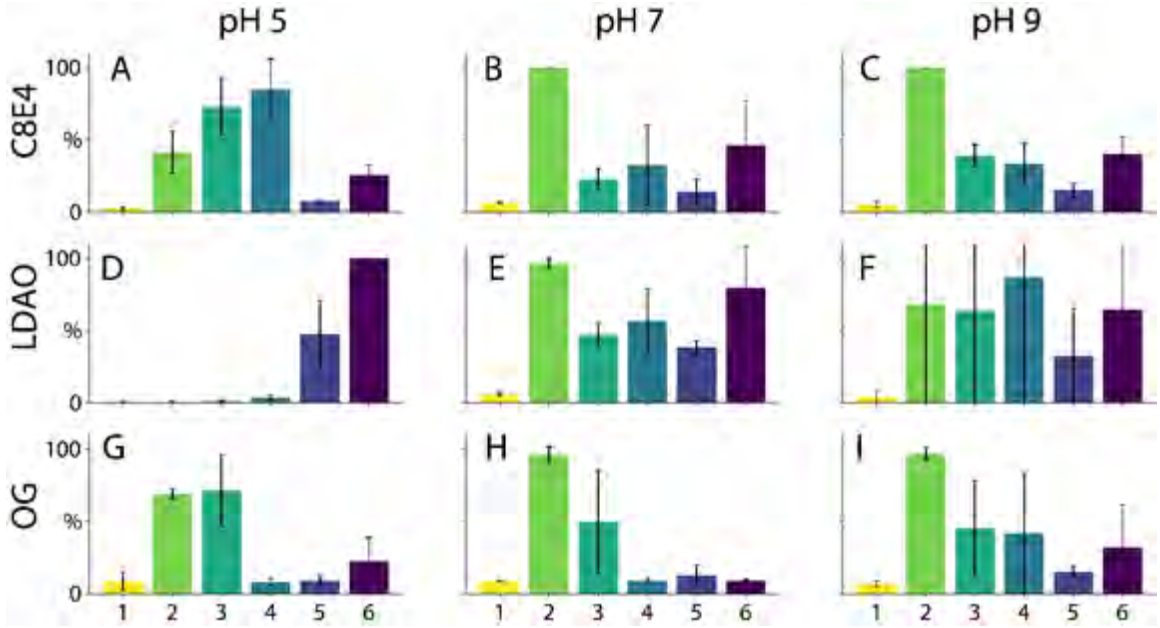

Figure 4-18: The average relative peak areas measured by native MS of different oligomeric states of full-length AM2 S31N (at 50 µM per monomer) at pH 5 (A, D, G), pH 7 (B, E, H), and pH 9 (C, F, I) while solubilized in C8E4 (A–C), LDAO (D–F), and OG (G–I). Error bars indicate the standard deviation of measurements from triplicate samples.

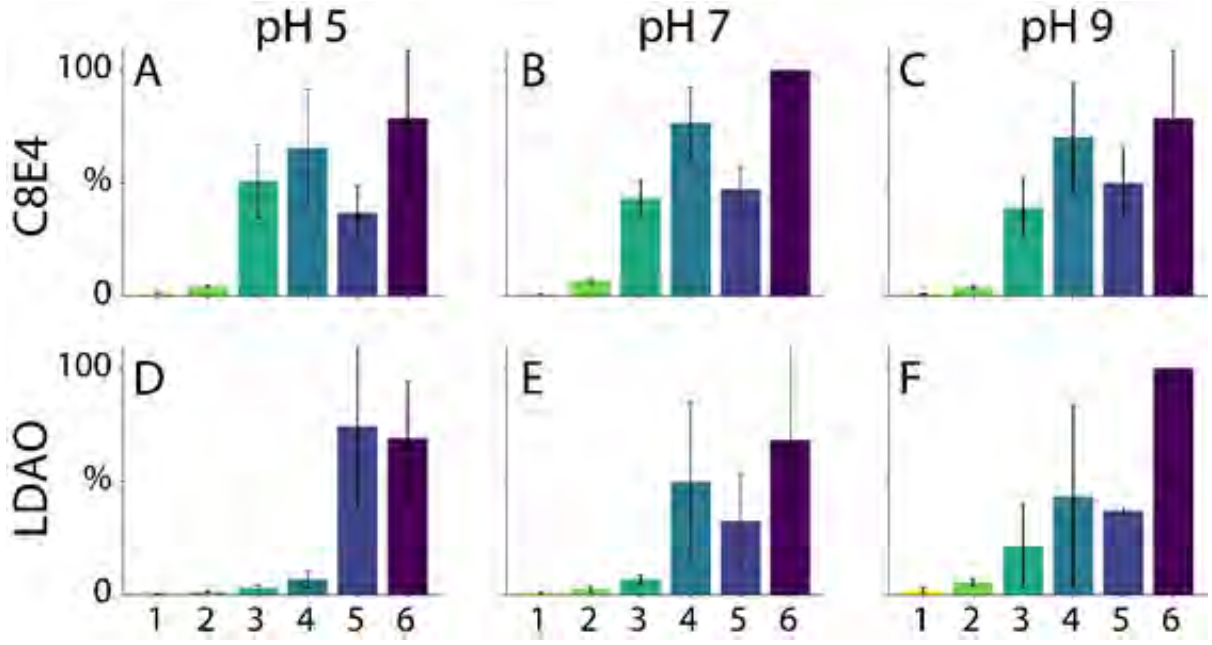

Figure 4-19: The average relative peak areas of the different oligomeric states of the TM domain of AM2 S31N (at 50 μM monomer) at pH 5 (A, D), pH 7 (B, E), and pH 9 (C, F) while in C8E4 (A–C) and LDAO detergents (D–F). The error bars indicate the standard deviation of measurements from triplicate samples.

towards dimer, suggesting the mutation may affect the oligomeric state distribution in some conditions.

One important limitation of these experiments is that we only observed shifts in the oligomeric state distribution in C8E4 detergent at pH 9. It has been previously found that amantadine preferentially binds under basic conditions, so it is not surprising that we only measured changes at higher pH.[268] The lack of response in other detergents may be because these detergents cause AM2 to form oligomers with lower drug binding affinity or oligomers with stronger protein-protein interactions that are not easily altered by the drug. AM2 shows the least oligomeric specificity in C8E4, so this set of conditions is perhaps most susceptible to shifts in the oligomeric state distribution caused by the drug.

Table 4-1: Mass defect shifts for binding different stoichiometries of amantadine in nanodiscs made of DPPC lipids. Contributions from AM2 and MSP are not included, so measured mass defect values will correspond to the values from Table S1 plus the shift indicated here.

Amantadine Stoichiometry	1	2	3	4
Mass Defect Shift	0.21	0.41	0.62	0.82

Another limitation is that only very small signals for drug bound to AM2 were observed, despite the high concentrations added and clear shifts in the oligomeric state distribution induced by drug binding. The lack of signal from bound drug is likely due to gas-phase dissociation of the drug inside the mass spectrometer, where the activation required to remove the detergent micelle also likely removes the small (151 Da) bound drug. Thus, we cannot comment on whether drug is

Table 4-2: Mass defect values for nanodiscs with different stoichiometries of AM2 that contain 2 × 22044 Da MSP belts with DMPC, DMPG, or DPPC lipids.

AM2 Stoichiometry	DMPC	DMPG	DPPC
0	0.03	0.09	0.09
1	0.44	0.81	0.16
2	0.86	0.51	0.25
3	0.28	0.22	0.34
4	0.70	0.92	0.43
5	0.12	0.63	0.51
6	0.54	0.34	0.60

binding in detergents, only on changes in observed oligomeric state as drug is added. Previous work by Pielak *et al.* suggested that amantadine may not be able to bind to AM2 under certain detergent conditions, such as in DHPC micelles, so detergents may be affecting drug binding. In any case, many AM2 structures have amantadine or an analogous AM2 inhibitor added, and our data suggest that the addition of inhibitors may help stabilize the monodisperse tetramer.[193, 255, 269]

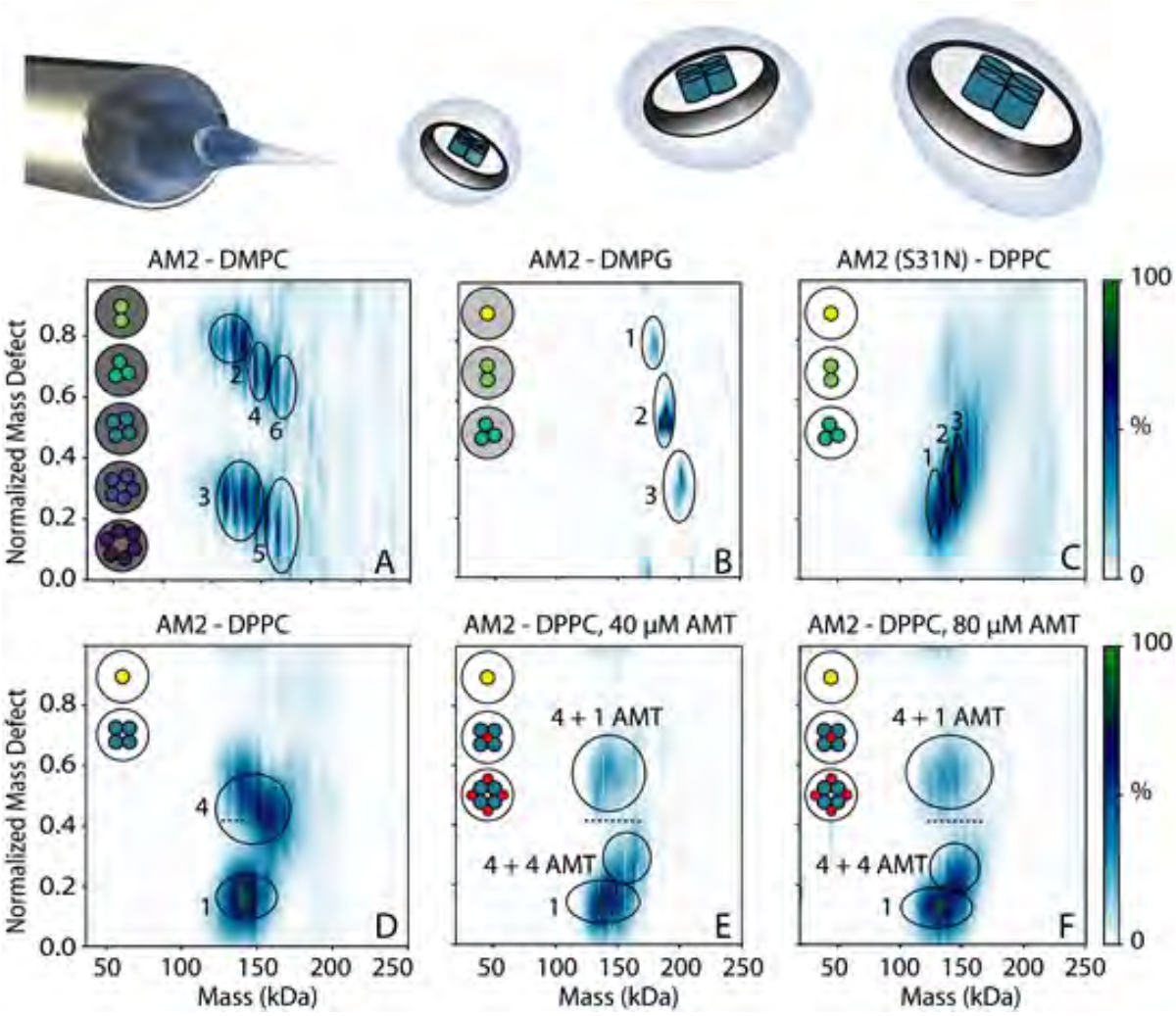

Figure 4-20: Native MS intensities as a function of normalized mass defect versus mass for (all except C) wild type and (C) S31N AM2 in nanodiscs with (A) DMPC, (B) DMPG, (C–F) DPPC lipids. (E) 40 µM and (F) 80 µM amantadine (AMT) were added and shifts of the tetramer from the dashed reference line indicate 1 or 4 AMT bound. Illustrations to the upper left indicate observed stoichiometries, which are circled and annotated. The cartoon shown above shows a schematic of directly ionizing intact AM2 nanodiscs.

4.3.4 AM2 IN NANODISCS SHOWS LIPID SENSITIVITY AND DRUG BINDING

After screening AM2 in a range of detergent and pH conditions, we characterized its oligomerization in lipid bilayers by assembling AM2 into nanodiscs of different lipid types at a 4:1 ratio of AM2 per nanodisc. Using the shifts in the overall mass of the nanodisc measured by native MS, as well as mass defect analysis (Table 4-2), we determined the stoichiometry of AM2 embedded within the intact nanodiscs.[153, 157] We first incorporated AM2 into 1,2-dimyristoyl-*sn*-glycero-3-phosphocholine (DMPC) nanodiscs, which showed AM2 stoichiometries from two through six (Figure 4-20A). We then incorporated AM2 into 1,2-dimyristoyl-*sn*-glycero-3-phosphorylglycerol (DMPG) nanodiscs, which showed less incorporation for the AM2 and only stoichiometries of one, two, or three within the nanodisc (Figure 4-20B). In both lipids, AM2 had a non-selective distribution of oligomers. In contrast, when AM2 was incorporated into 1,2-dipalmitoyl-*sn*-glycero-3-phosphocholine (DPPC) nanodiscs, it incorporated with stoichiometries of only one and four, which shows that AM2 forms specific tetramers in DPPC bilayers under these conditions (Figure 4-20D). The increased oligomeric specificity in DPPC nanodiscs may be due to the increased thickness or saturation of the lipid bilayer.[29, 270]

We next added amantadine to the DPPC nanodiscs and measured drug binding by native MS. Without amantadine, there were two clear mass defect distributions for monomer and tetramer, respectively. Upon adding 40 μM amantadine, the mass defect of the monomer did not shift, confirming that monomeric AM2 did not bind the drug. However, there were clear shifts in the mass defect of nanodiscs with AM2 tetramers. The first shift corresponded to AM2 tetramers with one amantadine bound (Figure 4-20E and Table 4-3). Interestingly, there was also a second shift in the mass defect that corresponded to AM2 tetramer with four amantadine bound. At 80 μM amantadine, the relative intensity of the single-bound state diminished, and the four-bound state

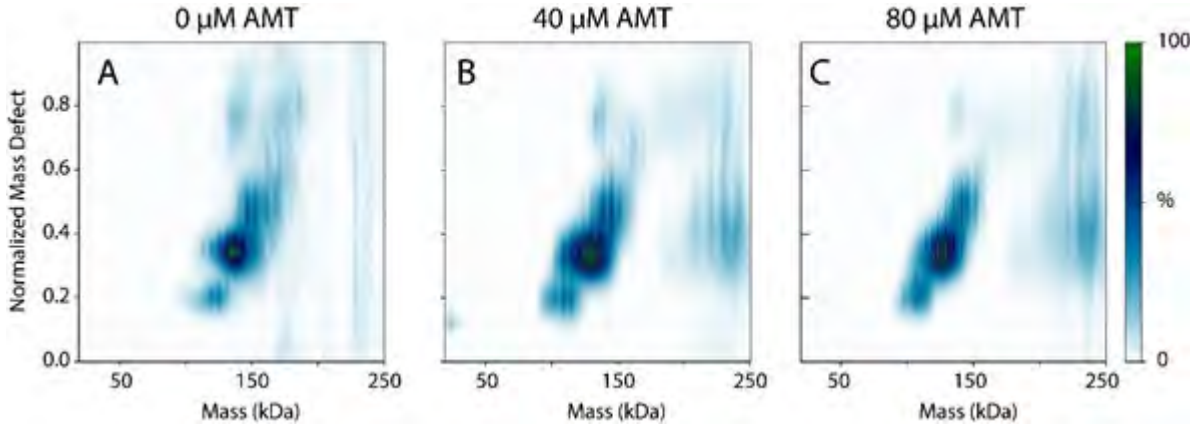

Figure 4-21: Native MS intensities as a function of normalized mass defect versus mass for S31N full-length AM2 in DPPC nanodiscs with (A) 0 µM, (B) 40 µM, and (C) 80 µM amantadine.

became more abundant. DMPC nanodiscs also showed shifts characteristic of drug binding, but the more complex oligomeric state distribution prevented conclusive assignments.

These data agree with existing structures that show AM2 can have one drug bound at lower concentration and four drugs bound at higher concentrations.[193, 271] Specifically, the allosteric binding site located at the helix interface has been previously shown by solution NMR.[193] Surface plasmon resonance experiments further demonstrated the coexistence of pore binding and allosteric binding sites in AM2.[271] Recent high-resolution X-ray crystal structures showed that amantadine binds specifically to the pore of the AM2 channel at a one drug per channel ratio at low drug concentrations.[3] Additionally, at high drug concentrations, rimantadine, an amantadine analog, also binds non-specifically to the AM2 helix interface at a four drug per channel ratio.[271] Overall, our results from native MS are consistent with prior literature describing binding of amantadine to AM2 in first a 1:4 and a 4:4 ratio, with the later more prevalent at high concentration.

To confirm specificity of drug binding, we incorporated drug-resistant AM2 S31N into DPPC nanodiscs (Figure 4-20C). AM2 S31N assembled into DPPC nanodiscs in stoichiometries

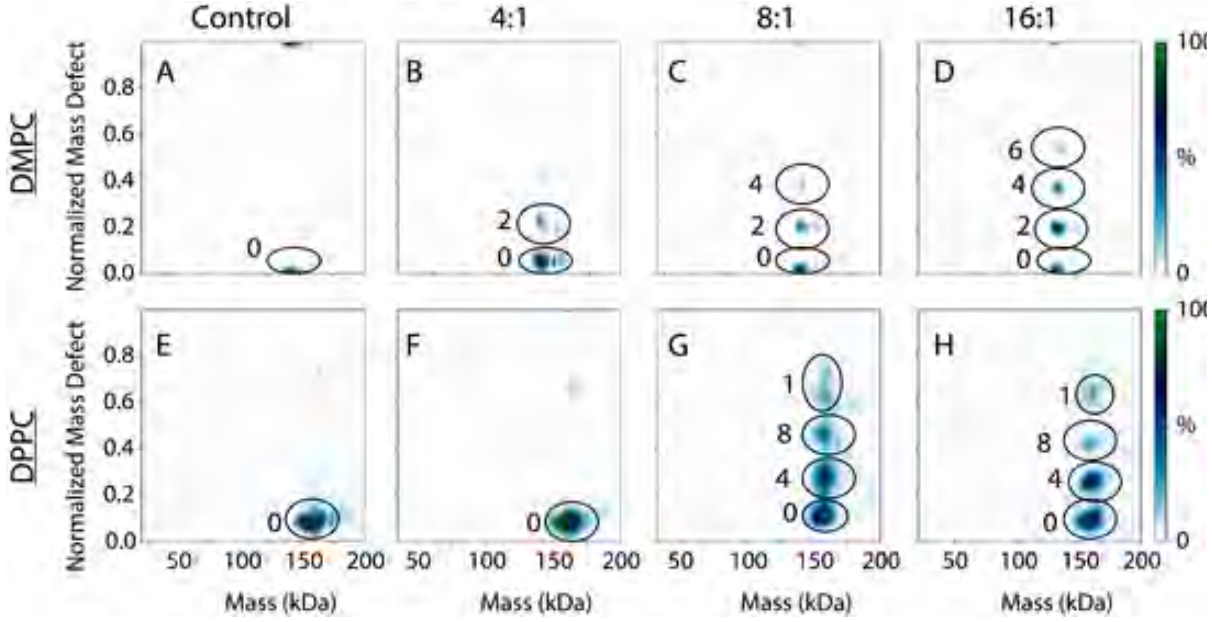

Figure 4-22: Native MS intensities as a function of normalized mass defect versus mass for the WT TM-AM2 in DMPC nanodiscs (A–D) and DPPC nanodiscs (E–H), with no TM-AM2 added (A, E), a 4:1 ratio (B, F), an 8:1 ratio (C, G), and a 16:1 ratio of TM-AM2 to nanodisc.

of one, two, and three, suggesting that the mutant did not form specific complexes. Thus, the oligomerization of AM2 S31N appears to be different from the wild type in nanodiscs (Figures 4-16 and 4-20). Importantly, AM2 S31N nanodiscs did not show any mass defect shifts upon addition of amantadine, confirming specificity of drug binding (Figure 4-21).

4.3.4 AM2 TM Domain Behavior in Nanodiscs

Finally, we investigated the oligomerization of TM-AM2 in lipid nanodiscs by directly adding TM-AM2 to pre-formed nanodiscs. With increasing concentrations of TM-AM2 in DMPC nanodiscs, we measured a mixture of zero, two, four, and six TM-AM2 incorporated into the nanodisc (Figure 4-22 A–D). There have been previous studies of TM-AM2 where has been observed as a dimer of dimers,[250] so it is not surprising that TM-AM2 incorporated in units of two in the nanodisc. Our TM-AM2 results also differed from the more random pattern of incorporation

that we measured with the full-length AM2. The difference between the full-length and TM AM2 reveals that the disordered cytosolic region of the full-length AM2 may influence the oligomerization of AM2 within DMPC lipid bilayers. In contrast, with DPPC nanodiscs, we saw a very similar trend to the full-length AM2 (Figure 4-22 E–H), with TM-AM2 being incorporated in units of four but with a small amount of monomer present.

4.4 DISCUSSION

Here, we used native MS to study the oligomerization of full-length and TM-AM2 in different pH conditions, detergents, lipid bilayers, and with added drug. In nearly all the detergent and pH combinations screened, AM2 had different patterns of oligomerization, which reveals two

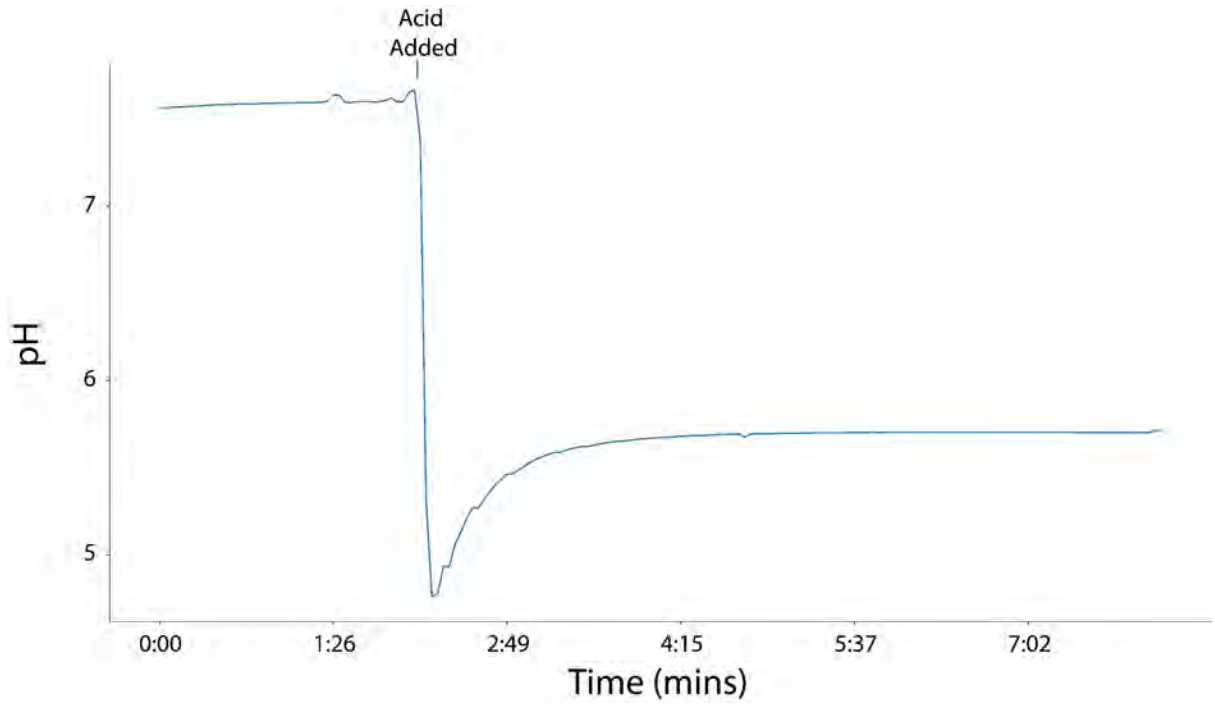

Figure 4-23: Liposomal proton flux assay of WT full-length AM2 embedded within POPC liposomes. The assay was performed by adding acid to the external solution. The pH was measured as protons were transported by full-length AM2 to the interior of the liposome, which increased the pH of the external solution.

key conclusions. First, AM2 is not exclusively a tetramer. Second, AM2 can be sensitive to its chemical environment, showing different oligomeric states in different pH and lipid/detergent conditions. There are two potential interpretations of these surprising results. On one hand, it may be that the tetramer is the true physiological state of AM2. In this case, our results reveal that it can be challenging to capture the pure tetramer in detergent and even some lipid bilayers. Native MS thus reveals conditions that favor or disfavor the true physiological oligomer. For example, AM2 has a strong propensity to form tetramers in DPPC nanodiscs. In contrast, our results with OG and DPC detergents do not show monodisperse tetramer as would be expected from past NMR and AUC studies in these detergents.[3, 7, 255, 257, 272] It could be that differences in protein or detergent concentrations, peptide length, or other experimental conditions caused these discrepancies. Our results generally show more robust tetramer in bilayers over detergents, with drug added, and with the TM peptide over the full-length, so these conditions may favor tetramer. Past research has shown significant changes in structure depending on bilayer/detergent conditions, and these structural changes could go beyond conformation to include changes to the oligomeric state.[250]

However, another interpretation of our results is that the oligomeric states of AM2 are more complex than previously thought. It is very challenging to measure the oligomeric state distribution for small membrane proteins like this, especially if they form polydisperse oligomers.[273] Past studies may have underestimated the true polydispersity due to limitations of the analysis techniques. For example, crystallization could push AM2 to form tetramer complexes or select for conditions where structurally monodisperse tetramers are present. Most X-ray structures of AM2 were collected in LCP, which could favor tetramers.[194, 274, 275] It is challenging to directly measure the oligomeric state distribution for homo-oligomers with NMR without advanced techniques that are not always employed.[276] Furthermore, many structural studies have been conducted in the

presence of high drug concentrations, which may bias the drug towards a monodisperse tetramer, as we saw here (Figure 4-16). Native MS, despite the potential biases outlined above, provides a direct analysis of the oligomeric state distribution of AM2 that could reveal previously unseen oligomers. Past native MS studies have shown similar oligomeric pore-forming proteins, such as the mechanosensitive channel of large conductance (MscL),[115] also form polydisperse oligomeric complexes that are sensitive to the local chemical environment. Conversely, other native MS studies have shown similarly small oligomeric membrane protein complexes to form specific monodisperse oligomers.[277]

These results could present several new hypotheses for AM2 structure and function in a physiological context. First, AM2 is known to be activated by lower pH.[278] Our results in LDAO detergent may suggest that this could be aided by shifts in oligomeric state distribution (Figure 4-6). Other detergents do not show as clear of a shift, but higher oligomers are preferred at lower pH in several different conditions. It may be that AM2 forms smaller oligomers at neutral pH, but acidic conditions in the endosome trigger formation of larger oligomeric pores that cause the influenza virus to fuse with the endosomal membrane and release the nucleic acid cargo for replication.[279]

Our results also suggest that changes in the lipid environment may affect the oligomerization of AM2 (Figure 4-20). DPPC nanodiscs showed specific tetramers whereas DMPC nanodiscs showed less selective complexes. The thickness and fluidity of the lipid bilayer are known to influence AM2 activity, and these functional changes may be due, in part, to changes in the oligomeric state distribution.[270, 280] Different lipid compositions in different intracellular organelle membranes or between different virus strains may contribute to altering AM2 activity.[281]

Finally, our results propose a new potential mechanism of drug activity where the drug may affect oligomerization. It likely still blocks the channel directly or by inducing conformational changes, but it may have the added effect of altering the oligomeric state distribution. Similar effects of AM2 stabilization by drug binding have also been observed in solution and solid-state NMR studies.[255, 282, 283] Clearly, extensive future studies will be required to test all these hypotheses, but our results shed new light on AM2 oligomerization and prompt a fresh perspective on its mechanisms that may extend to other viroporins.

These experiments also mark a technical milestone in using native MS to measure drug binding to a membrane protein in an intact lipid bilayer. High-resolution native MS enabled detection of a 151 Da drug bound to a roughly 150 kDa intact nanodisc complex containing a polydisperse mixture of lipids and AM2. We were able to simultaneously determine the stoichiometry of the bound drug as well as which AM2 oligomer it was binding. Importantly, nanodiscs seemed to better preserve the drug bound complex inside the mass spectrometer than detergent micelles, which were unable to capture much of the bound drug. We suspect that the nanodisc better protects the protein-drug complex by preserving the membrane protein in its surrounding lipid bilayer.

4.5 CONCLUSION

In conclusion, we discovered that AM2 is more polydisperse than previously thought and can be influenced by both the pH and the surrounding membrane environment. In some conditions, AM2 assembles into specific complexes, but others create a dynamic mixture of oligomers. Overall, the application of new analytical approaches revealed unexpected biophysical insights

into the polydispersity and pharmacology of AM2 that may have implications for the structures and functions of other viroporins.

*This chapter was reproduced in party with permissions from Townsend, J.A., Sanders, H.M., Rolland, A.D., et al. Influenza AM2 Channel is Sensitive to Its Chemical Environment. *Anal Chem.* **2021.** 93 (*48*), 16273-16281. Copyright 2021 American Chemical Society. The published version may be found online at https://pubs.acs.org/doi/10.1021/acs.analchem.1c04660. This chapter contains ion mobility data that was collected by Henry Sanders, computational modeling that was collected by Amber Rolland and James Prell, the M2 plasmid was provided by Jun Wang, and guidance for the AUC experiments was provided by Nancy Horton and Chad Park.

CHAPTER 5 DIFFERENCES IN OLIGOMERIZATION OF THE SARS-COV-2 ENVELOPE PROTEIN, POLIOVIRUS VP4, AND HIV VPU

5.1 INTRODUCTION

In Chapter 4, we leveraged native MS to reveal the unexpected polydispersity of M2 from Influenza A,[155] which suggested that other viroporins may also have complex oligomeric behavior. To better understand whether this polydispersity existed in all viroporins, we applied native MS to examine the oligomerization for a wider range of viroporins, including the envelope protein (E protein) from SARS-CoV-2, VP4 from Poliovirus, and viral protein U (Vpu) from HIV. The SARS-CoV-2 E protein is known to self-assemble within bilayers and is believed to specifically transport cations, including K^+, Na^+, and Ca^{2+}.[53, 284] Previous structural work of the transmembrane domain of the E protein suggests that it forms a pentamer.[5] Thus, we used native MS to investigate the oligomerization of the full-length E protein in diverse chemical environments.

Polio VP4 self-assembles to transport RNA during the viral infection cycle.[285] Currently, there is little structural information on VP4, but it is believed that the functional form of VP4 is an oligomer.[286] Previous experiments using chemical crosslinking and SDS-PAGE suggest that VP4 assembles into a hexameric complex.[287] Myristylation of the N-terminus is believed to be important in driving oligomerization and function.[288] However, there are still many questions surrounding the oligomerization of VP4 and how this may be influenced by its environment.

Finally, HIV Vpu is known to self-assemble and selectively transport monovalent cations across the bilayer.[45] There have been several different oligomeric states of Vpu proposed, ranging from dimer to octomer,[289] but Vpu is most commonly described as a pentameric complex.[290-293] However, currently there are no structures of Vpu that have been solved as an oligomeric complex

Table 5-1: The amino acid sequences and monomer molecular weight of all three viroporins analyzed in this study.

Protein	Sequence	Molecular Weight
E Protein	GSMYSFVSEETGTLIVNSVLLFLAFVVFLLVTLAILTALR LCAYCCNIVNVSLVKPTVYVYSRVKNLNSSRVPDLLV	8,475 Da
VP4	SNAMGAQVSSQKVGAHENSNRAYGGSTINYTTINY YRDSASNAASKQDFSQDPSKFTEPIKDVLIKTSPMLN	7,804 Da
Vpu	MQPIQIAIAALVVAIIIAIVVWSIVIIEYRKILRQRKIDRLIDRLIER AEDSGNESEGEISALVEMGVEMGHHAPWDIDDLAENLYFQ	10,026 Da

and very little structural data of the full-length Vpu, even in its monomer form. Thus, there is still some debate around the patterns of oligomerization of the full-length Vpu.[2]

Using native MS, we explored their oligomeric state distribution of the full-length forms of the E protein, VP4, and Vpu in a wide range of chemical environments, including different types of detergent, solution pH, ionic strength, and temperature. We observed a range of specificities in the oligomeric states of these proteins, ranging from the dynamic and polydisperse stoichiometries of Vpu to the more specific dimeric complexes of the E protein. Together, the results reveal diverse patterns of self-assembly of viroporins.

5.2 METHODS

5.2.1 Protein Expression and Purification

E Protein Expression and Purification:

As previously described,[59] he plasmid for the KSI-E protein (UniProt ID: P0DTC4) fusion protein was transformed into C43 *E. coli* cells and grown LB media to an optical density (O.D.) of 0.5–0.6. Overexpression was induced with isopropyl ß-D-1-thiogalactopyranoside (IPTG) at a

final concentration of 1 mM for 3 hours at 37 °C before harvesting cells. Cells were then resuspended in lysis buffer (20 mM HEPES, 500 mM NaCl, pH 7.8). Cells were then lysed using a LM20 Microfluidizer High Sheer Homogenizer. After lysis, Triton X-100 was then added to a final concentration of 1% (v/v) to the lysate and the solution was stirred at room temperature for 1 hour. Lysate was then clarified 48,380×g for 30 minutes at 4 °C. Supernatant was then discarded. The pellet remaining after centrifugation contains inclusion bodies with the protein of interest. This pellet was then resuspended with solubilization buffer (20 mM HEPES, 500 mM NaCl, 1% Fos-choline-16, 1 mM TCEP, pH 7.8) and stirred a room temperature for at least 2 hours, or until the inclusion bodies have been completely solubilized. The solubilized pellet is then centrifuged at 40,000×g for 30 minutes at 15 °C. Supernatant was then filtered.

Prior to purification, a HisTrap HP 5 mL column was equilibrated with 10 column volumes of binding buffer (20 mM HEPES, 500 mM NaCl, 20 mM imidazole, 0.1% Fos-choline-16, pH 7.8). The sample was then loaded to a 5 mL HisTrap HP column *(GE Healthcare)*, then washed with approximately 10–20 column volumes of the binding buffer. Afterwards, the column was washed with another 10–20 column volumes of washing buffer (20 mM HEPES, 500 mM NaCl, 50 mM imidazole, 0.1% Fos-choline-16, pH 7.8). The sample was then eluted from the column with HPC elution buffer (20 mM HEPES, 500 mM NaCl, 500 mM imidazole, 0.1% Fos-choline-16, pH 7.8). Eluted protein was pooled and then dialyzed overnight at room temperature with a 10 kDa membrane for against 4 L of dialysis buffer (20 mM HEPES, 50 mM NaCl, 1 mM EDTA, pH 7.8). The next day, thrombin was added to cleave to fusion protein at a final concentration of 10 U/mg and incubate again overnight.

After the cleavage of the fusion protein, a reverse nickel purification was performed with a HisTrap HP 5 mL column to separate the histidine tagged KSI protein from the E protein. The

column was equilibrated with the binding buffer, and the sample was loaded to the column with the flowthrough collected. The purity of the sample was confirmed with sodium dodecyl sulfate-polyacrylamide gel electrophoresis (SDS-PAGE) and MS. The final sequence and mass of each protein is provided in Table 1.

VP4 Expression and Purification

Polio VP4 (UniProt ID: Q84868) with a TEV-cleavable 10 × His-MBP-tag was overexpressed in T7 Express lysY Competent *E. coli* (High Efficiency). Cells were grown at 37 °C in terrific broth media (Thermo Fisher Scientific) to an O.D. of 0.6–0.8. Overexpression was induced with IPTG at a final concentration of 1 mM for three hours, and cells were harvested by centrifugation. Cells were resuspended in lysis buffer containing 150 mM NaCl, 50 mM Tris, 20 mM imidazole at pH 7.4, and protease inhibitor. After resuspension, cells were lysed as described above. We found that the MBP-VP4 construct was soluble, so no detergent was added until after cleavage of the MBP tag (see below). The lysate was clarified through centrifugation at 25,000×g for 20 minutes. Prior to protein purification, a HisTrap HP 5 ml column (GE Healthcare) was equilibrated with buffer A (150 mM NaCl, 50 mM Tris, 20 mM imidazole at pH 7.4). The sample was then filtered using 0.45 μm PES filter, loaded to the column, and washed with 60 column volumes of buffer A. To remove any nonspecific protein binding, the column was then washed with 30 column volumes of 5% buffer B (150 mM NaCl, 50 mM Tris, 400 mM imidazole at pH 7.4). His-MBP-VP4 was then eluted with 100% buffer B. It was then concentrated using 10k MWCO at 4,000×g for 30 minutes at 4 °C. N-Dodecyl-β-D-maltoside (DDM, Anatrace) 0.025%, 5 mM BME, and 2 mg/ml TEV (1:50 TEV to protein) were added to the concentrated His-MBP-VP4, and the mixture was then transferred into a 2k MWCO dialysis cassette.

After the cleavage of the fusion protein, a reverse nickel purification was performed with a HisTrap HP 5 mL column to separate the histidine tagged MBP from VP4. The column was equilibrated with Buffer A containing 0.025% DDM. The sample was then loaded to the column and the flowthrough of the cleaved VP4 was collected. Residual salts from the protein purification process were removed using a C18 column with a gradient run from HPLC buffer A (0.1% TFA in water) to HPLC buffer B (0.1% TFA in acetonitrile). The final VP4 product was confirmed by SDS-PAGE and MS.

Vpu Expression and Purification:

Full-length Vpu (UniProt ID: P05919) was transformed into pLysY *E. coli* cells and grown in terrific broth to an O.D. of 0.6–0.8. Overexpression was induced with IPTG at a final concentration of 1 mM for 2 hours at 37 °C. Cells were then harvested by centrifugation. Cell pellets were resuspended in a lysis buffer containing 50 mM Tris, 150 mM NaCl, 20 mM imidazole, 0.1% DDM detergent, as well as protease inhibitor. Resuspended cells were stirred at 4 °C for 3–4 hours and then lysed as above. Lysate was then clarified at 48,380×g for 20 minutes. Lysate was clarified using 0.2 μm pore size filter. Prior to protein purification, a HisTrap HP 5 mL column was equilibrated with loading buffer (50 mM Tris, 150 mM NaCl, 20 mM imidazole, and 0.05% DDM, pH 7.4). Sample was then loaded to column and washed with 10–15 column volumes of loading buffer. Nonspecific binding reduced by washing the column with buffer containing 5% elution buffer (50 mM Tris, 150 mM NaCl, 0.4 M imidazole, and 0.025% DDM, pH 7.4). The sample was then eluted from the column with 100% elution buffer. The 10x histidine tag was then cleaved from Vpu by incubating the eluted protein with TEV protease overnight at 4 °C. A reverse nickel purification was performed the next day to remove the TEV and cleaved His tag. Purity of the sample was confirmed with SDS-PAGE and MS.

5.2.2 Mass Spectrometry Sample Preparation

A series of ammonium acetate solutions were prepared for native MS. All solutions were prepared at a concentration of 0.2 M ammonium acetate, unless stated otherwise. The pH of solutions was adjusted to 5, 7, and 9 using acetatic acid or ammonium hydroxide. Detergents lauryldimethylamine-N-oxide (LDAO), tetraethylene glycol monooctyl ether (C8E4), dodecylphosphorylcholine (DPC) were purchased from Anatrace. Triton X-100, which was purchased from Sigma Aldrich. All solutions were prepared by adding twice the critical micelle concentration (CMC) of the detergent, unless stated otherwise. Viroporins were exchanged into each of these ammonium acetate solutions using BioSpin 6 columns (Bio-Rad) and diluted to a final protein concentration of 20 μM (per monomer) for the E Protein, Vpu, and VP4. Buffer exchanged protein samples were allowed to equilibriate at room temperature for several minutes prior to analysis, but no change was observed over time.

5.2.3 Native Mass Spectrometry

All native MS experiments were performed using a Q-Exactive HF Orbitrap (Thermo Scientific) mass spectromter that has ultrahigh mass range modifications as previously described.[155] Nano-electrospray ionization was performed using homemade borrosillicate needles that were pulled with a P-1000 micropipette puller (Sutter Instruments).

Viroporin samples were ionized in positive ion mode with a spray voltage of 1.1−1.5 kV. E Protein and Vpu samples were analyzed with a range of 2,000−10,000 *m/z*. The trapping gas pressure within the mass spectrometer was set to 3. Activation with 50 V of higher-energy collisional dissociation (HCD) energy was applied. To aid in the desolvation of samples, 10−50 V of source fragmentation were also applied to each sample. VP4 samples were analyzed with a

range of 500–4,000 *m/z* at a resolution setting of 240,000. All mass spectrometry data was collected in triplicate. Spectra are shown for a single representative replicate.

The native mass spectra for viroporins in detergent were deconvolved using UniDec as previously described.[155, 183] The settings for deconvolution of viroporins in all detergent conditions included the application of a curved background subtraction of 10, a mass range of 1,000−70,000 Da, a charge range of 1−50, and a FWHM of 1 *m/z.*

5.2.4 Functional Studies

Material and reagents

$CaCl_2 \cdot 2H_2O$, 2-[4-(2-hydroxyethyl) piperazin-1-yl]ethanesulfonic acid (HEPES), toluene, and acetone were purchased from Fisher Scientific. NaCl was purchased from EMD Millipore. HNO_3 was purchased from Macron. Cholesterol was purchased from Sigma Aldrich. (Tridecafluoro-1,1,2,2-tetrahydrooctyl)dimethylchlorosilane (PFDCS) was purchased from Gelest, Inc. 1,2-Dioleoyl-*sn*-glycero-3-phosphocholine (DOPC), 1-palmitoyl-2-oleoyl-*sn*-glycero-3-phosphocholine (POPC), and 1,2-diphytanoyl-*sn*-glycero-3-phosphocholine (DPhPC) were purchased from Avanti Polar Lipids. Borosilicate glass capillaries were purchased from World Precision Instruments.

Pipet aperture fabrication and black lipid membrane (BLM) formation.

The pipet apertures were prepared from 1.5 mm O.D., 1.0 mm I.D. borosilicate glass capillaries. Cleaned capillaries were pulled with a Sutter P-97 puller. To prepare a ~10 μm aperture and a rounded orifice geometry, the tapers of the glass pipets were cut and fire polished with a Narishige MF-900 microforge. Subsequently, the apertures were surface modified with PFDCS,

following a previously established gas phase silanization protocol.[294] Silanized pipets were rinsed and dried before use.

DOPC, POPC, and DPhPC lipids dissolved in chloroform were dried under a gentle stream of argon and lyophilized overnight. Immediately before using, the lyophilized lipids were resuspended in *n*-decane. BLMs were formed following a previously established tip-dip technique.[295] Briefly, the tip of the aperture was moved across the interfaces of air, 10 mg/mL resuspended lipids in *n*-decane, and the recording buffers. Formed BLMs across the apertures were kept submerged in the buffer to reconstitute the viroporins.

Current and membrane conductance characterization

The recording buffer composition of the recording bath was consistent for current recordings and membrane conductance measurements (0.5 M NaCl and 2.5 mM HEPES, pH 7.0). To test the selectivity on the transported ion, calcium buffer was also prepared but with other compositions controlled (0.5 M $CaCl_2$ and 2.5 mM HEPES, pH 7.0). Single channel recordings (SCRs) were conducted under voltage bias (-70 mV) and were presented after filtered at 500 Hz. Membrane conductance was measured with a previously established protocol. Briefly, the mean current from 21 different membrane potential states was recorded independently and the conductance was calculated from the I-V correlations.

5.3 RESULTS AND DISCUSSION

Here, we investigated three viroporins—the E protein from SARS-CoV-2, VP4 from Polio, and Vpu from HIV—in a wide range of chemical environments to try to better understand the patterns of oligomerization of this class of proteins. The chemical environment was altered by changing the solution conditions of the protein prior to ionization (Figure 5-1A). Native mass spectrometry was performed on each sample (Figure 5-1B), and we then deconvolved this data (Figure 5-1C) to determine the relative intensities of different oligomeric states (Figure 5-1D). The

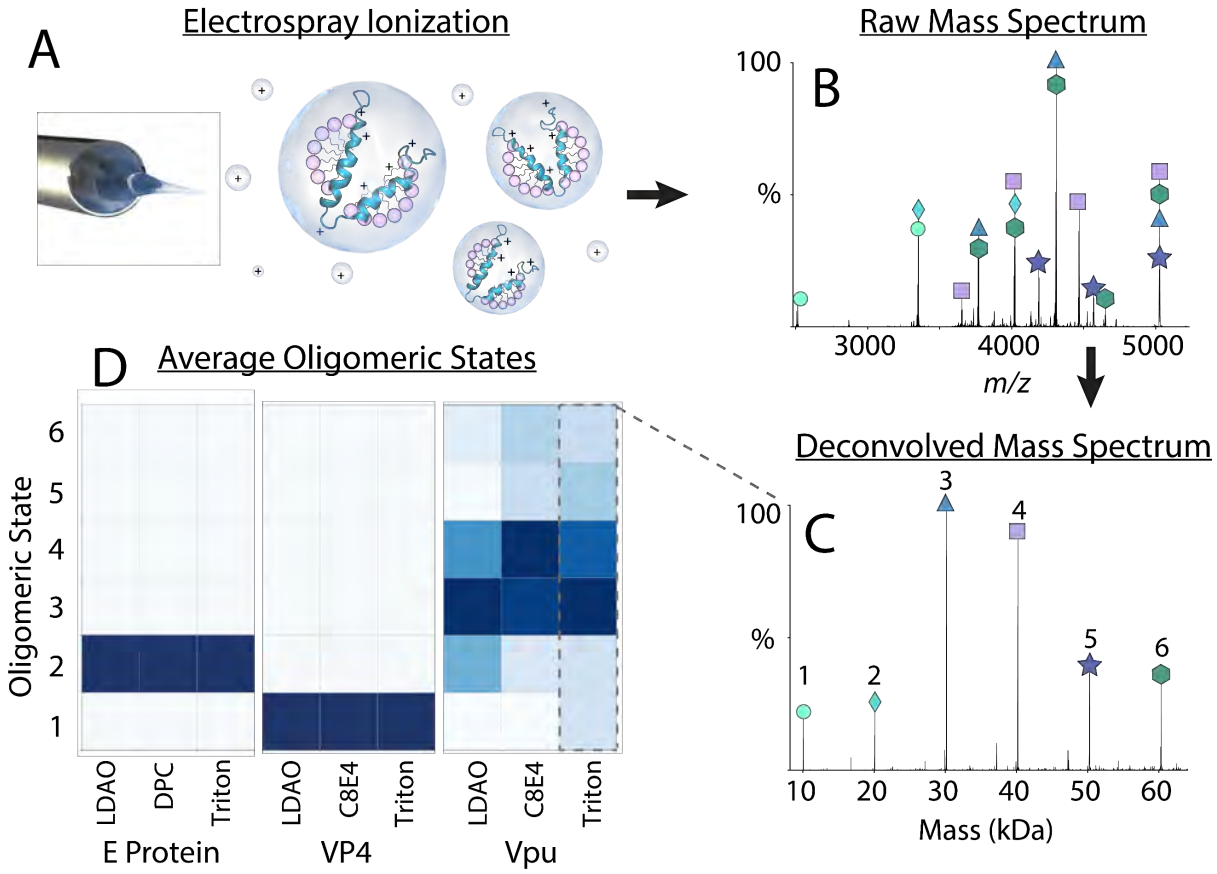

Figure 5-17: Workflow illustrating the process of studying the oligomeric states of viroporins in varied detergents. Electrospray ionization (A) is performed on the protein in detergent, yielding a raw mass spectrum of the sample (B), which is deconvolved into a zero-charge mass spectrum (C). The resulting peak intensities for different oligomers across different proteins and detergent conditions are averaged and displayed on a grid plot (D).

oligomeric state of the protein was determined by dividing the measured complex mass by the mass of the monomeric unit (shown in Table 5-1). Due to differences in ionization efficiency[296] and ion transmission,[297, 298] the native MS intensities do not necessarily directly mirror the concentration of each oligomer species in solution, but the distrubution in native MS signal intensities provide a qualitative picture of the oligomeric states present. Screening the oligomeric states of viroporins in a variety of different chemical conditions can provide insight on the structure and interactions of these viroporins.

5.3.1 SARS-CoV-2 E Protein

First, we performed native MS on the E protein in several different detergent conditions. For these initial experiments, we added twice the CMC of each detergent. We discovered that the E protein assembled exclusively as a dimer in LDAO, DPC, and Triton X-100 detergents (Figure 5-1D). Under all these detergent conditions, we observed residual Fos-Choline-16 detergents from the initial protein purification bound to the E protein. Together, this data indicates that the E protein forms specific dimers in these conditions instead of the expected pentamer.

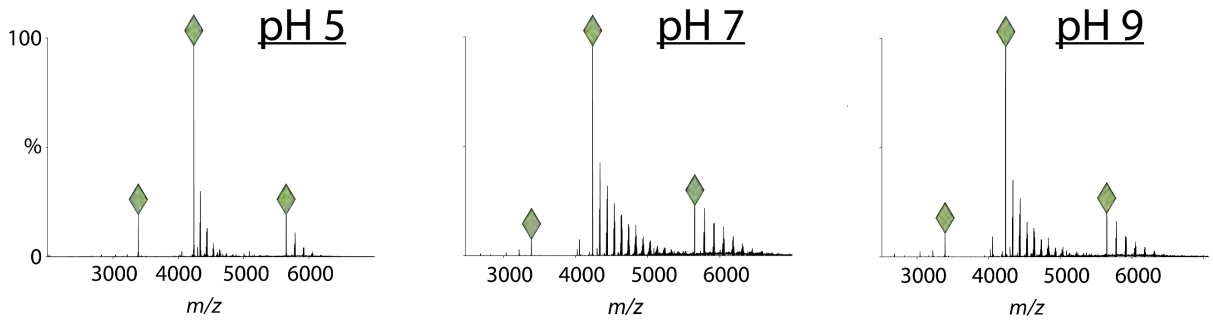

Figure 5-18: Representative raw mass spectra of the E protein in 0.2 M ammonium acetate solution with pH 5, 7, and 9 and LDAO detergent. The additional peaks in each spectrum correspond to Fos-Choline-16 detergents from the initial purification that that remained bound through the buffer exchange.

Next, we tested the influence of solution pH on the oligomeric state of the E Protein. We analyzed the E protein at pH values of 5, 7, and 9. The pH of the solution did not influence E protein oligomerization (Figure 5-2), and only dimer was observed in all conditions. Because the E protein has three cysteine residues, we also compared the E protein in both reducing and non-reducing conditions at neutral pH. Under both reducing and non-reducing conditions, the E protein was only a dimer.

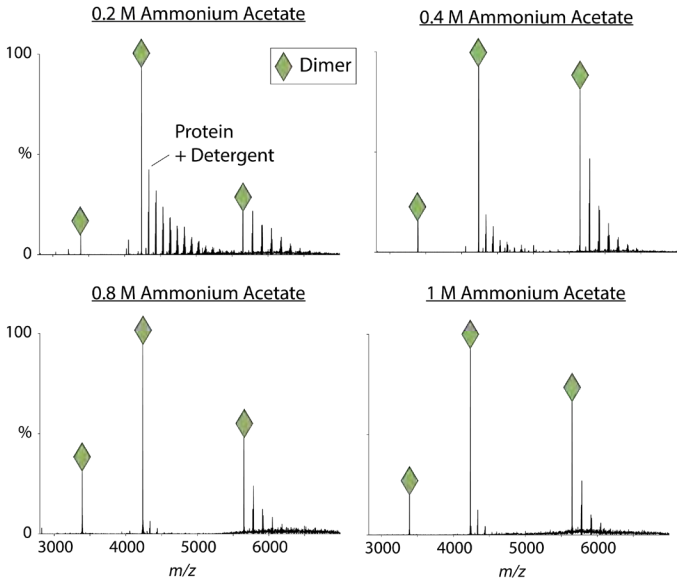

Figure 5-3: Representative raw mass spectra of the E protein solutions with LDAO and varying concentrations of ammonium acetate (labeled above). The additional peaks in each spectrum correspond to Fos-Choline-16 detergents from the initial purification that that remained bound through the buffer exchange.

We also investigated the influence of ionic strength on oligomerization. We did not measure any difference in the oligomeric state in the E protein under lower (0.05 M ammonium acetate) or higher (up to 1 M ammonium acetate) ionic strength conditions. However, the number of adducted Fos-Choline-16 detergents on the protein diminished under higher ionic strength conditions (Figure 5-3). This higher concentration of ions likely outcompetes the adducted Fos-Choline-16. Importantly, because the adducted Fos-Choline-16 could be almost fully removed without disrupting the dimer, these experiments suggest that the residual Fos-Choline-16 was not likely driving dimer formation.

Next, we investigated the effect of detergent concentration on the oligomerization of the E protein by adjusting the concentration of LDAO from 0.5 –2×CMC. At lower detergent concentrations, we discovered a small peak that corresponded to the mass for the E protein as a trimer, as shown in Figure 5-4. This E protein trimer was not measured under any other conditions tested. Thus, lower concentrations of detergent can affect oligomerization of the E protein, which may indicate the lower levels of lipid per protein would affect its oligomeric state in bilayers.

To test the stability of this E protein dimer, we increased the solution temperature on the sample with a variable temperature source.[299] The temperatures applied ranged from 15–55 °C, with 10 °C steps. The E protein dimer was present during these temperature ramps at lower temperatures. However, the peak for the dimer became less abundant relative to small detergent clusters at 45 °C, and the dimer was no longer present the 55 °C and above (Figure 5-5). Interestingly, a clear signal for the monomer did not appear at these higher temperatures where the dimer was less abundant. Instead, the signal for the E protein disappeared altogether, which suggests that the unstable monomer might aggregate at these temperatures.

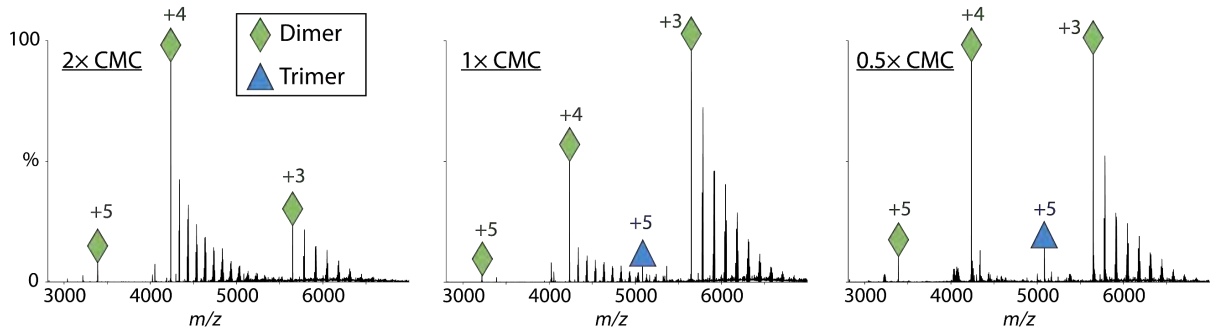

Figure 5-4: Representative raw mass spectra of the E protein 0.2 M ammonium acetate with varying concentrations of LDAO detergent. The CMC of LDAO is 0.025%. Additional detergents bound to the protein in each spectrum are Fos-Choline-16 detergents, residual from the initial protein purification.

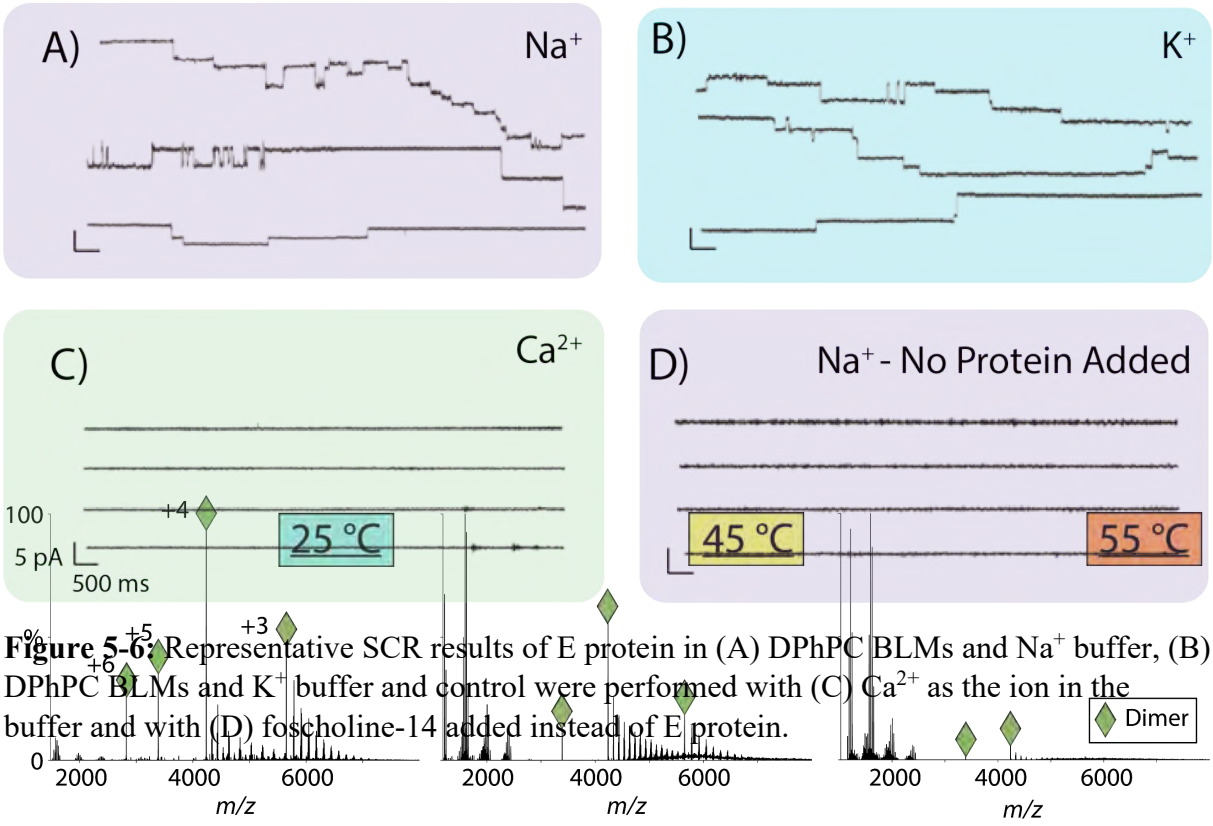

Figure 5-6: Representative SCR results of E protein in (A) DPhPC BLMs and Na^+ buffer, (B) DPhPC BLMs and K^+ buffer and control were performed with (C) Ca^{2+} as the ion in the buffer and with (D) foscholine-14 added instead of E protein.

Figure 5-5: Representative raw mass spectra of the E protein solubilized in 0.2 M ammonium acetate and 0.05% LDAO detergent. The spectra shown show the E protein with the solution temperature at 25, 45, and 55 °C. The charge states of the E protein are labeled under the 25 °C condition. The additional peaks in each spectrum correspond to Fos-Choline-16 detergents from the initial purification that that remained bound through the buffer exchange.

To validate the activity of the E protein, we also performed electrophysiology studies. These studies were performed using single channel recording under a controlled holding potential of -70 mV. The E protein exhibited flux activity with both Na^+ and K^+ ions (Figure 5-6A and B), but different step magnitudes were observed throughout the measurement. The predominant magnitudes of step changes in current were observed to be ~1, 2, 3, and 7 pA in BLMs with DPhPC. These differences in step magnitudes suggested that the E protein may form channels of different stoichiometries. Additionally, solutions containing Ca^{2+} instead of Na^+ or K^+ did not appear to have ion flux activity (Figure 5-6C). As a control, the same experiment was also

performed with just Fos-choline-16 added to the bilayer, which is the same buffer that the E protein was solubilized in prior to being incorporated in the bilayer. There was not any ion conductance measured upon adding this detergent to the bilayer at the same concentration (Figure 5-6D), which indicates that the ion conductance is due to the transport of ions from the E protein.

Previous structural work of the E protein proposed that it assembles into a pentameric structure.[57] However, the full-length E protein assembled nearly exclusively into dimers under all detergent conditions tested with native MS (Figure 5-1 and 5-4). The only conditions where oligomers besides dimer were measured for the E protein were in solutions that contained lower concentrations of detergent than the CMC, where low intensities of trimer were measured (Figure 5-5). Past structures of the E protein pentamer were solved using NMR with the E protein reconstituted into lipid bilayers. However, the protein-to-lipid ratio in these samples is much lower than physiological ratios,[300] which has the potential to drive the assembly of oligomers. These higher oligomers could be Driven by similar effects as the trimer we observed at low detergent concentrations (Figure 5-5). It is also possible that a lipid environment is necessary to drive the E protein to assemble into a pentamer.

Although we detected a monodisperse dimer, ion conductance experiments performed on E protein suggested more polydisperse oligomers, due to the differences in magnitudes of steps in conductance across the bilayer (Figure 5-6). The discrepancies between the native MS results and electrophysiology results may reveal that the detergents selected may not be an appropriate mimetic for the E protein and might not reflect the variety of oligomeric states that could be present in a natural lipid bilayer. Conversely, if the dimer is the functional form of the E protein, this raises two possible mechanisms , 1) that the E protein is able to transport ions in its dimeric form and that this dimer is able to have multiple conductance states, or 2) that the E protein dimers could be

transient and function more as a carpet model rather than a more traditional ion channel, allowing for multiple conductance states.[301] The behavior of the E protein is complex and will require further investigation to better understand the relationship between its oligomerization and ion channel function.

5.3.2 Polio VP4

Next, we used native MS to investigate the oligomeric states of polio VP4 in a range of chemical environments. Parameters including detergent type, detergent concentration, ionic strength, and solution pH were all screened. Across all the conditions screened, VP4 was a monomer, as shown in Figure 5-7. This lack of oligomerization is unlike any of the other viroporins characterized with native MS, which all oligomerized in detergents.

Prior studies demonstrated that VP4 oligomerizes and transports RNA across the cell membrane.[285] VP4 is known to be myristoylated on its N-terminal side, and myristylation drives faster assembly of oligomers than unmodified protomers.[302] Our studies revealed that the un-myristoylated form of VP4 does not assemble oligomers in detergent. Additionally, VP4 is known to participate in a variety of protein-protein interactions throughout the viral infection cycle, and

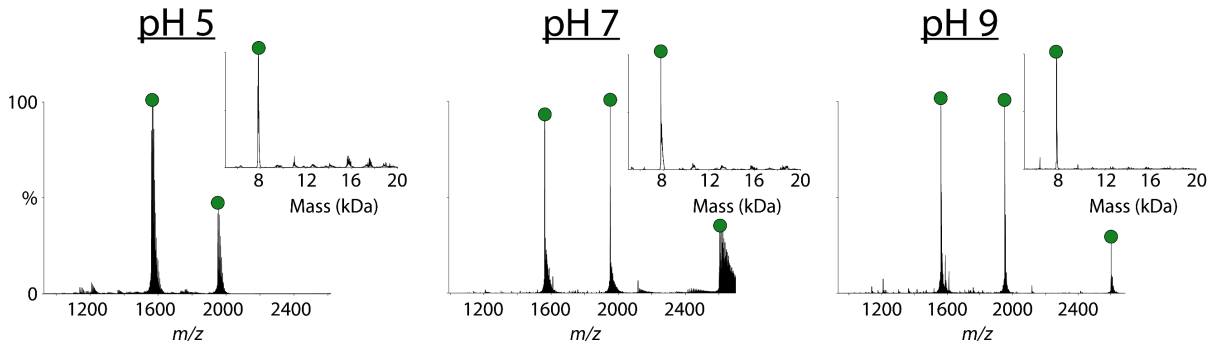

Figure 5-7: Representative native raw mass spectra of VP4 that has been buffer exchanged into solutions containing 0.2 M ammonium acetate and C8E4 detergent that are pH 5, 7, and 9. The deconvolved mass spectra are inset.

it is possible that some of these other accessory proteins may be necessary for oligomerization.[303] Future experiments with the myristoylated proteoform of VP4 will be necessary to better understand these processes, but our results show no oligomerization of the unmodified protein.

5.3.3 HIV-Vpu

Finally, we used native MS to study HIV Vpu oligomerization in different chemical environments. We first tested how Vpu was influenced by the type of detergent used (Figure 5-8). When Vpu was solubilized in tetraethylene glycol monooctyl ether (C8E4) detergent, we observed a mix of oligomers ranging from dimer to hexamer (Figure 5-8A). Similarly, in Triton X-100 detergent, we measured oligomers of monomer through hexamer (Figure 5-8B). However, in LDAO detergent, we observed fewer oligomers, detecting only monomer, dimer, and trimer (Figure 5-8C).

Interestingly, although we measured a range of oligomers in all three detergent conditions screened, the oligomeric state profile of Vpu was not significantly influenced by the concentration

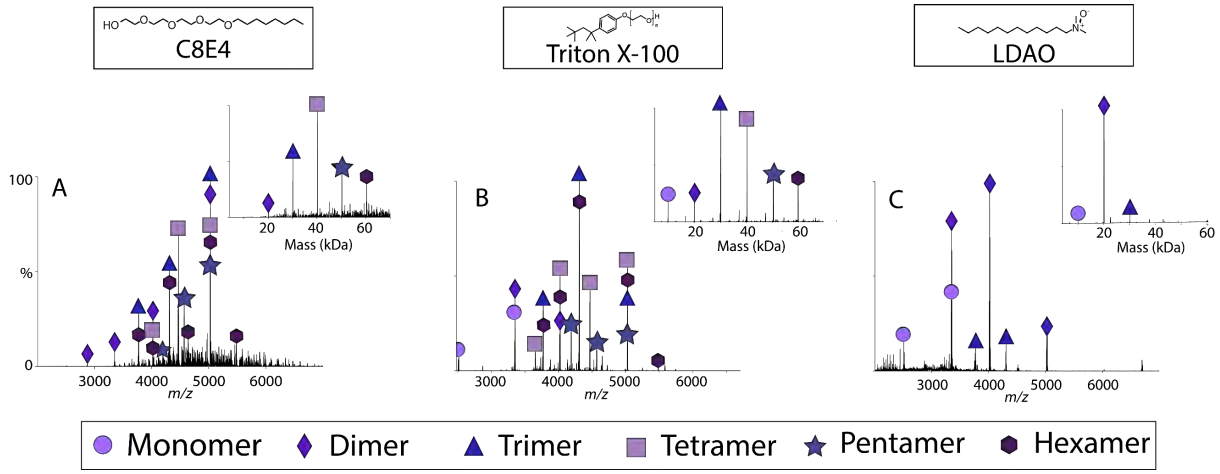

Figure 5-8: Representative native raw mass spectra of Vpu that has been solubilized in 0.2 M ammonium acetate with (A) C8E4 detergent, (B)Triton X-100 detergent, and (C) LDAO detergent. The deconvolved spectra of each condition are inset, and oligomeric states are annotated with shapes.

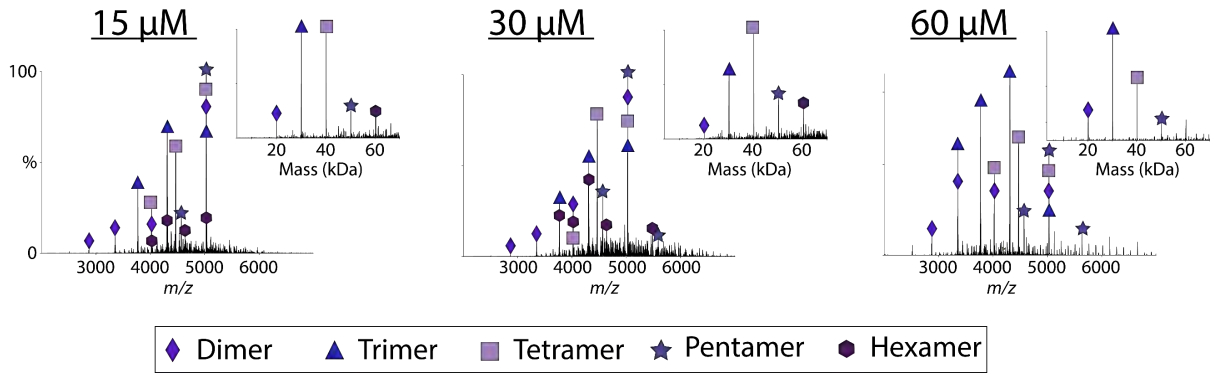

Figure 5-9: Representative native raw mass spectra of Vpu in 0.2 M ammonium acetate and C8E4 where the concentration of protein monomer is at 15, 30, and 60 µM. The deconvolved mass spectra are inset.

of the protein in solution in these conditions. In each of the detergents used, we screened the protein in concentrations of 60, 30, and 15 µM, and the oligomeric state profile did not significantly vary across these protein concentrations (Figure 5-9). We also characterized the oligomeric state of Vpu in a range of solution pH conditions. In LDAO detergent at pH values of 5, 7, and 9, the oligomeric state of Vpu was very similar, as shown in Figure 5-10. Thus, Vpu oligomerization is not significantly influenced by protein concentration or changes in the solution pH.

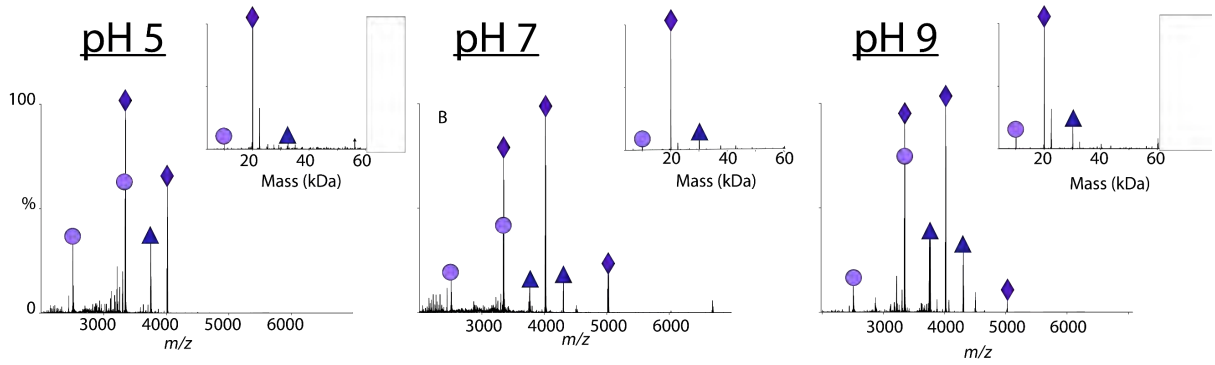

Figure 5-10: Representative native raw mass spectra of Vpu in 0.2 M ammonium acetate and LDAO where the solution pH is 5, 7, and 9. The deconvolved mass spectra are inset.

To validate the activity of the Vpu while in a bilayer, we performed electrophysiology assays of Vpu embedded in BLM's. We first embedded Vpu in BLM's made up of POPC, DOPC, and DPhPC lipids (Figure 5-11A–C). Under the controlled membrane potential (-70 mV), the magnitude of current step changes indicates Na^+ fluxes exhibited a minimum increment of ~1.5 pA. The other two predominant magnitudes of the current step changes were ~2.5 and ~5 pA, which were consistent from all tested membrane compositions (Figure 5-11A). This result suggested that the Vpu channels had more than one pore stoichiometry. Also, the same predominant step magnitudes indicated that the lipids that were tested had limited effects on the ion permeability of Vpu.

To probe specificity of Vpu ion transport, electrophysiology assays were also performed using buffer containing Ca^{2+} ions instead of Na^+. Under these conditions, Vpu did not transport Ca^{2+} ions across the bilayer (Figure 5-11B). Controls were also performed where DDM detergent was added directly to the bilayers

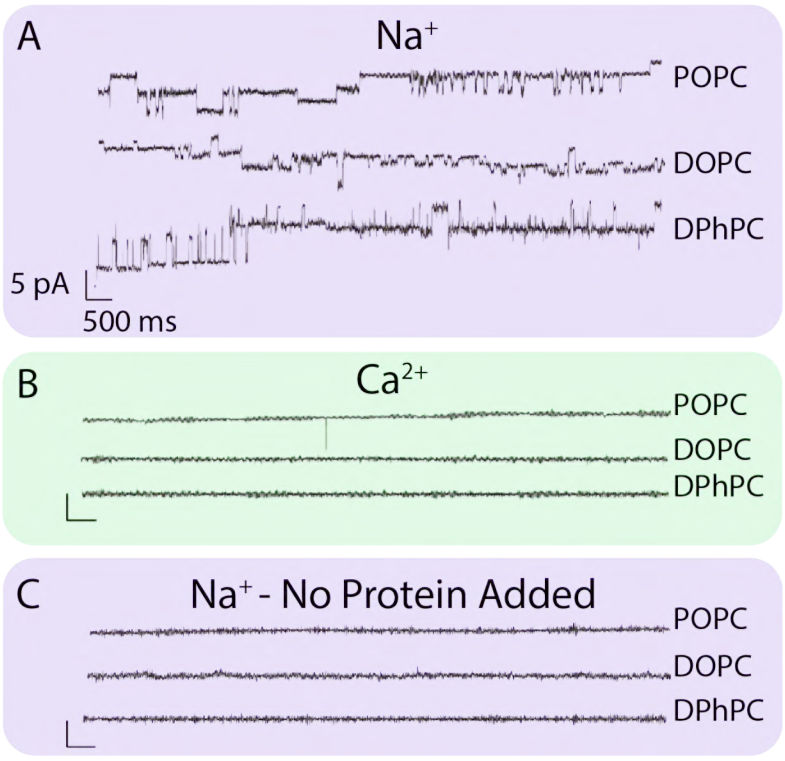

Figure 5-11: Representative SCR results of Vpu embedded in bilayers made of POPC, DOPC, and DPhPC with A) Na+ and B) Ca2+ buffer. As a control, C) DDM detergent was added instead without Vpu to a bilayer with Na+ buffer.

Table 5-2: Table summarizing the trends in oligomerization and behavior across each of the three viroporins characterized with native MS above.

	E Protein	VP4	Vpu
Average Oligomeric State	Dimer	Monomer	Varied
Substrate	Na^+/K^+	RNA	Na^+/K^+
Influenced by Detergent Type?	X	X	✓
Influenced by Detergent Concentration?	✓	X	-
Influenced by Protein Concentration?	X	X	X

instead of Vpu (Figure 5-11C). No ion flux was detected in these assays without the addition of Vpu.

Overall, the oligomerization of Vpu appears to be polydisperse and dynamic. A range of oligomers were measured for this protein, and these varied oligomeric states are influenced by the detergent environment. The electrophysiology data of Vpu (Figure 5-11) reveals different step magnitudes for the flux of monovalent cations, which supports the existence of multiple oligomeric states of Vpu.

Vpu exhibited the most complex and polydisperse behavior of the three viroporins investigated here. Vpu assembled into oligomers that varied between different detergent environments, as shown in Figure 5-8. Within the literature on Vpu, there is still ongoing debate on its oligomeric state.[41, 44, 45, 304, 305] There is currently no structural information of the full length Vpu forming an oligomeric complex, but there has been one structure solved of full-length Vpu in its monomeric form.[2, 47, 48] Some previous studies have suggested that Vpu assembles into fixed pentameric complexes,[306] whereas other studies found that Vpu assembles into a broader range of oligomers.[289, 307-309] Interestingly, some previous studies suggested that higher solution ionic strengths droved Vpu to assemble into large oligomeric complexes.[307] Additionally, the

electrophysiology assays performed revealed that single channels Vpu had different magnitudes of ion current across the bilayer (Figure 5-11A–C). These results suggested that Vpu ion transport behavior is more varied than those of a binary ON/OFF state of canonical ion channels.[310] Thus, Vpu may form ion channels of different stoichiometries. We hypothesized that these larger channels may exist to enable the transport of larger cations, such as Ca^{2+}. However, when the membranes containing Vpu were surrounded by a buffer containing Ca^{2+} instead of Na^{+}, no ion conductance was measured. It is possible that these varied oligomers are all specific monovalent cation channels. Further studies will be necessary to better understand the physiological roles of the different oligomers of Vpu.

5.3.4 Comparison of Viroporins

Most of the literature on viroporins suggests that they oligomerize into channels within the lipid bilayer.[23, 28] Influenza A M2 is the best characterized viroporin to date, and most literature suggests that it forms a specific tetrameric complex.[10, 35, 192, 311] However, native MS performed on M2 in a range of chemical environments, including varied solution pH, different detergents, and a range of different lipid environments revealed a variety of oligomers of M2 that had been previously undetected, as discussed in depth in Chapter 4.[155] This study raised the question of whether other viroporins from other viruses may also have more varied oligomers and more complexity than initially thought.

We used native MS to study the oligomerization of three different full-length viroporins, the E protein, Vpu, and VP4. We investigated the patterns of oligomerization of these viroporins in different chemical environments, including a range of different detergents, pH conditions, and ionic strength conditions (Table 5-2). These experiments revealed that the patterns of

oligomerization varied widely across proteins, with the E protein forming stable dimers, VP4 remaining monomeric, and Vpu exhibiting highly dynamic behaviors that varied across detergents, as shown in Figure 12. Many of these oligomers had not previously been detected for these viroporins.

Our results vary in how they compare with the existing literature on these viroporins. For example, the native MS data on Vpu somewhat agrees with earlier studies. Applying a wide range of analytical tools, Lu et al reported oligomers of various sizes, ranging from monomer through octamer for the transmembrane domain of Vpu.[289] This largely supports the behavior we observed for Vpu (Figures 5-8–5-10).

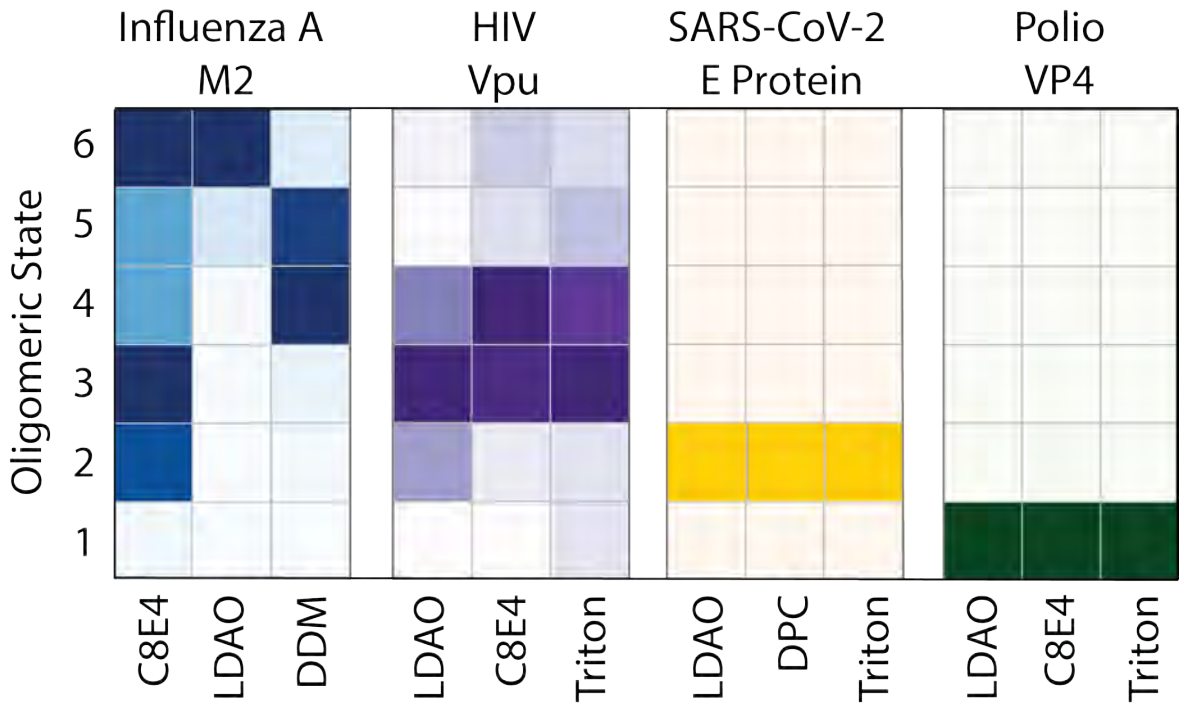

Figure 5-12: Grid showing the average oligomeric state intensities, ranging from monomer through hexamer, of viroporins M2, Vpu, E Protein, and VP4 in different types of detergent. The darker the color shown, the higher the abundance of that oligomer.

In contrast, our results disagree with most of the literature for the E protein and M2. Prior studies of both the E protein and M2 indicate that both proteins assemble into monodisperse oligomers, suggesting that M2 assembles into strictly a tetramer[3, 312] and the E protein into a pentamer.[5] However, our results with native MS reveal a previously undetected polydispersity for M2[155] and the assembly of a specific dimer for the E protein (Figures 5-2–5-5). These results are fundamentally different from the reported behavior for both M2 and E protein.

Given how many of our results differed from the literature, we wanted to rule out the possibility of experimental bias. One potential artifact of this analysis could be that native MS could be artificially generating oligomers that were not truly there in the sample. However, this was unlikely because under identical experimental conditions to the other viroporins tested, we only measured VP4 in its monomeric form. Another potential artifact is that native MS could potentially disrupt or break apart specific oligomers. This also seemed to be unlikely because we measured the E protein as a highly specific dimer. A final potential artifact could be that native MS was biasing our results, only allowing us to detect certain oligomer species. However, this artifact is also unrealistic because we were able to measure Vpu as a wide range of oligomers.

Having ruled out these possible artifacts, this left two possible interpretations of our results. The first interpretation is that these results may reveal the potential biases surrounding the use of different detergents in the analysis of membrane proteins, in which case the physiological oligomeric state of these viroporins may be very different from what we have measured here. In this case, this work emphasizes the need to carefully select membrane mimetics in the analysis of membrane proteins to avoid potential artifacts.[67, 78, 313]

Another possible interpretation of these results is that the oligomerization of viroporins may be more dynamic than previously thought. Most of the literature surrounding viroporins suggests that they assemble into these fixed complexes and that these monodisperse assemblies are the only physiological form.[5, 22, 37, 290, 314] However, most viruses genetically encode a relatively small number of proteins. Due to their small genome size,[315] as well as high mutation rates and frequently changing environmental fitness conditions,[316] each viral protein may play a variety of roles in the viral life cycle,[20] which can be done by creating small protein units that can self-assemble and form different oligomers that can carry out different biochemical functions.[317, 318] It is possible that viroporins may assemble into a range of oligomeric states to carry out these different functions, and that different chemical environments may trigger oligomer formation. These studies differed from previous structural investigations of viroporins because the full-length construct was used, as opposed to the transmembrane domain used in many previous viroporin studies, which may explain some of the different oligomeric states measured here.[319]

The differences In these results from the literature could be attributed to the analytical challenges associated with studying the oligomeric state of small membrane proteins, especially in instances where these proteins may assemble into polydisperse mixture of oligomers.[23] It is possible that many earlier studies underestimated the complexity of some of these proteins. Most of the earlier structural work on viroporins has been performed either with coupling cross-linking with SDS-PAGE or with NMR, which is limited in its ability to determine the oligomeric state of homo-oligomeric proteins without additional advanced techniques that are not always performed.[42, 90, 320-323] Additionally, with NMR, low concentrations of detergent and high concentrations of protein are often used, which can drive nonspecific oligomers.[324, 325] Conversely,

a unique advantage of native MS is that it allows for the direct measurement of the polydisperse oligomeric state distribution of viroporins.

These experiments reveal a previously underexplored differences in the behavior of viroporin complexes. Among the viroporins characterized here, there are few similarities. This includes little sequence or structural homology and highly varied patterns in oligomerization. It is possible that many of these novel oligomeric states have their own underexplored biochemical function. Overall, these results indicate that viroporins are far more diverse than previously thought.

5.4 CONCLUSION

In conclusion, we uncovered the oligomeric states of viroporins E protein, VP4, and Vpu. The behavior of these proteins varied widely, with the E protein forming dimers, VP4 not oligomerizing at all, and Vpu forming polydisperse and dynamic oligomers. Many of these oligomeric states have not been previously reported. The characterization of these viroporins may allow for a better understanding of virus biochemistry and the development of therapeutics in the future.

*This chapter includes data on VP4 that was expressed, purified, and analyzed by Oluwaseun Fapohunda. Michael Taylor and his laboratory members aided in the purification of VP4. This chapter also includes electrophysiology activity assays that were performed by Zhihan Wang and Craig Aspinwall. Brian Kloss aided in expression screening and plasmid design for viroporins Vpu and VP4. Sang Ho Park, and Stanley Opella also provided the E protein plasmid and aided in the development of a purification protocol for the E protein.

CHAPTER 6 CONCLUSIONS AND FUTURE DIRECTIONS

6.1 CONCLUSIONS

Viral infections pose a serious risk to human health globally because of the current lack of effective treatments against viral infections. [326,327] There are a variety of analytical challenges associated with studying viral proteins, as well as designing specific compounds to target viral proteins. Many antiviral compounds are designed to target proteases within the virus.[328] These proteases play important roles in the virus, as many viruses express one long single polypeptide chain that is then cleaved into its individual proteins by a viral protease.[329] Although targeting this main protease can be initially effective at attenuating viral growth, proteases can be prone to mutations that render these inhibitors ineffective.[330-332]

There are also analytical challenges associated with characterizing other viral structural proteins that could make suitable targets for antivirals. One challenge is that many of the structural proteins in enveloped viruses are hydrophobic membrane-embedded proteins. Although not all viruses are enveloped, some of the most clinically relevant viruses, such are HIV, influenza, and SARS-CoV-2, are all enveloped viruses. The hydrophobic properties of these structural proteins make them challenging to study with many conventional techniques, such as X-ray crystallography.[333] Hydrophobic proteins also require some form of a membrane mimetic for solubility. Additionally, many viroporins are relatively small proteins, making it challenging to study with traditional structural biology techniques, such as cryo-EM.[334]

Many viroporins are also known to oligomerize and form polydisperse transient complexes.[20] The complex behavior of viral proteins allows for viruses, which generally encode

few proteins, to modulate protein activities through different oligomeric states or generate different functional forms of proteins.[335] Viral proteins generally have diverse interactions and can have multifunctionality.[20] However, this can lead to challenges in characterizing viral proteins due to the intrinsic polydispersity in the sample. Many analytical techniques, such as chemical cross-linking and NMR are limited in their ability to characterize polydisperse samples and typically just provide an average of the sample.

Viroporins are understudied but attractive potential therapeutic targets. Most of the existing literature on viroporins suggests that these proteins will self-oligomerize within bilayers into fixed oligomeric complexes that typically form channels in the membrane.[22, 26, 27] Viroporins play other important roles in the viral infection cycle, including inducing membrane curvature, driving viral budding, and participating in critical protein-protein interactions.[24] By deleting viroporins from the viral genome, viral growth can be attenuated.[233, 336] It has also been postulated that viroporin channel activity could be blocked by a single small molecule inhibitor.[337]

To help overcome some of the limitations associated with determining the oligomerization of membrane proteins, in Chapter 2 we reviewed mass defect analysis as a technique to determine the oligomeric state of membrane proteins while in an intact lipid bilayer. We outlined methods and experimental details of coupling native MS with nanodiscs to determine the stoichiometry of proteins in a lipid bilayer. We also provided examples of how mass defect analysis has been applied and the variety of behaviors, both in patterns of oligomerization as well as lipid specificities, that can be identified using mass defect analysis. Additionally, we provided strategies for disambiguating mass defect assignments to allow for more confidence in mass defect assignments. The unique combination of native MS and nanodiscs provides a novel platform for characterizing the oligomeric state of small, polydisperse membrane proteins, such as viroporins.

Due to the small size of viroporins, many of the complexes that they assemble are fairly fragile. Even with the gentle conditions applied during native MS, these complexes can still be susceptible to unwanted gas-phase dissociation. However, this dissociation can be mitigated with the addition of charge reducing agents.[124] In Chapter 3, we identified a range of novel charge reducing agents for native MS. These charge reducing agents were inspired by a previously identified charge reducing agent, imidazole.[338] We determined that derivatives of imidazole, particularly those with alkyl substituents at the 2 position on the ring, we more effective at charge reducing and were amenable with a wide range analytes.[183] The addition of charge reducing agents can allow for the preservation and measurement of fragile protein oligomers.

The best characterized viroporin to-date is the viroporin M2 from influenza A. M2 currently is the only viroporin that has been approved as a therapeutic target, but resistance to this drug has become widespread.[35, 339] Currently, there are dozens of structures of M2 in the PDB, many with the protein embedded in different membrane mimetics, as well as in different solution environments. Notably, in many structures solved of M2, there was high concentration of the drug added to the sample prior to analysis. These high concentrations of amantadine were thought to stabilize the complex for structural studies. The majority of these structures were solved using NMR, which as discussed above, can be limited in its ability to capture sample polydispersity. Every structure currently in the PDB of M2 shows that this protein forms a fixed tetrameric structure. There have not been any other oligomers shown for M2 in the recent literature. However, among all the structures of M2, there are differences among these tetrameric forms. These differences suggest that perhaps the chemical environment surrounding M2 may have a significant influence on the proteins' overall structure.

In Chapter 4, we used native MS to characterize the influence of these varied chemical environments on M2.[155] We were initially surprised to find that when solubilized in detergent, M2 did not form the rigid, tetrameric structure that had been previously described in the literature. Instead, in most conditions we measured a mixture of oligomers, with this tetrameric complex not even the most abundant species in many of the samples. Additionally, we found that the type of detergent used as well as the solution pH had a notable impact on the oligomeric state of the protein. Interestingly, we found the M2 formed a specific hexameric complex, with no other abundant oligomer species, only in LDAO detergent at pH 5. This hexameric species had not been previously reported in the literature. Here, we also found that titrating in high concentrations of the drug to M2 while in detergent prior to MS analysis drove M2 to form specific tetrameric complexes. These surprising results led us to speculate that perhaps many of the tetrameric structures of M2 in the PDB may have been driven to this tetrameric form of the protein and that this tetramer may not be the native conformation of the protein. Overall, the behavior of M2 in detergent revealed a far more polydisperse protein complex than previous studies, which led us to speculate that perhaps these other oligomers of M2 may perform a range of biochemical functions that have not yet been discovered.

In Chapter 4, we also coupled nanodiscs with native MS to determine the oligomeric state of M2 while in a lipid bilayer, revealing that the oligomeric state of M2 is also sensitive to its lipid environment. In DMPC and DMPG nanodiscs, we found that M2 formed a polydisperse range of oligomers, similar to how M2 behaved in many of the detergent environments. Interestingly, M2 assembled into a more specific complex, primarily as a mixture of tetramer and monomer, in DPPC type lipids, suggesting that bilayer thickness and fluidity may influence M2 oligomerization.

Chapter 4 also marked a technical milestone for native mass spectrometry. There is an ongoing debate in the field of M2 research of whether the stoichiometry of drug binding is one drug per tetramer or four drug per tetramer.[192] Here, we added amantadine in varying concentrations to M2-DPPC nanodiscs. These experiments were the first time that native MS was used to directly measure the binding of a drug to a membrane protein in an intact bilayer. These experiments revealed not only the binding of amantadine to the M2-nanodisc complex, but we were also able to resolve the stoichiometry of the binding, showing both the one bound and four bound states of the drug to the tetramer.

After the surprising results with M2, we wanted to characterize other viroporins to determine whether they may also be more polydisperse than previously thought. In Chapter 5, we used native MS to characterize the oligomeric state of viroporins Vpu from HIV, E protein from SARS-CoV-2, and VP4 from Polio. There is far less literature on these additional viroporins than there is for M2. There have been a variety of oligomeric states proposed for Vpu and not yet been conclusively determined. For the E protein, there has been a structure solved with NMR suggesting that it forms a pentameric channel. There is very little known about the structure or oligomerization of VP4.

When characterizing these additional viroporins, we found that Vpu assembled into a wide range of oligomers that were also sensitive to their detergent environment, like M2 in Chapter 4. However, unlike Vpu and M2, both the E protein and VP4 did not assemble into a polydisperse mixture of oligomers. Instead, the E protein appeared to form a fixed dimeric complex in nearly all the environments screened. We only measured VP4 as a monomer and it did not appear to oligomerize in any environment at all.

Overall, we found that the patterns of oligomerization among viroporins are more complex than the literature had suggested. The experiments discussed in this thesis are the first reports of native MS to probe viroporin oligomerization. MS is a technique that typically excels at characterizing sample polydispersity, a sample parameter that most analytical techniques are limited in. Additionally, MS is not limited by the small size of these viral proteins, unlike some structural techniques, such as cryo-EM. Here, native MS revealed previously unseen oligomers of viroporins, with some of these viroporins being previously extensively studied. It is possible that these varied oligomers that were measured in Chapters 4 and 5 are not physiologically relevant and could instead be distorted by our purification process, the addition of detergents, or perhaps an artifact of the measurement with mass spectrometry. It is also possible that we have uncovered new oligomers of these proteins, all of which may have their own distinct function in the viral life cycle. In this case, the identification of these novel oligomeric states could ultimately enable the discovery of new aspects of virus biochemistry and the viral infection cycle. Additionally, the identification of these novel oligomers may also enable the development of therapeutic compounds in the future.

We found that some viroporins readily assembled into polydisperse mixtures, while others did not appear to oligomerize at all. There are very few similarities across viroporins as a class of proteins and very little sequence homology.[26] "Viroporins" are named after their ability to assemble into pore-forming ion transporters. Beyond ion transport, viroporins have varied and diverse roles in the viral life cycle, including protein-protein interactions and roles in signaling.[336] Given the significant differences in sequence, structure, function, and patterns of oligomerization, it is possible that many of the small membrane spanning viral proteins that have been labeled as

"viroporins" may not be appropriate to classify in the same structural family. Across viruses, the most common feature among all of these proteins is that they are just small viral proteins.[23]

6.2 FUTURE DIRECTIONS:

As shown in Chapter 4, the local lipid environment can play a critical role in the oligomerization of viroporins.[155] Lipid nanodiscs are a more native membrane mimetic than detergent micelles.[67, 149] It has also been proposed that viruses may remodel their host's membranes to suite their own biochemical needs.[340, 341] Moving forward, viroporins could be characterized in a wider range of lipid environments using nanodiscs, native MS, and mass defect analysis. In these experiments, additional considerations should be made for the types of lipids used and their relevancy in the viral life cycle.

To improve the understanding of the entire viroporin protein class, these methods should be extended to viroporins from other viruses. There has been some preliminary structural work on p7 from hepatitis C, making it a potential target for native MS. Similarly, there has also been preliminary work on the behavior of viroporin P2B from picornavirus. It would be interesting to compare the native MS results of these viroporins with what is known about them in the literature.

As the oligomeric state of viroporins is further characterized in varied lipid environments, the activity of viroporins should also be further investigated. In Chapter 5, we used electrophysiology to identify the ion transport functions of viroporins in a handful of PC type BLM's. In the future, the activity of viroporins should be further characterized in parallel lipid environments to the experiments performed in nanodiscs. These additional experiments could allow for conclusions to be drawn on the relationship between the oligomeric state of the viroporin and its function.

Additional experiments should also be performed using native MS on viroporins that have been surrounded by natural lipid extracts that can better mimic the physiological environment of viroporins. One challenge with creating nanodiscs of natural lipid extracts is that due to the sample polydispersity, intact nanodiscs of natural lipid extracts cannot be analyzed with native MS. The protein would have to be ejected from the bilayer. However, when trying to eject viroporins from nanodiscs inside the mass spectrometer, the signal for the viroporin is overwhelmed by the signal for the MSP belt, making it impossible to determine the proteins oligomeric state. To overcome this, I propose that viroporins be embedded into liposomes formed of natural lipid extracts and ejected from the liposome inside the mass spectrometer. This would provide a far more native environment without suppressing the signal for the viroporin.

Future experiments surrounding viroporins should include using native MS as a tool to screen potential antiviral compounds. These experiments could be performed first in detergent, for ease and simplicity, as well as in nanodiscs of varying lipids to better replicate a more native environment. Additionally, similar experiments to those performed in this thesis can be performed on viroporins that contain mutations from variants of the same virus, which will allow for us to better understand the influence of these variants on viroporin structures, as well as better design therapeutics that are resistant to these mutations. Overall, understanding the patterns of oligomerization of viroporins will be beneficial in better understanding virus biochemistry and key in the rational design of potential therapeutics.

REFERENCES

1. Jumper, J.; Evans, R.; Pritzel, A.; Green, T.; Figurnov, M.; Ronneberger, O.; Tunyasuvunakool, K.; Bates, R.; Žídek, A.; Potapenko, A.; Bridgland, A.; Meyer, C.; Kohl, S. A. A.; Ballard, A. J.; Cowie, A.; Romera-Paredes, B.; Nikolov, S.; Jain, R.; Adler, J.; Back, T.; Petersen, S.; Reiman, D.; Clancy, E.; Zielinski, M.; Steinegger, M.; Pacholska, M.; Berghammer, T.; Bodenstein, S.; Silver, D.; Vinyals, O.; Senior, A. W.; Kavukcuoglu, K.; Kohli, P.; Hassabis, D., Highly accurate protein structure prediction with AlphaFold. *Nature* **2021,** *596* (7873), 583-589.

2. Zhang, H.; Lin, E. C.; Das, B. B.; Tian, Y.; Opella, S. J., Structural determination of virus protein U from HIV-1 by NMR in membrane environments. *Biochimica et Biophysica Acta (BBA) - Biomembranes* **2015**, *1848* (11, Part A), 3007-3018.

3. Stouffer, A. L.; Acharya, R.; Salom, D.; Levine, A. S.; Di Costanzo, L.; Soto, C. S.; Tereshko, V.; Nanda, V.; Stayrook, S.; DeGrado, W. F., Structural basis for the function and inhibition of an influenza virus proton channel. *Nature* **2008,** *451* (7178), 596-599.

4. Jo, S.; Kim, T.; Iyer, V. G.; Im, W., CHARMM-GUI: A web-based graphical user interface for CHARMM. *Journal of Computational Chemistry* **2008,** *29* (11), 1859-1865.

5. Somberg, N. H.; Wu, W. W.; Medeiros-Silva, J.; Dregni, A. J.; Jo, H.; DeGrado, W. F.; Hong, M., SARS-CoV-2 Envelope Protein Forms Clustered Pentamers in Lipid Bilayers. *Biochemistry* **2022,** *61* (21), 2280-2294.

6. Nishimura, K.; Kim, S.; Zhang, L.; Cross, T. A., The Closed State of a H+ Channel Helical Bundle Combining Precise Orientational and Distance Restraints from Solid State NMR. *Biochemistry* **2002,** *41* (44), 13170-13177.

7. Wu, Y.; Canturk, B.; Jo, H.; Ma, C.; Gianti, E.; Klein, M. L.; Pinto, L. H.; Lamb, R. A.; Fiorin, G.; Wang, J.; DeGrado, W. F., Flipping in the Pore: Discovery of Dual Inhibitors That Bind in Different Orientations to the Wild-Type versus the Amantadine-Resistant S31N Mutant of the Influenza A Virus M2 Proton Channel. *JACS* **2014,** *136* (52), 17987-17995.

8. Acharya, R.; Carnevale, V.; Fiorin, G.; Levine, B. G.; Polishchuk, A. L.; Balannik, V.; Samish, I.; Lamb, R. A.; Pinto, L. H.; DeGrado, W. F.; Klein, M. L., Structure and mechanism of proton transport through the transmembrane tetrameric M2 protein bundle of the influenza A virus. *PNAS* **2010,** *107* (34), 15075-1508

9. Cady, S. D.; Mishanina, T. V.; Hong, M., Structure of Amantadine-Bound M2 Transmembrane Peptide of Influenza A in Lipid Bilayers from Magic-Angle-Spinning Solid-State NMR: The Role of Ser31 in Amantadine Binding. *J of Mol Bio* **2009,** *385* (4), 1127-1141.

10. Thomaston, J. L.; Konstantinidi, A.; Liu, L.; Lambrinidis, G.; Tan, J.; Caffrey, M.; Wang, J.; Degrado, W. F.; Kolocouris, A., X-ray Crystal Structures of the Influenza M2 Proton Channel Drug-Resistant V27A Mutant Bound to a Spiro-Adamantyl Amine Inhibitor Reveal the Mechanism of Adamantane Resistance. *Biochemistry* **2020,** *59* (4), 627-634.

11. Mahmoudabadi, G.; Phillips, R., A comprehensive and quantitative exploration of thousands of viral genomes. *eLife* **2018,** *7*, e31955.

12. Campillo-Balderas, J. A.; Lazcano, A.; Becerra, A., Viral Genome Size Distribution Does not Correlate with the Antiquity of the Host Lineages. *Frontiers in Ecology and Evolution* **2015,** *3*.

13. Kristensen David, M.; Cai, X.; Mushegian, A., Evolutionarily Conserved Orthologous Families in Phages Are Relatively Rare in Their Prokaryotic Hosts. *J of Bacteriol* **2011,** *193* (8), 1806-1814.

14. Raoult, D.; Audic, S.; Robert, C.; Abergel, C.; Renesto, P.; Ogata, H.; La Scola, B.; Suzan, M.; Claverie, J.-M., The 1.2-Megabase Genome Sequence of Mimivirus. *Science* **2004**, *306* (5700), 1344-1350.

15. DiMaio, D., Viruses, Masters at Downsizing. *Cell Host & Microbe* **2012,** *11* (6), 560-561.

16. Belshaw, R.; Pybus, O. G.; Rambaut, A., The evolution of genome compression and genomic novelty in RNA viruses. *Genome Res* **2007,** *17* (10), 1496-504.

17. Hobson, S. D.; Rosenblum, E. S.; Richards, O. C.; Richmond, K.; Kirkegaard, K.; Schultz, S. C., Oligomeric structures of poliovirus polymerase are important for function. *Embo j* **2001,** *20* (5), 1153-63.

18. Dubuisson, J., Hepatitis C virus proteins. *World J Gastroenterol* **2007,** *13* (17), 2406-15.

19. Faust, T. B.; Binning, J. M.; Gross, J. D.; Frankel, A. D., Making Sense of Multifunctional Proteins: Human Immunodeficiency Virus Type 1 Accessory and Regulatory Proteins and Connections to Transcription. *Annual Review of Virology* **2017,** *4* (1), 241-260.

20. Jayaraman, B.; Smith, A. M.; Fernandes, J. D.; Frankel, A. D., Oligomeric viral proteins: small in size, large in presence. *Crit Rev Biochem Mol Biol* **2016,** *51* (5), 379-394.

21. Tokuriki, N.; Oldfield, C. J.; Uversky, V. N.; Berezovsky, I. N.; Tawfik, D. S., Do viral proteins possess unique biophysical features? *Trends Biochem Sci* **2009,** *34* (2), 53-59.

22. Gonzalez, M. E.; Carrasco, L., Viroporins. *FEBS Letters* **2003,** *552* (1), 28-34.

23. Opella, S. J., Relating structure and function of viral membrane-spanning miniproteins. *Curr Opin Virol* **2015,** *12*, 121-125.

24. To, J.; Torres, J., Beyond Channel Activity: Protein-Protein Interactions Involving Viroporins. In *Virus Protein and Nucleoprotein Complexes*, Harris, J. R.; Bhella, D., Eds. Springer Singapore: Singapore, 2018; pp 329-377.

25. To, J.; Surya, W.; Torres, J., Chapter Eight - Targeting the Channel Activity of Viroporins. In *Adv Protein Chem Struct Biol*, Donev, R., Ed. Academic Press: 2016; Vol. 104, pp 307-355.

26. Hyser, J. M., *Viroporins*. Electrophysiology of Unconventional Channels and Pores. 2015 Jul 16;18:153-81. doi: 10.1007/978-3-319-20149-8_7. eCollection 2015.

27. To, J.; Surya, W.; Torres, J., Targeting the Channel Activity of Viroporins. *Adv Protein Chem Struct Biol* **2016,** *104*, 307-355.

28. Nieva, J. L.; Madan, V.; Carrasco, L., Viroporins: structure and biological functions. *Nat Rev Microbiol* **2012,** *10* (8), 563-574.

29. Pielak, R. M.; Chou, J. J., Influenza M2 proton channels. *Biochimica et biophysica acta* **2011,** *1808* (2), 522-529.

30. Cady, S. D.; Wang, J.; Wu, Y.; DeGrado, W. F.; Hong, M., Specific binding of adamantane drugs and direction of their polar amines in the pore of the influenza M2 transmembrane domain in lipid bilayers and dodecylphosphocholine micelles determined by NMR spectroscopy. *JACS* **2011,** *133* (12), 4274-4284.

31. Chizhmakov, I. V.; Geraghty, F. M.; Ogden, D. C.; Hayhurst, A.; Antoniou, M.; Hay, A. J., Selective proton permeability and pH regulation of the influenza virus M2 channel expressed in mouse erythroleukaemia cells. *J. Physiol.* **1996,** *494 (Pt 2)* (2), 329-36.

32. Cross, T. A.; Dong, H.; Sharma, M.; Busath, D. D.; Zhou, H.-X., M2 protein from influenza A: from multiple structures to biophysical and functional insights. *Curr Opin Virol* **2012,** *2* (2), 128-133.

33. Sakaguchi, T., [Structure and function of the influenza virus M2 ion channel protein]. *Nihon Rinsho* **1997,** *55* (10), 2587-92.

34. Nisar, T.; Sutherland-Foggio, H.; Husar, W., Antiviral amantadine. *The Lancet Neurology* **2019,** *18* (12), 1080.

35. Cady, S. D.; Hong, M., Amantadine-induced conformational and dynamical changes of the influenza M2 transmembrane proton channel. *PNAS* **2008,** *105* (5), 1483-1488.

36. Grambas, S.; Bennett, M. S.; Hay, A. J., Influence of amantadine resistance mutations on the pH regulatory function of the M2 protein of influenza A viruses. *Virology* **1992,** *191* (2), 541-549.

37. Cady, S. D.; Luo, W.; Hu, F.; Hong, M., Structure and function of the influenza A M2 proton channel. *Biochemistry* **2009,** *48* (31), 7356-64.

38. Pielak, R. M.; Schnell, J. R.; Chou, J. J., Mechanism of drug inhibition and drug resistance of influenza A M2 channel. *PNAS* **2009,** *106* (18), 7379-84.

39. Nomaguchi, M.; Fujita, M.; Adachi, A., Role of HIV-1 Vpu protein for virus spread and pathogenesis. *Microbes and Infection* **2008,** *10* (9), 960-967.

40. Ruiz, A.; Guatelli, J. C.; Stephens, E. B., The Vpu protein: new concepts in virus release and CD4 down-modulation. *Curr HIV Res* **2010,** *8* (3), 240-52.

41. Schubert, U.; Ferrer-Montiel, A. V.; Oblatt-Montal, M.; Henklein, P.; Strebel, K.; Montal, M., Identification of an ion channel activity of the Vpu transmembrane domain and its involvement in the regulation of virus release from HIV-1-infected cells. *FEBS Letters* **1996,** *398* (1), 12-18.

42. Ewart, G. D.; Sutherland, T.; Gage, P. W.; Cox, G. B., The Vpu protein of human immunodeficiency virus type 1 forms cation-selective ion channels. *J Virol* **1996,** *70* (10), 7108-15.

43. Schubert, U.; Ferrer-Montiel, A. V.; Oblatt-Montal, M.; Henklein, P.; Strebel, K.; Montal, M., Identification of an ion channel activity of the Vpu transmembrane domain and its involvement in the regulation of virus release from HIV-1-infected cells. *FEBS Lett* **1996,** *398* (1), 12-8.

44. Schubert, U.; Henklein, P.; Boldyreff, B.; Wingender, E.; Strebel, K.; Porstmann, T., The Human Immunodeficiency Virus Type 1 Encoded Vpu Protein is Phosphorylated by Casein Kinase-2 (CK-2) at Positions Ser52 and Ser56 within a Predicted α-Helix-Turn-α-Helix-Motif. *J Mol Bio* **1994,** *236* (1), 16-25.

45. Strebel, K., HIV-1 Vpu — an ion channel in search of a job. *Biochimica et Biophysica Acta (BBA) - Biomembranes* **2014,** *1838* (4), 1074-1081.

46. Cordes, F. S.; Kukol, A.; Forrest, L. R.; Arkin, I. T.; Sansom, M. S. P.; Fischer, W. B., The structure of the HIV-1 Vpu ion channel: modelling and simulation studies. *Biochimica et Biophysica Acta (BBA) - Biomembranes* **2001,** *1512* (2), 291-298.

47. Park, S. H.; De Angelis, A. A.; Nevzorov, A. A.; Wu, C. H.; Opella, S. J., Three-dimensional structure of the transmembrane domain of Vpu from HIV-1 in aligned phospholipid bicelles. *Biophys J* **2006,** *91* (8), 3032-3042.

48. Park, S. H.; Mrse, A. A.; Nevzorov, A. A.; Mesleh, M. F.; Oblatt-Montal, M.; Montal, M.; Opella, S. J., Three-dimensional Structure of the Channel-forming Trans-membrane Domain of Virus Protein "u" (Vpu) from HIV-1. *J of Mol Bio* **2003,** *333* (2), 409-424.

49. Wilson, L.; Gage, P.; Ewart, G., Hexamethylene amiloride blocks E protein ion channels and inhibits coronavirus replication. *Virology* **2006,** *353* (2), 294-306.

50. Schoeman, D.; Fielding, B. C., Is There a Link Between the Pathogenic Human Coronavirus Envelope Protein and Immunopathology? A Review of the Literature. *Front Microbiol* **2020,** *11*, 2086.

51. De Maio, F.; Lo Cascio, E.; Babini, G.; Sali, M.; Della Longa, S.; Tilocca, B.; Roncada, P.; Arcovito, A.; Sanguinetti, M.; Scambia, G.; Urbani, A., Improved binding of SARS-CoV-2 Envelope protein to tight junction-associated PALS1 could play a key role in COVID-19 pathogenesis. *Microbes and Infection* **2020,** *22* (10), 592-597.

52. Wilson, L.; McKinlay, C.; Gage, P.; Ewart, G., SARS coronavirus E protein forms cation-selective ion channels. *Virology* **2004,** *330* (1), 322-331.

53. Verdiá-Báguena, C.; Nieto-Torres, J. L.; Alcaraz, A.; DeDiego, M. L.; Torres, J.; Aguilella, V. M.; Enjuanes, L., Coronavirus E protein forms ion channels with functionally and structurally-involved membrane lipids. *Virology* **2012,** *432* (2), 485-494.

54. Ortego, J.; Ceriani, J. E.; Patiño, C.; Plana, J.; Enjuanes, L., Absence of E protein arrests transmissible gastroenteritis coronavirus maturation in the secretory pathway. *Virology* **2007,** *368* (2), 296-308.

55. Kuzmin, A.; Orekhov, P.; Astashkin, R.; Gordeliy, V.; Gushchin, I., Structure and dynamics of the SARS-CoV-2 envelope protein monomer. *Proteins: Structure, Function, and Bioinformatics* **2022,** *90* (5), 1102-1114.

56. Lin, M.-H.; Chen, C.-P.; Fischer, W. B., Patch formation of a viral channel forming protein within a lipid membrane – Vpu of HIV-1. *Molecular BioSystems* **2016,** *12* (4), 1118-1127.

57. Mandala, V. S.; McKay, M. J.; Shcherbakov, A. A.; Dregni, A. J.; Kolocouris, A.; Hong, M., Structure and drug binding of the SARS-CoV-2 envelope protein transmembrane domain in lipid bilayers. *Nat Struc & Mol Bio* **2020,** *27* (12), 1202-1208.

58. Torres, J.; Wang, J.; Parthasarathy, K.; Liu, D. X., The transmembrane oligomers of coronavirus protein E. *Biophys J* **2005,** *88* (2), 1283-90.

59. Park, S. H.; Siddiqi, H.; Castro, D. V.; De Angelis, A. A.; Oom, A. L.; Stoneham, C. A.; Lewinski, M. K.; Clark, A. E.; Croker, B. A.; Carlin, A. F.; Guatelli, J.; Opella, S. J., Interactions of SARS-CoV-2 envelope protein with amilorides correlate with antiviral activity. *PLOS Pathogens* **2021,** *17* (5), e1009519.

60. Simons, K., Cell membranes: A subjective perspective. *Biochimica et Biophysica Acta (BBA) - Biomembranes* **2016,** *1858* (10), 2569-2572.

61. Subczynski, W. K.; Wisniewska, A., Physical properties of lipid bilayer membranes: relevance to membrane biological functions. *Acta Biochim Pol* **2000,** *47* (3), 613-25.

62. Brown, M. F., Modulation of rhodopsin function by properties of the membrane bilayer. *Chemistry and Physics of Lipids* **1994,** *73* (1), 159-180.

63. Krogh, A.; Larsson, B.; von Heijne, G.; Sonnhammer, E. L. L., Predicting transmembrane protein topology with a hidden markov model: application to complete genomes11Edited by F. Cohen. *J of Mol Bio* **2001,** *305* (3), 567-580.

64. Almén, M. S.; Nordström, K. J. V.; Fredriksson, R.; Schiöth, H. B., Mapping the human membrane proteome: a majority of the human membrane proteins can be classified according to function and evolutionary origin. *BMC Biology* **2009,** *7* (1), 50.

65. Li, F.; Egea, P. F.; Vecchio, A. J.; Asial, I.; Gupta, M.; Paulino, J.; Bajaj, R.; Dickinson, M. S.; Ferguson-Miller, S.; Monk, B. C.; Stroud, R. M., Highlighting membrane protein structure and function: A celebration of the Protein Data Bank. *J of Bio Chem* **2021,** *296*, 100557.

66. Keener, J. E.; Zhang, G.; Marty, M. T., Native Mass Spectrometry of Membrane Proteins. *Anal Chem* **2021,** *93* (1), 583-597.

67. Seddon, A. M.; Curnow, P.; Booth, P. J., Membrane proteins, lipids and detergents: not just a soap opera. *Biochimica et Biophysica Acta (BBA) - Biomembranes* **2004,** *1666* (1), 105-117.

68. Kotov, V.; Bartels, K.; Veith, K.; Josts, I.; Subhramanyam, U. K. T.; Günther, C.; Labahn, J.; Marlovits, T. C.; Moraes, I.; Tidow, H.; Löw, C.; Garcia-Alai, M. M., High-throughput stability screening for detergent-solubilized membrane proteins. *Scientific Reports* **2019,** *9* (1), 10379.

69. Arachea, B. T.; Sun, Z.; Potente, N.; Malik, R.; Isailovic, D.; Viola, R. E., Detergent selection for enhanced extraction of membrane proteins. *Protein Expr Purif* **2012,** *86* (1), 12-20.

70. Denisov, I. G.; Sligar, S. G., Nanodiscs for structural and functional studies of membrane proteins. *Nat Struc & Mol Bio* **2016,** *23* (6), 481-486.

71. Sligar, S. G.; Denisov, I. G., Nanodiscs: A toolkit for membrane protein science. *Protein Science* **2021,** *30* (2), 297-315.

72. Bayburt, T. H.; Grinkova, Y. V.; Sligar, S. G., Self-assembly of discoidal phospholipid bilayer nanoparticles with membrane scaffold proteins. *Nano Lett.* **2002,** *2* (8), 853-856.

73. Conrard, L.; Tyteca, D., Regulation of Membrane Calcium Transport Proteins by the Surrounding Lipid Environment. *Biomolecules* **2019,** *9* (10).

74. Jiang, Y.; Thienpont, B.; Sapuru, V.; Hite, R. K.; Dittman, J. S.; Sturgis, J. N.; Scheuring, S., Membrane-mediated protein interactions drive membrane protein organization. *Nat Comm* **2022,** *13* (1), 7373.

75. Pal, S.; Chakraborty, H.; Chattopadhyay, A., Lipid Headgroup Charge Controls Melittin Oligomerization in Membranes: Implications in Membrane Lysis. *J Phys Chem B* **2021,** *125* (30), 8450-8459.

76. Bagheri, Y.; Ali, A. A.; You, M., Current Methods for Detecting Cell Membrane Transient Interactions. *Frontiers in Chemistry* **2020,** *8*.

77. Brown, M. F., Curvature forces in membrane lipid-protein interactions. *Biochem* **2012,** *51* (49), 9782-95.

78. Orwick-Rydmark, M.; Arnold, T.; Linke, D., The Use of Detergents to Purify Membrane Proteins. *Curr Protoc Protein Sci* **2016,** *84*, 4.8.1-4.8.35.

79. Kermani, A. A., A guide to membrane protein X-ray crystallography. *The FEBS Journal* **2021,** *288* (20), 5788-5804.

80. Edwards, G. B.; Muthurajan, U. M.; Bowerman, S.; Luger, K., Analytical Ultracentrifugation (AUC): An Overview of the Application of Fluorescence and Absorbance AUC to the Study of Biological Macromolecules. *Current Protocols in Molecular Biology* **2020,** *133* (1), e131.

81. Ebel, C., Sedimentation velocity to characterize surfactants and solubilized membrane proteins. *Methods* **2011,** *54* (1), 56-66.

82. Cole, J. L.; Lary, J. W.; T, P. M.; Laue, T. M., Analytical ultracentrifugation: sedimentation velocity and sedimentation equilibrium. *Methods Cell Biol* **2008,** *84*, 143-79.

83. Amartely, H.; Avraham, O.; Friedler, A.; Livnah, O.; Lebendiker, M., Coupling Multi Angle Light Scattering to Ion Exchange chromatography (IEX-MALS) for protein characterization. *Scientific Reports* **2018,** *8* (1), 6907.

84. Some, D.; Amartely, H.; Tsadok, A.; Lebendiker, M., Characterization of Proteins by Size-Exclusion Chromatography Coupled to Multi-Angle Light Scattering (SEC-MALS). *JoVE* **2019,** (148), e59615.

85. Wu, D.; Piszczek, G., Standard protocol for mass photometry experiments. *European Biophysics Journal* **2021,** *50* (3), 403-409.

86. Sonn-Segev, A.; Belacic, K.; Bodrug, T.; Young, G.; VanderLinden, R. T.; Schulman, B. A.; Schimpf, J.; Friedrich, T.; Dip, P. V.; Schwartz, T. U.; Bauer, B.; Peters, J. M.; Struwe, W. B.; Benesch, J. L. P.; Brown, N. G.; Haselbach, D.; Kukura, P., Quantifying the heterogeneity of macromolecular machines by mass photometry. *Nat Commun* **2020,** *11* (1), 1772.

87. Olerinyova, A.; Sonn-Segev, A.; Gault, J.; Eichmann, C.; Schimpf, J.; Kopf, A. H.; Rudden, L. S. P.; Ashkinadze, D.; Bomba, R.; Frey, L.; Greenwald, J.; Degiacomi, M. T.; Steinhilper, R.; Killian, J. A.; Friedrich, T.; Riek, R.; Struwe, W. B.; Kukura, P., Mass Photometry of Membrane Proteins. *Chem* **2021,** *7* (1), 224-236.

88. Wang, X.; Lee, H. W.; Liu, Y.; Prestegard, J. H., Structural NMR of protein oligomers using hybrid methods. *J Struct Biol* **2011,** *173* (3), 515-29.

89. Martin, J. W.; Yan, A. K.; Bailey-Kellogg, C.; Zhou, P.; Donald, B. R. In *A Geometric Arrangement Algorithm for Structure Determination of Symmetric Protein Homo-oligomers from NOEs and RDCs*, Research in Computational Molecular Biology, Berlin, Heidelberg, 2011; Bafna, V.; Sahinalp, S. C., Eds. Springer Berlin Heidelberg: Berlin, Heidelberg, 2011; pp 222-237.

90. Sala, D.; Cerofolini, L.; Fragai, M.; Giachetti, A.; Luchinat, C.; Rosato, A., A protocol to automatically calculate homo-oligomeric protein structures through the integration of evolutionary constraints and NMR ambiguous contacts. *Computational and Structural Biotechnology Journal* **2020,** *18*, 114-124.

91. Luo, W.; Hong, M., Determination of the Oligomeric Number and Intermolecular Distances of Membrane Protein Assemblies by Anisotropic 1H-Driven Spin Diffusion NMR Spectroscopy. *JACS* **2006,** *128* (22), 7242-7251.

92. Yu, H., Extending the size limit of protein nuclear magnetic resonance. *PNAS* **1999,** *96* (2), 332-334.

93. Kozak, S.; Lercher, L.; Karanth, M. N.; Meijers, R.; Carlomagno, T.; Boivin, S., Optimization of protein samples for NMR using thermal shift assays. *J Biomol NMR* **2016,** *64* (4), 281-9.

94. Park, S. H.; Das, B. B.; De Angelis, A. A.; Scrima, M.; Opella, S. J., Mechanically, Magnetically, and "Rotationally Aligned" Membrane Proteins in Phospholipid Bilayers Give Equivalent Angular Constraints for NMR Structure Determination. *J Phys Chem B* **2010,** *114* (44), 13995-14003.

95. Gaber, A.; Gunčar, G.; Pavšič, M., Proper evaluation of chemical cross-linking-based spatial restraints improves the precision of modeling homo-oligomeric protein complexes. *BMC Bioinformatics* **2019,** *20* (1), 464.

96. Banerjee, R.; Günsel, U.; Mokranjac, D., Chemical Crosslinking in Intact Mitochondria. *Methods Mol Biol* **2017,** *1567*, 139-154.

97. Yang, B.; Tang, S.; Ma, C.; Li, S.-T.; Shao, G.-C.; Dang, B.; DeGrado, W. F.; Dong, M.-Q.; Wang, P. G.; Ding, S.; Wang, L., Spontaneous and specific chemical cross-linking in live cells to capture and identify protein interactions. *Nat Comm* **2017,** *8* (1), 2240.

98. Merkley, E. D.; Cort, J. R.; Adkins, J. N., Cross-linking and mass spectrometry methodologies to facilitate structural biology: finding a path through the maze. *J Struct Funct Genomics* **2013,** *14* (3), 77-90.

99. Wang, Z.; Lu, W.; Rajapaksha, P.; Wilkop, T.; Cai, Y.; Wei, Y., Comparison of in vitro and in vivo oligomeric states of a wild type and mutant trimeric inner membrane multidrug transporter. *Biochem Biophys Rep* **2018,** *16*, 122-129.

100. Muzzopappa, F.; Hummert, J.; Anfossi, M.; Tashev, S. A.; Herten, D.-P.; Erdel, F., Detecting and quantifying liquid–liquid phase separation in living cells by model-free calibrated half-bleaching. *Nat Comm* **2022,** *13* (1), 7787.

101. Weiss, M., Challenges and artifacts in quantitative photobleaching experiments. *Traffic* **2004,** *5* (9), 662-71.

102. Barth, M.; Schmidt, C., Native mass spectrometry—A valuable tool in structural biology. *Journal of Mass Spectrometry* **2020,** *55* (10), e4578.

103. Heuvel, R. H. H. v. d.; Heck, A. J. R., Native protein mass spectrometry: from intact oligomers to functional machineries. *Current Opinion in Chemical Biology* **2004,** *8* (5), 519-526.

104. Leney, A. C.; Heck, A. J. R., Native Mass Spectrometry: What is in the Name? *J Am Soc Mass Spectrom* **2017,** *28* (1), 5-13.

105. Urban, P. L., Quantitative mass spectrometry: an overview. *Philos Trans A Math Phys Eng Sci* **2016,** *374* (2079).

106. Bui, D. T.; Li, Z.; Kitov, P. I.; Han, L.; Kitova, E. N.; Fortier, M.; Fuselier, C.; Granger Joly de Boissel, P.; Chatenet, D.; Doucet, N.; Tompkins, S. M.; St-Pierre, Y.; Mahal, L. K.; Klassen, J. S., Quantifying Biomolecular Interactions Using Slow Mixing Mode (SLOMO) Nanoflow ESI-MS. *ACS Cent Sci* **2022,** *8* (7), 963-974.

107. Free, T., Native mass spectrometry: a powerful tool for structural biology? *BioTechniques* **2019,** *67* (5), 204-206.

108. Snyder, D. T.; Harvey, S. R.; Wysocki, V. H., Surface-induced Dissociation Mass Spectrometry as a Structural Biology Tool. *Chemical Reviews* **2022,** *122* (8), 7442-7487.

109. Konijnenberg, A.; Butterer, A.; Sobott, F., Native ion mobility-mass spectrometry and related methods in structural biology. *Biochimica et Biophysica Acta (BBA) - Proteins and Proteomics* **2013,** *1834* (6), 1239-1256.

110. Karch, K. R.; Snyder, D. T.; Harvey, S. R.; Wysocki, V. H., Native Mass Spectrometry: Recent Progress and Remaining Challenges. *Annual Review of Biophysics* **2022,** *51* (1), 157-179.

111. Marty, M. T., Nanodiscs and mass spectrometry: Making membranes fly. *International Journal of Mass Spectrometry* **2020,** *458*, 116436.

112. Laganowsky, A.; Reading, E.; Hopper, J. T. S.; Robinson, C. V., Mass spectrometry of intact membrane protein complexes. *Nat Protoc* **2013,** *8* (4), 639-651.

113. Laganowsky, A.; Reading, E.; Hopper, J. T.; Robinson, C. V., Mass spectrometry of intact membrane protein complexes. *Nat. Protoc.* **2013,** *8* (4), 639-51.

114. Reading, E.; Liko, I.; Allison, T. M.; Benesch, J. L.; Laganowsky, A.; Robinson, C. V., The role of the detergent micelle in preserving the structure of membrane proteins in the gas phase. *Angew Chem Int Ed* **2015,** *54* (15), 4577-81.

115. Reading, E.; Walton, T. A.; Liko, I.; Marty, M. T.; Laganowsky, A.; Rees, D. C.; Robinson, C. V., The Effect of Detergent, Temperature, and Lipid on the Oligomeric State of MscL Constructs: Insights from Mass Spectrometry. *Chem. Biol.* **2015,** *22* (5), 593-603.

116. Olinares, P. D. B.; Kang, J. Y.; Llewellyn, E.; Chiu, C.; Chen, J.; Malone, B.; Saecker, R. M.; Campbell, E. A.; Darst, S. A.; Chait, B. T., Native Mass Spectrometry-Based Screening for Optimal Sample Preparation in Single-Particle Cryo-EM. *Structure* **2021,** *29* (2), 186-195.e6.

117. Cong, X.; Liu, Y.; Liu, W.; Liang, X.; Russell, D. H.; Laganowsky, A., Determining Membrane Protein–Lipid Binding Thermodynamics Using Native Mass Spectrometry. *JACS* **2016,** *138* (13), 4346-4349.

118. Gault, J.; Donlan, J. A. C.; Liko, I.; Hopper, J. T. S.; Gupta, K.; Housden, N. G.; Struwe, W. B.; Marty, M. T.; Mize, T.; Bechara, C.; Zhu, Y.; Wu, B.; Kleanthous, C.; Belov, M.; Damoc, E.; Makarov, A.; Robinson, C. V., High-resolution mass spectrometry of small molecules bound to membrane proteins. *Nat Meth* **2016,** *13* (4), 333-336.

119. Zhou, M.; Morgner, N.; Barrera, N. P.; Politis, A.; Isaacson, S. C.; Matak-Vinković, D.; Murata, T.; Bernal, R. A.; Stock, D.; Robinson, C. V., Mass spectrometry of intact V-type ATPases reveals bound lipids and the effects of nucleotide binding. *Science* **2011,** *334* (6054), 380-385.

120. Sahin, C.; Reid, D. J.; Marty, M. T.; Landreh, M., Scratching the surface: native mass spectrometry of peripheral membrane protein complexes. *Biochem Soc Trans* **2020,** *48* (2), 547-558.

121. Hellwig, N.; Peetz, O.; Ahdash, Z.; Tascón, I.; Booth, P. J.; Mikusevic, V.; Diskowski, M.; Politis, A.; Hellmich, Y.; Hänelt, I.; Reading, E.; Morgner, N., Native mass spectrometry goes more native: investigation of membrane protein complexes directly from SMALPs. *Chemical Communications* **2018,** *54* (97), 13702-13705.

122. Frick, M.; Schwieger, C.; Schmidt, C., Liposomes as Carriers of Membrane-Associated Proteins and Peptides for Mass Spectrometric Analysis. *Angewandte Chemie International Edition* **2021,** *60* (20), 11523-11530.

123. Marty, M. T.; Hoi, K. K.; Robinson, C. V., Interfacing Membrane Mimetics with Mass Spectrometry. *Accounts of Chemical Research* **2016,** *49* (11), 2459-2467.

124. Petroff, J. T., 2nd; Tong, A.; Chen, L. J.; Dekoster, G. T.; Khan, F.; Abramson, J.; Frieden, C.; Cheng, W. W. L., Charge Reduction of Membrane Proteins in Native Mass Spectrometry Using Alkali Metal Acetate Salts. *Anal Chem* **2020,** *92* (9), 6622-6630.

125. Konermann, L.; Ahadi, E.; Rodriguez, A. D.; Vahidi, S., Unraveling the Mechanism of Electrospray Ionization. *Anal Chem* **2013,** *85* (1), 2-9.

126. Yang, Y.; Niu, C.; Bobst, C. E.; Kaltashov, I. A., Charge Manipulation Using Solution and Gas-Phase Chemistry to Facilitate Analysis of Highly Heterogeneous Protein Complexes in Native Mass Spectrometry. *Anal Chem* **2021,** *93* (7), 3337-3342.

127. Lomeli, S. H.; Yin, S.; Ogorzalek Loo, R. R.; Loo, J. A., Increasing charge while preserving noncovalent protein complexes for ESI-MS. *J Am Soc Mass Spectrom* **2009,** *20* (4), 593-596.

128. Going, C. C.; Xia, Z.; Williams, E. R., New supercharging reagents produce highly charged protein ions in native mass spectrometry. *Analyst* **2015,** *140* (21), 7184-7194.

129. Frieden, C., Protein oligomerization as a metabolic control mechanism: Application to apoE. *Protein Sci* **2019,** *28* (4), 837-842.

130. Kim, J.; Wu, S.; Tomasiak, T. M.; Mergel, C.; Winter, M. B.; Stiller, S. B.; Robles-Colmanares, Y.; Stroud, R. M.; Tampé, R.; Craik, C. S.; Cheng, Y., Subnanometre-resolution electron cryomicroscopy structure of a heterodimeric ABC exporter. *Nature* **2015,** *517* (7534), 396-400.

131. Nöll, A.; Thomas, C.; Herbring, V.; Zollmann, T.; Barth, K.; Mehdipour, A. R.; Tomasiak, T. M.; Brüchert, S.; Joseph, B.; Abele, R.; Oliéric, V.; Wang, M.; Diederichs, K.; Hummer, G.; Stroud,

R. M.; Pos, K. M.; Tampé, R., Crystal structure and mechanistic basis of a functional homolog of the antigen transporter TAP. *PNAS* **2017,** *114* (4), E438-E447.

132. Nooren, I. M. A.; Thornton, J. M., Structural Characterisation and Functional Significance of Transient Protein–Protein Interactions. *J Mol Bio* **2003,** *325* (5), 991-1018.

133. Acuner Ozbabacan, S. E.; Engin, H. B.; Gursoy, A.; Keskin, O., Transient protein–protein interactions. *Protein Engineering, Design and Selection* **2011,** *24* (9), 635-648.

134. Šachl, R.; Čujová, S.; Singh, V.; Riegerová, P.; Kapusta, P.; Müller, H.-M.; Steringer, J. P.; Hof, M.; Nickel, W., Functional Assay to Correlate Protein Oligomerization States with Membrane Pore Formation. *Anal Chem* **2020,** *92* (22), 14861-14866.

135. Chung, I., Optical measurement of receptor tyrosine kinase oligomerization on live cells. *Biochim Biophys Acta Biomembr* **2017,** *1859* (9 Pt A), 1436-1444.

136. Park, P. S.; Filipek, S.; Wells, J. W.; Palczewski, K., Oligomerization of G protein-coupled receptors: past, present, and future. *Biochemistry* **2004,** *43* (50), 15643-56.

137. Palczewski, K., Oligomeric forms of G protein-coupled receptors (GPCRs). *Trends Biochem Sci* **2010,** *35* (11), 595-600.

138. Sleno, R.; Hébert, T. E., The Dynamics of GPCR Oligomerization and Their Functional Consequences. *Int Rev Cell Mol Biol* **2018,** *338*, 141-171.

139. Hashimoto, K.; Panchenko, A. R., Mechanisms of protein oligomerization, the critical role of insertions and deletions in maintaining different oligomeric states. *PNAS* **2010,** *107* (47), 20352-20357.

140. Xie, X.; Cheng, Y.-S.; Wen, M.-H.; Calindi, A.; Yang, K.; Chiu, C.-W.; Chen, T.-Y., Quantifying the Oligomeric States of Membrane Proteins in Cells through Super-Resolution Localizations. *J Phys Chem B* **2018,** *122* (46), 10496-10504.

141. Avci, F. G.; Akbulut, B. S.; Ozkirimli, E., Membrane Active Peptides and Their Biophysical Characterization. *Biomolecules* **2018,** *8* (3).

142. Helbig, A. O.; Heck, A. J.; Slijper, M., Exploring the membrane proteome--challenges and analytical strategies. *J Proteomics* **2010,** *73* (5), 868-78.

143. Wang, X.; Mu, Z.; Li, Y.; Bi, Y.; Wang, Y., Smaller Nanodiscs are Suitable for Studying Protein Lipid Interactions by Solution NMR. *The Protein Journal* **2015,** *34* (3), 205-211.

144. Padmanabha Das, K. M.; Shih, W. M.; Wagner, G.; Nasr, M. L., Large Nanodiscs: A Potential Game Changer in Structural Biology of Membrane Protein Complexes and Virus Entry. *Front Bioeng Biotechnol* **2020,** *8*, 539.

145. Borch, J.; Hamann, T., The nanodisc: a novel tool for membrane protein studies. *Biol Chem* **2009,** *390* (8), 805-14.

146. Botelho, A. V.; Huber, T.; Sakmar, T. P.; Brown, M. F., Curvature and Hydrophobic Forces Drive Oligomerization and Modulate Activity of Rhodopsin in Membranes. *Biophys J* **2006,** *91* (12), 4464-4477.

147. Gupta, K.; Donlan, J. A. C.; Hopper, J. T. S.; Uzdavinys, P.; Landreh, M.; Struwe, W. B.; Drew, D.; Baldwin, A. J.; Stansfeld, P. J.; Robinson, C. V., The role of interfacial lipids in stabilizing membrane protein oligomers. *Nature* **2017,** *541* (7637), 421-424.

148. Marty, M. T.; Zhang, H.; Cui, W.; Gross, M. L.; Sligar, S. G., Interpretation and Deconvolution of Nanodisc Native Mass Spectra. *J Am Soc Mass Spectrom* **2014,** *25* (2), 269-277.

149. Kostelic, M. M.; Zak, C. K.; Jayasekera, H. S.; Marty, M. T., Assembly of Model Membrane Nanodiscs for Native Mass Spectrometry. *Anal Chem* **2021,** *93* (14), 5972-5979.

150. Kostelic, M. M.; Ryan, A. M.; Reid, D. J.; Noun, J. M.; Marty, M. T., Expanding the Types of Lipids Amenable to Native Mass Spectrometry of Lipoprotein Complexes. *J. Am. Soc. Mass Spectrom.* **2019,** *30* (8), 1416-1425.

151. Keener, J. E.; Zambrano, D. E.; Zhang, G.; Zak, C. K.; Reid, D. J.; Deodhar, B. S.; Pemberton, J. E.; Prell, J. S.; Marty, M. T., Chemical additives enable native mass spectrometry measurement of membrane protein oligomeric state within intact nanodiscs. *JACS* **2019,** *141* (2), 1054-1061.

152. Walker, L. R.; Marty, M. T., Lipid tails modulate antimicrobial peptide membrane incorporation and activity. *Biochimica et Biophysica Acta (BBA) - Biomembranes* **2022,** *1864* (4), 183870.

153. Walker, L. R.; Marzluff, E. M.; Townsend, J. A.; Resager, W. C.; Marty, M. T., Native Mass Spectrometry of Antimicrobial Peptides in Lipid Nanodiscs Elucidates Complex Assembly. *Analytical Chemistry* **2019,** *91* (14), 9284-9291.

154. Walker, L. R.; Marty, M. T., Revealing the Specificity of a Range of Antimicrobial Peptides in Lipid Nanodiscs by Native Mass Spectrometry. *Biochemistry* **2020,** *59* (23), 2135-2142.

155. Townsend, J. A.; Sanders, H. M.; Rolland, A. D.; Park, C. K.; Horton, N. C.; Prell, J. S.; Wang, J.; Marty, M. T., Influenza AM2 Channel Oligomerization Is Sensitive to Its Chemical Environment. *Anal Chem* **2021,** *93* (48), 16273-16281.

156. Marty, M. T.; Zhang, H.; Cui, W.; Blankenship, R. E.; Gross, M. L.; Sligar, S. G., Native Mass Spectrometry Characterization of Intact Nanodisc Lipoprotein Complexes. *Anal Chem* **2012,** *84* (21), 8957-8960.

157. Keener, J. E.; Zambrano, D. E.; Zhang, G.; Zak, C. K.; Reid, D. J.; Deodhar, B. S.; Pemberton, J. E.; Prell, J. S.; Marty, M. T., Chemical Additives Enable Native Mass Spectrometry Measurement of Membrane Protein Oligomeric State within Intact Nanodiscs. *JACS* **2019,** *141* (2), 1054-1061.

158. Marty, M. T.; Baldwin, A. J.; Marklund, E. G.; Hochberg, G. K. A.; Benesch, J. L. P.; Robinson, C. V., Bayesian Deconvolution of Mass and Ion Mobility Spectra: From Binary Interactions to Polydisperse Ensembles. *Analytical Chemistry* **2015,** *87* (8), 4370-4376.

159. Denisov, I. G.; Grinkova, Y. V.; Lazarides, A. A.; Sligar, S. G., Directed Self-Assembly of Monodisperse Phospholipid Bilayer Nanodiscs with Controlled Size. *Journal of the American Chemical Society* **2004,** *126* (11), 3477-3487.

160. Reid, D. J.; Rohrbough, J. G.; Kostelic, M. M.; Marty, M. T., Investigating Antimicrobial Peptide–Membrane Interactions Using Fast Photochemical Oxidation of Peptides in Nanodiscs. *J Am Soc Mass Spectrom* **2022,** *33* (1), 62-67.

161. Reid, D. J.; Keener, J. E.; Wheeler, A. P.; Zambrano, D. E.; Diesing, J. M.; Reinhardt-Szyba, M.; Makarov, A.; Marty, M. T., Engineering Nanodisc Scaffold Proteins for Native Mass Spectrometry. *Anal Chem* **2017,** *89* (21), 11189-11192.

162. Marty, M. T.; Hoi, K. K.; Gault, J.; Robinson, C. V., Probing the Lipid Annular Belt by Gas-Phase Dissociation of Membrane Proteins in Nanodiscs. *Angewandte Chemie International Edition* **2016,** *55* (2), 550-554.

163. Roach, P. J.; Laskin, J.; Laskin, A., Higher-Order Mass Defect Analysis for Mass Spectra of Complex Organic Mixtures. *Anal Chem* **2011,** *83* (12), 4924-4929.

164. Swansiger, A. K.; Marty, M. T.; Prell, J. S., Fourier-Transform Approach for Reconstructing Macromolecular Mass Defect Profiles. *J Am Soc Mass Spectrom* **2022,** *33* (1), 172-180.

165. Fouquet, T. N. J., The Kendrick analysis for polymer mass spectrometry. *Journal of Mass Spectrometry* **2019,** *54* (12), 933-947.

166. Kendrick, E., A Mass Scale Based on CH2 = 14.0000 for High Resolution Mass Spectrometry of Organic Compounds. *Anal Chem* **1963,** *35* (13), 2146-2154.

167. Lerno, L. A., Jr.; German, J. B.; Lebrilla, C. B., Method for the identification of lipid classes based on referenced Kendrick mass analysis. *Anal Chem* **2010,** *82* (10), 4236-45.

168. Hustin, J.; Kune, C.; Far, J.; Eppe, G.; Debois, D.; Quinton, L.; De Pauw, E., Differential Kendrick's Plots as an Innovative Tool for Lipidomics in Complex Samples: Comparison of Liquid Chromatography and Infusion-Based Methods to Sample Differential Study. *J Am Soc Mass Spectrom* **2022,** *33* (12), 2273-2282.

169. Sleno, L., The use of mass defect in modern mass spectrometry. *Journal of Mass Spectrometry* **2012,** *47* (2), 226-236.

170. Zubarev, R. A.; Makarov, A., Orbitrap Mass Spectrometry. *Anal Chem* **2013,** *85* (11), 5288-5296.

171. Cleary, S. P.; Prell, J. S., Liberating Native Mass Spectrometry from Dependence on Volatile Salt Buffers by Use of Gábor Transform. *ChemPhysChem* **2019,** *20* (4), 519-523.

172. LaPlante Kerry, L.; Woodmansee, S., Activities of Daptomycin and Vancomycin Alone and in Combination with Rifampin and Gentamicin against Biofilm-Forming Methicillin-Resistant Staphylococcus aureus Isolates in an Experimental Model of Endocarditis. *Antimicrobial Agents and Chemotherapy* **2009,** *53* (9), 3880-3886.

173. Rose, W. E.; Leonard, S. N.; Sakoulas, G.; Kaatz, G. W.; Zervos, M. J.; Sheth, A.; Carpenter, C. F.; Rybak, M. J., daptomycin activity against Staphylococcus aureus following vancomycin exposure in an in vitro pharmacodynamic model with simulated endocardial vegetations. *Antimicrob Agents Chemother* **2008,** *52* (3), 831-6.

174. Johnson, A. R.; Carlson, E. E., Collision-Induced Dissociation Mass Spectrometry: A Powerful Tool for Natural Product Structure Elucidation. *Anal Chem* **2015,** *87* (21), 10668-10678.

175. Zhang, G.; Keener, J. E.; Marty, M. T., Measuring Remodeling of the Lipid Environment Surrounding Membrane Proteins with Lipid Exchange and Native Mass Spectrometry. *Anal Chem* **2020,** *92* (8), 5666-5669.

176. Sanders, H. M.; Kostelic, M. M.; Zak, C. K.; Marty, M. T., Lipids and EGCG Affect α-Synuclein Association and Disruption of Nanodiscs. *Biochemistry* **2022,** *61* (11), 1014-1021.

177. Gevaert, K.; Impens, F.; Ghesquière, B.; Van Damme, P.; Lambrechts, A.; Vandekerckhove, J., Stable isotopic labeling in proteomics. *Proteomics* **2008,** *8* (23-24), 4873-85.

178. Johnson, D. T.; Di Stefano, L. H.; Jones, L. M., Fast photochemical oxidation of proteins (FPOP): A powerful mass spectrometry-based structural proteomics tool. *J Biol Chem* **2019,** *294* (32), 11969-11979.

179. Konermann, L.; Pan, J.; Liu, Y. H., Hydrogen exchange mass spectrometry for studying protein structure and dynamics. *Chem Soc Rev* **2011,** *40* (3), 1224-34.

180. Reid Deseree, D. T., Wang Zhihan, Aspinwall Craig, Marty Michael., Daptomycin-Membrane Interactions Using Native MS and Fast Photochemical Oxidation of Peptides in Nanodiscs. *ChemRxiv* **2022**.

181. Sanders, H.; Chalyavi, F.; Fields, C.; Kostelic, M. M.; Li, M.-H.; Raleigh, D.; Zanni, M.; Marty, M. T., Interspecies Variation Affects IAPP Membrane Binding. *ChemRxiv* **2023**.

182. Kaldmäe, M.; Österlund, N.; Lianoudaki, D.; Sahin, C.; Bergman, P.; Nyman, T.; Kronqvist, N.; Ilag, L. L.; Allison, T. M.; Marklund, E. G.; Landreh, M., Gas-Phase Collisions with Trimethylamine-N-Oxide Enable Activation-Controlled Protein Ion Charge Reduction. *J Am Soc Mass Spectrom* **2019,** *30* (8), 1385-1388.

183. Townsend, J. A.; Keener, J. E.; Miller, Z. M.; Prell, J. S.; Marty, M. T., Imidazole Derivatives Improve Charge Reduction and Stabilization for Native Mass Spectrometry. *Anall Chem* **2019,** *91* (22), 14765-14772.

184. Pacholarz, K. J.; Barran, P. E., Use of a charge reducing agent to enable intact mass analysis of cysteine-linked antibody-drug-conjugates by native mass spectrometry. *EuPA Open Proteomics* **2016,** *11*, 23-27.

185. Jiang, J.; Daniels, B. V.; Fu, D., Crystal Structure of AqpZ Tetramer Reveals Two Distinct Arg-189 Conformations Associated with Water Permeation through the Narrowest Constriction of the Water-conducting Channel*. *J Bio Chem* **2006,** *281* (1), 454-460.

186. Ringler, P.; Borgnia, M. J.; Stahlberg, H.; Maloney, P. C.; Agre, P.; Engel, A., Structure of the water channel AqpZ from Escherichia coli revealed by electron crystallography. *J Mol Biol* **1999,** *291* (5), 1181-90.

187. Epand, R. M.; Epand, R. F., Lipid domains in bacterial membranes and the action of antimicrobial agents. *Biochimica et Biophysica Acta (BBA) - Biomembranes* **2009,** *1788* (1), 289-294.

188. Savini, F.; Loffredo, M. R.; Troiano, C.; Bobone, S.; Malanovic, N.; Eichmann, T. O.; Caprio, L.; Canale, V. C.; Park, Y.; Mangoni, M. L.; Stella, L., Binding of an antimicrobial peptide to bacterial cells: Interaction with different species, strains and cellular components. *Biochimica et Biophysica Acta (BBA) - Biomembranes* **2020,** *1862* (8), 183291.

189. Mondal, S.; Khelashvili, G.; Weinstein, H., Not Just an Oil Slick: How the Energetics of Protein-Membrane Interactions Impacts the Function and Organization of Transmembrane Proteins. *Biophys J* **2014,** *106* (11), 2305-2316.

190. Bieschke, J.; Russ, J.; Friedrich, R. P.; Ehrnhoefer, D. E.; Wobst, H.; Neugebauer, K.; Wanker, E. E., EGCG remodels mature alpha-synuclein and amyloid-beta fibrils and reduces cellular toxicity. *PNAS* **2010,** *107* (17), 7710-5.

191. Fernandes, L.; Cardim-Pires, T. R.; Foguel, D.; Palhano, F. L., Green Tea Polyphenol Epigallocatechin-Gallate in Amyloid Aggregation and Neurodegenerative Diseases. *Front Neurosci* **2021,** *15*, 718188.

192. Cady, S. D.; Schmidt-Rohr, K.; Wang, J.; Soto, C. S.; DeGrado, W. F.; Hong, M., Structure of the amantadine binding site of influenza M2 proton channels in lipid bilayers. *Nature* **2010,** *463* (7281), 689-692.

193. Schnell, J. R.; Chou, J. J., Structure and mechanism of the M2 proton channel of influenza A virus. *Nature* **2008,** *451* (7178), 591-595.

194. Thomaston, J. L.; Polizzi, N. F.; Konstantinidi, A.; Wang, J.; Kolocouris, A.; DeGrado, W. F., Inhibitors of the M2 Proton Channel Engage and Disrupt Transmembrane Networks of Hydrogen-Bonded Waters. *Journal of the American Chemical Society* **2018,** *140* (45), 15219-15226.

195. Keating, A. R.; Wesdemiotis, C., Rapid and simple determination of average molecular weight and composition of synthetic polymers via electrospray ionization-mass spectrometry and a Bayesian universal charge deconvolution. *Rapid Communications in Mass Spectrometry* **2023,** *37* (8), e9478.

196. Wu, D.; Li, J.; Struwe, W. B.; Robinson, Carol V., Probing N-glycoprotein microheterogeneity by lectin affinity purification-mass spectrometry analysis. *Chem Sci* **2019,** *10* (19), 5146-5155.

197. Wu, D.; Struwe, W. B.; Harvey, D. J.; Ferguson, M. A. J.; Robinson, C. V., N-glycan microheterogeneity regulates interactions of plasma proteins. *PNAS* **2018,** *115* (35), 8763-8768.

198. Hopper, J. T.; Robinson, C. V., Mass spectrometry quantifies protein interactions--from molecular chaperones to membrane porins. *Angew. Chem. Int. Ed.* **2014,** *53* (51), 14002-15.

199. Frick, M.; Schmidt, C., Mass spectrometry-A versatile tool for characterising the lipid environment of membrane protein assemblies. *Chem Phys Lipids* **2019,** *221*, 145-157.

200. Jovcevski, B.; Pukala, T. L., Mass Spectrometry and Its Applications. In *Biomolecular and Bioanalytical Techniques*, 2019; pp 219-253.

201. Bolla, J. R.; Agasid, M. T.; Mehmood, S.; Robinson, C. V., Membrane Protein-Lipid Interactions Probed Using Mass Spectrometry. *Annu. Rev. Biochem* **2019,** *88*, 85-111.

202. Fabris, D., A role for the MS analysis of nucleic acids in the post-genomics age. *J. Am. Soc. Mass Spectrom.* **2010,** *21* (1), 1-13.

203. Hofstadler, S. A.; Griffey, R. H., Analysis of Noncovalent Complexes of DNA and RNA by Mass Spectrometry. *Chem. Rev.* **2001,** *101* (2), 377-390.

204. Marty, M. T.; Zhang, H.; Cui, W.; Blankenship, R. E.; Gross, M. L.; Sligar, S. G., Native mass spectrometry characterization of intact nanodisc lipoprotein complexes. *Anal. Chem.* **2012,** *84* (21), 8957-60.

205. Marty, M. T.; Hoi, K. K.; Robinson, C. V., Interfacing Membrane Mimetics with Mass Spectrometry. *Acc Chem Res* **2016,** *49* (11), 2459-2467.

206. Mehmood, S.; Marcoux, J.; Hopper, J. T. S.; Allison, T. M.; Liko, I.; Borysik, A. J.; Robinson, C. V., Charge Reduction Stabilizes Intact Membrane Protein Complexes for Mass Spectrometry. *J. Am. Chem. Soc.* **2014,** *136* (49), 17010-17012.

207. Sun, J.; Kitova, E. N.; Klassen, J. S., Method for Stabilizing Protein−Ligand Complexes in Nanoelectrospray Ionization Mass Spectrometry. *Anal. Chem.* **2007,** *79* (2), 416-425.

208. Sun, N.; Soya, N.; Kitova, E. N.; Klassen, J. S., Nonspecific interactions between proteins and charged biomolecules in electrospray ionization mass spectrometry. *J. Am. Soc. Mass Spectrom.* **2010,** *21* (3), 472-81.

209. Hall, Z.; Politis, A.; Bush, M. F.; Smith, L. J.; Robinson, C. V., Charge-State Dependent Compaction and Dissociation of Protein Complexes: Insights from Ion Mobility and Molecular Dynamics. *J. Am. Chem. Soc.* **2012,** *134* (7), 3429-3438.

210. Bornschein, R. E.; Hyung, S.-J.; Ruotolo, B. T., Ion Mobility-Mass Spectrometry Reveals Conformational Changes in Charge Reduced Multiprotein Complexes. *J. Am. Soc. Mass. Spectrom.* **2011,** *22* (10), 1690.

211. Lemaire, D.; Marie, G.; Serani, L.; Laprévote, O., Stabilization of Gas-Phase Noncovalent Macromolecular Complexes in Electrospray Mass Spectrometry Using Aqueous Triethylammonium Bicarbonate Buffer. *Anal. Chem.* **2001,** *73* (8), 1699-1706.

212. Bagal, D.; Kitova, E. N.; Liu, L.; El-Hawiet, A.; Schnier, P. D.; Klassen, J. S., Gas Phase Stabilization of Noncovalent Protein Complexes Formed by Electrospray Ionization. *Anal. Chem.* **2009,** *81* (18), 7801-7806.

213. Patrick, J. W.; Laganowsky, A., Generation of Charge-Reduced Ions of Membrane Protein Complexes for Native Ion Mobility Mass Spectrometry Studies. *J. Am. Soc. Mass Spectrom.* **2019,** *30* (5), 886-892.

214. Gault, J.; Lianoudaki, D.; Kaldmae, M.; Kronqvist, N.; Rising, A.; Johansson, J.; Lohkamp, B.; Lain, S.; Allison, T. M.; Lane, D. P.; Marklund, E. G.; Landreh, M., Mass Spectrometry Reveals the Direct Action of a Chemical Chaperone. *J. Phys. Chem. Lett.* **2018,** *9* (14), 4082-4086.

215. Kaldmae, M.; Osterlund, N.; Lianoudaki, D.; Sahin, C.; Bergman, P.; Nyman, T.; Kronqvist, N.; Ilag, L. L.; Allison, T. M.; Marklund, E. G.; Landreh, M., Gas-Phase Collisions with Trimethylamine-N-Oxide Enable Activation-Controlled Protein Ion Charge Reduction. *J. Am. Soc. Mass Spectrom.* **2019,** *30* (8), 1385-1388.

216. Walker, L. R.; Marzluff, E. M.; Townsend, J. A.; Resager, W. C.; Marty, M. T., Native Mass Spectrometry of Antimicrobial Peptides in Lipid Nanodiscs Elucidates Complex Assembly. *Anal. Chem.* **2019,** *91* (14), 9284-9291.

217. Reid, D. J.; Keener, J. E.; Wheeler, A. P.; Zambrano, D. E.; Diesing, J. M.; Reinhardt-Szyba, M.; Makarov, A.; Marty, M. T., Engineering Nanodisc Scaffold Proteins for Native Mass Spectrometry. *Anal. Chem.* **2017,** *89* (21), 11189-11192.

218. Ritchie, T. K.; Grinkova, Y. V.; Bayburt, T. H.; Denisov, I. G.; Zolnerciks, J. K.; Atkins, W. M.; Sligar, S. G., Reconstitution of Membrane Proteins in Phospholipid Bilayer Nanodiscs. In *Methods Enzymol.*, Nejat, D., Ed. Academic Press: San Diego, CA, 2009; Vol. 464, pp 211-231.

219. Reid, D. J.; Diesing, J. M.; Miller, M. A.; Perry, S. M.; Wales, J. A.; Montfort, W. R.; Marty, M. T., MetaUniDec: High-Throughput Deconvolution of Native Mass Spectra. *J. Am. Soc. Mass Spectrom.* **2019,** *30* (1), 118-127.

220. van de Waterbeemd, M.; Fort, K. L.; Boll, D.; Reinhardt-Szyba, M.; Routh, A.; Makarov, A.; Heck, A. J., High-fidelity mass analysis unveils heterogeneity in intact ribosomal particles. *Nat. Methods* **2017,** *14* (3), 283-286.

221. Marty, M. T.; Baldwin, A. J.; Marklund, E. G.; Hochberg, G. K.; Benesch, J. L.; Robinson, C. V., Bayesian deconvolution of mass and ion mobility spectra: from binary interactions to polydisperse ensembles. *Anal. Chem.* **2015,** *87* (8), 4370-6.

222. Marty, M. T.; Hoi, K. K.; Gault, J.; Robinson, C. V., Probing the Lipid Annular Belt by Gas-Phase Dissociation of Membrane Proteins in Nanodiscs. *Angew. Chem. Int. Ed. Engl.* **2016,** *55* (2), 550-4.

223. Fifen, J. J.; Dhaouadi, Z.; Nsangou, M., Revision of the thermodynamics of the proton in gas phase. *J. Phys. Chem. A* **2014,** *118* (46), 11090-7.

224. Hunter, E. P. L.; Lias, S. G., Evaluated gas phase basicities and proton affinities of molecules: An update. *J. Phys. Chem. Ref. Data* **1998,** *27* (3), 413-656.

225. Quintyn, R. S. Applying Tandem Mass Spectrometry coupled with Ion Mobility to probe the Structure of Non-Covalent Protein Complexes and their Interactions with Ligands, Peptides and other Proteins. PhD Dissertation, The Ohio State University, 2015.

226. Pagel, K.; Hyung, S. J.; Ruotolo, B. T.; Robinson, C. V., Alternate dissociation pathways identified in charge-reduced protein complex ions. *Anal Chem* **2010,** *82* (12), 5363-72.

227. Dongré, A. R.; Jones, J. L.; Somogyi, Á.; Wysocki, V. H., Influence of Peptide Composition, Gas-Phase Basicity, and Chemical Modification on Fragmentation Efficiency: Evidence for the Mobile Proton Model. *J. Am. Chem. Soc.* **1996,** *118* (35), 8365-8374.

228. Marty, M. T.; Zhang, H.; Cui, W.; Gross, M. L.; Sligar, S. G., Interpretation and deconvolution of nanodisc native mass spectra. *J. Am. Soc. Mass Spectrom.* **2014,** *25* (2), 269-77.

229. Catalina, M. I.; van den Heuvel, R. H.; van Duijn, E.; Heck, A. J., Decharging of globular proteins and protein complexes in electrospray. *Chemistry* **2005,** *11* (3), 960-8.

230. Prell, J. S.; O'Brien, J. T.; Steill, J. D.; Oomens, J.; Williams, E. R., Structures of Protonated Dipeptides: The Role of Arginine in Stabilizing Salt Bridges. *J. Am. Chem. Soc.* **2009,** *131* (32), 11442-11449.

231. Roscioli, J. R.; McCunn, L. R.; Johnson, M. A., Quantum Structure of the Intermolecular Proton Bond. *Science* **2007,** *316* (5822), 249-254.

232. Luis Nieva, J.; Carrasco, L., Viroporins: Structures and Functions beyond Cell Membrane Permeabilization. *Viruses* **2015,** *7* (10), 5169-5171.

233. Nieva, J. L.; Madan, V.; Carrasco, L., Viroporins: structure and biological functions. *Nat Rev Microbiol* **2012,** *10* (8), 563-74.

234. Li, F.; Ma, C.; Hu, Y.; Wang, Y.; Wang, J., Discovery of Potent Antivirals against Amantadine-Resistant Influenza A Viruses by Targeting the M2-S31N Proton Channel. *ACS Infect Dis* **2016,** *2* (10), 726-733.

235. Wang, J., M2 as a target to combat influenza drug resistance: what does the evidence say? *Future Virology* **2016,** *11* (1), 1-4.

236. Mould, J. A.; Drury, J. E.; Frings, S. M.; Kaupp, U. B.; Pekosz, A.; Lamb, R. A.; Pinto, L. H., *J. Biol. Chem.* **2000,** *275* (40), 31038-31050.

237. OuYang, B.; Dong, Y.; Chou, J. J., Structural and Functional Properties of Viral Membrane Proteins. In *Advances in Membrane Proteins*, Cao, Y., Ed. Springer Singapore: Singapore, 2018; pp 147-181.

238. Zhou, H.-X.; Cross, T. A., Modeling the membrane environment has implications for membrane protein structure and function: Influenza A M2 protein. *Protein Sci.* **2013,** *22* (4), 381-394.

239. Jalily, P. H.; Duncan, M. C.; Fedida, D.; Wang, J.; Tietjen, I., Put a cork in it: Plugging the M2 viral ion channel to sink influenza. *Antiviral Res.* **2020,** *178*, 104780-104780.

240. Holsinger, L. J.; Nichani, D.; Pinto, L. H.; Lamb, R. A., Influenza A virus M2 ion channel protein: a structure-function analysis. *J. Virol.* **1994,** *68* (3), 1551-1563.

241. Saotome, K.; Duong-Ly, K. C.; Howard, K. P., Influenza A M2 protein conformation depends on choice of model membrane. *Biopolymers* **2015,** *104* (4), 405-11.

242. Kawano, K.; Yano, Y.; Matsuzaki, K., A dimer is the minimal proton-conducting unit of the influenza a virus M2 channel. *J. Mol. Biol.* **2014,** *426 14*, 2679-91.

243. Marty, M. T., Nanodiscs and Mass Spectrometry: Making Membranes Fly. *Int. J. Mass spectrom.* **2020,** *458*, 116436.

244. Ritchie, T. K.; Grinkova, Y. V.; Bayburt, T. H.; Denisov, I. G.; Zolnerciks, J. K.; Atkins, W. M.; Sligar, S. G., Chapter 11 - Reconstitution of membrane proteins in phospholipid bilayer nanodiscs. *Methods Enzymol* **2009,** *464*, 211-231.

245. Hopper, J. T. S.; Sokratous, K.; Oldham, N. J., Charge state and adduct reduction in electrospray ionization–mass spectrometry using solvent vapor exposure. *Anal. Biochem.* **2012,** *421* (2), 788-790.

246. Marty, M. T., Eliminating Artifacts in Electrospray Deconvolution with a SoftMax Function. *J. Am. Soc. Mass Spectrom.* **2019,** *30* (10), 2174-2177.

247. Bush, M. F.; Hall, Z.; Giles, K.; Hoyes, J.; Robinson, C. V.; Ruotolo, B. T., Collision Cross Sections of Proteins and Their Complexes: A Calibration Framework and Database for Gas-Phase Structural Biology. *Anal. Chem.* **2010,** *82* (22), 9557-9565.

248. Salbo, R.; Bush, M. F.; Naver, H.; Campuzano, I.; Robinson, C. V.; Pettersson, I.; Jorgensen, T. J.; Haselmann, K. F., Traveling-wave ion mobility mass spectrometry of protein complexes: accurate calibrated collision cross-sections of human insulin oligomers. *Rapid Commun. Mass Spectrom.* **2012,** *26* (10), 1181-93.

249. Schrodinger, LLC, The PyMOL Molecular Graphics System, Version 1.8. 2015.

250. Andreas, L. B.; Reese, M.; Eddy, M. T.; Gelev, V.; Ni, Q. Z.; Miller, E. A.; Emsley, L.; Pintacuda, G.; Chou, J. J.; Griffin, R. G., Structure and Mechanism of the Influenza A M218–60 Dimer of Dimers. *J. Am. Chem. Soc.* **2015,** *137* (47), 14877-14886.

251. Cho, K. J.; Schepens, B.; Seok, J. H.; Kim, S.; Roose, K.; Lee, J.-H.; Gallardo, R.; Van Hamme, E.; Schymkowitz, J.; Rousseau, F.; Fiers, W.; Saelens, X.; Kim, K. H., Structure of the Extracellular Domain of Matrix Protein 2 of Influenza A Virus in Complex with a Protective Monoclonal Antibody. *J. Virol.* **2015,** *89* (7), 3700-3711.

252. Rolland, A. D.; Prell, J. S., Computational Insights into Compaction of Gas-Phase Protein and Protein Complex Ions in Native Ion Mobility-Mass Spectrometry. *Trends Analyt. Chem.* **2019,** *116*, 282-291.

253. Ewing, S. A.; Donor, M. T.; Wilson, J. W.; Prell, J. S., Collidoscope: An Improved Tool for Computing Collisional Cross-Sections with the Trajectory Method. *J. Am. Soc. Mass Spectrom.* **2017,** *28* (4), 587-596.

254. Schuck, P., Size-Distribution Analysis of Macromolecules by Sedimentation Velocity Ultracentrifugation and Lamm Equation Modeling. *Biophys. J.* **2000,** *78* (3), 1606-1619.

255. Wang, J.; Wu, Y.; Ma, C.; Fiorin, G.; Wang, J.; Pinto, L. H.; Lamb, R. A.; Klein, M. L.; Degrado, W. F., Structure and inhibition of the drug-resistant S31N mutant of the M2 ion channel of influenza A virus. *Proc. Natl. Acad. Sci. U.S.A.* **2013,** *110* (4), 1315-20.

256. Acharya, R.; Carnevale, V.; Fiorin, G.; Levine, B. G.; Polishchuk, A. L.; Balannik, V.; Samish, I.; Lamb, R. A.; Pinto, L. H.; DeGrado, W. F.; Klein, M. L., Structure and mechanism of proton transport through the transmembrane tetrameric M2 protein bundle of the influenza A virus. *Proc. Natl. Acad. Sci. U.S.A.* **2010,** *107* (34), 15075-80.

257. Thomaston, J. L.; DeGrado, W. F., Crystal structure of the drug-resistant S31N influenza M2 proton channel. *Protein Sci.* **2016,** *25* (8), 1551-1554.

258. Mehmood, S.; Allison, T. M.; Robinson, C. V., Mass Spectrometry of Protein Complexes: From Origins to Applications. *Annu. Rev. Phys. Chem.* **2015,** *66* (1), 453-474.

259. Ma, C.; Wang, J., Functional studies reveal the similarities and differences between AM2 and BM2 proton channels from influenza viruses. *Biochim. Biophys. Acta Biomembr.* **2018,** *1860* (2), 272-280.

260. Cady, S. D.; Luo, W.; Hu, F.; Hong, M., Structure and function of the influenza A M2 proton channel. *Biochemistry* **2009,** *48* (31), 7356-7364.

261. Reading, E.; Liko, I.; Allison, T. M.; Benesch, J. L. P.; Laganowsky, A.; Robinson, C. V., The Role of the Detergent Micelle in Preserving the Structure of Membrane Proteins in the Gas Phase. *Angew. Chem. Int. Ed.* **2015,** *54* (15), 4577-4581.

262. Laganowsky, A.; Reading, E.; Allison, T. M.; Ulmschneider, M. B.; Degiacomi, M. T.; Baldwin, A. J.; Robinson, C. V., Membrane proteins bind lipids selectively to modulate their structure and function. *Nature* **2014,** *510* (7503), 172-175.

263. Sacco, M. D.; Ma, C.; Lagarias, P.; Gao, A.; Townsend, J. A.; Meng, X.; Dube, P.; Zhang, X.; Hu, Y.; Kitamura, N.; Hurst, B.; Tarbet, B.; Marty, M. T.; Kolocouris, A.; Xiang, Y.; Chen, Y.; Wang, J., Structure and inhibition of the SARS-CoV-2 main protease reveal strategy for developing dual inhibitors against M^{pro} and cathepsin L. *Science Advances* **2020,** *6* (50), eabe0751.

264. Gabelica, V.; Rosu, F.; De Pauw, E., A Simple Method to Determine Electrospray Response Factors of Noncovalent Complexes. *Anal. Chem.* **2009,** *81* (16), 6708-6715.

265. Ruotolo, B. T.; Benesch, J. L.; Sandercock, A. M.; Hyung, S. J.; Robinson, C. V., Ion mobility-mass spectrometry analysis of large protein complexes. *Nat. Protoc.* **2008,** *3* (7), 1139-52.

266. Watkins, L. C.; DeGrado, W. F.; Voth, G. A., Influenza A M2 Inhibitor Binding Understood through Mechanisms of Excess Proton Stabilization and Channel Dynamics. *Journal of the American Chemical Society* **2020,** *142* (41), 17425-17433.

267. Hu, Y.; Hau, R. K.; Wang, Y.; Tuohy, P.; Zhang, Y.; Xu, S.; Ma, C.; Wang, J., Structure-Property Relationship Studies of Influenza A Virus AM2-S31N Proton Channel Blockers. *ACS Med. Chem. Lett.* **2018,** *9* (11), 1111-1116.

268. Salom, D.; Hill, B. R.; Lear, J. D.; DeGrado, W. F., pH-Dependent Tetramerization and Amantadine Binding of the Transmembrane Helix of M2 from the Influenza A Virus. *Biochemistry* **2000,** *39* (46), 14160-14170.

269. Pielak, Rafal M.; Oxenoid, K.; Chou, James J., Structural Investigation of Rimantadine Inhibition of the AM2-BM2 Chimera Channel of Influenza Viruses. *Structure* **2011,** *19* (11), 1655-1663.

270. van Meer, G.; Voelker, D. R.; Feigenson, G. W., Membrane lipids: where they are and how they behave. *Nat Rev Mol Cell Biol* **2008,** *9* (2), 112-24.

271. Rosenberg, M. R.; Casarotto, M. G., Coexistence of two adamantane binding sites in the influenza A M2 ion channel. *Proc. Natl. Acad. Sci. U.S.A.* **2010,** *107* (31), 13866-71.

272. Stouffer, A. L.; Nanda, V.; Lear, J. D.; DeGrado, W. F., Sequence Determinants of a Transmembrane Proton Channel: An Inverse Relationship between Stability and Function. *J. Mol. Biol.* **2005,** *347* (1), 169-179.

273. Wilson, J. W.; Rolland, A. D.; Klausen, G. M.; Prell, J. S., Ion Mobility-Mass Spectrometry Reveals That α-Hemolysin from Staphylococcus aureus Simultaneously Forms Hexameric and Heptameric Complexes in Detergent Micelle Solutions. *Anal. Chem.* **2019,** *91* (15), 10204-10211.

274. Thomaston, J. L.; Alfonso-Prieto, M.; Woldeyes, R. A.; Fraser, J. S.; Klein, M. L.; Fiorin, G.; DeGrado, W. F., High-resolution structures of the M2 channel from influenza A virus reveal dynamic pathways for proton stabilization and transduction. *Proceedings of the National Academy of Sciences* **2015,** *112* (46), 14260-14265.

275. Thomaston, J. L.; Woldeyes, R. A.; Nakane, T.; Yamashita, A.; Tanaka, T.; Koiwai, K.; Brewster, A. S.; Barad, B. A.; Chen, Y.; Lemmin, T.; Uervirojnangkoorn, M.; Arima, T.; Kobayashi, J.; Masuda, T.; Suzuki, M.; Sugahara, M.; Sauter, N. K.; Tanaka, R.; Nureki, O.; Tono, K.; Joti, Y.; Nango, E.; Iwata, S.; Yumoto, F.; Fraser, J. S.; DeGrado, W. F., XFEL structures of the influenza M2 proton channel: Room temperature water networks and insights into proton conduction. *Proceedings of the National Academy of Sciences* **2017,** *114* (51), 13357-13362.

276. Yang, J.; Piai, A.; Shen, H.-B.; Chou, J. J., An Exhaustive Search Algorithm to Aid NMR-Based Structure Determination of Rotationally Symmetric Transmembrane Oligomers. *Sci. Rep.* **2017,** *7* (1), 17373.

277. Heck, A. J. R., Native mass spectrometry: a bridge between interactomics and structural biology. *Nature Methods* **2008,** *5* (11), 927-933.

278. Liang, R.; Swanson, J. M. J.; Madsen, J. J.; Hong, M.; DeGrado, W. F.; Voth, G. A., Acid activation mechanism of the influenza A M2 proton channel. *Proc. Natl. Acad. Sci. U.S.A.* **2016,** *113* (45), E6955-E6964.

279. To, J.; Torres, J., Viroporins in the Influenza Virus. *Cells* **2019,** *8* (7), 654.

280. Hu, F.; Luo, W.; Cady, S. D.; Hong, M., Conformational plasticity of the influenza A M2 transmembrane helix in lipid bilayers under varying pH, drug binding, and membrane thickness. *Biochim. Biophys. Acta* **2011,** *1808* (1), 415-423.

281. Ivanova, P. T.; Myers, D. S.; Milne, S. B.; McClaren, J. L.; Thomas, P. G.; Brown, H. A., Lipid Composition of the Viral Envelope of Three Strains of Influenza Virus—Not All Viruses Are Created Equal. *ACS Infectious Diseases* **2015,** *1* (9), 435-442.

282. Thomaston, J. L.; Wu, Y.; Polizzi, N.; Liu, L.; Wang, J.; DeGrado, W. F., X-ray Crystal Structure of the Influenza A M2 Proton Channel S31N Mutant in Two Conformational States: An Open and Shut Case. *J. Am. Chem. Soc.* **2019,** *141* (29), 11481-11488.

283. Williams, J. K.; Tietze, D.; Wang, J.; Wu, Y.; DeGrado, W. F.; Hong, M., Drug-induced conformational and dynamical changes of the S31N mutant of the influenza M2 proton channel investigated by solid-state NMR. *J. Am. Chem. Soc.* **2013,** *135* (26), 9885-9897.

284. Medeiros-Silva, J.; Somberg, N. H.; Wang, H. K.; McKay, M. J.; Mandala, V. S.; Dregni, A. J.; Hong, M., pH- and Calcium-Dependent Aromatic Network in the SARS-CoV-2 Envelope Protein. *Journal of the American Chemical Society* **2022,** *144* (15), 6839-6850.

285. Karunatilaka, K. S.; Filman, D. J.; Strauss, M.; Loparo, J. J.; Hogle, J. M., Real-Time Imaging of Polioviral RNA Translocation across a Membrane. *mBio* **2021,** *12* (1), e03695-20.

286. Hogle, J. M., Poliovirus cell entry: common structural themes in viral cell entry pathways. *Annu Rev Microbiol* **2002,** *56*, 677-702.

287. Panjwani, A.; Strauss, M.; Gold, S.; Wenham, H.; Jackson, T.; Chou, J. J.; Rowlands, D. J.; Stonehouse, N. J.; Hogle, J. M.; Tuthill, T. J., Capsid Protein VP4 of Human Rhinovirus Induces Membrane Permeability by the Formation of a Size-Selective Multimeric Pore. *PLOS Pathogens* **2014,** *10* (8), e1004294.

288. Paul, A. V.; Schultz, A.; Pincus, S. E.; Oroszlan, S.; Wimmer, E., Capsid protein VP4 of poliovirus is N-myristoylated. *Proc Natl Acad Sci U S A* **1987,** *84* (22), 7827-31.

289. Lu, J.-X.; Sharpe, S.; Ghirlando, R.; Yau, W.-M.; Tycko, R., Oligomerization state and supramolecular structure of the HIV-1 Vpu protein transmembrane segment in phospholipid bilayers. *Protein Sci* **2010,** *19* (10), 1877-1896.

290. Padhi, S.; Khan, N.; Jameel, S.; Priyakumar, U. D., Molecular Dynamics Simulations Reveal the HIV-1 Vpu Transmembrane Protein to Form Stable Pentamers. *PLOS ONE* **2013,** *8* (11), e79779.

291. Hussain, A.; Das, S. R.; Tanwar, C.; Jameel, S., Oligomerization of the human immunodeficiency virus type 1 (HIV-1) Vpu protein--a genetic, biochemical and biophysical analysis. *Virol J* **2007,** *4*, 81-81.

292. Khan, N.; Geiger, J. D. Role of Viral Protein U (Vpu) in HIV-1 Infection and Pathogenesis *Viruses* [Online], 2021.

293. Rosenberg, M. R.; Weaver, L. M.; Casarotto, M. G., Probing interactions of Vpu from HIV-1 with amiloride-based compounds. *Biochimica et Biophysica Acta (BBA) - Biomembranes* **2016,** *1858* (4), 733-739.

294. Bright, L. K.; Baker, C. A.; Agasid, M. T.; Ma, L.; Aspinwall, C. A., Decreased Aperture Surface Energy Enhances Electrical, Mechanical, and Temporal Stability of Suspended Lipid Membranes. *ACS Applied Materials & Interfaces* **2013,** *5* (22), 11918-11926.

295. Ehrlich, B. E., [31] Planar lipid bilayers on patch pipettes: Bilayer formation and ion channel incorporation. In *Methods Enzymol*, Academic Press: 1992; Vol. 207, pp 463-470.

296. Kiontke, A.; Oliveira-Birkmeier, A.; Opitz, A.; Birkemeyer, C., Electrospray Ionization Efficiency Is Dependent on Different Molecular Descriptors with Respect to Solvent pH and Instrumental Configuration. *PLoS One* **2016,** *11* (12), e0167502.

297. Cox, J. T.; Marginean, I.; Smith, R. D.; Tang, K., On the ionization and ion transmission efficiencies of different ESI-MS interfaces. *J Am Soc Mass Spectrom* **2015,** *26* (1), 55-62.

298. Guo, C.; Diao, Z.; Liu, J.; Yang, B.; Zhang, J., Quantification and evaluation of ion transmission efficiency in two-stage vacuum chamber miniature mass spectrometer. *Journal of Mass Spectrometry* **2022,** *57* (3), e4816.

299. McCabe, J. W.; Shirzadeh, M.; Walker, T. E.; Lin, C.-W.; Jones, B. J.; Wysocki, V. H.; Barondeau, D. P.; Clemmer, D. E.; Laganowsky, A.; Russell, D. H., Variable-Temperature Electrospray Ionization for Temperature-Dependent Folding/Refolding Reactions of Proteins and Ligand Binding. *Analytical Chemistry* **2021,** *93* (18), 6924-6931.

300. Yang, N. J.; Hinner, M. J., Getting across the cell membrane: an overview for small molecules, peptides, and proteins. *Methods Mol Biol* **2015,** *1266*, 29-53.

301. Diamond, G.; Beckloff, N.; Weinberg, A.; Kisich, K. O., The roles of antimicrobial peptides in innate host defense. *Curr Pharm Des* **2009,** *15* (21), 2377-92.

302. Moscufo, N.; Simons, J.; Chow, M., Myristoylation is important at multiple stages in poliovirus assembly. *Journal of Virology* **1991,** *65* (5), 2372-2380.

303. Moscufo, N.; Chow, M., Myristate-protein interactions in poliovirus: interactions of VP4 threonine 28 contribute to the structural conformation of assembly intermediates and the stability of assembled virions. *J Virol* **1992,** *66* (12), 6849-57.

304. Majeed, S.; Adetuyi, O.; Borbat, P. P.; Majharul Islam, M.; Ishola, O.; Zhao, B.; Georgieva, E. R., Insights into the oligomeric structure of the HIV-1 Vpu protein. *J Struct Biol* **2023,** *215* (1), 107943.

305. Herrero, L.; Monroy, N.; González, M. E., HIV-1 Vpu Protein Mediates the Transport of Potassium in Saccharomyces cerevisiae. *Biochemistry* **2013,** *52* (1), 171-177.

306. Hussain, A.; Das, S. R.; Tanwar, C.; Jameel, S., Oligomerization of the human immunodeficiency virus type 1 (HIV-1) Vpu protein – a genetic, biochemical and biophysical analysis. *Virol J* **2007,** *4* (1), 81.

307. Chen, C.-P.; Lin, M.-H.; Chan, Y.-T.; Chen, L.-C.; Ma, C.; Fischer, W. B., Membrane protein assembly: two cytoplasmic phosphorylated serine sites of Vpu from HIV-1 affect oligomerization. *Scientific Reports* **2016,** *6* (1), 28866.

308. Saman, M.; Oluwatosin, A.; Md Majharul, I.; Bo, Z.; Elka, R. G., Oligomeric polymorphism of HIV-1 Vpu protein in lipid environment and in solution. *bioRxiv* **2022**, 2022.08.26.505453.

309. Sharpe, S.; Yau, W.-M.; Tycko, R., Structure and Dynamics of the HIV-1 Vpu Transmembrane Domain Revealed by Solid-State NMR with Magic-Angle Spinning. *Biochemistry* **2006,** *45* (3), 918-933.

310. Santa Cruz Garcia, A. B.; Schnur, K. P.; Malik, A. B.; Mo, G. C. H., Gasdermin D pores are dynamically regulated by local phosphoinositide circuitry. *Nature Communications* **2022,** *13* (1), 52.

311. Cross, T. A.; Sharma, M.; Yi, M.; Zhou, H.-X., Influence of solubilizing environments on membrane protein structures. *Trends Biochem Sci* **2011,** *36* (2), 117-125.

312. Cady, S. D.; Schmidt-Rohr, K.; Wang, J.; Soto, C. S.; Degrado, W. F.; Hong, M., Structure of the amantadine binding site of influenza M2 proton channels in lipid bilayers. *Nature* **2010,** *463* (7281), 689-92.

313. Zhou, H.-X.; Cross, T. A., Influences of Membrane Mimetic Environments on Membrane Protein Structures. *Annual Review of Biophysics* **2013,** *42* (1), 361-392.

314. Georgieva, E. R.; Borbat, P. P.; Norman, H. D.; Freed, J. H., Mechanism of influenza A M2 transmembrane domain assembly in lipid membranes. *Scientific Reports* **2015,** *5* (1), 11757.

315. Chaitanya, K. V., *Structure and Organization of Virus Genomes*. Genome and Genomics. 2019 Nov 18:1-30. doi: 10.1007/978-981-15-0702-1_1.

316. Duffy, S., Why are RNA virus mutation rates so damn high? *PLoS Biol* **2018,** *16* (8), e3000003.

317. Xue, B.; Mizianty, M. J.; Kurgan, L.; Uversky, V. N., Protein intrinsic disorder as a flexible armor and a weapon of HIV-1. *Cellular and Molecular Life Sciences* **2012,** *69* (8), 1211-1259.

318. D'Orso, I.; Frankel, A. D., HIV-1 Tat: Its Dependence on Host Factors is Crystal Clear. *Viruses* **2010,** *2* (10), 2226-2234.

319. Xia, X.; Cheng, A.; Wang, M.; Ou, X.; Sun, D.; Mao, S.; Huang, J.; Yang, Q.; Wu, Y.; Chen, S.; Zhang, S.; Zhu, D.; Jia, R.; Liu, M.; Zhao, X. X.; Gao, Q.; Tian, B., Functions of Viroporins in the Viral Life Cycle and Their Regulation of Host Cell Responses. *Front Immunol* **2022,** *13*, 890549.

320. Lee, J.; Chen, J.; Brooks, C. L., 3rd; Im, W., Application of solid-state NMR restraint potentials in membrane protein modeling. *J Magn Reson* **2008,** *193* (1), 68-76.

321. Lacapère, J.-J.; Pebay-Peyroula, E.; Neumann, J.-M.; Etchebest, C., Determining membrane protein structures: still a challenge! *Trends Biochem Sci* **2007,** *32* (6), 259-270.

322. Sugrue, R. J.; Hay, A. J., Structural characteristics of the M2 protein of influenza a viruses: Evidence that it forms a tetrameric channe. *Virology* **1991,** *180* (2), 617-624.

323. Holsinger, L. J.; Alams, R., Influenza virus M2 integral membrane protein is a homotetramer stabilized by formation of disulfide bonds. *Virology* **1991,** *183* (1), 32-43.

324. Stanczak, P.; Horst, R.; Serrano, P.; Wüthrich, K., NMR characterization of membrane protein-detergent micelle solutions by use of microcoil equipment. *J Am Chem Soc* **2009,** *131* (51), 18450-6.

325. Zoonens, M.; Catoire, L. J.; Giusti, F.; Popot, J.-L., NMR study of a membrane protein in detergent-free aqueous solution. *Proceedings of the National Academy of Sciences* **2005,** *102* (25), 8893-8898.

326. Han, Y.; Pan, J.; Ma, Y.; Zhou, D.; Xu, W., Protein-based biomaterials for combating viral infections: Current status and future prospects for development. *Biosafety and Health* **2022,** *4* (2), 87-94.

327. Bahrampour Juybari, K.; Pourhanifeh, M. H.; Hosseinzadeh, A.; Hemati, K.; Mehrzadi, S., Melatonin potentials against viral infections including COVID-19: Current evidence and new findings. *Virus Research* **2020,** *287*, 198108.

328. Hsu, J. T.; Wang, H. C.; Chen, G. W.; Shih, S. R., Antiviral drug discovery targeting to viral proteases. *Curr Pharm Des* **2006,** *12* (11), 1301-14.

329. Sharma, A.; Gupta, S. P., *Fundamentals of Viruses and Their Proteases*. Viral Proteases and Their Inhibitors. 2017:1-24. doi: 10.1016/B978-0-12-809712-0.00001-0. Epub 2017 Jul 14.

330. Sasi, V. M.; Ullrich, S.; Ton, J.; Fry, S. E.; Johansen-Leete, J.; Payne, R. J.; Nitsche, C.; Jackson, C. J., Predicting Antiviral Resistance Mutations in SARS-CoV-2 Main Protease with Computational and Experimental Screening. *Biochemistry* **2022,** *61* (22), 2495-2505.

331. Chatterjee, S.; Bhattacharya, M.; Dhama, K.; Lee, S.-S.; Chakraborty, C., Resistance to nirmatrelvir due to mutations in the Mpro in the subvariants of SARS-CoV-2 Omicron: Another concern? *Molecular Therapy - Nucleic Acids* **2023,** *32*, 263-266.

332. Sargsyan, K.; Mazmanian, K.; Lim, C., A strategy for evaluating potential antiviral resistance to small molecule drugs and application to SARS-CoV-2. *Scientific Reports* **2023,** *13* (1), 502.

333. Carpenter, E. P.; Beis, K.; Cameron, A. D.; Iwata, S., Overcoming the challenges of membrane protein crystallography. *Curr Opin Struct Biol* **2008,** *18* (5), 581-586.

334. Zhang, Y.; Tammaro, R.; Peters, P. J.; Ravelli, R. B. G., Could Egg White Lysozyme be Solved by Single Particle Cryo-EM? *Journal of Chemical Information and Modeling* **2020,** *60* (5), 2605-2613.

335. Amiar, S.; Husby, M. L.; Wijesinghe, K. J.; Angel, S.; Bhattarai, N.; Gerstman, B. S.; Chapagain, P. P.; Li, S.; Stahelin, R. V., Lipid-specific oligomerization of the Marburg virus matrix protein VP40 is regulated by two distinct interfaces for virion assembly. *Journal of Biological Chemistry* **2021,** *296*, 100796.

336. Scott, C.; Griffin, S., Viroporins: structure, function and potential as antiviral targets. *Journal of General Virology* **2015,** *96* (8), 2000-2027.

337. Nieto-Torres, J. L.; Verdiá-Báguena, C.; Castaño-Rodriguez, C.; Aguilella, V. M.; Enjuanes, L., Relevance of Viroporin Ion Channel Activity on Viral Replication and Pathogenesis. *Viruses* **2015,** *7* (7), 3552-73.

338. Marcoux, J.; Champion, T.; Colas, O.; Wagner-Rousset, E.; Corvaïa, N.; Van Dorsselaer, A.; Beck, A.; Cianférani, S., Native mass spectrometry and ion mobility characterization of trastuzumab emtansine, a lysine-linked antibody drug conjugate. *Protein Science* **2015,** *24* (8), 1210-1223.

339. Lampejo, T., Influenza and antiviral resistance: an overview. *Eur J Clin Microbiol Infect Dis* **2020,** *39* (7), 1201-1208.

340. Chukkapalli, V.; Heaton, N. S.; Randall, G., Lipids at the interface of virus-host interactions. *Curr Opin Microbiol* **2012,** *15* (4), 512-8.

341. Rosenwasser, S.; Mausz, M. A.; Schatz, D.; Sheyn, U.; Malitsky, S.; Aharoni, A.; Weinstock, E.; Tzfadia, O.; Ben-Dor, S.; Feldmesser, E.; Pohnert, G.; Vardi, A., Rewiring Host Lipid Metabolism by Large Viruses Determines the Fate of Emiliania huxleyi, a Bloom-Forming Alga in the Ocean *The Plant Cell* **2014,** *26* (6), 2689-2707.